THE CONSTRAINED DISCRETE-TIME STATE-DEPENDENT RICCATI EQUATION TECHNIQUE FOR UNCERTAIN NONLINEAR SYSTEMS

BY

INSU CHANG

DISSERTATION

Submitted in partial fulfillment of the requirements
for the degree of Doctor of Philosophy in Aerospace Engineering
in the Graduate College of the
University of Illinois at Urbana-Champaign, 2016

Urbana, Illinois

Doctoral Committee:

Professor Joseph Bentsman, Chair and Director of Research
Professor N. Sri Namachchivaya
Professor Petros G. Voulgaris
Professor Andrew G. Alleyne

Abstract

The objective of the thesis is to introduce a relatively general nonlinear controller/estimator synthesis framework using a special type of the state-dependent Riccati equation technique. The continuous time state-dependent Riccati equation (SDRE) technique is extended to discrete-time under input and state constraints, yielding constrained (C) discrete-time (D) SDRE, referred to as CD-SDRE. For the latter, stability analysis and calculation of a region of attraction are carried out. The derivation of the D-SDRE under state-dependent weights is provided. Stability of the D-SDRE feedback system is established using Lyapunov stability approach. Receding horizon strategy is used to take into account the constraints on D-SDRE controller. Stability condition of the CD-SDRE controller is analyzed by using a switched system. The use of CD-SDRE scheme in the presence of constraints is then systematically demonstrated by applying this scheme to problems of spacecraft formation orbit reconfiguration under limited performance on thrusters. Simulation results demonstrate the efficacy and reliability of the proposed CD-SDRE.

The CD-SDRE technique is further investigated in a case where there are uncertainties in nonlinear systems to be controlled. First, the system stability under each of the controllers in the robust CD-SDRE technique is separately established. The stability of the closed-loop system under the robust CD-SDRE controller is then proven based on the stability of each control system comprising switching configuration. A high fidelity dynamical model of spacecraft attitude motion in 3-dimensional space is derived with a partially filled fuel tank, assumed to have the first fuel slosh mode. The proposed robust CD-SDRE controller is then applied to the spacecraft attitude control system to stabilize its motion in the presence of uncertainties characterized by the first fuel slosh mode. The performance of the robust CD-SDRE technique is discussed.

Subsequently, filtering techniques are investigated by using the D-SDRE technique. Detailed derivation of the D-SDRE-based filter (D-SDREF) is provided under the assumption of Gaussian noises and the stability condition of the error signal between the measured signal and the estimated signals is proven to be input-to-state stable. For the non-Gaussian distributed noises, we propose a filter by combining the D-SDREF

and the particle filter (PF), named the combined D-SDRE/PF. Two algorithms for the filtering techniques are provided. Several filtering techniques are compared with challenging numerical examples to show the reliability and efficacy of the proposed D-SDREF and the combined D-SDRE/PF.

To my parents, for their unconditional love and support.

Acknowledgements

THIS thesis could not have been accomplished without the support from several incredibly talented and insightful people around me. First, and foremost, I would like to express my deepest gratitude and appreciation to my advisor, Professor Joseph Bentsman for the many years of invaluable help and guidance. Without his enthusiastic guidance and support, this thesis could not have been published.

I would like to acknowledge my thesis committee members: Professors N Sri Namachchivaya, Petros Voulgaris, and Andrew Alleyne for their insightful comments and critique for the improvement of my thesis.

I would like to thank Caterpillar Inc. for giving me a chance to work on many challenging projects over the last three years. I would like to thank John Wunning, Andrew Braun, Salim Jaliwala, Dwight Holloway, Yanchai Zhang, James Chase, Navya Yadma & Madhusudhan Kallam, Venkata Dandibhotla, Kanak Paradkar, Manh Phan, Vijay Janardhan, Vishal Murali, Jeremy Lee, and Dan Monroe (CCRI), and Winnie Wong (Cobham) at Caterpillar and Albert Wray, Yongliang Zhu, Kyle Davis, Nima Alam, Francisco Green at Caterpillar Trimble Control Technologies. Special thanks to Wei Li, who was a talented engineer as well as a good supervisor to me at Caterpillar.

I cannot forget to express my gratitude to Electric Power Research Institute (EPRI) for giving me a chance to work on a very interesting project. I would especially like to acknowledge Mark Little, John Sorge (Southern Company), and Cyrus Taft (Taft Engineering).

I would like to extend my gratitude to Dr. Fred Hadaegh, Dr. Behçet Açıkmeşe (University of Texas) and Dr. Lars Blackmore (Space-X) at NASA Jet Propulsion Laboratory (JPL) for the collaboration of the swarm project with the University of Illinois.

My sincere appreciation goes to Professors Sang-Young Park and Chandeok Park at Yonsei University for their insightful comments and suggestions for my research project. I could have not finished my studies without their help.

I would also acknowledge my research colleagues in Control Systems Design and Applications Labo-

ratory at the University of Illinois for their support: Vivek Natarajan (Tel Aviv University), Bryan Petrus (Nucor Steel), Zhelin Chen, Scott Ding, Ya Wang (Beijing Institute of Technology), Huirong Zhao (Southeast University), and Shu Zhang (Bloomberg).

I am grateful to my friends Alaa Alokaily (Lam Research), Anand Gopa Kumar (HRST), Chang Geun Yoo (Oak Ridge National Laboratory), Dukhee Yoon (Samsung), Jong Woo Kim, Jung Wook Pyo, Kim Doang Nguyen, Kyung Min Lee , Mazhar Islam, Sungjin Choi, and Wei Du (Garmin International) for enlightening and often amusing conversations.

Last of all, my sincere thanks goes to my family, especially my parents, for their love, support, and sacrifice. The dissertation is dedicated to my family.

Insu Chang

Urbana, Illinois

November 2015

Table of Contents

List of Tables

List of Figures

Part I

Introduction and Preliminaries

Chapter 1

Introduction

1.1 Research Background

CONTROL field has been enriched in the past 40 years with several advanced control techniques. However, a number of unresolved problems in the applicability of control to real industrial systems still remain (Çimen, 2010). The state-dependent Riccati equation (SDRE) technique, which emerged in the 1960's (Pearson, 1962) and was popularized in the 1990's (Cloutier, 1997; Mracek and Cloutier, 1998), has been among the candidate techniques for addressing these problems for quite some time. The SDRE techniques are general design methods that provide a systematic and effective means of designing nonlinear controllers, observers, and filters (Cloutier, 1997). One of the merits of the SDRE approach to nonlinear systems is to use the state-dependent coefficient (SDC) factorization that recasts a nonlinear system's dynamics into a form resembling linear dynamics. Then, the SDRE is used to generate the feedback control law. The SDRE techniques overcome many of the difficulties of existing methodologies such as feedback linearization, and deliver computationally efficient algorithms that are highly effective in a variety of practical applications (Çimen, 2010). Due to such benefits, SDRE has been applied to various control problems: autopilot design (Cloutier and Stansbery, 2001), satellite attitude and orbit control (Chang et al., 2009, 2010b), missile guidance and control systems (Vaddi et al., 2009), an underactuated robot (Erdem, 2001), a magnetically levitated ball (Erdem and Alleyne, 2004), helicopters (Bogdanov and Wan, 2007), a pendulum problem (Suzuki et al., 2004), underwater vehicle control problems (Naik and Singh, 2007; Geranmehr and Nekoo, 2015), polynomial differential games (Jiménez-Lizárraga et al., 2015), medical problems (Banks et al., 2006; Nazari et al., 2015), and others.

Although the SDRE technique has been evaluated successfully, the estimation of a stability region for the SDRE-controlled systems is an open problem. An analytical solution of the SDRE is generally not known (Bracci et al., 2006) since the algebraic state-dependent Riccati equation is solved numerically. There have

been many attempts to solve this problem. Some notable results are as follows: McCaffrey and Banks (2001) proposed a stability test for determining the size of the region of attraction (ROA) on which large-scale asymptotic stability holds for the SDRE algorithm by using the geometrical construction of a viscosity-type Lyapunov function. The stability region estimates for the SDRE feedback are very close to the true domain of attraction than conservative estimates in the existing literature. $\mathcal{S}$-procedure (Boyd et al., 1994) was applied to check the stability condition (Shamma and Cloutier, 2003). Here, Hurwitz $A_{\text{cl}}(x)$ was considered. Erdem and Alleyne (2002) suggested a method to satisfy high-order dynamical systems by using vector norms. By determining the overvaluing matrix for the given dynamical system, the method shows the maximum boundary for the SDRE-controlled dynamical systems. However, this method is complicated from the computational standpoint for medium and high order systems (Bracci et al., 2006). Langson and Alleyne (2002) tried to find a stable upper boundary for the SDRE controlled system. Seiler (2003) introduced a method to estimate the stability region by turning the stability problem into a semi-definite programming problem, called the Sum-of-Squares (SOS) program (Parrilo, 2000). By using the SOS program, the largest values of decision variables satisfying the Lyapunov stability condition are found. However, if the dimension of the system matrix for the SDRE is greater than two, it takes a large set of internal variables to find the optimal values for maximizing the stability region for the SDRE feedback system. Erdem and Alleyne (2004) proposed an analytical solution to estimate the asymptotic stability region for the second-order system controlled by the SDRE technique. Bracci et al. (2006) proposed another method to estimate the ROA. This procedure is an alternative to the method proposed by (Erdem and Alleyne, 2002), and is based on the Lyapunov local stability theorem (Khalil, 2002). Chen et al. (2015) investigated the global stability of the SDRE feedback system for a certain condition. In this thesis, we propose a way to estimate the exponential stability region of the SDRE feedback system.

The SDRE technique was originally developed for continuous-time systems (Cloutier, 1997; Mracek and Cloutier, 1998; Çimen, 2012). However, it is desirable to use a discrete-time SDRE for direct applications to real embedded systems. To this end, the discrete-time version of the SDRE, called D-SDRE, has been studied as well. The optimization of the D-SDRE was investigated by using a concept of model predictive control (MPC) (Dutka et al., 2005). Hassan (2012) used D-SDRE to design an observer-based controller. The D-SDRE can also be used in designing nonlinear filter systems (Nemra and Aouf, 2010; Jaganath et al., 2005). In this thesis, we derive a D-SDRE feedback controller analytically by using the Hamiltonian

(Bryson, Jr. and Ho, 1975) with state-dependent weighting matrices

The derivation and the analysis of the D-SDRE without and with constraints conditions, the latter named constrained discrete-time state-dependent Riccati equation (CD-SDRE), are the main contributions of this thesis. The constraint problem has been addressed through anti-windup (Kothare et al., 1994; Kothare and Morari, 1999) and model predictive control (MPC) (Mayne et al., 2000; Rawlings and Mayne, 2009; Grüne and Pannek, 2011). MPC has been applied to a linear quadratic regulation (LQR) under input/state constraints (Scokaert and Rawlings, 1998; Bemporad et al., 2002; Johansen et al., 2002; Johansen, 2003; Grieder et al., 2004; Ding et al., 2004; Lee and Khargonekar, 2007; Zhao and Lin, 2008; Ferrante and Ntogramatzidis, 2013). However, to the best of our knowledge, there are no specific results on SDRE (or D-SDRE) with constraints on the inputs or states.

The CD-SDRE controller described above is for deterministic nonlinear systems. However, uncertainties are ubiquitous in any systems. Therefore, the robustness of the CD-SDRE controller for such uncertain nonlinear systems in the presence of constraints on the states/inputs should be investigated, which is another main objective of the thesis. Based on the stability proof of the D-SDRE controller, we establish a robust D-SDRE feedback controller, which is proven to be exponentially stable in its ROA. The linear matrix inequalities (de Oliveira et al., 1999; Ramos and Peres, 2001) are used to prove the stability condition. The stability analysis of the robust D-SDRE controller in the presence of constraints on the states/input, called a robust CD-SDRE controller, is then investigated through the use of a concept of a switched system.

As a second part of the thesis, we investigate filtering techniques. The filtering techniques have been one of the central topics in industry as well as academia for more than 50 years since online recursive linear filters/observers were introduced in the 1960's (Kalman, 1960; Kalman and Bucy, 1961; Luenberger, 1966). The filtering techniques have not only been a popular research topic but also been used as a crucial application to control, estimation, optimization, and signal processing (Gelb, 1974; Bryson, Jr. and Ho, 1975; Anderson and Moore, 1979; Goodwin and Sin, 1984; Widrow and Stearns, 1985; Brown and Hwang, 1997; Doucet et al., 2000; Rawlings and Mayne, 2009; Lewis et al., 2012), just to name a few. Among the various filtering techniques developed so far, the extended Kalman filter (EKF) has been one of the main filtering techniques especially in industry since it is simple to design and easy to be implemented in a system. However, stable operation has been a main problem in using the EKF.

Other filtering techniques have emerged to overcome the weaknesses of the EKF. One of the notable

filtering techniques is the unscented Kalman filter (UKF) (Julier and Uhlmann, 1997, 2004). Unlike the EKF, it does not use the lienarization such as Jacobian. Instead, it uses full nonlinear dynamical models to propagate some meaningful samples called sigma points and estimates the states of the system from the behaviors of the sigma points. Direct applicability of the nonlinear dynamical models gives high chances to avoid the instability of the filtering systems. Unlike random particles in Monte Carlo method, the sigma points are chosen deterministically so that they show certain mean and covariance (Julier and Uhlmann, 2004). Rao et al. (2003) investigated a filter design by means of a concept of receding horizon in MPC (Clarke et al., 1987a,b; Mayne et al., 2000), called the moving horizon estimator (MHE). Unlike EKF or UKF which use only one step measurement to predict the states for the next step, MHE uses several prior measurements and predicts the states for finite horizons by using a constrained optimization technique. More accurate estimates of the states are expected than those by EKF or UKF (Rawlings and Mayne, 2009). Sequential Monte Carlo (SMC) methods or particle filters (PF) were introduced to increase the accuracy of the states especially in the presence of non-Gaussian noises in a system (Gordon et al., 1993). However, it should be noted that UKF or PF use samples and MHE uses optimization technique. Moreover, the MHE uses several measurement data and predicts states for finite horizons while the Kalman filters predict only one step ahead. These can cause significant computational burden in a system so that such a fact might limit their applicability to various systems specifically in which fast sampling time or less computational power are critical. Moreover, the performance of PF significantly decreases as the dimension of the state increases. It is also vulnerable to unmodeled disturbances (Rawlings and Mayne, 2009).

Another notable filtering technique is the state-dependent Riccati equation-based filter (SDREF), which is based on the SDRE technique. Beside the SDRE technique specifically for the controller development, the SDREF has also been investigated theoretically and applied to practical problems (Xin and Balakrishnan, 2002; Jaganath et al., 2005; Çimen and Merttopçuoğlu, 2008; Nemra and Aouf, 2010; Beikzadeh and Taghirad, 2012b,a; Batmani and Khaloozadeh, 2012), to name a few. The SDREF can overcome the linearization issue in EKF while it can also reduce the computational load which is a critical problem in particle-based filters such as UKF or PF. However, more analytical analysis on the stability of the SDREF should be studied. Moreover, most of the filtering techniques are designed under the assumption of Gaussian noises. There might be many cases where noises in a system do not follow the normal distribution. In these cases, PF is widely used. One of the strengths of the PF is the ability to estimate the state in the

presence of non-Gaussian noises while it has so called curse of dimensionality and is sensitive to ummodeled noises (Rawlings and Mayne, 2009). de Freitas et al. (2000) provided a filter by combining EKF and PF to improve the performance of the PF. However, it still has a linearization issue of the EKF part. van der Merwe et al. (2000) tried to combine UKF and PF, called the unscented particle filter (UPF). Rawlings and Mayne (2009) introduced a filter which contains MHE and PF. Although improved performance can be expected from the filters, there is a trade-off: the computational burden will be increased due to the sigma points in the UKF part and the longer horizons in the MHE part. In this thesis, we first start the discussion with observer design through the use of the D-SDRE technique. Then, we propose a discrete-time version of the SDREF, named D-SDREF. The proposed filter does not require the linearization like the EKF. It does not need several samples as in UKF or PF. Thereby, it can reduce the computational burden while it can estimate the real state values accurately. Then, a new filter is investigated by combining the D-SDREF and PF so that the proposed filter can have the strengths of both filters.

1.2 Outline and Contributions

The main contributions of this thesis are:
In Part II, we discuss the CD-SDRE controllers for discrete-time nonlinear systems.

- In Chapter 5, we derive the D-SDRE feedback controller analytically by using the Hamiltonian (Bryson, Jr. and Ho, 1975). To make the system more general, we allow weights on the performance index to be minimized to be dependent on states while previous studies assumed that they are constant or time-varying. Instead of using the discrete algebraic Riccati equation (DARE), a generalized discrete-time Riccati equation is derived and used. By doing so, more accurate optimization results can be expected since DARE's assumption of steady-state conditions can lead to significant errors in a controlled system. A condition for stability is proven by using the Lyapunov stability criteria (Khalil, 2002). We suggest a way to find an ROA of the D-SDRE feedback system through the use of linear matrix inequality (LMI) methods (Boyd et al., 1994; de Oliveira et al., 1999; Ramos and Peres, 2001). We investigate the stability condition of the CD-SDRE feedback system as a switched one due to the characteristics of the controller. We suggest two algorithms for CD-SDRE: a regulation problem and a reference tracking problem. The analysis of the algorithms indicates that CD-SDRE

can perform in an optimal sense in the presence of the input/state constraints.

- In Chapter 6, the proposed CD-SDRE is evaluated by using challenging problems in spacecraft orbit reconfiguration problems. We apply the proposed CD-SDRE controller to spacecraft orbit reconfiguration problems which have limited actuator performance. It is interesting to note that trajectory optimization techniques have been widely used for the reconfiguration problems (Scharf et al., 2003, 2004). However, many of the previous studies show that the optimization techniques are based on open-loop control methods which might be vulnerable to internal/external disturbances. Moreover, most of them are not real-time trajectory optimizers. In order to overcome such problems, numerous closed-loop tracking control methods have been suggested (Scharf et al., 2004). In this case, by using *a priori* designed reference trajectories, the control methods calculate proper control signals to make each spacecraft follows its reference. However, depending on the size of orbits and initial conditions (positions and velocities of spacecraft), excessively large initial control inputs might be inevitable in the tracking control which are not desirable, since, in general, an actuator's effort corresponding to a large control signal cannot be generated by a real thruster in a small spacecraft. Moreover, such improper control signals can make the motions of the spacecraft unstable. Therefore, the actuator saturation problem should be considered when designing a control system. Although the input saturation problem is prevalent in real systems, many of the advanced control methods cannot take it into account explicitly. For realistic results in this work, high-fidelity dynamical models of orbits for the reference and deputy spacecraft are derived in the presence of the oblateness of the Earth (J_2 perturbation) and atmospheric drag. The simulations show the reliable results by using the proposed CD-SDRE technique.

- In Chapter 7, we extend our scope of the CD-SDRE technique to a case of controlling a class of uncertain nonlinear system. A rigorous analysis of a robust state-feedback SDRE (or D-SDRE) controller for uncertain nonlinear systems is investigated. The performance of the proposed robust CD-SDRE-based feedback controller in the presence of uncertainties is evaluated through its application to the attitude motion control of a spacecraft with a partially filled fuel tank. Unlike predictable disturbance sources such as gravity-gradient/aerodynamic torques, magnetic fields, or solar radiation pressure, the partially filled fuel tank can generate unwanted disturbances to the spacecraft: as the spacecraft consumes fuel for orbit maintenance or momentum dumping, the volume of fuel in the tank shrinks.

Then, the rest of the fuel can generate a reaction force and excite spacecraft motion by using its movement, called fuel slosh effect (Vreeburg, 2005; Bryson, Jr., 1994). It has been a challenging problem for a long time and many researchers have tried to handle the disturbances (Peterson et al., 1989; Agrawal, 1993; Vreeburg, 2005; Reyhanoglu and Hervas, 2011; Hervas et al., 2013). To better address the fuel slosh effect, another objective of the thesis is to provide an accurate dynamical model of a spacecraft attitude motion in 3-dimensional space in the presence of the effect. Most of the previous studies listed above, especially for controlling the motion of the spacecraft, have focused on a planar motion, i.e., 2-dimensional space, of a spacecraft, like a hovercraft, to investigate the fuel slosh dynamics (Bryson, Jr., 1994; Reyhanoglu and Hervas, 2011; Hervas et al., 2013). The proposed models might provide an insight of how to attenuate the disturbance. However, equations of motion for this system have never been derived in 3-dimensional space, and simpler and less representative 2-dimensional models have been widely studied instead. Therefore, unlike the previous studies listed above, we show the equations of motion in 3-dimensional space. Under the assumption of the first fuel slosh mode (Bryson, Jr., 1994), the fuel can be considered as ice moving in the fuel tank. It is interesting to note that it is analogous to motion of spacecraft which are connected by inelastic tethers (Chang et al., 2010b).

In Part III, we investigate the design of the observer/filters based on the D-SDRE technique.

- In Chapter 8, we derive the D-SDRE-based observer for the deterministic nonlinear system. Detailed procedure for deriving the D-SDRE Observer is provided by using a one-step process. The error between the actual state and its corresponding estimated state via the D-SDRE Observer is studied analytically to show its boundedness by using the input-to-state stability (ISS) analysis (Sontag, 1989; Jiang and Wang, 2001). The D-SDRE Observer is evaluated by using the Lorenz attractor as an example.

- In Chapter 9, one of the main contributions of the thesis in the filtering part, we investigate the D-SDREF for stochastic nonlinear systems in the presence of Gaussian noises. First, we provide detailed procedure for deriving the D-SDREF by using a two-step process with an assumption of Gaussian noises. Theoretical proofs are provided to show that the state error between the measured signal and the estimated one by the D-SDREF is ISS. The algorithm of the D-SDREF is provided.

The D-SDREF has several benefits compared to other filtering techniques. Unlike the EKF, the D-SDREF does not need linearization of the stochastic system so that it can capture the nonlinearities of the system. Moreover, it does not require demanding computational power since it does not use many samples like UKF, MHE, or PF. or it only relies on the current states while the MHE uses longer horizons (Rawlings and Mayne, 2009). In order to apply the D-SDREF to stochastic systems with non-Gaussian distributed noises, we propose a new filter by combining the D-SDREF and PF, named the combined D-SDRE/PF. The proposed filter has strengths and overcomes the weaknesses of both filters. The proposed combined D-SDRE/PF can guarantee better performance than EKF/PF while maintain lower computation cost than UPF or MHE/PF. We provide an algorithm of the combined D-SDRE/PF. Finally, we evaluate the performance of the proposed D-SDREF and the combined D-SDRE/PF by using challenging numerical examples: estimates of the states of the pendubot (Spong and Block, 1995; Fantoni et al., 2000) and the Rössler attractor (Rössler, 1976; Pikovsky et al., 1996). The proposed filtering techniques show outstanding performance to estimate accurate states while the existing filtering techniques listed above have difficulty in estimating the states with high accuracy compared to the proposed filters.

As independent studies which can provide good tools for the two parts listed above, a stability analysis of the continuous-time SDRE feedback system is investigated. Moreover, we propose a gain-tuning algorithm which can be widely applied to many practical problems as well as the CD-SDRE to estimate the parameters in the MPC and D-SDRE.

- In Chapter 3, we discuss the exponential stability of the continuous-time SDRE feedback system and how to estimate its ROA. The objective of the study is to estimate the exponential stability region for the SDRE feedback systems by the motivation of contraction theory (Lohmiller and Slotine, 1998), which is closely related to the incremental stability (Angeli, 2002) in the sense that both of them consider the incremental dynamics for stability conditions. By applying the contraction analysis to the SDRE controlled systems and interpreting it as polytopic linear differential inclusions (LDIs) (Boyd et al., 1994), we can guarantee the exponential stability of the systems. Moreover, the stability condition can be interpreted as an incremental exponential stability, which has stronger characteristics than exponential convergence (Pham et al., 2009). Furthermore, the ROA estimated by the proposed method is an invariant set, which is essential because any trajectories starting from an invariant set

can be guaranteed to stay in it forever (Khalil, 2002).

- In Chapter 4, we investigate an automatic gain-tuning method, named the automatic-gain tuner via the particle swarm optimization (AGT-PSO). The AGT-PSO calculates optimal values of user-defined system parameters which is expected to be time/cost efficient and labor efficient in the sense that it automatically tunes the system parameters with little background knowledge of the controller. Moreover, the performance of the system is shown to be significantly improved with the new parameters, obtained by the AGT-PSO.

Chapter 2 provides some background material for this thesis.

Chapter 2

Preliminaries

THE basic schemes of the D-LQR, nonlinear MPC, and ISS are briefly reviewed to help understand the contents of the thesis. In this thesis, we use the following function classes. A function $\gamma : \mathbb{R}_{\geq 0} \to \mathbb{R}_{\geq 0}$ is said to be of class $\mathcal{K}$ if it is continuous, strictly increasing, and $\gamma(0) = 0$. If γ is unbounded, it is said to be of class $\mathcal{K}_\infty$. A function $\beta : \mathbb{R}_{\geq 0} \times \mathbb{R}_{\geq 0} \to \mathbb{R}_{\geq 0}$ is said to be of class $\mathcal{KL}$ if $\beta(\cdot, k)$ is of class $\mathcal{K}$ for each fixed $k \geq 0$ and $\beta(\xi, k)$ is decreasing to zero as $k \to \infty$ for each fixed $\xi \geq 0$. Some notations are also defined which will be used throughout the thesis: $\mathbb{N} := \{1, 2, 3, \cdots\}$; $\mathbb{Z}_{\geq 0} := \mathbb{N} \cup \{0\}$; $\mathbb{Z}_{a:b} := \{z \in \mathbb{N} : z \geq a,\ z \leq b;\ a < b,\ a, b \in \mathbb{Z}_{\geq 0}\}$; $\mathbb{R} := (-\infty, +\infty)$; $\mathbb{R}_{\geq 0} := \{r \in \mathbb{R} : r \geq 0\}$.

2.1 Discrete-Time Linear Quadratic Regulator (D-LQR)

Suppose that there is a deterministic discrete-time linear time-varying system described by the following difference equation

$$\boldsymbol{x}_{k+1} = \boldsymbol{A}_k \boldsymbol{x}_k + \boldsymbol{B}_k \boldsymbol{u}_k, \quad \boldsymbol{x}(0) = \boldsymbol{x}_0 \tag{2.1}$$

where $\boldsymbol{x}_k \in \mathbb{R}^n$ and $\boldsymbol{u}_k \in \mathbb{R}^m$ are the state and the control input, respectively.

The objective of the D-LQR is to find the sequence of control inputs $\boldsymbol{u}_0, \boldsymbol{u}_1, \cdots, \boldsymbol{u}_{N-1}$ that minimizes the performance index:

$$J_0 = \frac{1}{2} \sum_{j=0}^{N-1} \Big(\boldsymbol{x}_j^\top \boldsymbol{Q}_j \boldsymbol{x}_j + \boldsymbol{u}_j^\top \boldsymbol{R}_j \boldsymbol{u}_j \Big) \tag{2.2}$$

where $\boldsymbol{Q}_j$ and $\boldsymbol{R}_j$ are assumed to be symmetric positive semi-definite and symmetric positive definite, respectively.

To this end, we use the Hamiltonian as below (Lewis et al., 2012):

$$\mathcal{H}_k = \frac{1}{2} \Big(\boldsymbol{x}_k^\top \boldsymbol{Q}_k \boldsymbol{x}_k + \boldsymbol{u}_k^\top \boldsymbol{R}_k \boldsymbol{u}_k \Big) + \boldsymbol{\lambda}_{k+1}^\top \Big(\boldsymbol{A}_k \boldsymbol{x}_k + \boldsymbol{B}_k \boldsymbol{u}_k \Big) \tag{2.3}$$

where $\boldsymbol{\lambda}_k \in \mathbb{R}^n$ is the Lagrange multiplier.

Then, by using the optimality conditions (Bryson, Jr. and Ho, 1975), the controller can be designed as

$$\begin{aligned} \boldsymbol{u}_k &= -\boldsymbol{R}_k^{-1}\boldsymbol{B}_k^\top \boldsymbol{\lambda}_{k+1} \\ &= -\big(\boldsymbol{B}_k^\top \boldsymbol{P}_{k+1}\boldsymbol{B}_k + \boldsymbol{P}_k\big)^{-1}\boldsymbol{B}_k^\top \boldsymbol{P}_{k+1}\boldsymbol{A}_k\boldsymbol{x}_k, \ \ \forall k \in \mathbb{Z}_{0:N-1} \end{aligned} \tag{2.4}$$

where $\boldsymbol{P}_k$ is the unique solution of the discrete-time Riccati equation at time k:

$$\boldsymbol{P}_k = \boldsymbol{Q}_k + \boldsymbol{A}_k^\top \Big(\boldsymbol{P}_{k+1} - \boldsymbol{P}_{k+1}\boldsymbol{B}_k\big(\boldsymbol{B}_k^\top \boldsymbol{P}_{k+1}\boldsymbol{B}_k + \boldsymbol{R}_k\big)^{-1}\boldsymbol{B}_k^\top \boldsymbol{P}_{k+1}\Big)\boldsymbol{A}_k. \tag{2.5}$$

The detailed derivation of the D-LQR is omitted here since it is straightforward and can be found in (Lewis et al., 2012; Kirk, 1970).

Remark 1 If the control horizon is considered $N \to \infty$, then (2.5) can be rewritten under the assumption that the state of (2.1) has a steady-state value:

$$\boldsymbol{P} = \boldsymbol{A}_k^\top \Big(\boldsymbol{P} - \boldsymbol{P}\boldsymbol{B}_k\big(\boldsymbol{B}_k^\top \boldsymbol{P}\boldsymbol{B}_k + \boldsymbol{R}_k\big)^{-1}\boldsymbol{B}_k^\top \boldsymbol{P}\Big)\boldsymbol{A}_k + \boldsymbol{Q}_k \tag{2.6}$$

which is called the discrete-time algebraic Riccati equation (DARE). It is widely used in D-LQR problems.

2.2 Model Predictive Control

MPC is a main tool in the CD-SDRE technique to handle constraints on states and control inputs. We briefly review the MPC in this section. More detailed information of the MPC can be found in (Mayne et al., 2000; Rawlings and Mayne, 2009; Magni et al., 2009; Grüne and Pannek, 2011).

Consider a discrete-time nonlinear system described by the nonlinear difference equation:

$$\boldsymbol{x}_{k+1} = \boldsymbol{f}(\boldsymbol{x}_k, \boldsymbol{u}_k), \quad \boldsymbol{x}(0) = \boldsymbol{x}_0 \quad \forall k \in \mathbb{Z}_{\geq 0} \tag{2.7}$$

where $\boldsymbol{f} : X \times U \mapsto X$ maps the current state $\boldsymbol{x}_k \in X \subseteq \mathbb{R}^n$ and the current control input $\boldsymbol{u}_k \in U \subseteq \mathbb{R}^m$ into the successor state $\boldsymbol{x}_{k+1} \in X \subseteq \mathbb{R}^n$.

It is assumed that the system (2.7) is subject to hard constraints on the state and the control input:

$$\boldsymbol{u}_k \in \mathbb{U}, \;\; \boldsymbol{x}_k \in \mathbb{X} \quad \forall k \in \mathbb{Z}_{\geq 0} \tag{2.8}$$

where $\mathbb{X} \subseteq X$, $\mathbb{U} \subseteq U$, which are assumed to be closed and convex, are constraint sets of the state and the control inputs, respectively.

Then, the purpose of MPC is to find a sequence of control inputs $\boldsymbol{\mu}(\cdot) \in \mathbb{U}$ such that the following performance index is minimized:

$$\begin{aligned} J_N(\boldsymbol{x}_0, \boldsymbol{\mu}(\cdot)) := & \sum_{j=k}^{k+N-1} \ell(\boldsymbol{x}_j, \boldsymbol{u}_j) + J_f(\boldsymbol{x}_{k+N}) \\ \text{s.t.} \;\; & \boldsymbol{x}_k \in \mathbb{X}, \;\; \boldsymbol{u}_k \in \mathbb{U} \;\; \text{and} \;\; (2.7) \;\; \forall k \in \mathbb{Z}_{\geq 0} \end{aligned} \tag{2.9}$$

where N is a finite horizon and $\ell(\cdot)$ is assumed to be continuous with $\ell(\mathbf{0}, \mathbf{0}) = 0$.

Therefore, by solving the optimal control problem, the optimal state and control sequence as functions of the initial state $\boldsymbol{x}_0$ and time k can be obtained; $\boldsymbol{\mu} = [\boldsymbol{u}^\top(0) \;\; \boldsymbol{u}^\top(1) \;\; \cdots \;\; \boldsymbol{u}^\top(N-1)]^\top \in \mathbb{R}^{Nm}$ is the optimization vector. In MPC, the first element in the optimal control action $\boldsymbol{\mu}(\cdot)$ is chosen for the control input at time k, i.e., $\boldsymbol{u}_k = \boldsymbol{\mu}(0)$ becomes the control input signal at time k, and the sequence is repeated for the next time step.

Remark 2 The constraints in (2.8) at time k can be expressed in the following matrix form

$$\boldsymbol{M}\boldsymbol{\mu} \leq \boldsymbol{W} + \boldsymbol{S}\boldsymbol{x}_k. \tag{2.10}$$

Then, the minimization of (2.9) becomes the convex quadratic programming (QP). The QP is widely used in MPC.

2.3 Input-to-State Stability

We introduce the concept of input-to-state stability (ISS) (Sontag, 1989; Jiang and Wang, 2001) which is used throughout the thesis.

Definition 1 *(Jiang and Wang, 2001) The discrete-time nonlinear system*

$$\boldsymbol{x}_{k+1} = \boldsymbol{f}(\boldsymbol{x}_k, \boldsymbol{u}_k) \tag{2.11}$$

is said to be input-to-state stable (ISS) if there exist $\beta \in \mathcal{KL}$, $\gamma \in \mathcal{K}$, and constant $\eta_1,\ \eta_2 \in \mathbb{R}_{\geq 0}$ such that

$$|\boldsymbol{x}_k| \leq \beta(|\boldsymbol{x}_0|, k) + \gamma(|\boldsymbol{u}|_{\mathcal{L}_\infty}) \quad \forall k \in \mathbb{Z}_{\geq 0} \tag{2.12}$$

for all $\boldsymbol{x}_0 \in \mathbb{X}$ and $\boldsymbol{u}_k \in \mathbb{U}$ satisfying that $|\boldsymbol{x}_0| < \eta_1$ and $|\boldsymbol{u}|_{\mathcal{L}_\infty} < \eta_2$.

Definition 2 *(Jiang and Wang, 2001) A continuous function $V : \mathbb{R}^n \to \mathbb{R}_{\geq 0}$ is said to be an ISS-Lyapunov function for (2.11) if the following hold:*

1. *There exist $\alpha_1,\ \alpha_2 \in \mathcal{K}_\infty$ such that*

$$\alpha_1(|\boldsymbol{\xi}|) \leq V(\boldsymbol{\xi}) \leq \alpha_2(|\boldsymbol{\xi}|) \quad \forall \boldsymbol{\xi} \in \mathbb{R}^n. \tag{2.13}$$

2. *There exist $\alpha_3 \in \mathcal{K}_\infty$ and $\sigma \in \mathcal{K}$ such that*

$$V(f(\boldsymbol{\xi}, \boldsymbol{\mu})) - V(\boldsymbol{\xi}) \leq -\alpha_3(|\boldsymbol{\xi}|) + \sigma(|\boldsymbol{\mu}|) \tag{2.14}$$

for all $\boldsymbol{\xi} \in \mathbb{R}^n$ and $\boldsymbol{\mu} \in \mathbb{R}^m$.

Chapter 3

Exponential Stability Region Estimates for the Continuous-Time SDRE

As a preliminary of the thesis, we investigate the exponential stability of the continuous-time state-dependent Riccati equation-based control. Some notable prior work has shown local asymptotic stability of SDRE by using numerical and analytical methods. In this chapter, we introduce a new strategy, based on contraction analysis and incremental stability analysis, to estimate the exponential stability region for the SDRE controlled system. Examples demonstrate the superiority of the proposed method.

The organization of this chapter is as follows: preliminaries of the continuous-time SDRE control, a brief introduction to contraction analysis are presented in Section 3.1. The stability proof of the SDRE controlled systems is described in Section 3.2. In Section 3.3, two numerical examples are presented to compare the results with other numerical methods. Finally, concluding remarks are stated in Section 3.4.

3.1 Preliminaries

3.1.1 State-Dependent Riccati Equation Technique

Consider a deterministic, infinite-horizon nonlinear optimal regulation problem, where the system is full-state observable, autonomous, nonlinear in the state, and affine in the input, represented in the form (Çimen, 2008)

$$\dot{\boldsymbol{x}}(t) = \boldsymbol{f}(\boldsymbol{x}) + \boldsymbol{B}(\boldsymbol{x})\boldsymbol{u}(t), \quad \boldsymbol{x}(0) = \boldsymbol{x}_0 \tag{3.1}$$

where $\boldsymbol{x} \in \mathbb{R}^n$ is the state vector and $\boldsymbol{u} \in \mathbb{R}^m$ is the input vector.

The SDRE technique is a nonlinear control design method for the direct construction of nonlinear feedback controllers. Through the state-dependent coefficient (SDC) factorization, system designers can represent the nonlinear equations of motion as linear structures with state-dependent coefficients. Then, the LQR technique can be applied to this state-dependent state-space equation. Thus, the following procedure

is similar to the LQR method, except that all matrices may depend on the states. Based on this concept, the state-space equation for the nonlinear system described in (3.1) can be expressed as a linear-like state-space equation using the direct SDC factorization as:

$$\dot{\boldsymbol{x}} = \boldsymbol{A}(\boldsymbol{x})\boldsymbol{x} + \boldsymbol{B}(\boldsymbol{x})\boldsymbol{u} \tag{3.2}$$

where the factorization for $\boldsymbol{f}(\boldsymbol{x}) = \boldsymbol{A}(\boldsymbol{x})\boldsymbol{x}$ is possible if and only if $\boldsymbol{f}(\boldsymbol{0}) = \boldsymbol{0}$ and $\boldsymbol{f}(\boldsymbol{x})$ is continuously differentiable. Note that $\boldsymbol{A}(\boldsymbol{x})$ is not a unique matrix because there could be many possible choices in the direct SDC factorization (Cloutier, 1997). For this system, the SDRE technique finds an input $\boldsymbol{u}(t)$ that *approximately* minimizes the following performance index:

$$J = \frac{1}{2}\int_0^\infty \left(\boldsymbol{x}^\top \boldsymbol{Q}(\boldsymbol{x})\boldsymbol{x} + \boldsymbol{u}^\top \boldsymbol{R}(\boldsymbol{x})\boldsymbol{u}\right) \mathrm{d}t \tag{3.3}$$

where $\boldsymbol{Q}(\boldsymbol{x})$ is a symmetric positive semi-definite matrix with quadratic form and $\boldsymbol{R}(\boldsymbol{x})$ is a symmetric positive definite matrix with quadratic form for all $\boldsymbol{x} \in \mathbb{R}^n$. Also, it is assumed that $\boldsymbol{f}(\boldsymbol{0}) = \boldsymbol{0}$ and $\boldsymbol{B}(\boldsymbol{x}) \neq \boldsymbol{0}$. It should be noted that $\boldsymbol{Q}(\boldsymbol{x})$ and $\boldsymbol{R}(\boldsymbol{x})$ are not only allowed to be constant, but can also be varied as functions of states. As these state-dependent matrices are applied to the algebraic Riccati equation (ARE), the following state-dependent Riccati equation is obtained (Cloutier, 1997):

$$\begin{aligned} &\boldsymbol{P}(\boldsymbol{x})\boldsymbol{A}(\boldsymbol{x}) + \boldsymbol{A}^\top(\boldsymbol{x})\boldsymbol{P}(\boldsymbol{x}) + \boldsymbol{Q}(\boldsymbol{x}) \\ &\qquad - \boldsymbol{P}(\boldsymbol{x})\boldsymbol{B}(\boldsymbol{x})\boldsymbol{R}^{-1}(\boldsymbol{x})\boldsymbol{B}^\top(\boldsymbol{x})\boldsymbol{P}(\boldsymbol{x}) = \boldsymbol{0} \end{aligned} \tag{3.4}$$

The optimal feedback control gain matrix, which is a state-dependent $m \times n$ variable gain matrix, and the $m \times 1$ input control can be calculated in the same way as the LQR technique except for the state dependence:

$$\begin{aligned} \boldsymbol{K}(\boldsymbol{x}) &= \boldsymbol{R}^{-1}(\boldsymbol{x})\boldsymbol{B}^\top(\boldsymbol{x})\boldsymbol{P}(\boldsymbol{x}) \\ \boldsymbol{u} &= -\boldsymbol{K}(\boldsymbol{x})\boldsymbol{x} \end{aligned} \tag{3.5}$$

where $\boldsymbol{P}(\boldsymbol{x}) \in \mathbb{R}^{n\times n}$ is the unique positive-definite solution of the SDRE (3.4).

As with the LQR technique, the SDRE technique also constructs a closed-loop system with direct state

feedback controller $\boldsymbol{u}(t)$ as a regulator. However, the feedback gain, $\boldsymbol{K}(\boldsymbol{x})$, of the SDRE technique depends on the states. Hence, state-dependent control inputs are applied to the plant. Because the state-space equation (3.2) should be computed for every state and control input, (3.4) and (3.5) should be calculated at each time step. Because the SDRE technique can be considered as the LQR method for each time step, the matrix $\boldsymbol{P}(\boldsymbol{x})$ in (3.4) becomes a unique solution of the algebraic Riccati equation at the particular state, $\boldsymbol{x}(t)$, which means it has constant values at each given state. Therefore, solving the ARE in (3.4) for each $\boldsymbol{x}$ is feasible and can be done either on-line or off-line (Erdem, 2001).

Controllability is critical because it is a sufficient condition for the existence of a solution to the SDRE. In general, a linear time-invariant system is controllable if and only if the $n \times nm$ controllability matrix $\boldsymbol{W}_{\text{ctrl}}$ has full rank (i.e., $rank(\boldsymbol{W}_{\text{ctrl}}) = n$). The controllability of the SDRE can be determined by pointwise controllability ($\boldsymbol{W}_{\text{ctrl}}(\boldsymbol{x})$) of the SDC factorization

$$\boldsymbol{W}_{\text{ctrl}}(\boldsymbol{x}) = \left[\boldsymbol{B}(\boldsymbol{x}) \;\; \boldsymbol{A}(\boldsymbol{x})\boldsymbol{B}(\boldsymbol{x}) \;\; \boldsymbol{A}^2(\boldsymbol{x})\boldsymbol{B}(\boldsymbol{x}) \;\cdots\; \boldsymbol{A}^{n-1}(\boldsymbol{x})\boldsymbol{B}(\boldsymbol{x})\right]. \tag{3.6}$$

Thus, the selection of ($\boldsymbol{A}(\boldsymbol{x})$ and $\boldsymbol{B}(\boldsymbol{x})$) can affect the controllability of the system.

3.1.2 Contraction Theory

The new method proposed in this chapter is motivated by contraction analysis, a relatively new nonlinear stability tool for exponential stability for the nonlinear systems. It is a generalized version of Krasovskii's theorem (Khalil, 2002), which provides a sufficient, asymptotic convergence result. Readers are referred to (Lohmiller and Slotine, 1998) for more detailed information about contraction analysis.

Consider a general deterministic system of the form

$$\dot{\boldsymbol{x}}(t) = \boldsymbol{f}(\boldsymbol{x}, \boldsymbol{u}(\boldsymbol{x}, t), t) \tag{3.7}$$

where $\boldsymbol{f} : \mathbb{R}^n \times \mathbb{R}^m \times \mathbb{R} \longmapsto \mathbb{R}^n$ is a nonlinear vector function and $\boldsymbol{x} \in \mathbb{R}^n$ is the state vector. This nonlinear system can be thought of as an n-dimensional fluid flow, where $\dot{\boldsymbol{x}}$ is the n-dimensional "velocity" vector at the n-dimensional position $\boldsymbol{x}$ and time t. Assuming that $\boldsymbol{f}(\boldsymbol{x}, \boldsymbol{u}(\boldsymbol{x}, t), t)$ is continuously differentiable, the

exact differential relation can be obtained by (3.7):

$$\delta\dot{\boldsymbol{x}}(t) = \frac{\partial \boldsymbol{f}}{\partial \boldsymbol{x}}(\boldsymbol{x}, \boldsymbol{u}(\boldsymbol{x}, t), t)\delta\boldsymbol{x} \tag{3.8}$$

where $\delta\boldsymbol{x}$ is a virtual displacement of the systems. Note that $\delta\boldsymbol{x}$ defines a linear tangent differential form, and $\delta\boldsymbol{x}^\top\delta\boldsymbol{x}$ the associated quadratic tangent form, both of which are differentiable with respect to time t.

Consider two neighboring trajectories in the flow field (3.7), and the virtual displacement $\delta\boldsymbol{x}$ between them. The squared distance (quadratic virtual length) between these two trajectories can be defined as $\delta\boldsymbol{x}^\top\delta\boldsymbol{x}$, leading from (3.8) to the rate of change

$$\frac{\mathrm{d}}{\mathrm{d}t}(\delta\boldsymbol{x}^\top\delta\boldsymbol{x}) = 2\delta\boldsymbol{x}^\top\delta\dot{\boldsymbol{x}} = 2\delta\boldsymbol{x}^\top\frac{\partial \boldsymbol{f}}{\partial \boldsymbol{x}}\delta\boldsymbol{x}. \tag{3.9}$$

Denoting by $\lambda_{\max}(\boldsymbol{x}, t)$ the largest eigenvalue of the symmetric part of the Jacobian $\frac{\partial \boldsymbol{f}}{\partial \boldsymbol{x}}$, we have

$$\frac{\mathrm{d}}{\mathrm{d}t}(\delta\boldsymbol{x}^\top\delta\boldsymbol{x}) \leq 2\lambda_{\max}\delta\boldsymbol{x}^\top\delta\boldsymbol{x} \tag{3.10}$$

and hence,

$$\|\delta\boldsymbol{x}\| \leq \|\delta\boldsymbol{x}_0\|e^{\int_0^t \lambda_{\max}(\boldsymbol{x},t)\mathrm{d}t} \tag{3.11}$$

Assuming that $\lambda_{\max}$ is uniformly strictly negative, then from (3.11) any infinitesimal length $\|\delta\boldsymbol{x}\|$ converges exponentially to zero.

3.1.3 Generalized Contraction Analysis

The line vector δx defined in (3.8) can also be expressed using the differential coordinate transformation (Lohmiller and Slotine, 1998), and leads to a generalization of the previous definition of squared length as

$$\begin{aligned} \delta\boldsymbol{z} &= \boldsymbol{\Theta}(\boldsymbol{x}, t)\delta\boldsymbol{x}, \\ \delta\boldsymbol{z}^\top\delta\boldsymbol{z} &= \delta\boldsymbol{x}^\top\boldsymbol{M}\delta\boldsymbol{x} \end{aligned} \tag{3.12}$$

where $\boldsymbol{\Theta}(\boldsymbol{x}, t)$ and $\boldsymbol{M} = \boldsymbol{\Theta}^\top\boldsymbol{\Theta}$ denote a square matrix and a symmetric and continuously differentiable metric, respectively. Therefore, exponential convergence of $\delta\boldsymbol{z}$ to $\mathbf{0}$ implies exponential convergence of $\delta\boldsymbol{x}$ to $\mathbf{0}$.

The time derivative of $\delta \boldsymbol{z} = \boldsymbol{\Theta} \delta \boldsymbol{x}$ can be computed as

$$\begin{aligned} \frac{\mathrm{d}}{\mathrm{d}t} \delta \boldsymbol{z} &= \dot{\boldsymbol{\Theta}} \delta \boldsymbol{x} + \boldsymbol{\Theta} \delta \dot{\boldsymbol{x}} \\ &= \left(\dot{\boldsymbol{\Theta}} + \boldsymbol{\Theta} \frac{\partial \boldsymbol{f}}{\partial \boldsymbol{x}} \right) \boldsymbol{\Theta}^{-1} \delta \boldsymbol{z} \triangleq \boldsymbol{H} \delta \boldsymbol{z}. \end{aligned} \tag{3.13}$$

The rate of change of squared length can be written

$$\frac{\mathrm{d}}{\mathrm{d}t} (\delta \boldsymbol{z}^\top \delta \boldsymbol{z}) = 2 \delta \boldsymbol{z}^\top \boldsymbol{H} \delta \boldsymbol{z}. \tag{3.14}$$

Therefore, if there exists a $\gamma > 0$, such that the symmetric part of $\boldsymbol{H}$ is negative definite, that is,

$$\frac{\boldsymbol{H} + \boldsymbol{H}^\top}{2} < -\gamma \boldsymbol{I}, \tag{3.15}$$

then the system is exponentially stable. It is helpful to recall that $\boldsymbol{H} = \boldsymbol{H}(\boldsymbol{x}, t)$.

By using the characteristics of contraction analysis, we will estimate the exponential stability region for the SDRE controlled systems in the next section.

3.2 Exponential Stability Analysis of the SDRE Feedback Systems

Given the nonlinear equation (3.1) under the assumption of an autonomous nonlinear equation, the equation can be rewritten in the form (3.2) by applying the SDC factorization. Moreover, by applying the control law (3.5) to the SDC factorization, the closed-loop form can be obtained as

$$\begin{aligned} \dot{\boldsymbol{x}} &= \big(\boldsymbol{A}(\boldsymbol{x}) - \boldsymbol{B}(\boldsymbol{x}) \boldsymbol{K}(\boldsymbol{x}) \big) \boldsymbol{x} \\ &= \big(\boldsymbol{A}(\boldsymbol{x}) - \boldsymbol{B}(\boldsymbol{x}) \boldsymbol{R}^{-1}(\boldsymbol{x}) \boldsymbol{B}^\top(\boldsymbol{x}) \boldsymbol{P}(\boldsymbol{x}) \big) \boldsymbol{x} \\ &=: \boldsymbol{A}_{\mathrm{cl}}(\boldsymbol{x}) \boldsymbol{x}. \end{aligned} \tag{3.16}$$

Furthermore, for simplicity, (3.16) can be written as $\dot{\boldsymbol{x}} = \boldsymbol{\phi}(\boldsymbol{x})$. Note that $\boldsymbol{\phi}(\boldsymbol{x}) \in \mathcal{G}$ where $\mathcal{G} = Co\{\boldsymbol{\phi}_1, \ \boldsymbol{\phi}_2, \ \cdots, \ \boldsymbol{\phi}_k\}$ is polytopic LDIs (Boyd et al., 1994). Here, $\boldsymbol{\phi}_i$ is obtained by an associated $\boldsymbol{x}_i$. Then for any $\boldsymbol{x}$ in its ROA $\mathcal{X}$, the following system describes the dynamics of the virtual displacement $\delta \boldsymbol{x}$

of the system (3.16),

$$\frac{\mathrm{d}}{\mathrm{d}t}(\delta\boldsymbol{x}^\top\delta\boldsymbol{x}) = 2\delta\boldsymbol{x}^\top\delta\dot{\boldsymbol{x}} = 2\delta\boldsymbol{x}^\top\boldsymbol{F}\delta\boldsymbol{x} \tag{3.17}$$

where $\boldsymbol{F} := \frac{\partial\boldsymbol{\phi}}{\partial\boldsymbol{x}} = \boldsymbol{A}_{\mathrm{cl}}(\boldsymbol{x}) + \frac{\partial}{\partial\boldsymbol{x}}\boldsymbol{A}_{\mathrm{cl}}(\boldsymbol{x})\boldsymbol{x}$ denotes a Jacobian of the system (3.16).

Now we define a new term below:

Definition 3 *The system (3.16) is said to be locally incrementally exponentially stable (IES) with an ROA $\mathcal{X} \subset \mathbb{R}^n$ if the system (3.17) is locally exponentially stable when initial condition of any two neighboring trajectories, say $\boldsymbol{x}_l(t_0)$ and $\boldsymbol{x}_m(t_0)$, are in $\mathcal{X}$ such that $\delta\boldsymbol{x}(t_0) = \boldsymbol{x}_l(t_0) - \boldsymbol{x}_m(t_0)$.*

By the definition, if the system (3.16) is locally IES with $\mathcal{X}$, then

$$\frac{\mathrm{d}}{\mathrm{d}t}(\delta\boldsymbol{x}^\top\delta\boldsymbol{x}) \leq -2\lambda\delta\boldsymbol{x}^\top\delta\boldsymbol{x} \quad \text{and} \quad \|\delta\boldsymbol{x}\| \leq \|\delta\boldsymbol{x}_0\|e^{-\int_0^t \lambda(\boldsymbol{x},t)\mathrm{d}t} \tag{3.18}$$

hold for any two neighboring trajectories $\boldsymbol{x}_l(\cdot)$ and $\boldsymbol{x}_m(\cdot)$ with $\boldsymbol{x}_l(t_0)$ and $\boldsymbol{x}_m(t_0)$ both in $\mathcal{X}$. Here, $\lambda(\boldsymbol{x},t) > 0$ is the smallest eigenvalue of the symmetric part of the Jacobian $\boldsymbol{F}$ in (3.17). Note that (3.18) clearly indicates that $\delta\boldsymbol{x}$ will converge to zero exponentially with the convergence rate λ.

The below theorem shows a condition of the locally IES ROA of nonlinear systems controlled by the SDRE technique.

Theorem 4 *For the system (3.16), suppose that there exist $\boldsymbol{M} = \boldsymbol{M}^\top > \boldsymbol{0}$ and $\alpha > 0$, such that the following matrix inequality holds*

$$\boldsymbol{M}\boldsymbol{F}_i + \boldsymbol{F}_i^\top\boldsymbol{M} + 2\alpha\boldsymbol{M} \leq \boldsymbol{0}. \quad \forall i = 1, 2, \cdots, k \tag{3.19}$$

where $\boldsymbol{F}_i := \frac{\partial\boldsymbol{\phi}_i}{\partial\boldsymbol{x}}$ and $\boldsymbol{F}_i \in \mathcal{F} := Co\{\boldsymbol{F}_1,\ \boldsymbol{F}_2,\ \cdots,\ \boldsymbol{F}_k\}$, where $\mathcal{F}$ is a polytope. Note that $\boldsymbol{F} \in \mathcal{F}$. Then the system (3.16) is locally IES with an ROA $\mathcal{X}$ if $\mathcal{X} = \mathcal{E}(\boldsymbol{M}, \boldsymbol{\rho}, \boldsymbol{r})$ is an invariant set for the system (3.16), where $\mathcal{E}(\boldsymbol{M}, \boldsymbol{\rho}, \boldsymbol{r}) := \{\boldsymbol{x} : (\boldsymbol{x} - \boldsymbol{\rho})^\top\boldsymbol{M}(\boldsymbol{x} - \boldsymbol{\rho}) \leq \boldsymbol{r}^2\}$.

Proof Since $\mathcal{X}$ is an invariant set for the system (3.16), any trajectories of this system with its initial state in $\mathcal{X}$ stays in $\mathcal{X}$ for all times. Consider the system described by (3.16) with $\boldsymbol{x}_l(t_0)$ and $\boldsymbol{x}_m(t_0)$ both in $\mathcal{X}$, which implies that both $\boldsymbol{x}_l(t)$ and $\boldsymbol{x}_m(t)$ are in $\mathcal{X}$ for all $t \geq t_0$. Then by pre and post-multiplying (3.19)

by $\delta \boldsymbol{x}^\top$ and $\delta \boldsymbol{x}$, the following holds for all $t \geq t_0$

$$\delta \boldsymbol{x}^\top (\boldsymbol{M}\boldsymbol{F}_i + \boldsymbol{F}_i^\top \boldsymbol{M} + 2\alpha \boldsymbol{M}) \delta \boldsymbol{x} \leq \boldsymbol{0} \qquad \forall i = 1, 2, \cdots, k. \tag{3.20}$$

Consider the virtual displacement $\delta \boldsymbol{x} := \boldsymbol{x}_l(\cdot) - \boldsymbol{x}_m(\cdot)$, where $\boldsymbol{x}_l,\ \boldsymbol{x}_m \in \mathcal{X}$ and corresponding quadratic virtual length $V = \delta \boldsymbol{x}^\top \boldsymbol{M} \delta \boldsymbol{x}$, where $\boldsymbol{M} = \boldsymbol{M}^\top > \boldsymbol{0}$ by the assumption. By differentiating the virtual length, the rate of the quadratic virtual length is derived as:

$$\begin{aligned} \dot{V} &= \delta \dot{\boldsymbol{x}}^\top \boldsymbol{M} \delta \boldsymbol{x} + \delta \boldsymbol{x}^\top \boldsymbol{M} \delta \dot{\boldsymbol{x}} \\ &= \delta \boldsymbol{x}^\top (\boldsymbol{F}_i^\top \boldsymbol{M} + \boldsymbol{M}\boldsymbol{F}_i) \delta \boldsymbol{x} \qquad \forall i = 1, 2, \cdots, k. \end{aligned} \tag{3.21}$$

Therefore, (3.20) implies the virtual length analysis satisfies the following condition:

$$\dot{V} \leq -2\alpha V \quad \forall t \geq t_0,$$

which implies that the contracting system (3.17) is locally exponentially stable. □

Remark 3 By Theorem 4, the stability condition of the SDRE feedback systems is interpreted as a stability condition of polytopic LDIs.

Remark 4 If we can establish the invariance of a set of $\mathcal{X} \subseteq X \subseteq \mathbb{R}^n$, then Theorem 4 suggests that proving the local stability of the system (3.16), with an ROA $\mathcal{X}$, only requires finding $\boldsymbol{M} = \boldsymbol{M}^\top > \boldsymbol{0}$ and satisfying LMIs (3.19).

The next theorem shows the ROA $\mathcal{X}$ obtained in the previous theorem is an invariant set for the system.

Theorem 5 *Consider the system described by (3.16) for some $X \subseteq \mathbb{R}^n$. Suppose that there exist $M = M^T > 0$ and $\alpha > 0$, such that the LMIs (3.19) hold. Then the system is locally IES with an ROA $\mathcal{X} = \mathcal{E}(M, \rho, r) \subseteq X$ if $\|M^{1/2}\rho\| \leq \alpha r \quad \forall t \geq t_0$.*

Proof To prove that $\mathcal{E}(M, \rho, r)$ is an invariant set for the system (3.16), consider the LMIs below:

$$MF_i + F_i^T M + 2\alpha M \leq 0 \quad \forall i = 1, 2, \cdots, k.$$

Post and pre-multiplying the above LMI by δx and its transpose, the inequality can be obtained

$$\delta x^T (MF_i + F_i^T M + 2\alpha M)\delta x \leq 0 \quad \forall i = 1, 2, \cdots, k. \tag{3.22}$$

If there exists $\rho \in \mathbb{R}^n$ such that $\delta x^T M \rho \geq 0$, then (3.22) can be rewritten with the definition of $V := \delta x^T M \delta x$ as

$$\dot{V} \leq -2\alpha V + 2\delta x^T M \rho. \tag{3.23}$$

Now, let $s := \|M^{1/2}\delta x\|$ and $\sigma := \|M^{1/2}\rho\|$. Note that $V = s^2$ and $\sigma \leq \alpha r$. By substituting s and σ into (3.23), then

$$\dot{V} \leq -2\alpha s^2 + 2s\sigma \leq -2\alpha s\,(s - r)\,. \tag{3.24}$$

Since $\alpha > 0$, the above inequality implies that $\dot{V} < 0 \ \ \forall s > r$. This implies that $V \leq r^2$ is an invariant ellipsoid for the system of δx. This indicates that $\mathcal{E}(M, \rho, r)$ is an invariant set for the system (3.16). □

Remark 5 If an ROA $\mathcal{X} \in X$ for a certain system is satisfied with Theorems 4 and 5, the ROA is an invariant set.

We proved the exponential stability condition of SDRE feedback systems and shows how to estimate the ROA. In the next section, the stability analysis will be evaluated with some numerical examples.

3.3 Numerical Validation

In this section, the exponentially stability analyses of two nonlinear systems controlled by the SDRE are examined. The first example is a simple second order nonlinear system (Shamma and Cloutier, 2003) and the other is attitude control of the aircraft (Etkin, 1972). Please note that an estimation method in (Bracci et al., 2006) is shown to be more accurate than prior studies. Hence, the simulation results of the proposed method in this chapter are compared with those by Bracci et al. (2006).

3.3.1 Case Study I: Second Order Nonlinear System

The first example is for a simple second order nonlinear feedback control system (Shamma and Cloutier, 2003). Consider the second-order nonlinear system:

$$\dot{\boldsymbol{x}} = \boldsymbol{A}(\boldsymbol{x})\boldsymbol{x} + \boldsymbol{B}\boldsymbol{u} = \begin{bmatrix} x_1 & 1 \\ 0 & 0 \end{bmatrix} \boldsymbol{x} + \begin{bmatrix} 0 \\ 1 \end{bmatrix} \boldsymbol{u}. \tag{3.25}$$

For simplicity, let us assume that the weighting matrices $\boldsymbol{Q}(\boldsymbol{x})$ and $\boldsymbol{R}(\boldsymbol{x})$, which are used in the algebraic Riccati equation as well as in the Lypunov equation for the method by Bracci et al. (2006), are constant such that $\boldsymbol{Q} = diag(100,\ 100)$ and $\boldsymbol{R} = 1$, respectively.

For estimation of the exponentially stable ROA $\mathcal{X} \subset \mathbb{R}^2$, the Jacobian of the nonlinear system (3.25), used in the virtual length analysis, can be obtained by (3.17). Now, let us define a convex set $X \in \mathbb{R}^2$. Then the exponentially stable region can be estimated. That is, if there exist $\boldsymbol{M} = \boldsymbol{M}^\top > \boldsymbol{0}$, $\alpha > 0$, such that (3.19) holds, then (3.25) is exponentially stable with an ROA $\mathcal{X} \subseteq X \subset \mathbb{R}^2$.

Figure 3.1 shows simulation results of the ROAs by the method by Bracci et al. (2006) and the proposed method. The circle in Figure 3.1 denotes the ROA estimated by Bracci et al. (2006). The dotted area shows the subset of the exponentially stable ROA for the system, obtained by the proposed method. Apparently, the exponentially stable region is global in $x_i \in [-3,\ 3],\ i = 1, 2$. Several state trajectories with different initial conditions are shown in Figure 3.1 (solid curves). Here, one can easily notice that even some state trajectories, which start from unstable region by the method by Bracci et al. (2006), still converge to the equilibrium point $\boldsymbol{x}_e = \boldsymbol{0}$. By the state trajectories, we can see the ROA estimated by the proposed method is more accurate.

The next simulation shows a more complicated example: an attitude control system of an aircraft.

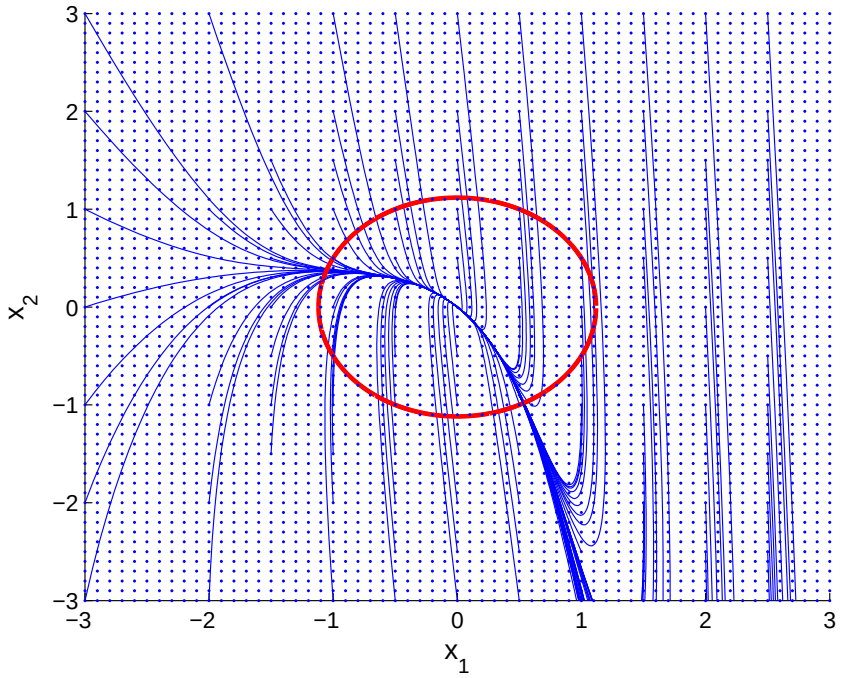

Figure 3.1: Comparison of the stability region estimates for Example 1. The circle denotes an asymptotic ROA estimated by Bracci et al. (2006). The dotted area (whole region) indicates a subset of the exponentially stable ROA estimated by the proposed method. State trajectories (solid curves) with several different initial conditions validate the ROA by the proposed method is more accurate.

3.3.2 Case Study II: Aircraft Attitude Control

In the second simulation, an aircraft attitude control system (Etkin, 1972) is examined. The rotational dynamics of an aircraft attitude motion is given as (Etkin, 1972; Bracci et al., 2006):

$$\begin{aligned} \dot{p} &= c_1 qr + c_2 pq + c_3 L + c_4 N \\ \dot{q} &= c_5 rp + c_6 (r^2 - p^2) + c_7 M \\ \dot{r} &= c_8 pq - c_2 qr + c_4 L + c_9 N \end{aligned} \tag{3.26}$$

where $\boldsymbol{x} = [p \;\; q \;\; r]^\top$ and $\boldsymbol{u} = [L \;\; M \;\; N]^\top$ are the states and the control inputs, respectively. Coefficients $c_1 - c_9$ are determined by moments of inertia of the aircraft. The values are set to $c_1 = 0.1806,\ c_2 = -0.0673,\ c_3 = 0.6415,\ c_4 = -0.0527,\ c_5 = 0.7420,\ c_6 = -0.0786,\ c_7 = 0.1332,\ c_8 = -0.8166$, and $c_9 = 0.1436$, respectively.

The dynamics can be rewritten by using the SDC factorization as

$$\dot{\boldsymbol{x}} = \boldsymbol{A}(\boldsymbol{x})\boldsymbol{x} + \boldsymbol{B}\boldsymbol{u} \tag{3.27}$$

where $\boldsymbol{A}(\boldsymbol{x}) = \begin{bmatrix} c_2 q & c_1 r & 0 \\ -c_6 p & 0 & c_5 p + c_6 r \\ 0 & c_8 p & -c_2 q \end{bmatrix}$ and $\boldsymbol{B} = \begin{bmatrix} c_3 & 0 & c_4 \\ 0 & c_7 & 0 \\ c_4 & 0 & c_9 \end{bmatrix}$.
The values of the weighting matrices $\boldsymbol{Q}$ and $\boldsymbol{R}$ were chosen from Bracci et al. (2006). The asymptotic ROA estimated by Bracci et al. (2006) and exponentially stable region can be estimated by using the similar ways to the previous example.

Figures 3.2–3.4 shows the simulation results of the stability analysis for (3.26). The analysis was performed in $x_i \in [-4,\ \ 4],\ i = 1, 2, 3$. An ellipsoid in Figure 3.2 denotes the ROA by Bracci et al. (2006). The radius of the ellipsoid is $r = 1.7205$. However, the proposed method shows the whole area as a subset of the exponentially stable ROA (the cube in Figure 3.2). For the evaluation of the results, Figure 3.3 shows several state trajectories with different initial conditions starting from $x_i \in [-4,\ 4],\ i = 1, 2, 3$). This figure shows all state trajectories converge to zero state ($\boldsymbol{x}_e = \boldsymbol{0}$) regardless of the initial condition, $\boldsymbol{x}_0 \in \mathcal{X}$. The complicated state trajectories in the figure can be explained by Figure 3.4, the state trajectories of $p,\ q$, and r with respect to time with an initial condition $[-4 \;\; -4 \;\; -4]^\top$), which shows the exponential convergence,

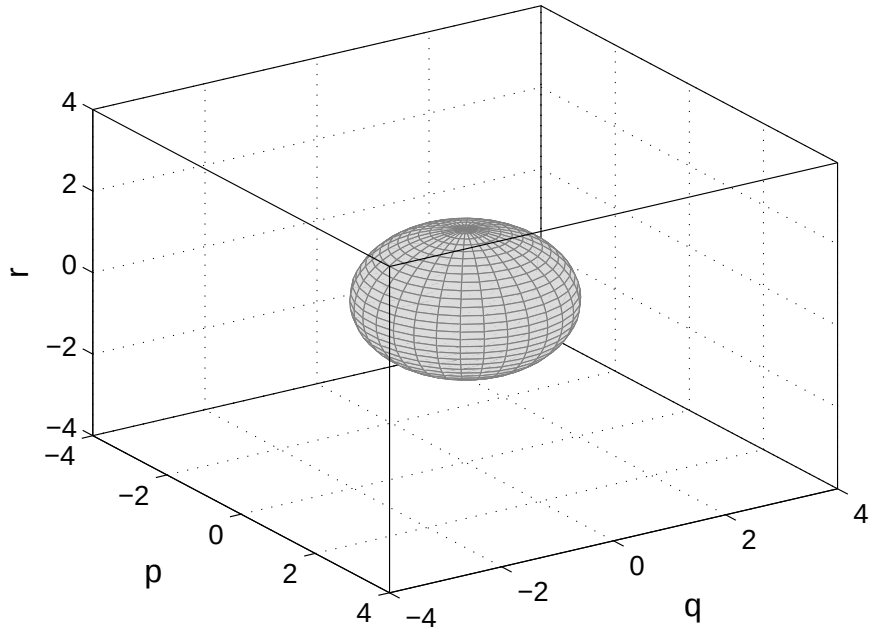

Figure 3.2: Comparison of the stability region estimates for Example 2. ROA by Bracci et al. (2006) (ellipsoid, $r = 1.7205$) and ROA by the proposed method (cube, whole area(subset))

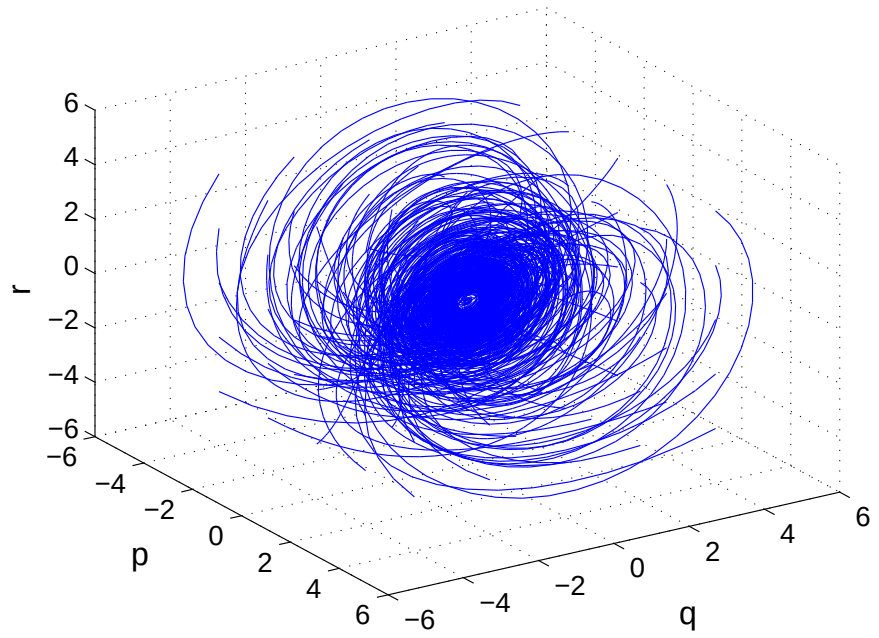

Figure 3.3: Comparison of the stability region estimates for Example 2. Several state trajectories with different initial conditions. In the whole area, all states are converged to the zero state ($x_e = 0$).

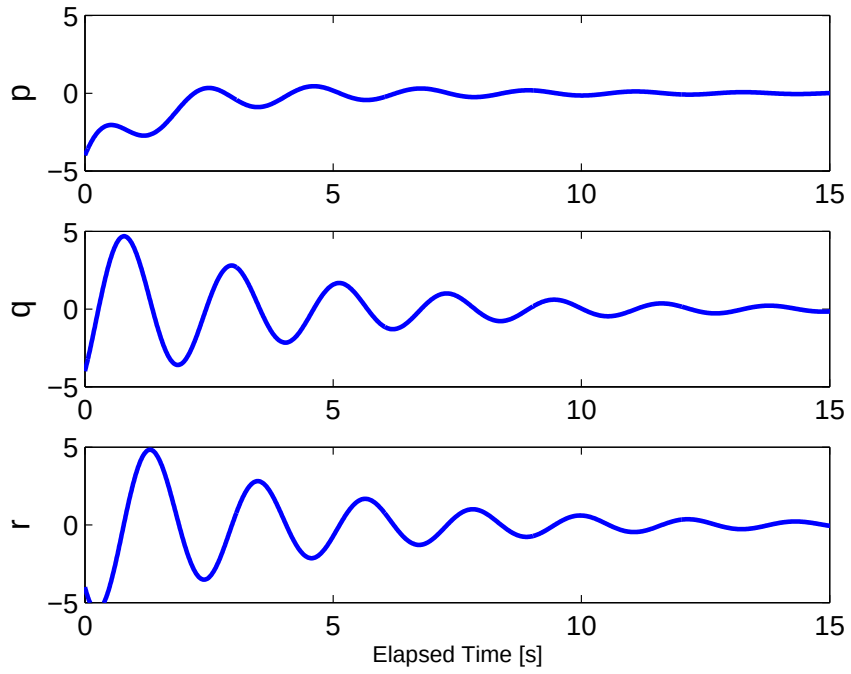

Figure 3.4: Comparison of the stability region estimates for Example 2. Time history of the state trajectories for a certain initial condition ($p = q = r = -4.0$). The figures show that all states approach 0 exponentially. Note that the convergent time is longer due to the small convergent rate ($\alpha = 0.153$). Moreover, the states are oscillated. It can explain the complicated trajectories in Figure 3.3.

although it shows the oscillatory motions of the states.

From the two examples, the superiority of the proposed method for estimating the exponentially stable ROA for the SDRE feedback systems is apparent. Note that the proposed method provides more accurate information than the prior work, so that the results could be more reliable.

3.4 Conclusions

We proposed a new method to estimate an ROA for the nonlinear system controlled by the SDRE controllers. The proposed method estimates the exponentially stable ROA for the SDRE feedback systems, while previous relevant work estimated the asymptotically stable ROAs in a conservative manner. The proposed method considers the contraction analysis, the incremental stability analysis, and the LMIs, specifically polytopic LDIs for the stability condition. Estimated ROAs by the method can be expected more accurate than those by prior studies. Through two examples, we demonstrated the reliability of the proposed method for estimating the ROA for nonlinear SDRE feedback systems.

Chapter 4

Automatic Gain-Tuner via Particle Swarm Optimization

In this chapter, we discuss an automatic gain tuning system, named the automatic gain-tuner via particle swarm optimization technique (AGT-PSO). The AGT-PSO calculates optimal values of user-defined system parameters which is expected to be time/cost efficient and labor efficient in the sense that it automatically tunes the system parameters with little background knowledge of the controller. Moreover, the performance of the system is shown to be significantly improved with the new parameters, obtained by the AGT-PSO. Even without any prior knowledge about control systems to be designed, system designers can tune the parameters of the controllers, which could have various forms, through the use of the AGT-PSO. It can be used to evaluate the existing control setups and will show suboptimal values of the parameters depending on the current setups. Examples with heavy industry machine tuning tools show the effectiveness and the reliability of the AGT-PSO.

4.1 Introduction

In modern society, structures of machines are becoming more sophisticated due to high demands such as fast response, fine accuracy, improved robustness, etc. For these systems to be feasible, several types of techniques of control and estimation should be used. Therefore, the overall structure of the control system may have a complex multi-loop. As the control system gets more complicated, the more gains or gains with more constraints may be used. In this case, tuning the gains might be a challenging problem since tuning a complex multi-loop control system or hierarchical structure requires considerable experience (Zhang et al., 2012). Unfortunately, however, the number of available qualified control engineers has decreased in today's industry although well trained engineers' skills become more important and there is a great need for high-fidelity tuning tools to maintain and improve the performance of complex control systems. Moreover,

although proportional-integral-derivative (PID) controllers are widely used in industry due to their simplicity and robustness in some sense, it is essential to consider new controllers for improved performance. Therefore, it is essential to develop automatic gain tuning methods so that they can replace experienced engineers and reduce time-cost to find "good" gains for the complex control systems.

The purpose of the current chapter is to investigate an automatic and simultaneous gain tuning algorithm for complex systems, especially for industrial machines. There is large volume of research on the automated tuning algorithms. First of all, several automatic tuning methods for PID-based controllers have been widely discussed in (Åström et al., 1993; Johnson and Moradi, 2005), and references therein. Crowe et al. (2003) studied the possibility of tuning PID controllers by using a new model-free gain tuning method, called the controller parameter cycling method. Kim et al. (2010) proposed a tuning method for a PID controller by using recursive least-square with linearization, which is expected to show fast response and good overall performance. Scaling and bandwidth-parameterization were also used to tune gains of a PID controller (Gao, 2003). A relay feedback technique was used in designing a PID controller for DC–DC converters (Stefanutti et al., 2007). A model-free gradient based tuning algorithm, called iterative feedback tuning (IFT), was extensively studied by (Hjalmarsson et al., 1998; Hjalmarsson, 2002) and references therein. Lequin et al. (2003) compared IFT with a conventional method for tuning PID controllers. Zhang et al. (2012) tuned a PID cluster controller for a boiler/turbine system through the use of IFT.

One might notice that the major target of the automatic gain tuning systems listed above is a PID-based controller. A reason of using such fixed gain controllers in industry is to avoid the possible abuse of adaptive schemes, which is more complicated than a fixed gain controller (Tan et al., 2002). However, there have been many attempts to apply different types of controllers to the existing systems such as linear quadratic regulator (LQR), linear quadratic Gaussian (LQG) control, gain scheduling, adaptive control, model predictive control, etc. Even in this case, there are gains and system parameters to be tuned. Therefore, it is essential to find "good" values of the parameters for reasonable performance of the system. For this, Sánchez et al. (2004) used a subspace identification method for a tuning algorithm which is for multivariable restricted structure control systems. A simultaneous perturbation stochastic approximation (SPSA) was used in multivariate stochastic approximation (Spall, 1992) and it was implemented in (Spall, 1998). As a direct method for constructing feedback controller, virtual reference feedback tuning (VRFT) for a linear system (Campi et al., 2002) and a nonlinear system (Campi and Savaresi, 2006) were investigated, respectively. As an

application, Rădac et al. (2011) applied IFT and SPSA to servo system control. By using the correlation method, iterative schemes (Karimi et al., 2004) and non-iterative schemes (Karimi et al., 2007) were studied for tuning controllers. However, most of the approaches listed above are related to gradient-based methods. Therefore, it might not be able to show optimized parameter values if a cost function to be minimized is neither convex nor smooth or the system has constraints on inputs or outputs. Therefore, these issues should be taken into account in the new gain tuning algorithms.

The main objective of the chapter is to show an automatic tuning algorithm of a controller of a complex system by using a global optimizer, particle swarm optimization (PSO), named as the automatic gain-tuner via PSO (AGT-PSO). The PSO, first introduced by Kennedy and Eberhart (1995), is a heuristic optimization algorithm, based on a swarm intelligence. It was developed through a simulation of a simplified social behavior, and was found to be robust in solving nonlinear optimization problems (Shi and Eberhart, 1998). Constraints can be included in finding optimal solutions in PSO (Parsopoulos and Vrahatis, 2002). The PSO technique can generate high-fidelity results with less calculation time and stable convergence characteristic than other stochastic methods such as genetic algorithms (GA) and simulated annealing (SA) (Eberhart and Shi, 1998; Gaing, 2004; Hassan et al., 2005). PSO also guarantees its reliability in non-smooth cost functions (Park et al., 2005). Due to the superiority of PSO, it has been widely applied to industrial as well as academic problems. For applications of a PID controller, Zhang et al. (2010) compared PSO, GA, and SA to tuning PID clusters for a boiler/turbine system. Convergence analysis and parameter selection of PSO were studied in (Trelea, 2003). Gaing (2004) applied PSO to find an optimal PID controller in an automatic voltage regulator system. Constrained PSO was investigated to design a PID controller (Kim et al., 2008). The performance of feedback linearization control for an industrial heavy machine was compared by using IFT and PSO (Bentsman et al., 2012). Applicability of PSO to tuning parameters of more sophisticated controllers such as gain scheduling, $\mathcal{L}_1$ adaptive control, limiting control, etc. was investigated (Chang et al., 2013), which showed overall significant improvement of the performance when using PSO.

We can summarize the contributions as follows:

- Unlike the existing tuning methods listed above, AGT-PSO can be applied to designing not only PID controllers but it can also be used to find optimal setups for various types of linear/nonlinear controllers. Moreover, AGT-PSO can be a useful tool for identification of open-loop and closed-loop systems.

- Unlike gradient-based tuning algorithms such as IFT and SPSA, AGT-PSO can obtain optimized solutions of the controlled systems even with non-smooth or non-convex cost functions due to the characteristics of PSO (Parsopoulos and Vrahatis, 2002; Park et al., 2005; Selvakumar and Thanushkodi, 2007; Niknam, 2010). It is of significant importance in industry due to the fact that such cost functions are common in industrial machines because of the complexity of the systems and constraints on inputs/outputs.

- AGT-PSO can obtain optimal values of a complex control system with shorter calculation time than those by heuristic methods, i.e., trial-and-error methods, which is the most common method of tuning system parameters in industry (Zhang et al., 2012). Moreover, the performance of the system can be improved significantly with AGT-PSO.

- Any prior knowledge of a control system is not needed to apply AGT-PSO to tuning parameters of the system. Moreover, control designers can use AGT-PSO not only to find optimal values of the gains without any prior knowledge (i.e., a wild initial guess is acceptable.) but also to verify optimality of the given initial setup of the gains.

- The existing optimizer, PSO, can be replaced with other optimization tools such as GA and SA depending on system designer's preference.

The organization of this chapter is as follows: The algorithm of AGT-PSO is introduced together with a brief introduction of PSO in Section 4.2. Subsequently, the performance of AGT-PSO is evaluated by applying it to two industrial examples in Section 4.3. Finally, conclusions are presented at the end of the chapter.

4.2 Automatic Gain-Tuner via Particle Swarm Optimization (AGT-PSO)

In AGT-PSO, an optimization technique plays a crucial role and PSO is used as the optimization technique. In this section, AGT is introduced together with a brief introduction of PSO. Readers are referred to (Kennedy and Eberhart, 1995; Clerc, 2006; Poli et al., 2007; Parsopoulos and Vrahatis, 2010) for details of PSO.

4.2.1 Particle Swarm Optimization (PSO)

The PSO is a population-based optimization technique where the population is called the swarm, defined as a set $\mathcal{S} = \{\boldsymbol{x}_1, \boldsymbol{x}_2, \cdots, \boldsymbol{x}_{N_p}\}$ and its individuals $\boldsymbol{x}_i$ $(i = 1, 2, \cdots, N_p)$ are called the particles, where N_p is the size of the swarm. For PSO, we consider the objective function to be minimized:

$$\min_{\boldsymbol{x}} V(\boldsymbol{x}), \quad \boldsymbol{x} \in \mathcal{D} \subset \mathbb{R}^n. \tag{4.1}$$

The swarm containing N_p particles is defined as the following form: $\boldsymbol{x}_i = \begin{bmatrix} \boldsymbol{x}_{i1} & \boldsymbol{x}_{i2} & \cdots & \boldsymbol{x}_{in} \end{bmatrix} \in \mathcal{D}, \ i = 1, 2, \cdots, N_p$ where $\mathcal{D}$ denotes the search space and we assume that $\mathcal{D}$ is the feasible space of the problem. The indices are arbitrarily assigned to particles and $V(\boldsymbol{x})$ is assumed to be available for all $\boldsymbol{x} \in \mathcal{D}$.
It is assumed that the particles move within the search space $\mathcal{D}$ iteratively. This is possible by adjusting their position using a proper position shift which is called velocity: $\boldsymbol{v}_i = \begin{bmatrix} \boldsymbol{v}_{i1} & \boldsymbol{v}_{i2} & \cdots & \boldsymbol{v}_{in} \end{bmatrix}, i = 1, 2, \cdots, N_p$.

We can express the current position of the ith particle and its velocity at the iteration counter k as $\boldsymbol{x}_i(k)$ and $\boldsymbol{v}_i(k)$, respectively. The velocity is updated iteratively through the use of information obtained in previous steps of the algorithm and updated to make the particles move through any region of $\mathcal{D}$. This is implemented in terms of a memory, where each particle can store the best position that it has ever visited during its search in $\mathcal{D}$, which is called the local best position. Then, a set can be defined by collecting the local best positions, $\mathcal{P} = \{\boldsymbol{p}_1, \boldsymbol{p}_2, \cdots, \boldsymbol{p}_{N_p}\}$ where the elements are defined as $\boldsymbol{p}_i(k) = \begin{bmatrix} \boldsymbol{p}_{i1}(k) & \boldsymbol{p}_{i2}(k) & \cdots & \boldsymbol{p}_{in}(k) \end{bmatrix} = \arg\min_k V_i(k) \in \mathcal{D}, \ i = 1, 2, \cdots, N_p$.

In PSO, the algorithm approximates the global minimizer with the best position ever visited by all particles. Let g be the index of the best position with the lowest function value in $\mathcal{P}$ at a given iteration k, i.e.,

$$\boldsymbol{p}_g(k) = \arg\min_i V(\boldsymbol{p}_i(k)) \tag{4.2}$$

which is also called global best position at a given iteration. Then, we define the new position and the

velocity by the following equations (Clerc and Kennedy, 2002):

$$\begin{aligned}\boldsymbol{x}_{ij}(k+1) &= \boldsymbol{x}_{ij}(k) + \boldsymbol{v}_{ij}(k+1),\\ \boldsymbol{v}_{ij}(k+1) &= \chi\Big(\boldsymbol{v}_{ij}(k) + c_1 R_1\big(\boldsymbol{p}_{ij}(k) - \boldsymbol{x}_{ij}(k)\big) + c_2 R_2\big(\boldsymbol{p}_{gj}(k) - \boldsymbol{x}_{ij}(k)\big)\Big)\end{aligned} \tag{4.3}$$

for all $i = 1, 2, \cdots, N_p,\ \ j = 1, 2, \cdots, n$ where R_1 and R_2 denote random variables uniformly distributed within $[0, 1]$; and c_1 and c_2 are the *cognitive* and *social* parameter, respectively. The parameter χ is called *constriction coefficient*. Among the ways to define the values of χ, c_1, and c_2, Clerc and Kennedy (2002) suggested the following formula:

$$\chi = \frac{2}{\phi - 2 + \sqrt{\phi^2 - 4\phi}} \tag{4.4}$$

where $\phi = c_1 + c_2 > 4$. Based on (4.4), the default parameter set of the constriction coefficient is as follows:

$$\chi = 0.729,\ \ c_1 = c_2 = 2.05. \tag{4.5}$$

At each iteration, the best positions are also updated after the update and evaluation of particles. Thus, we can define the new best position of x_i at iteration $k + 1$ as

$$\boldsymbol{p}_i(k+1) = \begin{cases} \boldsymbol{x}_i(k+1), & \text{if } V\big(\boldsymbol{x}_i(k+1)\big) \le V\big(\boldsymbol{p}_i(k)\big),\\ \boldsymbol{p}_i(k), & \text{otherwise.}\end{cases} \tag{4.6}$$

4.2.2 Algorithm of AGT-PSO

In this part, we introduce the mechanism of AGT-PSO.

1. Initial Setup for PSO

There are several parameters to be set up *a priori* in order to run PSO:

n : dimension of the problem (i.e., the number of parameters to be tuned in PSO)

N : swarm size (i.e., the number of particles)

k_{max} : the maximum number of iterations

tol : tolerance of the simulation

U : the vector of the upper bounds of the tuning parameters

L : the vector of the lower bounds of the tuning parameters

2. Initial Conditions

As mentioned in the previous section, the standard PSO uses U and L to generate initial conditions. However, it is not always necessary if good initial conditions or desired values of the tuning parameters are given. For this condition, a special parameter is defined:

RI : determination of the random initialization of the parameters

If $RI \leftarrow 1$, AGT-PSO starts with random initial conditions of the tuning parameters. If $RI \leftarrow 0$, on the other hand, users can define the initial conditions by themselves. This condition can be used to evaluate parameters which were tuned manually. In this case, a special function can be used to assign the user-defined initial conditions:

$$x_0 = \mathrm{TuningIC}(\mathrm{condition}) \tag{4.7}$$

where x_0 denotes the new initial conditions of the tuning parameters which were given externally depending on "condition."

For the case of $RI \leftarrow 1$, the random initial conditions are generated by using the following equation:

$$\mathrm{current\_position}(j,i) = \mathrm{rand} \times \big(U(j) - L(j)\big) + L(j) \tag{4.8}$$

where $j = 1, 2, \cdots, n$ and $i = 1, 2, \cdots, k_{maxRI}$. The function rand and the constant k_{maxRI} denote the uniform random number generator in $[0\ 1]$ and the maximum number of iterations for obtaining random

initial conditions, respectively.

3. Model Update

The tuning parameters can be directly applied to tuning systems. However, depending on the tuning systems, system models such as a dynamic model, a filter system, etc. must be updated by using the latest information of the tuning parameters. In this case, a special function is used:

$$[model\ parameters] = \text{Model\_Update}\big(\text{current\_position}(:, i), (other\ parameters)\big) \tag{4.9}$$

4. Evaluation of Performance Index (PI)

In optimization problems, defining performance indices (or cost functions) plays an important role. Therefore, more sophisticated performance index is recommended. In other words, a performance index V to be minimized for a given system can be simply defined as follows:

$$V = \frac{1}{2}\sum_{i=1}^{m} e_i^\top W_i e_i \tag{4.10}$$

where e_i is the error of the system to be minimized and $m \geq 1$ is the number of errors to be considered. Figure 4.1 shows the flowchart of the AGT-PSO.

Remark 6 The performance index in (4.10) is a simple form. If there are specific performance requirements such as rise time (t_r), settling time (t_s), and % overshoot (M_p), the performance index in (4.10) should be modified.

4.3 Performance Evaluation

In this section, we evaluate the performance of AGT-PSO with two examples from industry.

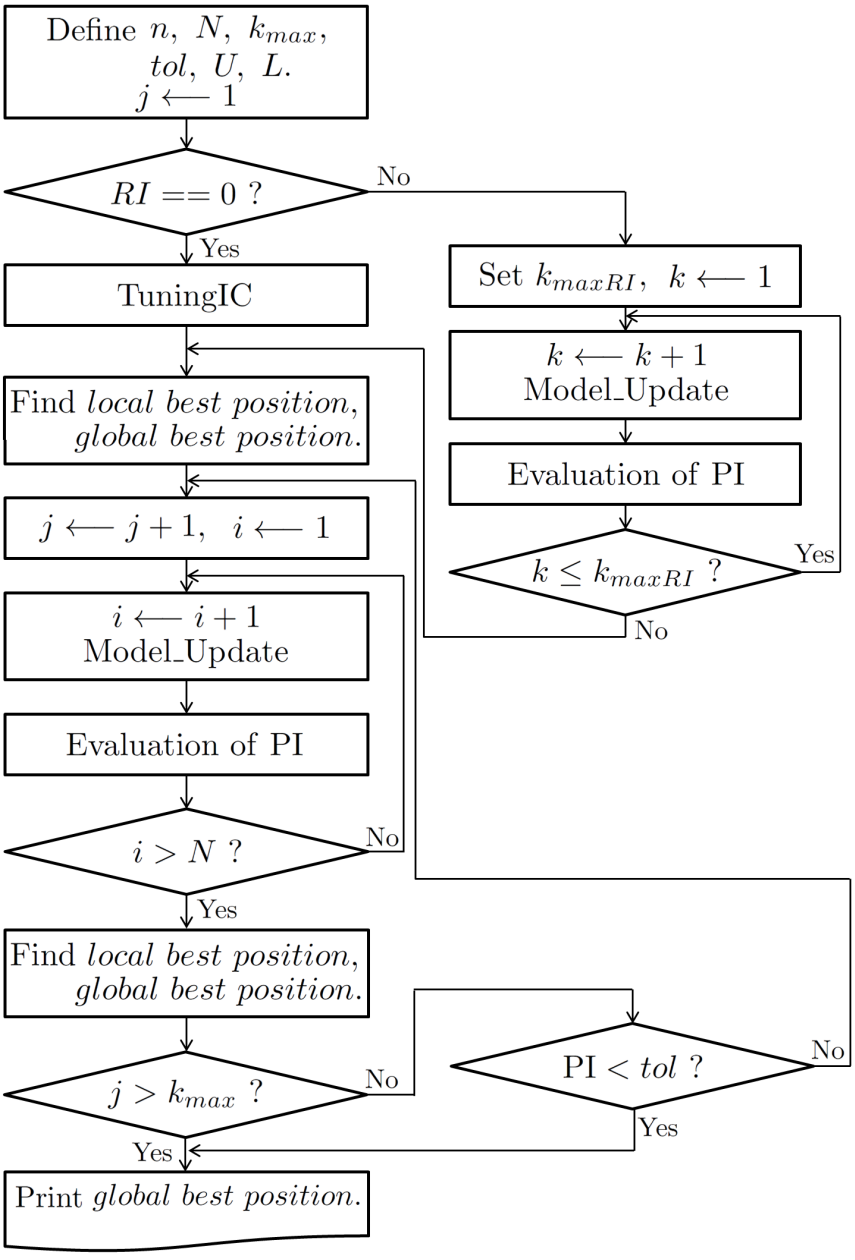

Figure 4.1: The schematic flowchart of the AGT-PSO

4.3.1 Case I: Tuning Gains in Feedback Linearization

In this simulation, we will show how AGT-PSO will work to tune gains in a control system – feedback linearization. For this, a sophisticated model (a small track-type tractor (STTT)) from Caterpillar Inc. is used which was designed in Simulink/MATLAB®.[1] The main objective of the simulation is to tune gains in the control system so that underspeed performance of the STTT is improved. First, we briefly analyze the control system.

Mathematical Description of the Controller

The control system was constructed by using a feedback linearization technique. Due to insufficient space, we omit the detailed derivation of the control system. Readers are referred to (Anderson, 2010) for the derivation. The feedback controller of the model is described as follows: there are mainly three gains to be able to be tune in this model: k_1, k_2, and k_3. We want to construct a mathematical model of the controller from the model. The input control u can be directly obtained in the following form:

$$\begin{aligned} u = T_{p,est} + k_3 \left(k_1^2 T + k_1 k_2 \dot{T}\right) \left(\frac{|P_L| + |P_R|}{\alpha \omega_p}\right) - k_3 \frac{T_{p,est} \dot{\omega}_p}{\omega_p} \\ + k_3 \frac{D_{m,l} P_L \dot{\omega}_p}{\omega_p} + k_3 \frac{D_{m,r} P_R \dot{\omega}_p}{\omega_p} \end{aligned} \tag{4.11}$$

where

$$\begin{aligned} T &= T_{p,lim,total} - T_{p,est} \\ P_L &= P_{f,left} - P_{r,left} \\ P_R &= P_{f,right} - P_{r,right}. \end{aligned}$$

The parameters α, $T_{p,lim,total}$, $T_{p,est}$, P_f, P_r, D_m, ω_p, and $\dot{\omega}_p$ denote a constant which is determined by physical information of the machine, the pump torque limit, the measured pump torque, the forward loop pressure, the reverse loop pressure, the motor displacement, the pump speed, and the rate of the pump speed,

[1] MATLAB and Simulink are registered trademarks of The MathWorks, Inc. See www.mathworks.com/trademarks for a list of additional trademarks.

respectively. The values of k_1, k_2, and k_3 were tuned manually and the values are set to

$$\begin{aligned} k_1 &= 43.9820 \\ k_2 &= \ 1.6000 \\ k_3 &= \ 0.0796. \end{aligned} \tag{4.12}$$

By using the current gains, we want to evaluate the performance of the controlled system in the next subsection for future references.

Test of Simulation

In order to evaluate the performance of the controller (4.11) with the current gains (4.12) and that obtained by using AGT-PSO, the model should be simulated under several conditions separately or simultaneously. For the test, we designed a comprehensive test model shown in Figure 4.2(a). The simulation condition comprises bank ram, forward-neutral-reverse (FNR) shifts, hill transition, and implement load. Notice that the main objective of the control system here is to minimize the effort of the underspeed control action, whose set point map can be found in Table 4.1.

Based on the mathematical description of the control system, we will obtain the optimal values of k_1, k_2, and k_3 through the use of AGT-PSO in the following subsection.

Performance of AGT-PSO for Tuning the Gains

In this subsection, the performance of AGT-PSO will be evaluated with the STTT model. For this, we tested two simulations with different assumptions: in the firs simulation, we assumed that the current gains (4.12) are the starting point of the PSO. In the second simulation, on the other hand, it was assumed that we do not know have *a priori* knowledge of the gains.

In the model, there are six variables (errors) to be considered: the torque error (T), the rate of torque error ($\dot{T}$), the motor speed errors ($e_{\omega_m,l}$(left) and $e_{\omega_m,r}$(right)), the engine speed error (e_{es}), and the underspeed error (e_{us}) which are defined as:

Table 4.1: Underspeed Set Point Map

		Desired Engine Speed						
		0	**950**	**1200**	**1600**	**1800**	**2100**	**2300**
Motor Speed	**500**	0	950	1150	1525	1700	1800	2200
	2000	0	950	1150	1525	1700	2000	2200

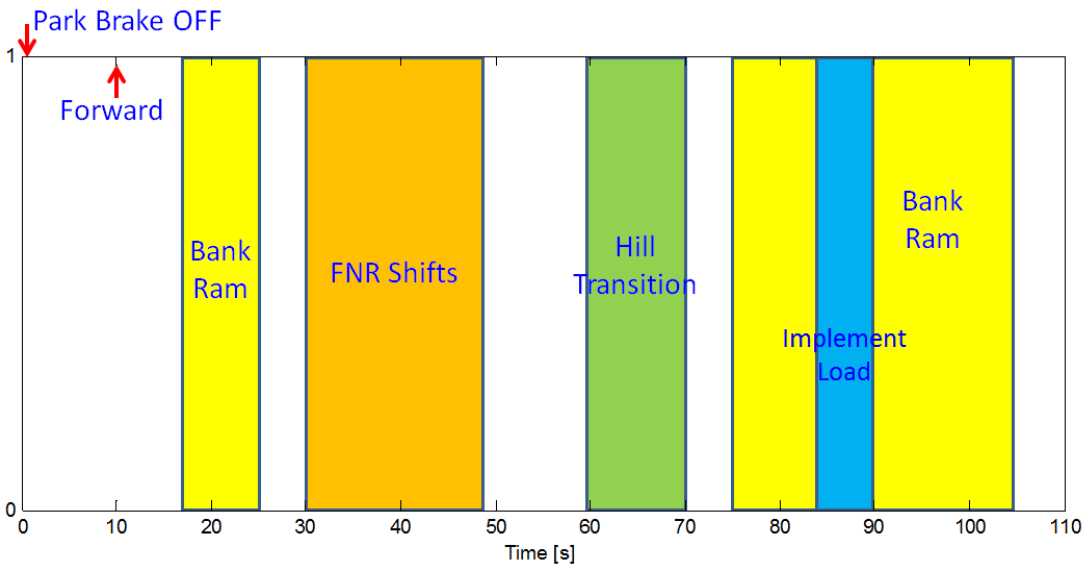

Figure 4.2: Specification of the tests and their activation time

$$\begin{cases} e_t & = T \\ \dot{e}_t & = \dot{T} \\ e_{\omega_m,l} & = \omega_{m,des,l} - \omega_{m,l} \\ e_{\omega_m,r} & = \omega_{m,des,r} - \omega_{m,r} \\ e_{es} & = \omega_{des} - \omega \\ e_{us} & = USSP - \omega. \end{cases} \tag{4.13}$$

where $USSP$ denotes the underspeed set point described in Table 4.1. It should be noted that it is meaningful to consider $e_{us} > 0$ due to the objective of the controller design. Therefore, e_{us} can be rewritten as follows:

$$e_{us} = \begin{cases} USSP - \omega, & \text{if } USSP > \omega \\ 0, & \text{otherwise.} \end{cases} \tag{4.14}$$

In order to define the performance index, weights $W_i,\ i = 1, 2, \cdots, 6$ must be defined:

$$W_1 = 5,\ W_2 = 10,\ W_3 = W_4 = W_5 = 0,\ W_6 = 20, \tag{4.15}$$

thereby the performance index to be minimized is defined in the following way:

$$V = \frac{1}{2}\Big(e_t^\top W_1 e_t + \dot{e}_t^\top W_2 \dot{e}_t + e_{us}^\top W_6 e_{us}\Big). \tag{4.16}$$

The search space $\mathcal{D}$ of the tunable gains k_1, k_2, and k_3 is chosen: $k_1 \in [10,\ 70],\ k_2 \in [0.3,\ 7],\ k_3 \in [0.05,\ 2]$. Moreover, the swarm size N and the maximum iteration k_{max} are set to $N = 30$ and $k_{max} = 30$, respectively.

Figures 4.3–4.5 shows the simulation results. Figure 4.3 shows the performance indices of the two simulations. Notice that "PSO with given IC" started the simulation with the current gains which was obtained manually shown in (4.12) and "PSO with random IC" did with random numbers in the search space $\mathcal{D}$. From the result of the dashed line, we can see that the current gains in (4.12) is not optimal and the performance index has been decreased from 2.9487×10^5 to 2.6924×10^5. On the other hand, the solid line shows that the performance index can be even further reduced with random initial conditions: 2.5932×10^5.

Table 4.2: Performance Improvement of the Engine Speed Drop [rpm] (Max Deviation w.r.t. the Desired Engine Speed)

	1st Bank Ram ($t \approx 18$ sec)		Hill Transition ($60 \sim 70$ sec)		2nd Bank Ram ($75 \sim 85$ sec)	
	Max Dev.	Improvement	Max Dev.	Improvement	Max Dev.	Improvement
Current Gains	-377.72	—	-123.70	—	-121.52	—
PSO w/ Given IC	-266.57	29.43%	-108.70	12.13%	-84.75	30.26%
PSO w/ Random IC	-200.31	46.97%	-85.20	31.12%	-63.79	47.51%

Table 4.3: Comparison of Performance Indices via AGT-PSO

PSO	Performance Index		Reduction (w.r.t.)	
	Iter = 0	Iter = 30	Iter = 0	Manual Tuning
w/ Given IC	2.9487×10^5	2.6924×10^5	8.69%	8.69%
w/ Random IC	2.6663×10^5	2.5932×10^5	2.74%	12.06%

Table 4.4: Optimal Gains via AGT-PSO

	Manual Tuning	AGT-PSO	
		w/ Given IC	w/ Random IC
k_1	43.9820	44.3072	24.9442
k_2	1.6000	2.8410	5.1157
k_3	0.0796	0.1382	0.2985

Table 4.5: Performance Improvement (Inputs) during the 1st Bank Ram Test ($t \approx 18$ sec)

	Torque Error (T)		Rate of Torque Error ($\dot{T}$)	
	Value [Nm]	Improvement	Value [Nm/s]	Improvement
Current Gains	-459.24	—	-2423.75	—
PSO w/ Given IC	-286.00	37.72%	-2020.00	16.66%
PSO w/ Random IC	-197.25	57.05%	-1782.50	26.46%

Detailed comparison can be found in Table 4.3. Figure 4.4 illustrates the history of tuning gains during 30 iterations. The final gains are shown in Table 4.4. Comparing Figures 4.2 and 4.5, we can find that there is no significant difference in FNR shits and implement load tests. In the first bank ram test, there is a big changes in the torque error and the rate of the torque error. Detailed information can be found in Table 4.5. From the table, we can easily find that the input changes can be significantly relieved by the gains obtained from the PSO with random initial conditions. However, it should be emphasized that the main objective of the controller design is to improve the underspeed performance which is shown in Figure 4.5. Table 4.2 shows the performance improvement in the first bank ram test, hill transition test, and the second bank ram test. The results also show the same conclusions: we can make the performance of the system by using the gains obtained by the PSO with random initial conditions.

Remark 7 Depending on restrictions or constraints of the machines, specific initial conditions should be used rather than starting AGT-PSO with random initial conditions, which is the reason why AGT-PSO has the condition $RI \longleftarrow 0$. Therefore, AGT-PSO can provide more flexible conditions to system designers.

4.3.2 Case II: Tuning Lookup Tables (Gain Scheduling)

The purpose of Case II is to design a control system for a medium wheel loader (MWL) so that we can balance the power, generated by an engine of the machine, to make the MWL move forward/backward and lift its bucket. For the simulation, a sophisticated model of MWL (MWL-980L) is used, developed by Caterpillar Inc. by using Simulink/MATLAB and Dynasty software.[2] Figure 4.6 shows how MWL-980L moves during its operation, illustrated by using Dynasty software. There are mainly two challenging tasks in this simulation. First, the system has a open-loop control system (see Figure 4.7). Second, the machine has "lookup tables," which are related to gain scheduling. Table 4.6) shows the five lookup tables which were tuned manually. Notice that gain-scheduling-based controllers are widely used in industry. Therefore, it will be of much significance if AGT-PSO could tune the lookup tables as well to increase the applicability in industry.

For the simulation, there are two performance requirements: time to 9KPH from 0KPH and tire revolutions until the machine lifts its bucket up from a stationary position. Detailed information of the requirements are listed in Table 4.7.

[2]Dynasty is a virtual prototyping and dynamic machine modeling software of Caterpillar Inc. that provides virtual simulation of multiple systems with multiple conditions.

Table 4.6: The Five Lookup Tables in the Open-Loop Controller in Figure 4.7

Trq Atmos

		Input1			
		70	80	90	100
Input2	700	125	125	125	125
	800	450	450	450	450
	1000	450	450	450	450
	1100	450	500	525	550
	1200	600	630	645	660
	1300	720	745.5	758.25	771
	1400	840	863.5	875.25	887
	1600	1030	1044.5	1051.75	1059
	1800	1440	1451	1456.5	1462
	1900	1575	1575	1575	1575
	2525	1575	1575	1575	1575

Trq US

Input	Output
400	700
500	700
700	700
800	700
850	700
900	700
950	1575
1050	1575
1300	1575
2200	1575

Trq Smoke Prox

Input	Output
0	450
1	450
5	450
10	500
15	600
25	1575
50	1575
100	1575

Trq Rate Inc

Input	Output
600	9
800	9
900	9
1000	9
1200	9
1500	9
1700	9
1900	9
2100	9
2500	9

Trq Rate Dec

Input	Output
600	–200
800	–100
900	–25
1000	–3.2
1200	–1.6
1500	–1.6
1700	–1.6
1900	–1.6
2100	–1.6
2500	–1.6

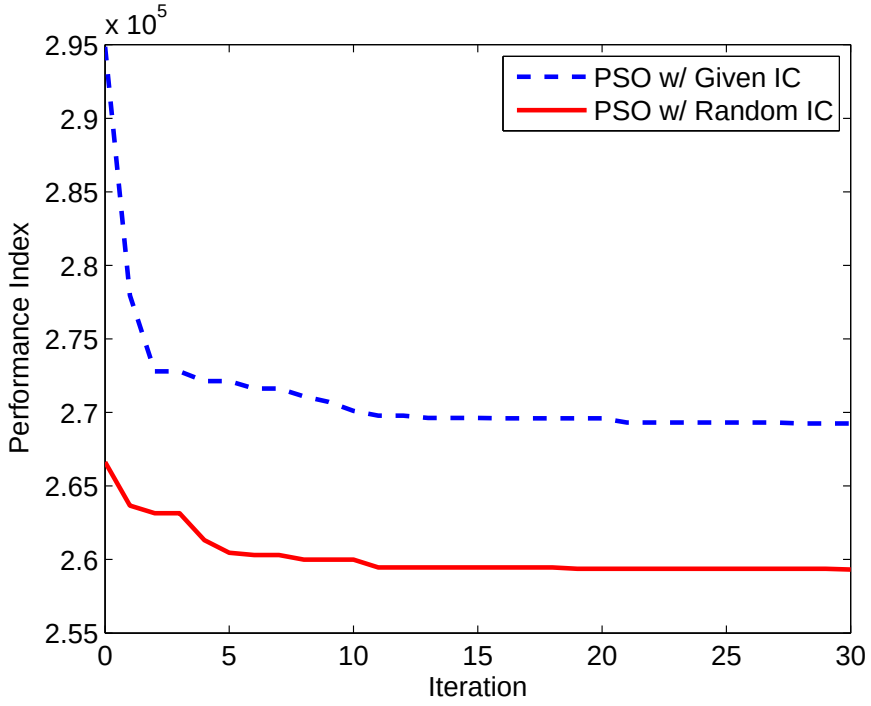

Figure 4.3: Time history of the performance index of the STTT simulation

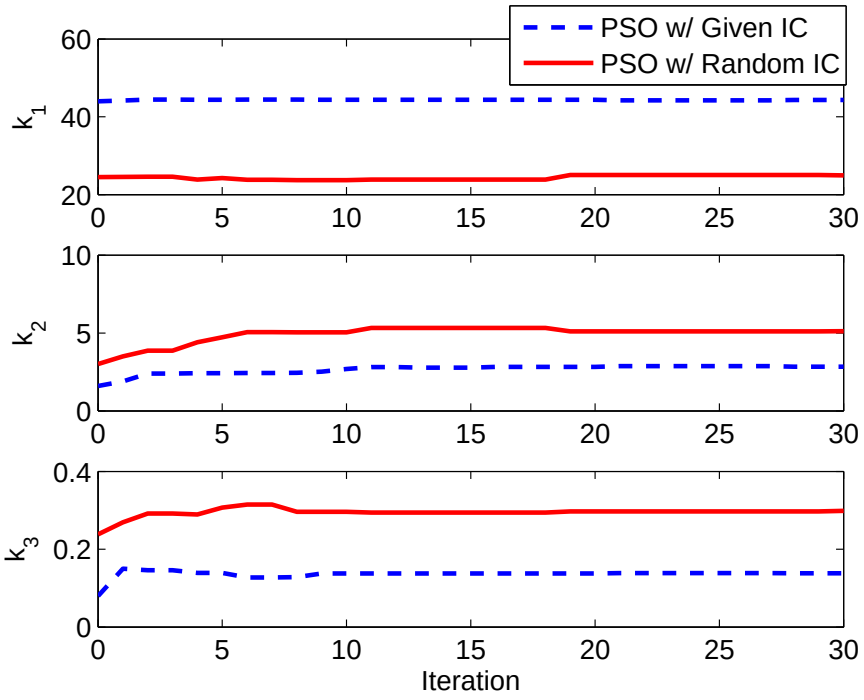

Figure 4.4: Time history of the gain variations of the STTT simulation

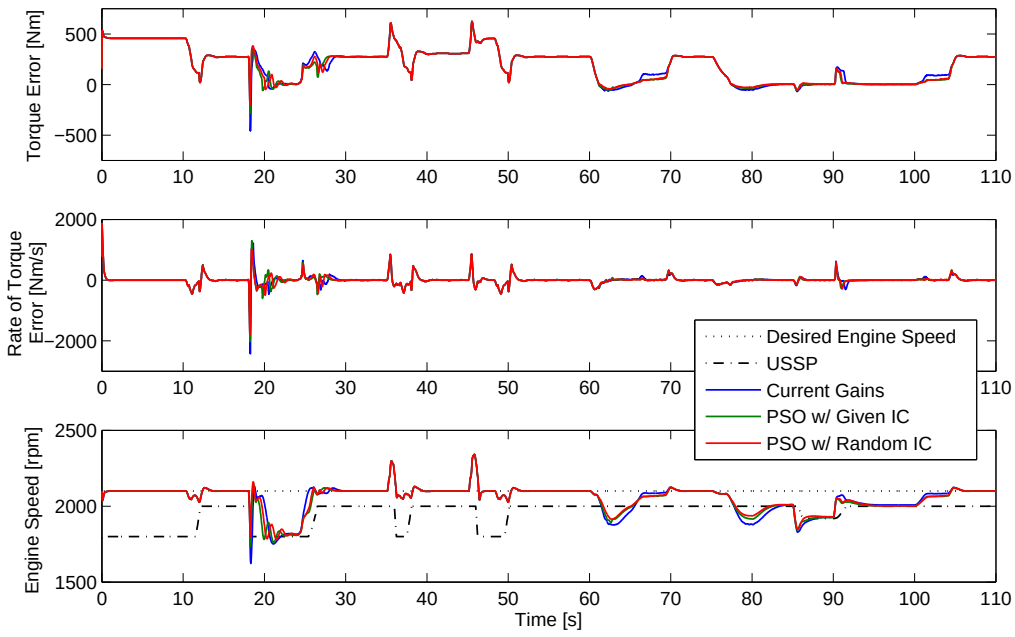

Figure 4.5: Comparison of the performance of the controllers of the STTT simulation

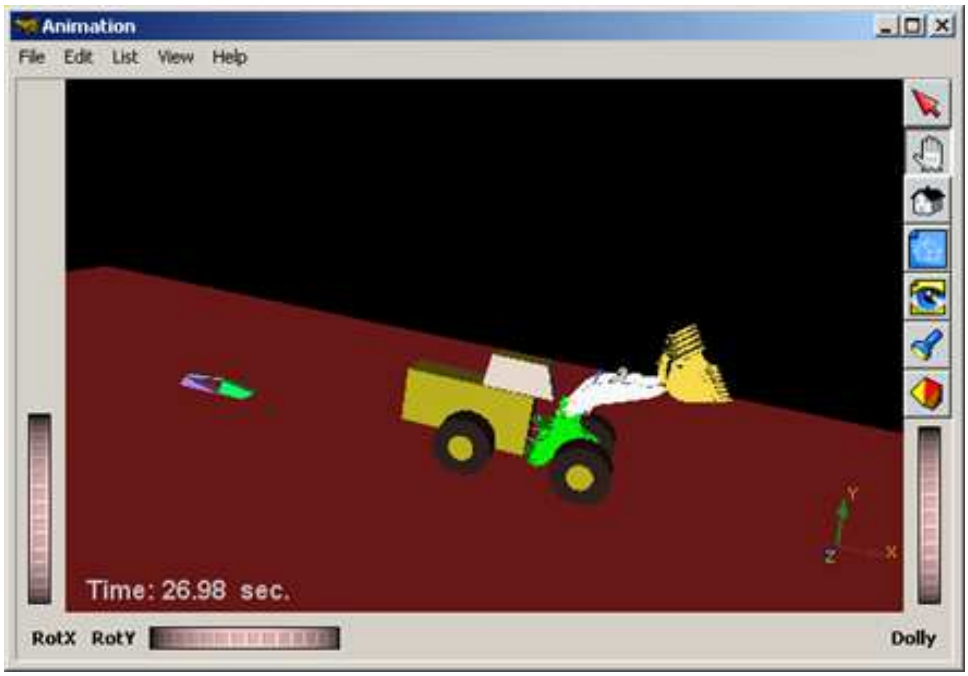

Figure 4.6: Capture of animation of the medium wheel loader (MWL) in Dynasty software. Requirements of the motion are shown in Table 4.7.

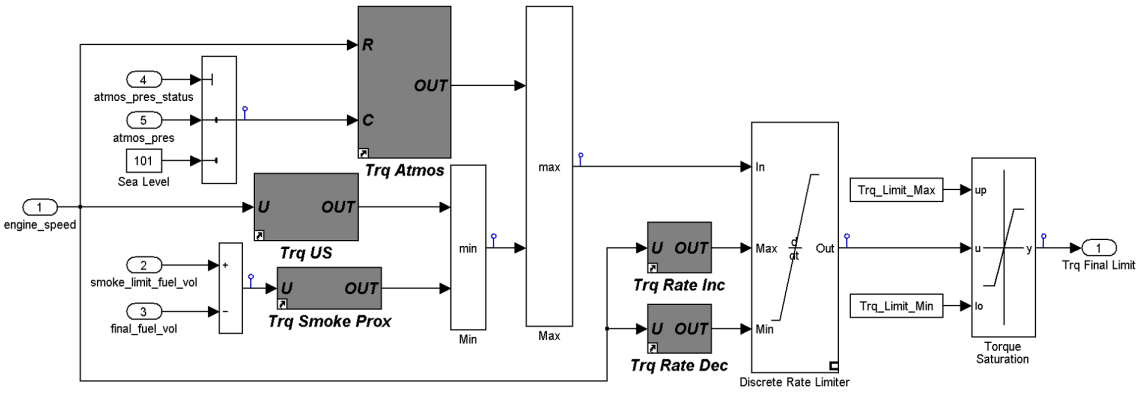

Figure 4.7: The block diagram of the open-loop controller (Simulink)

Table 4.7: Performance Requirements of the Second Simulation with respect to Altitudes

Altitude	Time to 9kph	Tire Revolution (full bucket lift)
0 ft	3.7 sec	
5,500 ft	≤ 4.4 sec	3.4 rev
10,000 ft	≤ 5.0 sec	

Concept of Tuning Lookup Tables

There are two ways to tune the lookup tables. The first approach is to tune the tables directly by selecting tuning points (i.e., inputs and outputs). However, the number of tuning knobs will increase in this case. The second approach, which is an alternative way to tune the lookup tables, is to define the shape of the lookup tables. Figure 4.8(a) illustrates the approach. Here, we assume that there are maximum (τ_{max}) and minimum (τ_{min}) of the output (say, torque (τ)). We can define a critical point of the input signal (x_c) and a slope (K). Then, the output within the boundary can be obtained by using a simple linear function:

$$\begin{cases} \tau(x) = \tau_{min}, & \text{if } \tau < \tau_{min} \\ \tau(x) = K(x - x_c) + \frac{\tau_{max}+\tau_{min}}{2}, & \text{if } \tau_{min} \leq \tau \leq \tau_{max} \\ \tau(x) = \tau_{max}, & \text{if } \tau > \tau_{max} \end{cases} \tag{4.17}$$

where it is assumed that the image of the critical point is located in the middle of the boundary, i.e., $\tau(x_c) = \frac{\tau_{max}+\tau_{min}}{2}$. With this concept, a lookup table can be defined by using the four variables: τ_{max}, τ_{min}, x_c, and K. Figure 4.8(b) shows the block diagram, designed in Simulink/MATLAB.

Remark 8 It should be noted that the description of the second approach is the simplest case under the assumption of linearity. However, more critical points together with slopes can be simply added to the concept.

Simulation Setup

Depending on the information of the tuning knobs, we have 20 tunable parameters: $\tau_{max,i}$, $\tau_{min,i}$, $x_{c,i}$, and K_i, $i = 1, 2, 3, 4, 5$ where i denotes the number of the lookup tables: Trq Atmos ($i = 1$), Trq US ($i = 2$), Trq Smoke Prox ($i = 3$), Trq Rate Inc ($i = 4$), and Trq Rate Dec ($i = 5$). However, due to physical limitations, the maxima of Trq Atmos, Trq US, and Trq Smoke Prox are given:

$$\tau_{max,1} = \tau_{max,2} = \tau_{max,3} = 1575 \text{ Nm}. \tag{4.18}$$

Therefore, we have 17 parameters to be tuned, i.e., $n = 17$. The search space $\mathcal{D}$ of the each parameter is defined as follows: $K_1,\ K_2 \in [0,\ 100]$, $K_3 \in [0,\ 200]$, $K_4 \in [0,\ 10]$, $K_5 \in [-10,\ 0]$, $\tau_{min,1}, \tau_{min,2}, \tau_{min,3} \in [100,\ 1575]$, $\tau_{min,4} \in [0,\ 50]$, $\tau_{min,5} \in [-500,\ 0]$, $\tau_{max,4} \in [0,\ 100], \tau_{max,5} \in [-500,\ 0]$, $x_{c,1}, x_{c,2}, x_{c,4}, x_{c,5} \in [0,\ 3000]$, $x_{c,3} \in [0,\ 20]$. For PSO, we set up the values of the important

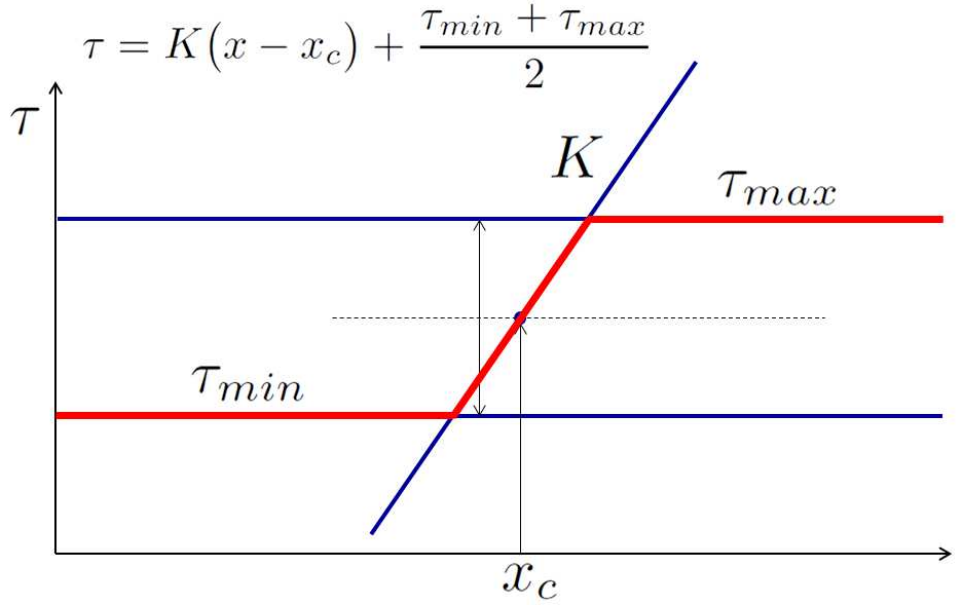

(a) Concept of defining a lookup table

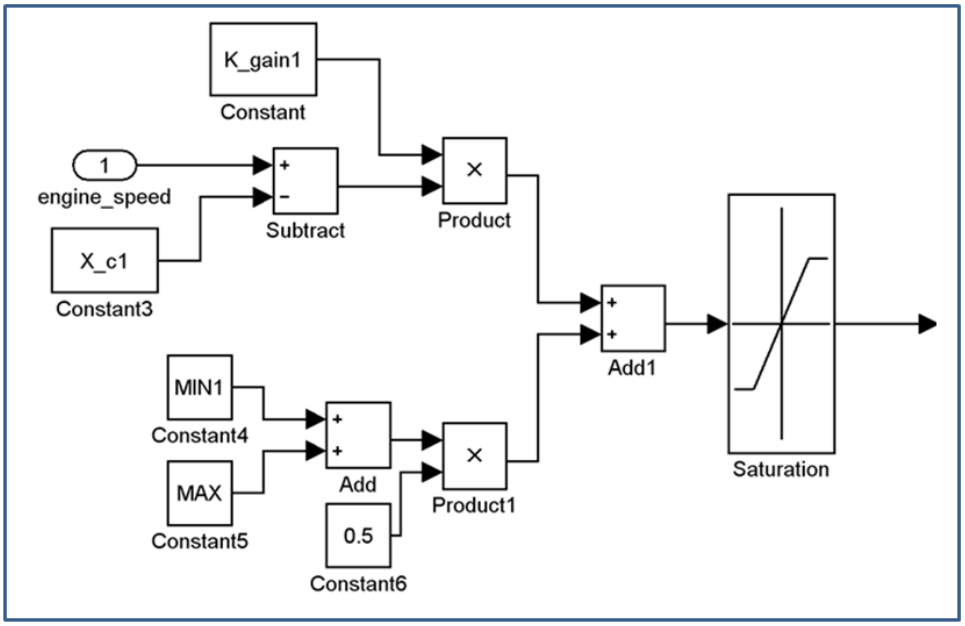

(b) Implementation of the concept in Simulink/MATLAB

Figure 4.8: Alternative approach to tune the lookup tables

parameters: $N = 40$, $k_max = 40$, $tol = 10^{-5}$. Moreover, it is assumed that we do not have good initial conditions of the parameters, i.e., $RI \longleftarrow 1$.

The performance index in this problem is constructed with two performance criteria: $e_{9\mathrm{KPH}}$ and e_{tire}, thereby it has the following form:

$$V = \frac{1}{2}\Big(e_{9\mathrm{KPH}}^{\top} W_1 e_{9\mathrm{KPH}} + e_{\mathrm{tire}}^{\top} W_2 e_{\mathrm{tire}}\Big) \tag{4.19}$$

where $e_{9\mathrm{KPH}}$ denotes the normalized time error to 9KPH (i.e., $e_{9\mathrm{KPH}} := (t - 3.7 - 20)/3.7$ for altitude = 0 ft)[3] and e_{tire} is the normalized tire revolution error (i.e., $e_{\mathrm{tire}} := (rev - 3.4)/3.4$).

Performance of AGT-PSO for Tuning the Lookup Tables

There are different performance requirements depending on the altitudes. Since the results are similar, we will show the results at the sea level (altitude = 0 ft). The history of the performance index is shown in Figure 4.9. Notice that the simulation was terminated at $j = 18$ since the value of the performance index (5.5826×10^{-6}) was lower than $tol = 10^{-5}$. The new five lookup tables are plotted[4] in Figure 4.10. The shape of the new lookup tables (solid lines) are different from the original ones in the sense that they have different slopes (K_i) and critical points ($x_{c,i}$) in most cases. The performance of the machine can be found in Figure 4.11. As can be seen from the two figures, the results by the new lookup tables meet the performance requirements in Table 4.7 while those by the original lookup tables failed to satisfy the requirements.

Remark 9 AGT-PSO not only provides optimal values of the parameters to be tuned, but it also shows meaningful results within a relatively short time while the manual tuning hardly does it as can be seen from the two simulation tests.

4.4 Conclusions

In this chapter, we introduced an automatic gain-tuner via particle swarm optimization. The suggested gain tuning system through the use of PSO has shown to be beneficiary in the sense that the obtained control gains are guaranteed to be *optimal* or *suboptimal*. Moreover, the performance of the controlled system

[3]The machine starts to move from 20 sec.

[4]For the simple comparison of the original lookup tables and new ones, obtained by using AGT-PSO, we plotted them instead of showing them in the form of tables such as Table 4.6.

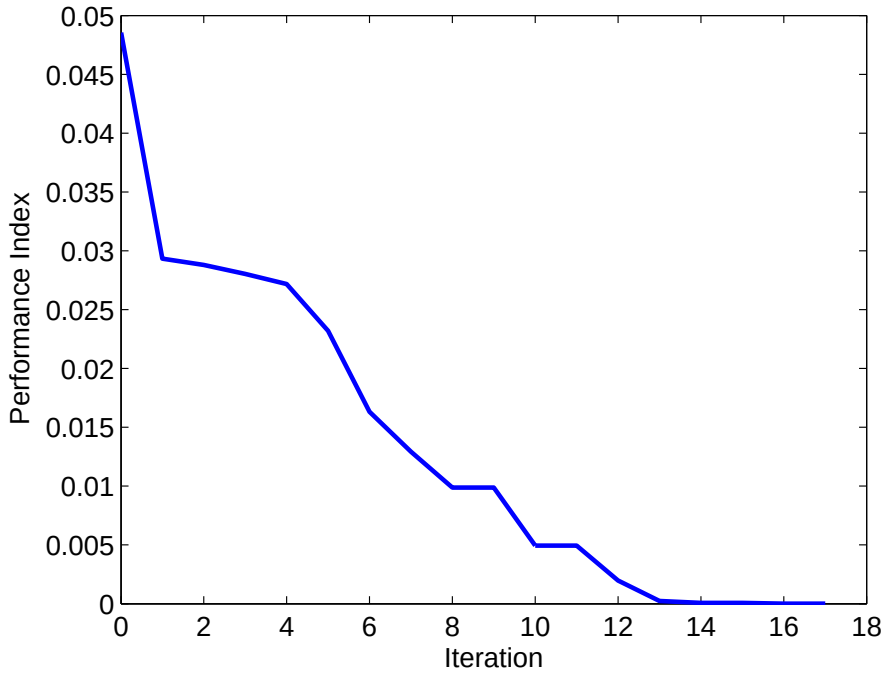

Figure 4.9: Time history of the performance index (altitude = 0 ft)

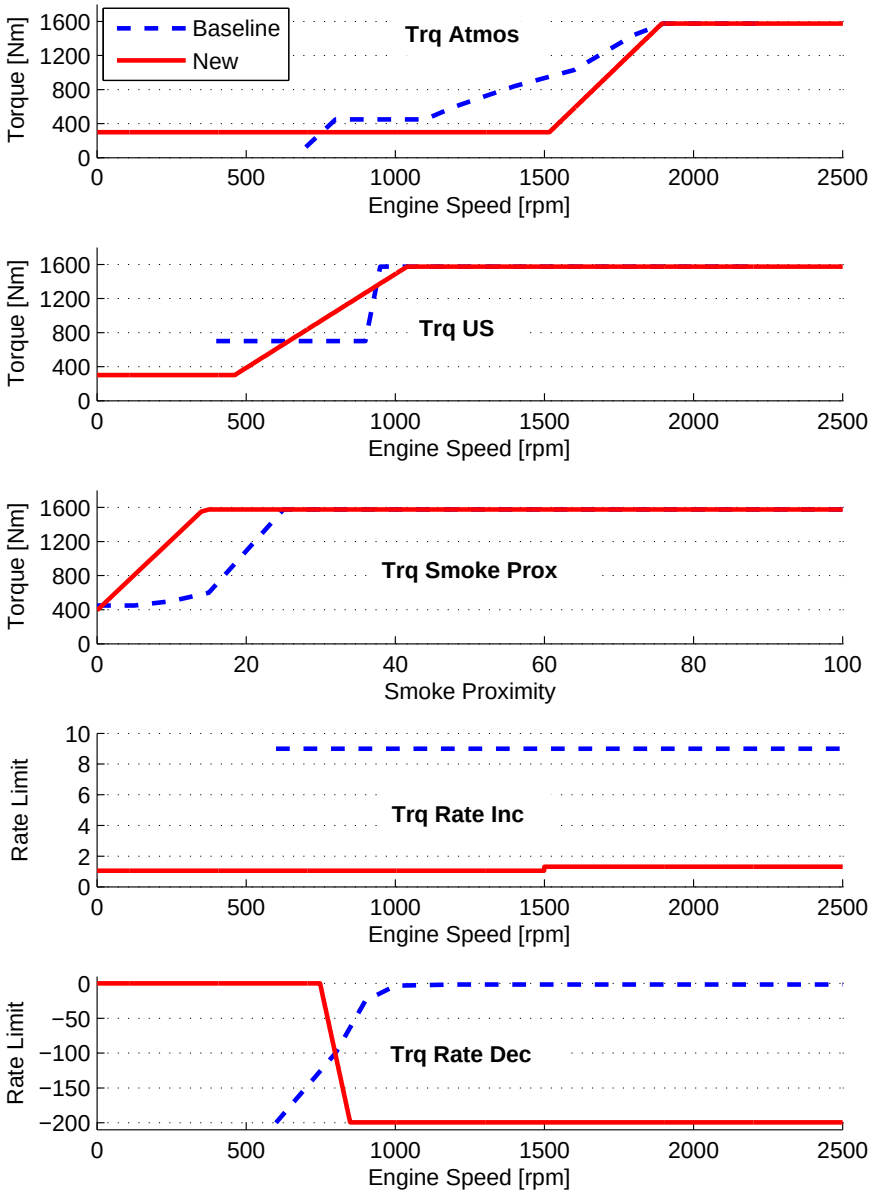

Figure 4.10: Comparison of the lookup tables (altitude = 0 ft)

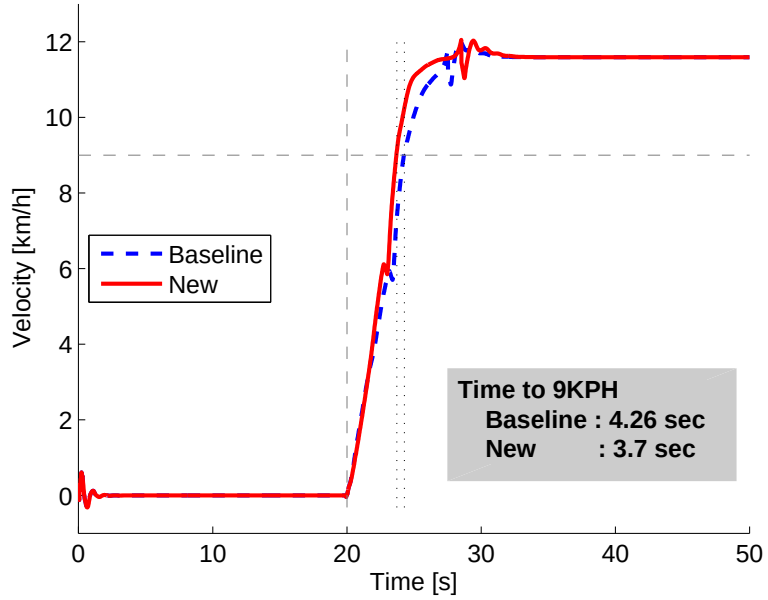

(a) Time to 9KPH

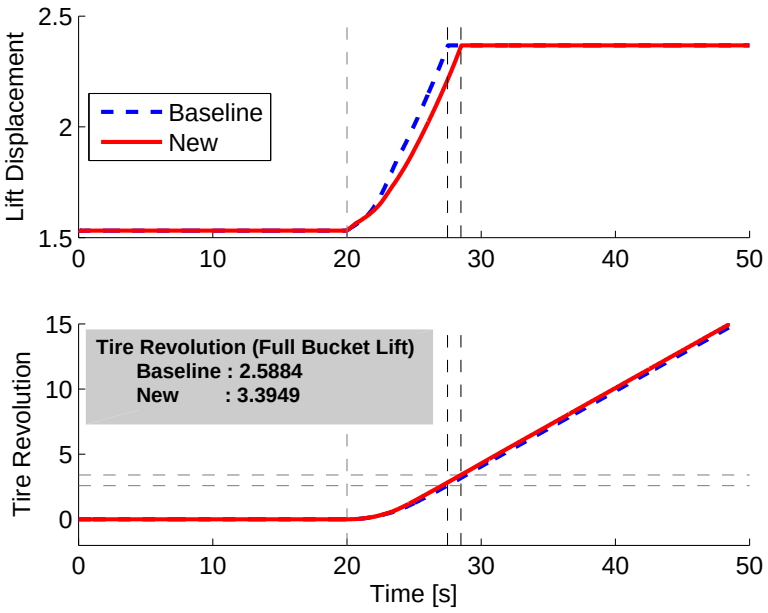

(b) Tire revolution

Figure 4.11: Comparison of the performance of the controllers (altitude = 0 ft)

could be modified by the designers' choice of the weights in the performance index. The main advantage of the automatic gain-tuners lies in the fact that it does not require any specific information to use it which in turn skills of the well-experienced control engineers can be easily replaed by the to tune parameters of the machines. AGT-PSO also provides the choice to start it with random initial conditions of the tunable parameters or meaningful initial conditions given *a priori*. It should be emphasized that AGT-PSO will significantly reduce time and labor to tune system parameters.

Part II

Constrained Discrete-Time State-Dependent Riccati Equation Technique

Chapter 5

Constrained Discrete-Time State-Dependent Riccati Equation Technique

THE objective of this chapter is to introduce the discrete-time state-dependent Riccati equation technique under input and state constraints, yielding constrained (C) discrete-time (D) SDRE, referred to as CD-SDRE. For the latter, stability analysis and calculation of a region of attraction are carried out. The derivation of the D-SDRE under state-dependent weights is provided. Stability of the D-SDRE feedback system is established using the Lyapunov stability approach. Receding horizon strategy is used to take into account the constraints on D-SDRE controller. Stability condition of the CD-SDRE controller is analyzed by using a switched system.

This chapter is organized as follows: In the following section, the derivation of D-SDRE, its stability condition, and estimates of a region of attraction of the D-SDRE feedback system are presented. The CD-SDRE is established in Section 5.2. Finally, concluding remarks are made in Section 5.3.

5.1 Generalized Discrete-Time State-Dependent Riccati Equation (D-SDRE) Technique

In this section, we derive the D-SDRE by using the optimality condition through the use of the Hamiltonian. Then, stability conditions of the D-SDRE feedback system are provided via the Lyapunov stability analysis. An ROA of a nonlinear system controlled by the D-SDRE feedback controller is investigated subsequently.

5.1.1 Derivation of the D-SDRE Feedback Controller

Consider the discrete-time nonlinear control-affine system described by using the nonlinear difference equation

$$\boldsymbol{x}_{k+1} = \boldsymbol{f}(\boldsymbol{x}_k) + \boldsymbol{B}(\boldsymbol{x}_k)\boldsymbol{u}_k \quad k \in \mathbb{Z}_{\geq 0} \tag{5.1}$$

where $\boldsymbol{x}_k \in X \subseteq \mathbb{R}^n$ and $\boldsymbol{u}_k \in U \subseteq \mathbb{R}^m$. It is assumed that $\boldsymbol{f}(\boldsymbol{0}) = \boldsymbol{0}$ and $\boldsymbol{f}(\boldsymbol{x}_k)$ is continuously differentiable. In this case, the model can be rearranged through the use of the SDC factorization (Cloutier, 1997):

$$\boldsymbol{x}_{k+1} = \boldsymbol{A}(\boldsymbol{x}_k)\boldsymbol{x}_k + \boldsymbol{B}(\boldsymbol{x}_k)\boldsymbol{u}_k. \tag{5.2}$$

We assume that $(\boldsymbol{A}(\boldsymbol{x}_k), \boldsymbol{B}(\boldsymbol{x}_k))$ is piecewise controllable for all $\boldsymbol{x}_k \in X$. For this system, the D-SDRE technique finds a control input $\boldsymbol{u}_k \in U$ at each time that approximately minimizes the following performance index:

$$J_0 = \frac{1}{2}\sum_{j=k}^{k+N-1}\Big(\boldsymbol{x}_j^\top \boldsymbol{Q}(\boldsymbol{x}_j)\boldsymbol{x}_j + \boldsymbol{u}_j^\top \boldsymbol{R}(\boldsymbol{x}_j)\boldsymbol{u}_j\Big) \tag{5.3}$$

where the weights $\boldsymbol{Q}(\boldsymbol{x}_j)$ and $\boldsymbol{R}(\boldsymbol{x}_j)$, which are assumed to be differentiable at $\boldsymbol{x}_k$ for all $k \in \mathbb{Z}_{\geq 0}$, are symmetric positive semi-definite and symmetric positive definite, respectively.

To find the optimal feedback controller $\boldsymbol{u}(\boldsymbol{x}_k)$, the Hamiltonian defined as below is used:

$$\mathcal{H}_k = \frac{1}{2}\Big(\boldsymbol{x}_k^\top \boldsymbol{Q}(\boldsymbol{x}_k)\boldsymbol{x}_k + \boldsymbol{u}_k^\top \boldsymbol{R}(\boldsymbol{x}_k)\boldsymbol{u}_k\Big) + \boldsymbol{\lambda}_{k+1}^\top\Big(\boldsymbol{f}(\boldsymbol{x}_k) + \boldsymbol{B}(\boldsymbol{x}_k)\boldsymbol{u}_k\Big). \tag{5.4}$$

Applying the optimality condition (Kirk, 1970; Bryson, Jr. and Ho, 1975), we obtain the three equations:

State equation

$$\boldsymbol{x}_{k+1} = \frac{\partial \mathcal{H}_k}{\partial \boldsymbol{\lambda}_{k+1}} = \boldsymbol{f}(\boldsymbol{x}_k) + \boldsymbol{B}(\boldsymbol{x}_k)\boldsymbol{u}_k \tag{5.5}$$

Costate equation

$$\boldsymbol{\lambda}_k = \frac{\partial \mathcal{H}_k}{\partial \boldsymbol{x}_k} = \bar{\boldsymbol{Q}} + \bar{\boldsymbol{A}}^\top \boldsymbol{\lambda}_{k+1} \tag{5.6}$$

Stationary condition

$$\boldsymbol{0} = \frac{\partial \mathcal{H}_k}{\partial \boldsymbol{u}_k} = \boldsymbol{B}(\boldsymbol{x}_k)^\top \boldsymbol{\lambda}_{k+1} + \boldsymbol{R}(\boldsymbol{x}_k)\boldsymbol{u}_k \tag{5.7}$$

where $\bar{\boldsymbol{Q}} := \boldsymbol{Q}(\boldsymbol{x}_k)\boldsymbol{x}_k + \frac{1}{2}\boldsymbol{x}_k^\top \frac{\partial \boldsymbol{Q}(\boldsymbol{x}_k)}{\partial \boldsymbol{x}_k}\boldsymbol{x}_k + \frac{1}{2}\boldsymbol{u}_k^\top \frac{\partial \boldsymbol{R}(\boldsymbol{x}_k)}{\partial \boldsymbol{x}_k}\boldsymbol{u}_k$ and $\bar{\boldsymbol{A}} := \boldsymbol{A}(\boldsymbol{x}_k) + \frac{\partial \boldsymbol{A}(\boldsymbol{x}_k)}{\partial \boldsymbol{x}_k}\boldsymbol{x}_k + \frac{\partial \boldsymbol{B}(\boldsymbol{x}_k)}{\partial \boldsymbol{x}_k}\boldsymbol{u}_k$.

To find the optimal solution, it is assumed that

$$\boldsymbol{\lambda}_k = \boldsymbol{P}_k \boldsymbol{x}_k. \tag{5.8}$$

Substituting (5.8) into (5.7) yields

$$\begin{aligned}
\boldsymbol{u}(\boldsymbol{x}_k) &= -\boldsymbol{R}(\boldsymbol{x}_k)^{-1}\boldsymbol{B}(\boldsymbol{x}_k)^\top \boldsymbol{\lambda}_{k+1} \\
&= -\boldsymbol{R}(\boldsymbol{x}_k)^{-1}\boldsymbol{B}(\boldsymbol{x}_k)^\top \boldsymbol{P}_{k+1}\left(\boldsymbol{A}(\boldsymbol{x}_k)\boldsymbol{x}_k + \boldsymbol{B}(\boldsymbol{x}_k)\boldsymbol{u}_k\right) \\
\Rightarrow \quad \boldsymbol{u}(\boldsymbol{x}_k) &= -\left(\boldsymbol{R}(\boldsymbol{x}_k) + \boldsymbol{B}(\boldsymbol{x}_k)^\top \boldsymbol{P}_{k+1}\boldsymbol{B}(\boldsymbol{x}_k)\right)^{-1}\boldsymbol{B}(\boldsymbol{x}_k)^\top \\
&\quad \times \boldsymbol{P}_{k+1}\boldsymbol{A}(\boldsymbol{x}_k)\boldsymbol{x}_k =: -\boldsymbol{K}(\boldsymbol{x}_k)\boldsymbol{x}_k
\end{aligned} \tag{5.9}$$

where $\boldsymbol{K}(\boldsymbol{x}_k) \in \mathbb{R}^{m\times n}$ is the optimal feedback control gain of the D-SDRE technique.

It should be noted that in order to obtain $\boldsymbol{K}(\boldsymbol{x}_k)$, $\boldsymbol{P}_k$ and $\boldsymbol{P}_{k+1}$ are needed, which are the solutions of the generalized discrete-time Riccati equation (GD-RE) at times k and $k+1$, respectively. Substituting (5.8), (5.5), and (5.9) into (5.6) and applying the matrix inversion lemma (Lewis et al., 2012) yield the following derivation:

$$\begin{aligned}
\boldsymbol{P}_k\boldsymbol{x}_k &= \bar{\boldsymbol{Q}} + \bar{\boldsymbol{A}}^\top \boldsymbol{\lambda}_{k+1} \\
&= \bar{\boldsymbol{Q}} + \bar{\boldsymbol{A}}^\top \boldsymbol{P}_{k+1}\boldsymbol{x}_{k+1} \\
&= \bar{\boldsymbol{Q}} + \bar{\boldsymbol{A}}^\top \boldsymbol{P}_{k+1}\left(\boldsymbol{A}(\boldsymbol{x}_k)\boldsymbol{x}_k + \boldsymbol{B}(\boldsymbol{x}_k)\boldsymbol{u}_k\right) \\
&= \bar{\boldsymbol{Q}} + \bar{\boldsymbol{A}}^\top \boldsymbol{P}_{k+1}\left(\boldsymbol{A}(\boldsymbol{x}_k)\boldsymbol{x}_k - \boldsymbol{B}(\boldsymbol{x}_k)\left(\boldsymbol{R}(\boldsymbol{x}_k) + \boldsymbol{B}^\top(\boldsymbol{x}_k)\boldsymbol{P}_{k+1}\boldsymbol{B}(\boldsymbol{x}_k)\right)^{-1}\boldsymbol{B}^\top(\boldsymbol{x}_k)\boldsymbol{P}_{k+1}\boldsymbol{A}(\boldsymbol{x}_k)\boldsymbol{x}_k\right) \\
&= \bar{\boldsymbol{Q}} + \bar{\boldsymbol{A}}^\top \boldsymbol{P}_{k+1}\left(\boldsymbol{I} - \boldsymbol{B}(\boldsymbol{x}_k)\left(\boldsymbol{R}(\boldsymbol{x}_k) + \boldsymbol{B}^\top(\boldsymbol{x}_k)\boldsymbol{P}_{k+1}\boldsymbol{B}(\boldsymbol{x}_k)\right)^{-1}\boldsymbol{B}^\top(\boldsymbol{x}_k)\boldsymbol{P}_{k+1}\right)\boldsymbol{A}(\boldsymbol{x}_k)\boldsymbol{x}_k \\
&= \bar{\boldsymbol{Q}} + \bar{\boldsymbol{A}}^\top \boldsymbol{P}_{k+1}\left(\boldsymbol{I} + \boldsymbol{B}(\boldsymbol{x}_k)\boldsymbol{R}^{-1}(\boldsymbol{x}_k)\boldsymbol{B}^\top(\boldsymbol{x}_k)\boldsymbol{P}_{k+1}\right)^{-1}\boldsymbol{A}(\boldsymbol{x}_k)\boldsymbol{x}_k.
\end{aligned}$$

Therefore, the GD-RE is obtained:

$$\begin{aligned}
\boldsymbol{P}_k = &\left(\boldsymbol{Q}(\boldsymbol{x}_k) + \frac{1}{2}\boldsymbol{x}_k^\top \frac{\partial \boldsymbol{Q}(\boldsymbol{x}_k)}{\partial \boldsymbol{x}_k} - \frac{1}{2}\boldsymbol{u}_k^\top \frac{\partial \boldsymbol{R}(\boldsymbol{x}_k)}{\partial \boldsymbol{x}_k}\boldsymbol{K}(\boldsymbol{x}_k)\right) \\
&+ \bar{\boldsymbol{A}}^\top \boldsymbol{P}_{k+1}\left(\boldsymbol{I} + \boldsymbol{B}(\boldsymbol{x}_k)\boldsymbol{R}(\boldsymbol{x}_k)^{-1}\boldsymbol{B}(\boldsymbol{x}_k)^\top \boldsymbol{P}_{k+1}\right)^{-1}\boldsymbol{A}(\boldsymbol{x}_k).
\end{aligned} \tag{5.10}$$

Remark 10 The algebraic Riccati equation (ARE) is used in LQR problems. In (Cloutier, 1997) and many other studies on SDRE, the ARE has been commonly used. Likewise, the DARE in (2.5) can be used for D-SDRE (Algorithm 1 in (Dutka et al., 2005)). In this case, there is an assumption that $\boldsymbol{A}(\boldsymbol{x}_k) =$

$\frac{\partial}{\partial \boldsymbol{x}_k}\left(\boldsymbol{f}(\boldsymbol{x}_k)+\boldsymbol{B}(\boldsymbol{x}_k)\boldsymbol{u}_k\right)\ \forall \boldsymbol{x}_k \in X$. However, it is not satisfied in general. Therefore, the feedback controller $\boldsymbol{u}_k$ may not work properly in an optimal sense unless $\frac{\partial \boldsymbol{A}(\boldsymbol{x}_k)}{\partial \boldsymbol{x}_k}\boldsymbol{x}_k+\frac{\partial \boldsymbol{B}(\boldsymbol{x}_k)}{\partial \boldsymbol{x}_k}\boldsymbol{u}_k=\boldsymbol{0}\ \forall \boldsymbol{x}_k \in X$.

Remark 11 In this chapter, $\boldsymbol{Q}$ and $\boldsymbol{R}$ in (5.3) are assumed to be dependent on the state $\boldsymbol{x}_k$, i.e., $\boldsymbol{Q}=\boldsymbol{Q}(\boldsymbol{x}_k)$ and $\boldsymbol{R}=\boldsymbol{R}(\boldsymbol{x}_k)$. For simplicity, $\boldsymbol{Q}$ and $\boldsymbol{R}$ can be considered to be independent on $\boldsymbol{x}_k$. Then, $\bar{\boldsymbol{Q}}=\boldsymbol{Q}$ in (5.6), and (5.10) becomes the same formula as that in Algorithm 2 in (Dutka et al., 2005). However, since $\boldsymbol{Q}$ and $\boldsymbol{R}$ affect the performance of an optimal control problem such as D-SDRE, it is more desirable to use state-dependent matrices rather than constant ones.

5.1.2 Stability Analysis of D-SDRE

It should be noted that the D-SDRE feedback controller is stabilizing the discrete-time nonlinear difference equation (5.1) or (5.2). In this part, we investigate the stability of the D-SDRE controller. Prior to that, we introduce exponential stability conditions.

Definition 6 *Consider the discrete-time nonlinear system*

$$\boldsymbol{\xi}_{k+1}=\boldsymbol{f}(\boldsymbol{\xi},\boldsymbol{\mu}). \tag{5.11}$$

Let (5.11) be a locally Lipschitz function in $\mathbb{X}\subseteq\mathbb{R}^n$ and $V:\mathbb{R}^n\to\mathbb{R}_{\geq 0}$ be a continuously differentiable function. Then (5.11) is said to be exponentially stable in $\mathbb{X}$ and V is called a Lyapunov function for (5.11) if the following hold:

1. *There exist $\alpha_1,\ \alpha_2\in\mathcal{K}_\infty$ such that*

$$\alpha_1(|\boldsymbol{\xi}|)\leq V(\boldsymbol{\xi})\leq\alpha_2(|\boldsymbol{\xi}|)\quad\forall\boldsymbol{\xi}\in\mathbb{R}^n. \tag{5.12}$$

2. *There exists $\alpha_3\in\mathcal{K}_\infty$ such that*

$$V(f(\boldsymbol{\xi},\boldsymbol{\mu}))-V(\boldsymbol{\xi})\leq-\alpha_3(|\boldsymbol{\xi}|)\ \ \forall\,\boldsymbol{\xi}\in\mathbb{R}^n. \tag{5.13}$$

Theorem 7 *The discrete-time nonlinear system (5.2) controlled by the D-SDRE technique (5.9) is exponentially stable in the ROA of the system $\mathcal{X}\subset\mathbb{X}$.*

Proof By substituting (5.9) into (5.2), we obtain the closed-loop form of the system:

$$\begin{aligned}\boldsymbol{x}_{k+1} = \Big\{\boldsymbol{A}(\boldsymbol{x}_k) - \boldsymbol{B}(\boldsymbol{x}_k)\Big(\boldsymbol{R}(\boldsymbol{x}_k) + \boldsymbol{B}(\boldsymbol{x}_k)^\top \boldsymbol{P}_{k+1}\boldsymbol{B}(\boldsymbol{x}_k)\Big)^{-1} \\ \times \boldsymbol{B}(\boldsymbol{x}_k)^\top \boldsymbol{P}_{k+1}\boldsymbol{A}(\boldsymbol{x}_k)\Big\}\boldsymbol{x}_k =: \boldsymbol{A}_{cl}(\boldsymbol{x}_k)\boldsymbol{x}_k.\end{aligned} \tag{5.14}$$

Then, we can derive the following equation by using the direct substitution into (5.14):

$$\boldsymbol{x}_{k+1} = \prod_{j=0}^{k} \boldsymbol{A}_{cl}(\boldsymbol{x}_j)\boldsymbol{x}_0. \tag{5.15}$$

By assumption in (5.2), $(\boldsymbol{A}(\boldsymbol{x}_k),\ \boldsymbol{B}(\boldsymbol{x}_k))$ is piecewise controllable for $\boldsymbol{x}_k \in X$, which implies that the system is stabilizable. Then, for $\zeta < 1$, there exist $c > 0$ and $0 \leq \sigma < \zeta$ such that

$$\|\boldsymbol{A}_{cl}(\boldsymbol{x}_k)\| \leq c\sigma_k \leq c\sigma_{max} \tag{5.16}$$

where $\sigma_{max} = \max_k \sigma_k$.

We need to find a Lyapunov function of (5.2). Given $\boldsymbol{D} = \boldsymbol{D}^\top > \boldsymbol{0}$, we can find $\boldsymbol{M}_k = \boldsymbol{M}_k^\top > \boldsymbol{0}$ for each k from the following equation:

$$\boldsymbol{A}_{cl}^\top(\boldsymbol{x}_k)\boldsymbol{M}_k\boldsymbol{A}_{cl}(\boldsymbol{x}_k) - \boldsymbol{M}_{k-1} = -\boldsymbol{D}. \tag{5.17}$$

Consider the following Lyapunov function candidate:

$$V(\boldsymbol{x}_k) = \boldsymbol{x}_k^\top \boldsymbol{M}_{k-1}\boldsymbol{x}_k. \tag{5.18}$$

It shows that $V(\boldsymbol{x}_k) \geq \lambda_{min}|\boldsymbol{x}_k|^2 =: \alpha_1(|\boldsymbol{x}_k|)$ and $V(\boldsymbol{x}_k) \leq \lambda_{max}|\boldsymbol{x}_k|^2 =: \alpha_2(|\boldsymbol{x}_k|)$ where

$$\begin{aligned}\lambda_{min} &= \min_k \lambda_{min}(\boldsymbol{M}_k) \\ \lambda_{max} &= \max_k \lambda_{max}(\boldsymbol{M}_k).\end{aligned} \tag{5.19}$$

Then, we can find $\alpha_3(|\boldsymbol{x}_k|)$ in Definition 6 from (5.2), (5.14)–(5.19):

$$\begin{aligned} V(\boldsymbol{x}_{k+1}) - V(\boldsymbol{x}_k) &= \boldsymbol{x}_{k+1}^\top \boldsymbol{M}_k \boldsymbol{x}_{k+1} - \boldsymbol{x}_k^\top \boldsymbol{M}_{k-1} \boldsymbol{x}_k \\ &= \boldsymbol{x}_k^\top \boldsymbol{A}_{cl}^\top \boldsymbol{M}_k \boldsymbol{A}_{cl} \boldsymbol{x}_k^\top - \boldsymbol{x}_k^\top \boldsymbol{M}_{k-1} \boldsymbol{x}_k \\ &= -\boldsymbol{x}_k^\top \boldsymbol{D} \boldsymbol{x}_k \leq -\lambda_{min}(\boldsymbol{D}) |\boldsymbol{x}_k|^2 =: -\alpha_3(|\boldsymbol{x}_k|), \end{aligned} \tag{5.20}$$

which implies that V in (5.18) is a Lyapunov function and therefore, the system (5.2) controlled by (5.9) is exponentially stable in its ROA. $\square$

5.1.3 Estimates of Region of Attraction (ROA) of D-SDRE

We consider a discrete-time nonlinear system controlled by the D-SDRE technique. We have shown that given the nonlinear system (5.1), under the assumption of an autonomous nonlinear equation, it can be rewritten in the form of (5.2) by using the SDC factorization. Moreover, by (5.9), the closed-loop system controlled by the D-SDRE feedback controller was obtained in (5.14). However, it should be emphasized that it is difficult to express $\boldsymbol{A}_{cl}(\boldsymbol{x}_k)$ in an analytic form due to the difficulty of an analytic expression of $\boldsymbol{P}_k$ and $\boldsymbol{P}_{k+1}$. Therefore, we should approach the problem in a different way: one can view this problem as a robust stability problem by assuming that $\boldsymbol{A}_{cl}(\boldsymbol{x}_k)$ is not precisely known, but it stays in $\mathcal{G}$, a convex, closed, and bounded domain (polytope) (Ramos and Peres, 2001), i.e.,

$$\mathcal{G} = \left\{ \boldsymbol{A}_{cl}(\alpha) : \boldsymbol{A}_{cl}(\alpha) = \sum_{i=1}^{L} \alpha_i \boldsymbol{A}_{cl,i};\ \sum_{i=1}^{L} \alpha_i = 1;\ \alpha_i \geq 0 \right\} \tag{5.21}$$

where $\boldsymbol{A}_{cl,i}$ are the vertices of the polytope $\mathcal{G}$.

Then, we have useful lemmas to find the ROA of the D-SDRE feedback system.

Lemma 8 *Suppose $\boldsymbol{A}_{cl}(\boldsymbol{x}_k)$ has uncertainties but belongs to $\mathcal{G}$ in (5.21). Then, (5.14) is robustly stable in $\mathcal{G}$ if there exists $\boldsymbol{P} = \boldsymbol{P}^\top > \boldsymbol{0}$ such that*

$$\boldsymbol{A}_{cl,i}^\top \boldsymbol{P} \boldsymbol{A}_{cl,i} - \boldsymbol{P} < -\rho \boldsymbol{I} \tag{5.22}$$

for all $i = 1, 2, \cdots, L$ and $\rho > 0$.

Proof See (de Oliveira et al., 1999; Jiang and Wang, 2001). □

Lemma 9 *Suppose $\boldsymbol{A}_{cl}(\boldsymbol{x}_k)$ has uncertainties but belongs to $\mathcal{G}$ in (5.21). Then, (5.14) is robustly stable in $\mathcal{G}$ if there exist $\boldsymbol{P}_i = \boldsymbol{P}_i^\top > \boldsymbol{0}$ and $\boldsymbol{G}$ such that*

$$\begin{bmatrix} \boldsymbol{P}_i & \boldsymbol{A}_{cl,i}^\top \boldsymbol{G}^\top \\ \boldsymbol{G}\boldsymbol{A}_{cl,i} & \boldsymbol{G} + \boldsymbol{G}^\top - \boldsymbol{P}_i \end{bmatrix} > \rho \boldsymbol{I} \tag{5.23}$$

for all $i = 1, 2, \cdots, L$ and $\rho > 0$.

Proof See (de Oliveira et al., 1999). □

Note that Lemmas 8 and 9 can be easily established by standard LMI solvers since $\boldsymbol{A}_{cl,i}$, the vertices of the polytope $\mathcal{G}$, are linear and so is (5.23) on $\boldsymbol{P}_i$. Therefore, the ROA of D-SDRE feedback control system, $\mathcal{X} \subseteq \mathbb{X} \subseteq X \subseteq \mathbb{R}^n$ can be obtained by the following way:

$$\mathcal{X} = \Big\{ \boldsymbol{x} \in X : \boldsymbol{A}_{cl}(\boldsymbol{x}) \in \mathcal{G} \text{ in (5.21)} \Big\}. \tag{5.24}$$

So far, we derived the D-SDRE feedback controller and proved the stability condition in an ROA which is obtained numerically via LMIs. Notice that we assumed that there are no constraints on the states or the control inputs. In order for the proposed control technique (CD-SDRE) to handle such constraints, MPC is used. In the next section, we discuss MPC, its stability condition, and finally CD-SDRE.

5.2 Constrained Discrete-Time State-Dependent Riccati Equation (CD-SDRE) Technique

In this section, we consider the D-SDRE technique with constraints on the states $\boldsymbol{x}_k$ and the control inputs $\boldsymbol{u}_k$. As a second part of the proposed CD-SDRE, MPC is presented. Stability analysis of the CD-SDRE is investigated subsequently. Finally, algorithms of CD-SDRE for regulation / tracking problems are provided.

5.2.1 Stability Analysis of MPC Mode

The proposed CD-SDRE uses MPC for two purposes: 1) to give directions to D-SDRE (guidance) by providing values of the parameters such as $\boldsymbol{P}_i$ in (5.10) and 2) to handle constraints on $\boldsymbol{x}_k$ or $\boldsymbol{u}_k$. Therefore, the proposed controller can be viewed as a hybrid system with two different controllers with a proper activation mode. We already showed the stability condition of the D-SDRE controller. We need to show that of the MPC controller.

Given a discrete-time nonlinear control-affine system (5.2), we want to find an optimal control sequence:

$$\boldsymbol{\mu}_N(\boldsymbol{x}_k, k) := \{\mu_k(\boldsymbol{x}_k, k), \mu_{k+1}(\boldsymbol{x}_k, k), \cdots, \mu_{k+N-1}(\boldsymbol{x}_k, k)\} \tag{5.25}$$

that minimizes the following performance index

$$J_N(\boldsymbol{x}_k) = \sum_{i=k}^{k+N-1} \left(\boldsymbol{x}_i^\top \boldsymbol{Q}(\boldsymbol{x}_i)\boldsymbol{x}_i + \boldsymbol{u}_i^\top \boldsymbol{R}(\boldsymbol{x}_i)\boldsymbol{u}_i \right) + \boldsymbol{x}_{k+N}^\top \boldsymbol{S}(\boldsymbol{x}_{k+N})\boldsymbol{x}_{k+N} \tag{5.26}$$

subject to (5.2), $\boldsymbol{x}_k \in \mathbb{X}$, and $\boldsymbol{u}_k \in \mathbb{U}$ where $\mathbb{X}$ is convex and closed in $\mathbb{R}^n$ and $\mathbb{U}$ is convex and compact in $\mathbb{R}^m$ both of which contain their origins.

An optimization technique such as dynamic program discussed in (Rawlings and Mayne, 2009) or PSO discussed in Chapter 4 can yield an optimal control sequence $\boldsymbol{\mu}_N(\boldsymbol{x}_k, k)$. Then the optimal controlled system satisfies

$$\boldsymbol{x}_{k+1} = \boldsymbol{A}(\boldsymbol{x}_k)\boldsymbol{x}_k + \boldsymbol{B}(\boldsymbol{x}_k)\boldsymbol{u}_k \tag{5.27}$$

where $\boldsymbol{u}_k := \mu_k(\boldsymbol{x}_k, k)$ in (5.25).

For the stability proof of the system controlled by MPC, we need assumptions as follows.

Assumption 10 *The stage cost and the terminal cost satisfy the bound conditions*

$$\begin{aligned} &\textstyle\sum_{i=k}^{k+N-1} \boldsymbol{x}_i^\top \boldsymbol{Q}(\boldsymbol{x}_i)\boldsymbol{x}_i + \boldsymbol{u}_i^\top \boldsymbol{R}(\boldsymbol{x}_i)\boldsymbol{u}_i \geq \alpha_1(|\boldsymbol{x}_k|) \\ &\boldsymbol{x}_{k+N}^\top \boldsymbol{S}(\boldsymbol{x}_{k+N})\boldsymbol{x}_{k+N} \leq \alpha_2(|\boldsymbol{x}_k|) \end{aligned}$$

$\forall \boldsymbol{x}_k \in \mathcal{X}_N$, $\forall \boldsymbol{u}_k \in \mathbb{U}$ *where* $\alpha_1(\cdot)$, $\alpha_2(\cdot) \in \mathcal{K}_\infty$ *and* $\mathcal{X}_N \in \mathbb{X}$ *is a region of attraction of the system controlled by MPC.*

Assumption 11 *The following inequality holds for all $k \in \mathbb{Z}_{\geq 0}$:*

$$\min_{\boldsymbol{u}\in\mathbb{U}} \sum_{i=k}^{k+N-1} \boldsymbol{x}_i^\top \boldsymbol{Q}(\boldsymbol{x}_i)\boldsymbol{x}_i + \boldsymbol{u}_i^\top \boldsymbol{R}(\boldsymbol{x}_i)\boldsymbol{u}_i + \boldsymbol{x}_{k+N}^\top \boldsymbol{S}(\boldsymbol{x}_{k+N})\boldsymbol{x}_{k+N} \leq \boldsymbol{x}_{k+N-1}^\top \boldsymbol{S}(\boldsymbol{x}_{k+N-1})\boldsymbol{x}_{k+N-1}.$$

By means of the assumptions, we can prove the following theorem.

Theorem 12 *Given the discrete-time nonlinear control-affine system in (5.2), the performance index in (5.26), and the optimal control sequence (5.25), there exist $\alpha_1(\cdot),\ \alpha_2(\cdot) \in \mathcal{K}_\infty$ such that $J_N(\cdot)$ satisfies the following inequalities:*

$$\begin{aligned} &J_N(\boldsymbol{x}_k) \geq \alpha_1(|\boldsymbol{x}_k|) \quad \forall \boldsymbol{x}_k \in \mathcal{X}_N \\ &J_N(\boldsymbol{x}_k) \leq \alpha_2(|\boldsymbol{x}_k|) \quad \forall \boldsymbol{x}_k \in \mathcal{X}_N \\ &J_N(\boldsymbol{x}_{k+1}) - J_N(\boldsymbol{x}_k) \leq -\alpha_1(|\boldsymbol{x}_k|) \quad \forall \boldsymbol{x}_k \in \mathcal{X}_N. \end{aligned} \tag{5.28}$$

Proof See Proposition 2.18 in (Rawlings and Mayne, 2009). □

Theorem 12 shows that the system controlled by MPC is exponentially stable in $\mathcal{X}_N$. However, it should be noted that the system is based on an open-loop control. For rigorous stability proof of the CD-SDRE controlled system, the open-loop control system should be approximately expressed as a closed-loop system. To the end, it is assumed that the control sequence generated by MPC can be expressed as

$$\boldsymbol{u}_k = \mu_N(\boldsymbol{x}_k, k) = -\boldsymbol{K}_{\mathrm{MPC}}\boldsymbol{x}_k - \boldsymbol{K}_{\mathrm{MPC},0} \tag{5.29}$$

In order to handle the modified control inputs, the given nonlinear system in (5.2) is transformed as follows:

$$\begin{bmatrix} \boldsymbol{x}_{k+1} \\ 1 \end{bmatrix} = \underbrace{\begin{bmatrix} \boldsymbol{A}(\boldsymbol{x}_k) - \boldsymbol{B}(\boldsymbol{x}_k)\boldsymbol{K}_{\mathrm{MPC}} & -\boldsymbol{B}(\boldsymbol{x}_k)\boldsymbol{K}_{\mathrm{MPC}} \\ \boldsymbol{0} & \boldsymbol{0} \end{bmatrix}}_{=:\breve{\boldsymbol{A}}_{cl}(\boldsymbol{x}_k)} \begin{bmatrix} \boldsymbol{x}_k \\ 1 \end{bmatrix}. \tag{5.30}$$

As we did in Theorem 7, we can prove the stability condition of the nonlinear system controlled by MPC.

Proposition 13 *The discrete-time nonlinear system (5.27) controlled by MPC (5.29) is exponentially stable in the ROA $\mathcal{X}_N \subseteq \mathbb{X}$.*

Proof The proof is straightforward from Theorem 7 by replacing $\boldsymbol{A}_{cl}(\boldsymbol{x}_k)$ by $\breve{\boldsymbol{A}}_{cl}(\boldsymbol{x}_k)$. □

It should be noted that the ROA of the system can be estimated by changing $\boldsymbol{A}_{cl}(\boldsymbol{x}_k)$ to $\breve{\boldsymbol{A}}_{cl}(\boldsymbol{x}_k)$ in Lemmas 8 and 9.

We have shown that the nonlinear discrete-time system controlled by D-SDRE and MPC is exponentially stable in its ROA. Notice that the two controllers are mutually exclusive: only one controller is activated during each sampling time. Therefore, it can be viewed as a switched system. In the next section, we will discuss the stability condition of such a switched system.

5.2.2 Stability Analysis of the Switched System (CD-SDRE)

As discussed in the previous sections, the proposed CD-SDRE controller contains two different controllers: D-SDRE and MPC, i.e.,

$$\boldsymbol{u}_k = \begin{cases} -\boldsymbol{K}_1(\boldsymbol{x}_k)\boldsymbol{x}_k, & \text{for D-SDRE} \\ -\breve{\boldsymbol{K}}_2(\boldsymbol{x}_k)\breve{\boldsymbol{x}}_k, & \text{for MPC} \end{cases} \tag{5.31}$$

where $\breve{\boldsymbol{x}}_k := \begin{bmatrix} \boldsymbol{x}_k^\top & 1 \end{bmatrix}^\top$.

Depending on the location of the estimates of the states and the inputs, the CD-SDRE activates only one controller to generate the proper control signals. In order to augment the two controllers to the nonlinear discrete-time system, we define the indicator function:

$$\boldsymbol{\eta}_k := \begin{bmatrix} \eta_k^1 & \eta_k^2 \end{bmatrix}^\top \tag{5.32}$$

where

$$\eta_k^i = \begin{cases} 1, & \text{if } \boldsymbol{K}_i \text{ is activated,} \\ 0, & \text{otherwise.} \end{cases} \tag{5.33}$$

By substituting (5.33) into the nonlinear discrete-time system (5.2) yields

$$\breve{\boldsymbol{x}}_{k+1} = \left(\breve{\boldsymbol{A}}(\boldsymbol{x}_k) - \sum_{i=1}^{2} \eta_k^i \boldsymbol{K}_i(\boldsymbol{x}_k) \right) \breve{\boldsymbol{x}}_k =: \breve{\boldsymbol{A}}_{cl}(\boldsymbol{x}_k, \boldsymbol{\eta}_k)\breve{\boldsymbol{x}}_k = \sum_{i=1}^{2} \eta_k^i \breve{\boldsymbol{A}}_{cl}^{\,i}(\boldsymbol{x}_k)\breve{\boldsymbol{x}}_k \tag{5.34}$$

where $\breve{\boldsymbol{A}}(\boldsymbol{x}_k) := \begin{bmatrix} \boldsymbol{A}(\boldsymbol{x}_k) & 0 \\ 0 & 0 \end{bmatrix}$ and $\breve{\boldsymbol{K}}_1(\boldsymbol{x}_k) := \begin{bmatrix} \boldsymbol{K}_1(\boldsymbol{x}_k) & 0 \\ 0 & 0 \end{bmatrix}$.

Then the following theorem shows the stability condition of the switched system.

Theorem 14 *Suppose there exist symmetric positive definite matrices $\boldsymbol{M}_k^1$ (D-SDRE) and $\boldsymbol{M}_k^2$ (MPC) such that*

$$\begin{bmatrix} \boldsymbol{M}_k^i & \breve{\boldsymbol{A}}_{cl}^{i\top} \boldsymbol{M}_k^j \\ \boldsymbol{M}_k^j \breve{\boldsymbol{A}}_{cl}^{i} & \boldsymbol{M}_k^j \end{bmatrix} > \mathbf{0} \quad \forall i,\ j \in \mathbb{Z}_{1:2}. \tag{5.35}$$

Then, the switched system (5.34) is exponentially stable in $\mathcal{X}_N$.

Proof We have shown the stability proofs of the nonlinear discrete-time system controlled by D-SDRE and MPC, respectively, i.e., there exist $\boldsymbol{M}_k^1$ and $\boldsymbol{M}_k^2$ such that

$$\begin{bmatrix} \boldsymbol{M}_k^1 & \breve{\boldsymbol{A}}_{cl}^{1\top} \boldsymbol{M}_k^1 \\ \boldsymbol{M}_k^1 \breve{\boldsymbol{A}}_{cl}^{1} & \boldsymbol{M}_k^1 \end{bmatrix} > \mathbf{0} \quad \text{and} \quad \begin{bmatrix} \boldsymbol{M}_k^2 & \breve{\boldsymbol{A}}_{cl}^{2\top} \boldsymbol{M}_k^2 \\ \boldsymbol{M}_k^2 \breve{\boldsymbol{A}}_{cl}^{2} & \boldsymbol{M}_k^2 \end{bmatrix} > \mathbf{0} \quad \forall k \in \mathbb{Z}_{\geq 0}. \tag{5.36}$$

Then the switched system can be expressed by using (5.36) together with η_k^l:

$$\begin{bmatrix} \boldsymbol{M}_k^i \sum_{l=1}^2 \eta_k^l & \breve{\boldsymbol{A}}_{cl}^{i\top} \boldsymbol{M}_k^j \sum_{l=1}^2 \eta_k^l \\ \boldsymbol{M}_k^j \sum_{l=1}^2 \eta_k^l \breve{\boldsymbol{A}}_{cl}^{i} & \boldsymbol{M}_k^j \sum_{l=1}^2 \eta_k^l \end{bmatrix} > \mathbf{0} \quad i, j \in \mathbb{Z}_{1:2}. \tag{5.37}$$

To prove the theorem, it is sufficient to show that the inequality holds for $i \neq j$. Let $\eta_k^1 = 1$ at time k and $\eta_k^2 = 1$ at time $k+1$. Then

$$\begin{bmatrix} \boldsymbol{M}_k^i & \breve{\boldsymbol{A}}_{cl}^{i\top} \boldsymbol{M}_{k+1}^j \\ \boldsymbol{M}_{k+1}^j \breve{\boldsymbol{A}}_{cl}^{i} & \boldsymbol{M}_{k+1}^j \end{bmatrix} > \mathbf{0}. \tag{5.38}$$

By Schur complement (Boyd et al., 1994), it is equivalent to the following inequality,

$$\breve{\boldsymbol{x}}_k^\top \left(\boldsymbol{M}_k^i - \breve{\boldsymbol{A}}_{cl}^{i\top} \boldsymbol{M}_{k+1}^j \breve{\boldsymbol{A}}_{cl}^{i} \right) \breve{\boldsymbol{x}}_k > \mathbf{0}. \tag{5.39}$$

We define a Lyapunov function candidate for the switched system as

$$V(\boldsymbol{x}_k) := \breve{\boldsymbol{x}}_k^\top \boldsymbol{M}_k(\boldsymbol{\eta}_k) \breve{\boldsymbol{x}}_k = \breve{\boldsymbol{x}}_k^\top \left(\sum_{l=1}^2 \eta_k^l \boldsymbol{M}_k^l \right) \breve{\boldsymbol{x}}_k \tag{5.40}$$

where $\boldsymbol{M}_k^i$ is symmetric positive definite which are defined above.

Hence, the following inequalities hold due to the definition of the $V(\boldsymbol{x}_k)$ and $\boldsymbol{M}_k^i$:

$$\begin{aligned} V(\boldsymbol{x}_k) &\geq \lambda_{min}(\min\{\boldsymbol{M}_k^1,\ \boldsymbol{M}_k^2\})|\boldsymbol{x}_k| =: \alpha_1(|\boldsymbol{x}_k|) \\ V(\boldsymbol{x}_k) &\leq \lambda_{max}(\max\{\boldsymbol{M}_k^1,\ \boldsymbol{M}_k^2\})|\boldsymbol{x}_k| =: \alpha_2(|\boldsymbol{x}_k|). \end{aligned} \tag{5.41}$$

By the definition of the Lyapunov function, we can derive the inequality

$$\begin{aligned} V(\boldsymbol{x}_{k+1}) - V(\boldsymbol{x}_k) &= \breve{\boldsymbol{x}}_{k+1}^\top \left(\sum_{l=1}^{2} \eta_{k+1}^l \boldsymbol{M}_{k+1}^l \right) \breve{\boldsymbol{x}}_{k+1} - \breve{\boldsymbol{x}}_k^\top \left(\sum_{l=1}^{2} \eta_k^l \boldsymbol{M}_k^l \right) \breve{\boldsymbol{x}}_k \\ &= -\breve{\boldsymbol{x}}_k^\top \left(\boldsymbol{M}_k^i - \breve{\boldsymbol{A}}_{cl}^{i\top} \boldsymbol{M}_{k+1}^j \breve{\boldsymbol{A}}_{cl,k}^i \right) \breve{\boldsymbol{x}}_k \leq -\alpha_3(|\boldsymbol{x}_k|) < 0 \end{aligned} \tag{5.42}$$

where $\alpha_3 \in \mathcal{K}_\infty$ by Definition 6.

This proves the theorem. $\square$

5.2.3 Regulation Problem of CD-SDRE

In order to provide an algorithm for the D-SDRE with constraints on the states and the control inputs, we define the problem first. Consider the discrete-time nonlinear control-affine system (5.2), described by using the nonlinear difference equation. Then, we want to design the D-SDRE state feedback controller $\boldsymbol{u}(\boldsymbol{x}_k)$ as in (5.9) such that the performance index is minimized:

$$J(\boldsymbol{x}_0, \boldsymbol{\mu}(\cdot)) := \sum_{j=k}^{k+N-1} \boldsymbol{x}_j^\top \boldsymbol{Q}(\boldsymbol{x}_j)\boldsymbol{x}_j + \boldsymbol{u}_j^\top \boldsymbol{R}(\boldsymbol{x}_j)\boldsymbol{u}_j \tag{5.43}$$

$$\text{s.t.} \quad \boldsymbol{x}_{k+1} = \boldsymbol{f}(\boldsymbol{x}_k) + \boldsymbol{B}(\boldsymbol{x}_k)\boldsymbol{u}_k,\ \ \boldsymbol{x}(0) = \boldsymbol{x}_0$$

$$\boldsymbol{x}_k \in \mathbb{X},\ \ \boldsymbol{u}_k \in \mathbb{U}\ \ \forall k \in \mathbb{Z}_{\geq 0}$$

where $\mathbb{X}$ and $\mathbb{U}$ are closed, bounded, and convex, and contain the origins in their interiors.

Then, Table 5.1 shows the algorithm of the CD-SDRE technique.

Notice that the algorithm in Table 5.1 is for the regulation problem where the reference is assumed to be constant. It can be extended to the case where the reference is time-varying; the algorithm in Table 5.2 introduced in the next section shows the reference tracking problem with constraints on states and control

Table 5.1: Algorithm of CD-SDRE (Regulation Problem)

1. ***Define sets and variables.***
2. Define $\mathbb{X} \subseteq \mathcal{X} \subseteq X \subseteq \mathbb{R}^n$ and $\mathbb{U} \subseteq U \subseteq \mathbb{R}^m$.
3. Define N.
4. For $k = 0 : 1 : k_f - 1$
5. Generate $\boldsymbol{u}_k, \cdots, \boldsymbol{u}_{k+N-1}$ that minimize (5.43).
6. Obtain estimates of $\boldsymbol{x}_{k+1}, \cdots, \boldsymbol{x}_{k+N}$ from Line 5.
7. Solve (5.10) to obtain $\boldsymbol{P}_{k+1}, \cdots, \boldsymbol{P}_{k+N}$.
8. Calculate $\boldsymbol{u}_k (:= \boldsymbol{u}(\boldsymbol{x}_k)), \boldsymbol{u}_{k+1}, \cdots, \boldsymbol{u}_{k+N-1}$ by using (5.9).
9. Apply $\boldsymbol{u}_k, \boldsymbol{u}_{k+1}, \cdots, \boldsymbol{u}_{k+N}$ to (5.2).
10. If $\boldsymbol{x}_k \in \mathbb{X}\ \forall k \in \mathbb{Z}_{k+1:k+N+1}$ in Line 9 and $\boldsymbol{u}_k \in \mathbb{U}\ \forall k \in \mathbb{Z}_{k:k+N}$ in Line 8
11. Choose $\boldsymbol{u}_k$ from Line 8.
12. Else
13. Choose $\boldsymbol{u}_k$ from Line 5.
14. End
15. End

inputs.

5.2.4 Reference Tracking Problem of CD-SDRE

We have discussed a regulation problem of CD-SDRE. In this part, we will design a tracking controller by using D-SDRE/CD-SDRE. It is assumed that we have a nonlinear control-affine difference system:

$$\boldsymbol{x}_{k+1} = \boldsymbol{f}(\boldsymbol{x}_k) + \boldsymbol{B}(\boldsymbol{x}_k)\boldsymbol{u}_k = \boldsymbol{A}(\boldsymbol{x}_k)\boldsymbol{x}_k + \boldsymbol{B}(\boldsymbol{x}_k)\boldsymbol{u}_k. \tag{5.44}$$

The purpose of the controller is to make the states $\boldsymbol{x}_k$ follow the references $\boldsymbol{x}_{d,k}$. In this case, a performance index to be minimized can be expressed as

$$J_0 := \frac{1}{2}\sum_{j=k}^{k+N-1} \left(\boldsymbol{x}_j - \boldsymbol{x}_{d,j}\right)^\top \boldsymbol{Q}(\boldsymbol{x}_j)\left(\boldsymbol{x}_j - \boldsymbol{x}_{d,j}\right) + \boldsymbol{u}_j^\top \boldsymbol{R}(\boldsymbol{x}_j)\boldsymbol{u}_j. \tag{5.45}$$

From (5.44), the Hamiltonian is expressed with the costate $\boldsymbol{\lambda} \in \mathbb{R}^n$:

$$\mathcal{H}_k := \frac{1}{2}\left(\left(\boldsymbol{x}_k - \boldsymbol{x}_{d,k}\right)^\top \boldsymbol{Q}(\boldsymbol{x}_k)\left(\boldsymbol{x}_k - \boldsymbol{x}_{d,k}\right) + \boldsymbol{u}_k^\top \boldsymbol{R}(\boldsymbol{x}_k)\boldsymbol{u}_k\right) + \boldsymbol{\lambda}_{k+1}^\top\left(\boldsymbol{f}(\boldsymbol{x}_k) + \boldsymbol{B}(\boldsymbol{x}_k)\boldsymbol{u}_k\right). \tag{5.46}$$

For the optimality condition (Kirk, 1970; Lewis et al., 2012) of the discrete-time system, we have three conditions:

1. State equation:

$$\boldsymbol{x}_{k+1} = \frac{\partial \mathcal{H}_k}{\partial \boldsymbol{\lambda}_{k+1}} = \boldsymbol{f}(\boldsymbol{x}) + \boldsymbol{B}(\boldsymbol{x}_k)\boldsymbol{u}_k = \boldsymbol{A}(\boldsymbol{x}_k)\boldsymbol{x}_k + \boldsymbol{B}(\boldsymbol{x}_k)\boldsymbol{u}_k. \tag{5.47}$$

2. Costate equation:

$$\begin{aligned}\boldsymbol{\lambda}_k = \frac{\partial \mathcal{H}_k}{\partial \boldsymbol{x}_k} &= \underbrace{\left(\boldsymbol{Q}(\boldsymbol{x}_k)\left(\boldsymbol{x}_k - \boldsymbol{x}_{d,k}\right) + \frac{1}{2}\left(\boldsymbol{x}_k - \boldsymbol{x}_{d,k}\right)^\top \frac{\partial \boldsymbol{Q}(\boldsymbol{x}_k)}{\partial \boldsymbol{x}_k}\left(\boldsymbol{x}_k - \boldsymbol{x}_{d,k}\right) + \frac{1}{2}\boldsymbol{u}_k^\top \frac{\partial \boldsymbol{R}(\boldsymbol{x}_k)}{\partial \boldsymbol{x}_k}\boldsymbol{u}_k\right)}_{=:\bar{\boldsymbol{Q}}} \\ &\quad + \left(\frac{\partial \boldsymbol{f}(\boldsymbol{x}_k)}{\partial \boldsymbol{x}_k} + \frac{\partial \boldsymbol{B}(\boldsymbol{x}_k)}{\boldsymbol{x}_k}\boldsymbol{u}_k\right)^\top \boldsymbol{\lambda}_{k+1} \\ &= \bar{\boldsymbol{Q}} + \underbrace{\left(\boldsymbol{A}(\boldsymbol{x}_k) + \frac{\partial \boldsymbol{A}(\boldsymbol{x}_k)}{\partial \boldsymbol{x}_k}\boldsymbol{x}_k + \frac{\partial \boldsymbol{B}(\boldsymbol{x}_k)}{\boldsymbol{x}_k}\boldsymbol{u}_k\right)^\top}_{=:\bar{\boldsymbol{A}}^\top(\boldsymbol{x}_k)} \boldsymbol{\lambda}_{k+1}. \end{aligned} \tag{5.48}$$

3. Stationary condition:

$$\boldsymbol{0} = \frac{\partial \mathcal{H}_k}{\partial \boldsymbol{u}_k} = \boldsymbol{R}(\boldsymbol{x}_k)\boldsymbol{u}_k + \boldsymbol{B}^\top(\boldsymbol{x}_k)\boldsymbol{\lambda}_{k+1}. \tag{5.49}$$

In order to find the optimal controller to handle the states and desired trajectories, it is reasonable to assume that the costate can be expressed by using two unknown variables as (Lewis et al., 2012)

$$\boldsymbol{\lambda}_k = \boldsymbol{P}_k \boldsymbol{x}_k - \boldsymbol{w}_k. \tag{5.50}$$

Then, the optimal controller is derived from (5.49),

$$\begin{aligned}\boldsymbol{u}_k &= -\boldsymbol{R}^{-1}(\boldsymbol{x}_k)\boldsymbol{B}^\top(\boldsymbol{x}_k)\boldsymbol{\lambda}_{k+1} = -\boldsymbol{R}^{-1}(\boldsymbol{x}_k)\boldsymbol{B}^\top(\boldsymbol{x}_k)\left(\boldsymbol{P}_{k+1}\boldsymbol{x}_{k+1} - \boldsymbol{w}_{k+1}\right) \\ &= -\boldsymbol{R}^{-1}(\boldsymbol{x}_k)\boldsymbol{B}^\top(\boldsymbol{x}_k)\boldsymbol{P}_{k+1}\left(\boldsymbol{A}(\boldsymbol{x}_k)\boldsymbol{x}_k + \boldsymbol{B}(\boldsymbol{x}_k)\boldsymbol{u}_k\right) + \boldsymbol{R}^{-1}(\boldsymbol{x}_k)\boldsymbol{B}^\top(\boldsymbol{x}_k)\boldsymbol{w}_{k+1}. \end{aligned} \tag{5.51}$$

Therefore, the optimal controller in (5.51) becomes

$$\begin{aligned}\boldsymbol{u}_k &= \left(\boldsymbol{R}(\boldsymbol{x}_k) + \boldsymbol{B}^\top(\boldsymbol{x}_k)\boldsymbol{P}_{k+1}\boldsymbol{B}(\boldsymbol{x}_k)\right)^{-1}\boldsymbol{B}^\top(\boldsymbol{x}_k)\left(-\boldsymbol{P}_{k+1}\boldsymbol{A}(\boldsymbol{x}_k)\boldsymbol{x}_k + \boldsymbol{w}_{k+1}\right) \\ &= -\underbrace{\left(\boldsymbol{R}(\boldsymbol{x}_k) + \boldsymbol{B}^\top(\boldsymbol{x}_k)\boldsymbol{P}_{k+1}\boldsymbol{B}(\boldsymbol{x}_k)\right)^{-1}\boldsymbol{B}^\top(\boldsymbol{x}_k)\boldsymbol{P}_{k+1}\boldsymbol{A}(\boldsymbol{x}_k)}_{=:\boldsymbol{K}_x(\boldsymbol{x}_k)}\boldsymbol{x}_k \\ &\quad + \underbrace{\left(\boldsymbol{R}(\boldsymbol{x}_k) + \boldsymbol{B}^\top(\boldsymbol{x}_k)\boldsymbol{P}_{k+1}\boldsymbol{B}(\boldsymbol{x}_k)\right)^{-1}\boldsymbol{B}^\top(\boldsymbol{x}_k)}_{=:\boldsymbol{K}_{\boldsymbol{w}}(\boldsymbol{x}_k)}\boldsymbol{w}_{k+1} \\ &= -\boldsymbol{K}_x(\boldsymbol{x}_k)\boldsymbol{x}_k + \boldsymbol{K}_{\boldsymbol{w}}(\boldsymbol{x}_k)\boldsymbol{w}_{k+1}. \end{aligned} \tag{5.52}$$

It should be noted from (5.52) that values of $\boldsymbol{P}_{k+1}$ and $\boldsymbol{\omega}_{k+1}$ are needed to determine $\boldsymbol{u}_k$. Thus, equations for obtaining $\boldsymbol{P}_{k+1}$ and $\boldsymbol{\omega}_{k+1}$ are essential. The equations are obtained as follows. Substituting the first equation in (5.51) into (5.44) yields

$$\begin{aligned}\boldsymbol{x}_{k+1} &= \boldsymbol{A}(\boldsymbol{x}_k)\boldsymbol{x}_k + \boldsymbol{B}(\boldsymbol{x}_k)\boldsymbol{u}_k \\ &= \boldsymbol{A}(\boldsymbol{x}_k)\boldsymbol{x}_k + \boldsymbol{B}(\boldsymbol{x}_k)\left(-\boldsymbol{R}^{-1}(\boldsymbol{x}_k)\boldsymbol{B}^\top(\boldsymbol{x}_k)\boldsymbol{P}_{k+1}\boldsymbol{x}_{k+1} + \boldsymbol{R}^{-1}(\boldsymbol{x}_k)\boldsymbol{B}^\top(\boldsymbol{x}_k)\boldsymbol{w}_{k+1}\right) \\ &= \boldsymbol{A}(\boldsymbol{x}_k)\boldsymbol{x}_k - \boldsymbol{B}(\boldsymbol{x}_k)\boldsymbol{R}^{-1}(\boldsymbol{x}_k)\boldsymbol{B}^\top(\boldsymbol{x}_k)\boldsymbol{P}_{k+1}\boldsymbol{x}_{k+1} + \boldsymbol{B}(\boldsymbol{x}_k)\boldsymbol{R}^{-1}(\boldsymbol{x}_k)\boldsymbol{B}^\top(\boldsymbol{x}_k)\boldsymbol{w}_{k+1}. \end{aligned} \tag{5.53}$$

Finally, the closed-loop nonlinear difference system becomes

$$\boldsymbol{x}_{k+1} = \left(\boldsymbol{I} + \boldsymbol{B}(\boldsymbol{x}_k)\boldsymbol{R}^{-1}(\boldsymbol{x}_k)\boldsymbol{B}^\top(\boldsymbol{x}_k)\boldsymbol{P}_{k+1}\right)^{-1}\left(\boldsymbol{A}(\boldsymbol{x}_k)\boldsymbol{x}_k + \boldsymbol{B}(\boldsymbol{x}_k)\boldsymbol{R}^{-1}(\boldsymbol{x}_k)\boldsymbol{B}^\top(\boldsymbol{x}_k)\boldsymbol{w}_{k+1}\right) \tag{5.54}$$

where $\boldsymbol{I} \in \mathbb{R}^{n\times n}$ is the identity matrix.

By substituting (5.54) into the costate equation in (5.48), the equations for $\boldsymbol{P}_k$ and $\boldsymbol{\omega}_k$ are obtained:

$$\begin{aligned}\boldsymbol{\lambda}_k &= \bar{\boldsymbol{Q}} + \bar{\boldsymbol{A}}^\top(\boldsymbol{x}_k)\left(\boldsymbol{P}_{k+1}\boldsymbol{x}_{k+1} - \boldsymbol{w}_{k+1}\right) \\ &= \bar{\boldsymbol{Q}} + \bar{\boldsymbol{A}}^\top(\boldsymbol{x}_k)\boldsymbol{P}_{k+1}\left(\boldsymbol{I} + \boldsymbol{B}(\boldsymbol{x}_k)R^{-1}(\boldsymbol{x}_k)\boldsymbol{B}^\top(\boldsymbol{x}_k)\boldsymbol{P}_{k+1}\right)^{-1}\left(\boldsymbol{A}(\boldsymbol{x}_k)\boldsymbol{x}_k\right. \\ &\quad \left. + \boldsymbol{B}(\boldsymbol{x}_k)\boldsymbol{R}^{-1}(\boldsymbol{x}_k)\boldsymbol{B}^\top(\boldsymbol{x}_k)\boldsymbol{w}_{k+1}\right) - \bar{\boldsymbol{A}}^\top(\boldsymbol{x}_k)\boldsymbol{w}_{k+1}. \end{aligned} \tag{5.55}$$

Substituting (5.50) into (5.55) and rearranging it yields

$$\begin{aligned}&\boldsymbol{Q}(\boldsymbol{x}_k)\boldsymbol{x}_k - \boldsymbol{Q}(\boldsymbol{x}_k)\boldsymbol{x}_{d,k} + \frac{1}{2}\left(\boldsymbol{x}_k - \boldsymbol{x}_{d,k}\right)^\top \frac{\partial \boldsymbol{Q}(\boldsymbol{x}_k)}{\partial \boldsymbol{x}_k}\left(\boldsymbol{x}_k - \boldsymbol{x}_{d,k}\right) + \frac{1}{2}\boldsymbol{u}_k^\top \frac{\partial \boldsymbol{R}(\boldsymbol{x}_k)}{\partial \boldsymbol{x}_k}\boldsymbol{u}_k \\ &+ \bar{\boldsymbol{A}}^\top(\boldsymbol{x}_k)\boldsymbol{P}_{k+1}\left(\boldsymbol{I} + \boldsymbol{B}(\boldsymbol{x}_k)\boldsymbol{R}^{-1}(\boldsymbol{x}_k)\boldsymbol{B}^\top(\boldsymbol{x}_k)\boldsymbol{P}_{k+1}\right)^{-1}\boldsymbol{A}(\boldsymbol{x}_k)\boldsymbol{x}_k \\ &+ \bar{\boldsymbol{A}}^\top(\boldsymbol{x}_k)\boldsymbol{P}_{k+1}\left(\boldsymbol{I} + \boldsymbol{B}(\boldsymbol{x}_k)\boldsymbol{R}^{-1}(\boldsymbol{x}_k)\boldsymbol{B}^\top(\boldsymbol{x}_k)\boldsymbol{P}_{k+1}\right)^{-1}\boldsymbol{B}(\boldsymbol{x}_k)\boldsymbol{R}^{-1}(\boldsymbol{x}_k)\boldsymbol{B}^\top(\boldsymbol{x}_k)\boldsymbol{w}_{k+1} \\ &- \bar{\boldsymbol{A}}^\top(\boldsymbol{x}_k)\boldsymbol{w}_{k+1} = \boldsymbol{P}_k\boldsymbol{x}_k - \boldsymbol{w}_k. \end{aligned} \tag{5.56}$$

Therefore, $\boldsymbol{P}_k$ and $\boldsymbol{w}_k$ can be found from (5.56) backwards with the conditions of $\boldsymbol{P}_N = \boldsymbol{0}$ and $\boldsymbol{w}_N = \boldsymbol{0}$:

$$\boldsymbol{P}_k = \boldsymbol{Q}(\boldsymbol{x}_k) + \bar{\boldsymbol{A}}^\top(\boldsymbol{x}_k)\boldsymbol{P}_{k+1}\left(\boldsymbol{I} + \boldsymbol{B}(\boldsymbol{x}_k)\boldsymbol{R}^{-1}(\boldsymbol{x}_k)\boldsymbol{B}^\top(\boldsymbol{x}_k)\boldsymbol{P}_{k+1}\right)^{-1}\boldsymbol{A}(\boldsymbol{x}_k) \tag{5.57}$$

$$\begin{aligned}\boldsymbol{w}_k = \boldsymbol{Q}(\boldsymbol{x}_k)\boldsymbol{x}_{d,k} - \frac{1}{2}\left(\boldsymbol{x}_k - \boldsymbol{x}_{d,k}\right)^\top \frac{\partial \boldsymbol{Q}(\boldsymbol{x}_k)}{\partial \boldsymbol{x}_k}\left(\boldsymbol{x}_k - \boldsymbol{x}_{d,k}\right) - \frac{1}{2}\boldsymbol{u}_k^\top \frac{\partial \boldsymbol{R}(\boldsymbol{x}_k)}{\partial \boldsymbol{x}_k}\boldsymbol{u}_k + \Big(\bar{\boldsymbol{A}}^\top(\boldsymbol{x}_k) \\ - \bar{\boldsymbol{A}}^\top(\boldsymbol{x}_k)\boldsymbol{P}_{k+1}\left(\boldsymbol{I} + \boldsymbol{B}(\boldsymbol{x}_k)\boldsymbol{R}^{-1}(\boldsymbol{x}_k)\boldsymbol{B}^\top(\boldsymbol{x}_k)\boldsymbol{P}_{k+1}\right)^{-1}\boldsymbol{B}(\boldsymbol{x}_k)\boldsymbol{R}^{-1}(\boldsymbol{x}_k)\boldsymbol{B}^\top(\boldsymbol{x}_k)\Big)\boldsymbol{w}_{k+1}.\end{aligned} \tag{5.58}$$

We summarized the CD-SDRE for the reference tracking in Table 5.2.

5.2.5 Extension to a Multi-Agent System

So far, we designed the D-SDRE controller for a single system. In this part, we extend it to a multi-agent system. For notational simplicity, we will omit the time k from the following equations unless otherwise needed for clarification. It is supposed that a specific agent, say jth agent, can communicate with other agents in the networked system, comprised of p agents. Then, the controller for the jth agent can be designed as follows:

$$\boldsymbol{u}_j = -\boldsymbol{K}_{\boldsymbol{x}_j}(\boldsymbol{x}_j)\boldsymbol{x}_j + \boldsymbol{K}_{\boldsymbol{\omega}_j}(\boldsymbol{x}_j)\boldsymbol{\omega}_j + \sum_{l\in\mathcal{N}_j, l\neq j}\left(\boldsymbol{K}_{\boldsymbol{x}_l}\boldsymbol{x}_l - \boldsymbol{K}_{\boldsymbol{\omega}_l}\boldsymbol{\omega}_l\right) \tag{5.59}$$

where $\mathcal{N}_j \subset \mathbb{Z}_{1:p}$ denotes a set containing the indices for the agents communicating with the jth agent in the networked system.

It should be emphasized that (5.59) can be reformulated to see tracking and diffusive coupling terms for synchronization of the motions among the agents:

$$\begin{aligned}\boldsymbol{u}_j = &\underbrace{-\left(\boldsymbol{K}_{\boldsymbol{x}_j}(\boldsymbol{x}_j) - \sum_{l\in\mathcal{N}_j, l\neq j}\boldsymbol{K}_{\boldsymbol{x}_l}\right)\boldsymbol{x}_j + \left(\boldsymbol{K}_{\boldsymbol{\omega}_j}(\boldsymbol{x}_j) - \sum_{l\in\mathcal{N}_j, l\neq j}\boldsymbol{K}_{\boldsymbol{\omega}_l}\right)\boldsymbol{\omega}_j}_{\text{tracking control}} \\ &\underbrace{+\sum_{l\in\mathcal{N}_j, l\neq j}\boldsymbol{K}_{\boldsymbol{x}_l}\left(\boldsymbol{x}_l - \boldsymbol{x}_j\right) - \sum_{l\in\mathcal{N}_j, l\neq j}\boldsymbol{K}_{\boldsymbol{\omega}_l}\left(\boldsymbol{\omega}_l - \boldsymbol{\omega}_j\right)}_{\text{synchronization}}.\end{aligned} \tag{5.60}$$

It is important to emphasize that the diffusive coupling gains $\boldsymbol{K}_{\boldsymbol{x}_l}$ and $\boldsymbol{K}_{\boldsymbol{\omega}_l}$ are chosen such that the tracking

Table 5.2: Algorithm of CD-SDRE (Tracking Problem)

1. ***Define sets and variables.***
2. Define $\mathbb{X} \subseteq \mathcal{X} \subseteq X \subseteq \mathbb{R}^n$ and $\mathbb{U} \subseteq U \subseteq \mathbb{R}^m$.
3. Define N.
4. For $k = 0 : 1 : k_f - 1$
5. Generate $\boldsymbol{u}_k, \cdots, \boldsymbol{u}_{k+N-1}$ that minimize (5.45).
6. Obtain estimates of $\boldsymbol{x}_{k+1}, \cdots, \boldsymbol{x}_{k+N}$ from Line 5.
7. Solve (5.57) and (5.58) to obtain $\boldsymbol{P}_{k+1}, \cdots, \boldsymbol{P}_{k+N}$ and $\boldsymbol{\omega}_{k+1}, \cdots, \boldsymbol{\omega}_{k+N}$.
8. Calculate $\boldsymbol{u}_k (:= \boldsymbol{u}(\boldsymbol{x}_k)), \boldsymbol{u}_{k+1}, \cdots, \boldsymbol{u}_{k+N-1}$ by using (5.52).
9. Apply $\boldsymbol{u}_k, \boldsymbol{u}_{k+1}, \cdots, \boldsymbol{u}_{k+N}$ to (5.44).
10. If $\boldsymbol{x}_k \in \mathbb{X}\ \forall k \in \mathbb{Z}_{k+1:k+N+1}$ in Line 9 and $\boldsymbol{u}_k \in \mathbb{U}\ \forall k \in \mathbb{Z}_{k:k+N}$ in Line 8
11. Choose $\boldsymbol{u}_k$ from Line 8.
12. Else
13. Choose $\boldsymbol{u}_k$ from Line 5.
14. End
15. End

control signal in (5.60) is guaranteed to exist. One way to choose them is using $\boldsymbol{K}_{\boldsymbol{x}_j}$ and $\boldsymbol{K}_{\boldsymbol{\omega}_j}$:

$$\boldsymbol{K}_{\boldsymbol{x}_l} = \frac{1}{1+\mathrm{card}(\mathcal{N}_j)}\boldsymbol{K}_{\boldsymbol{x}_j}(\boldsymbol{x}_j) \quad \text{and} \quad \boldsymbol{K}_{\boldsymbol{\omega}_l} = \frac{1}{1+\mathrm{card}(\mathcal{N}_j)}\boldsymbol{K}_{\boldsymbol{\omega}_j}(\boldsymbol{x}_j) \tag{5.61}$$

where $\mathrm{card}(\cdot)$ is the cardinality of the set. For example, if a bi-direction ring structure array is assumed for the networked system, $\boldsymbol{K}_{\boldsymbol{x}_l} = \frac{1}{3}\boldsymbol{K}_{\boldsymbol{x}_j}$ and $\boldsymbol{K}_{\boldsymbol{\omega}_l} = \frac{1}{3}\boldsymbol{K}_{\boldsymbol{\omega}_j}$, the tracking term of the controller in (5.60) becomes $\boldsymbol{u}_j = -\frac{1}{3}\boldsymbol{K}_{\boldsymbol{x}_j}(\boldsymbol{x}_j)\boldsymbol{x}_j + \frac{1}{3}\boldsymbol{K}_{\boldsymbol{\omega}_j}(\boldsymbol{x}_j)\boldsymbol{\omega}_j$.

By substituting (5.59) into (5.44), the closed-loop equation for the jth agent is expressed as:

$$\boldsymbol{x}_j^+ = \Bigg(\underbrace{\boldsymbol{A}_j(\boldsymbol{x}_j) - \boldsymbol{B}_j(\boldsymbol{x}_j)\boldsymbol{K}_{\boldsymbol{x}_j}(\boldsymbol{x}_j)}_{=:\boldsymbol{A}_{\mathrm{cl},j}(\boldsymbol{x}_j)}\Bigg)\boldsymbol{x}_j + \boldsymbol{B}_j(\boldsymbol{x}_j)\boldsymbol{K}_{\boldsymbol{\omega}_j}\boldsymbol{\omega}_j + \boldsymbol{B}_j(\boldsymbol{x}_j)\sum_{l\in\mathcal{N}_j, l\neq j}\boldsymbol{K}_{\boldsymbol{x}_l}\boldsymbol{x}_l - \boldsymbol{K}_{\boldsymbol{\omega}_l}\boldsymbol{\omega}_l \tag{5.62}$$

Therefore, from (5.62), the multi-agent system with p agents can be expressed in a matrix form as

$$\begin{aligned}\begin{bmatrix}\boldsymbol{x}_1\\ \boldsymbol{x}_2\\ \vdots\\ \boldsymbol{x}_p\end{bmatrix}^+ &= \begin{bmatrix}\boldsymbol{A}_{\mathrm{cl},1}(\boldsymbol{x}_1) & \delta_{1,2}\boldsymbol{B}_1(\boldsymbol{x}_1)\boldsymbol{K}_{\boldsymbol{x}_2} & \cdots & \delta_{1,p}\boldsymbol{B}_1(\boldsymbol{x}_1)\boldsymbol{K}_{\boldsymbol{x}_p}\\ \delta_{2,1}\boldsymbol{B}_2(\boldsymbol{x}_2)\boldsymbol{K}_{\boldsymbol{x}_1} & \boldsymbol{A}_{\mathrm{cl},2}(\boldsymbol{x}_2) & \cdots & \delta_{2,p}\boldsymbol{B}_2(\boldsymbol{x}_2)\boldsymbol{K}_{\boldsymbol{x}_p}\\ \vdots & \vdots & \ddots & \vdots\\ \delta_{p,1}\boldsymbol{B}_p(\boldsymbol{x}_p)\boldsymbol{K}_{\boldsymbol{x}_1} & \delta_{p,2}\boldsymbol{B}_p(\boldsymbol{x}_p)\boldsymbol{K}_{\boldsymbol{x}_2} & \cdots & \boldsymbol{A}_{\mathrm{cl},p}(\boldsymbol{x}_p)\end{bmatrix}\begin{bmatrix}\boldsymbol{x}_1\\ \boldsymbol{x}_2\\ \vdots\\ \boldsymbol{x}_p\end{bmatrix}\\ &+ \begin{bmatrix}\boldsymbol{B}_1(\boldsymbol{x}_1)\boldsymbol{K}_{\boldsymbol{\omega}_1} & -\delta_{1,2}\boldsymbol{B}_1(\boldsymbol{x}_1)\boldsymbol{K}_{\boldsymbol{\omega}_2} & \cdots & -\delta_{1,p}\boldsymbol{B}_1(\boldsymbol{x}_1)\boldsymbol{K}_{\boldsymbol{\omega}_p}\\ -\delta_{2,1}\boldsymbol{B}_2(\boldsymbol{x}_2)\boldsymbol{K}_{\boldsymbol{\omega}_1} & \boldsymbol{B}_2(\boldsymbol{x}_2)\boldsymbol{K}_{\boldsymbol{\omega}_2} & \cdots & -\delta_{2,p}\boldsymbol{B}_2(\boldsymbol{x}_2)\boldsymbol{K}_{\boldsymbol{\omega}_p}\\ \vdots & \vdots & \ddots & \vdots\\ -\delta_{p,1}\boldsymbol{B}_p(\boldsymbol{x}_p)\boldsymbol{K}_{\boldsymbol{\omega}_1} & -\delta_{p,1}\boldsymbol{B}_p(\boldsymbol{x}_p)\boldsymbol{K}_{\boldsymbol{\omega}_2} & \cdots & \boldsymbol{B}_p(\boldsymbol{x}_p)\boldsymbol{K}_{\boldsymbol{\omega}_p}\end{bmatrix}\begin{bmatrix}\boldsymbol{\omega}_1\\ \boldsymbol{\omega}_2\\ \vdots\\ \boldsymbol{\omega}_p\end{bmatrix}\end{aligned} \tag{5.63}$$

or in a simpler form as

$$\boldsymbol{x}^+ = \boldsymbol{A}_{\mathrm{cl}}(\boldsymbol{x})\boldsymbol{x} + \boldsymbol{G}(\boldsymbol{x})\boldsymbol{\omega} \tag{5.64}$$

where $\delta_{j,l} = 1$ if $l \in \mathcal{N}_j$, otherwise $\delta_{j,l} = 0$ for the jth agent ($1 \leq j \leq p$).

Stability Analysis

It should be noted that the D-SDRE feedback controller is stabilizing the discrete-time nonlinear difference equation in (5.1) or (5.2). In this part, we investigate the stability of the D-SDRE controller. We use the

following assumption for the stability analysis.

Assumption 15 *The desired trajectory $\boldsymbol{x}_d$ can be expressed as*

$$\boldsymbol{x}_d^+ = \boldsymbol{A}_m(\boldsymbol{x}_d, k)\boldsymbol{x}_d + \boldsymbol{G}_m(\boldsymbol{x}_d, k)\boldsymbol{\omega}_d \tag{5.65}$$

where $\boldsymbol{A}_m(\boldsymbol{x}_d, k) \in \mathbb{X}^{p\times p}$, $\boldsymbol{G}_m(\boldsymbol{x}_d, k) \in \mathbb{X}^{p\times p}$, and $\boldsymbol{\omega}_d \in \mathbb{X}^p$.

Lemma 16 *Given $\boldsymbol{A}_{\rm cl}(\boldsymbol{x})$ in (5.64) for all $\boldsymbol{x} \in \mathbb{X}^p$, there exist $\boldsymbol{M} = \boldsymbol{M}^\top > \boldsymbol{0}$ and $\rho_A > 0$ such that*

$$\boldsymbol{A}_{\rm cl}^\top(\boldsymbol{x})\boldsymbol{M}\boldsymbol{A}_{\rm cl} - \boldsymbol{M} < -\boldsymbol{D} \leq -\rho_A \boldsymbol{I} \tag{5.66}$$

for some $\boldsymbol{D} = \boldsymbol{D}^\top > 0$.

Proof A proof can be straightforwardly obtained from Theorem 7. □

Theorem 17 *Suppose the networked system comprised of p agents expressed in (5.64) is controlled with the tracking/synchronization controller in (5.59). Then, the networked system is ISS in its ROA.*

Proof Suppose such $\boldsymbol{M} = \boldsymbol{M}^\top > \boldsymbol{0}$ exists from Lemma 16. Then, the Lyapunov function candidate V for (5.64) is defined as

$$V(\boldsymbol{e}) := (\boldsymbol{x} - \boldsymbol{x}_d)^\top \boldsymbol{M} (\boldsymbol{x} - \boldsymbol{x}_d) = \boldsymbol{e}^\top \boldsymbol{M}\boldsymbol{e} > 0 \tag{5.67}$$

where $\boldsymbol{e} := \boldsymbol{x} - \boldsymbol{x}_d$.

Therefore,

$$\begin{aligned}
V(\boldsymbol{e}^+) - V(\boldsymbol{e}) &= \left(\boldsymbol{x}^+ - \boldsymbol{x}_d^+\right)^\top \boldsymbol{M} \left(\boldsymbol{x}^+ - \boldsymbol{x}_d^+\right) - \boldsymbol{e}^\top \boldsymbol{M}\boldsymbol{e} \\
&= \Big(\boldsymbol{A}_{\rm cl}(\boldsymbol{x})\boldsymbol{x} + \boldsymbol{G}(\boldsymbol{x})\boldsymbol{\omega} - \boldsymbol{A}_m(\boldsymbol{x}_d, k)\boldsymbol{x}_d - \boldsymbol{G}_m(\boldsymbol{x}_d, k)\boldsymbol{\omega}_d\Big)^\top \boldsymbol{M}\Big(\boldsymbol{A}_{\rm cl}(\boldsymbol{x})\boldsymbol{x} \\
&\quad + \boldsymbol{G}(\boldsymbol{x})\boldsymbol{\omega} - \boldsymbol{A}_m(\boldsymbol{x}_d, k)\boldsymbol{x}_d - \boldsymbol{G}_m(\boldsymbol{x}_d, k)\boldsymbol{\omega}_d\Big) - \boldsymbol{e}^\top \boldsymbol{M}\boldsymbol{e} \\
&= \boldsymbol{e}^\top \boldsymbol{A}_{\rm cl}^\top(\boldsymbol{x})\boldsymbol{M}\boldsymbol{A}_{\rm cl}(\boldsymbol{x})\boldsymbol{e} - \boldsymbol{e}^\top \boldsymbol{M}\boldsymbol{e} + \boldsymbol{\eta}^\top \boldsymbol{J} \otimes \boldsymbol{M}\boldsymbol{\eta} \\
&\leq -\rho_A \|\boldsymbol{e}\|_2 + \lambda_{\max}\big(\boldsymbol{J} \otimes \boldsymbol{M}\big)\|\boldsymbol{\eta}\|_2
\end{aligned} \tag{5.68}$$

where $\otimes$ denotes the Kronecker product, $\lambda_{\max}\big(\cdot\big)$ the maximum eigenvalue, $\boldsymbol{\eta} := \left[\boldsymbol{e}_{\boldsymbol{x}}^\top \ \boldsymbol{e}_{\boldsymbol{\omega}}^\top \ \boldsymbol{e}_{\boldsymbol{A}}^\top \ \boldsymbol{e}_{\boldsymbol{G}}^\top\right]^\top$, $\boldsymbol{e}_{\boldsymbol{x}} :=$

$\boldsymbol{A}_{\rm cl}(\boldsymbol{x})\big(\boldsymbol{x}-\boldsymbol{x}_d\big)$, $\boldsymbol{e}_{\boldsymbol{\omega}} := \boldsymbol{G}(\boldsymbol{x})\big(\boldsymbol{\omega}-\boldsymbol{\omega}_d\big)$, $\boldsymbol{e}_{\boldsymbol{A}} := \big(\boldsymbol{A}_{\rm cl}(\boldsymbol{x})-\boldsymbol{A}_m(\boldsymbol{x}_d,k)\big)\boldsymbol{x}_d$, $\boldsymbol{e}_{\boldsymbol{G}} := \big(\boldsymbol{G}(\boldsymbol{x})-\boldsymbol{G}_m(\boldsymbol{x}_d,k)\big)\boldsymbol{\omega}_d$, and $\boldsymbol{J} := \begin{bmatrix} \boldsymbol{0}_{np} & \boldsymbol{I}_{np} & \boldsymbol{I}_{np} & \boldsymbol{I}_{np} \\ \boldsymbol{I}_{np} & \boldsymbol{I}_{np} & \boldsymbol{I}_{np} & \boldsymbol{I}_{np} \\ \boldsymbol{I}_{np} & \boldsymbol{I}_{np} & \boldsymbol{I}_{np} & \boldsymbol{I}_{np} \end{bmatrix}$ where $\boldsymbol{I}_{np}$ is the $np \times np$ identity matrix.
Hence, the system is ISS for all $\boldsymbol{x} \in \mathbb{X}^p$ by Definitions 1 and 2. Therefore, the error $\boldsymbol{e} = \boldsymbol{x} - \boldsymbol{x}_d$ converges to a ball with the radius of $\frac{\lambda_{\max}\left(\boldsymbol{J}\otimes\boldsymbol{M}\right)}{\rho_A}\|\boldsymbol{\eta}\|_2$. $\square$

5.3 Conclusions

In conclusion, this chapter has considered the discrete-time nonlinear system with constraints on states/inputs, which is a critical issue in designing a control system. In this chapter, we have introduced and discussed a new control framework that can effectively handle such huddles though the use of D-SDRE-based controller with a help of MPC, named CD-SDRE. The MPC plays an important role in CD-SDRE in two ways: it not only estimates the parameters of the CD-SDRE but also works as guidance of the controller. Rigorous analyses of the stability of D-SDRE and CD-SDRE via Lyapunov stability condition can help one understand the performance of the technique. Algorithms of the proposed CD-SDRE could give one solid understand of its mechanism.

We have shown the derivation and analysis of the proposed CD-SDRE controller in this section. In the next chapter, we evaluate it with challenging problems in spacecraft orbit reconfiguration.

Chapter 6

Application of CD-SDRE to Spacecraft Orbit Reconfiguration

THE use of CD-SDRE scheme in the presence of constraints is then systematically demonstrated by applying this scheme to problems of spacecraft formation orbit reconfiguration under limited actuation performance. Simulation results demonstrate the efficacy and reliability of the proposed CD-SDRE.

6.1 Introduction

Based on the development of the CD-SDRE controller in the previous chapter, we validate it with challenging problems in this chapter. In order to validate the proposed control method, we apply the proposed CD-SDRE controller to spacecraft orbit reconfiguration problems which has limited actuator performance. It is interesting to note that trajectory optimization techniques have been widely used for the reconfiguration problems (Scharf et al., 2003, 2004). However, many of the previous studies show that the optimization techniques are based on open-loop control methods which might be vulnerable to internal/external disturbances. Moreover, most of them are not real-time trajectory optimizers. In order to overcome such problems, numerous closed-loop tracking control methods have been suggested (Scharf et al., 2004). In this case, by using *a priori* designed reference trajectories, the control methods calculate proper control signals to make each spacecraft follows its reference.

However, depending on the size of orbits and initial conditions (positions and velocities of spacecraft), excessively large initial control inputs might be inevitable in the tracking control which are not desirable, since, in general, an actuation effort corresponding to a large control signal cannot be generated by a real thruster in a small spacecraft. Moreover, such improper control signals can make the motions of the spacecraft unstable. Therefore, the actuator saturation problem should be considered when designing control systems. Although the input saturation problem is prevalent in real systems, many of the advanced control methods cannot take it into account explicitly. For realistic results, high-fidelity dynamic models of orbits

for the reference and deputy spacecraft are derived in the presence of Earth oblateness (J_2 perturbation) and atmospheric drag. The simulations show the reliable results by using the proposed CD-SDRE technique.

The rest of the chapter is organized as follows: Detailed dynamic models of spacecraft orbit reconfiguration are provided in Section 6.2. In Section 6.3, simulation results are discussed. Finally, concluding remarks are made in Section 6.4.

6.2 Nonlinear Dynamic Models of Reference and Relative Orbits

In this Section, we will derive exact nonlinear dynamic models of a reference (i.e., chief spacecraft) and relative orbits (i.e., deputy spacecraft) in the presence of perturbations such as the Earth oblateness (J_2) and the atmospheric drag. For the notational brevity, the abbreviations $s_{(\cdot)} = \sin(\cdot),\ c_{(\cdot)} = \cos(\cdot)$ are used.

6.2.1 Nonlinear Dynamic Model for Reference Orbit (Chief Spacecraft)

The main disturbance sources we consider in this work are the J_2 perturbation and the atmospheric drag. The gravitational potential with J_2 perturbation can be expressed as (Vallado, 2007):

$$U = -\frac{\mu}{r} - \frac{\mathfrak{J}_2}{r^3}\left(\frac{1}{3} - s_\phi^2\right) \tag{6.1}$$

where μ, r, and ϕ are, respectively, the gravitational parameter, distance between the center of the Earth and the position of the object, and the geocentric latitude. $\mathfrak{J}_2 := \frac{3}{2}J_2\mu R_e^2$ where $J_2 = 1.0826267 \times 10^3$ and R_e is the radius of the Earth.

From (6.1), we can derive the gradient of the gravitational potential as

$$\nabla U = \frac{\mu}{r^2}\hat{R} + \frac{\mathfrak{J}_2}{r^4}\left(1 - 3s_i^2 s_\theta^2\right)\hat{R} + \frac{\mathfrak{J}_2 s_i^2 s_{2\theta}}{r^4}\hat{S} + \frac{\mathfrak{J}_2 s_{2i} s_\theta}{r^4}\hat{W} \tag{6.2}$$

where $\begin{bmatrix}\hat{R} & \hat{S} & \hat{W}\end{bmatrix}$ are the unit vectors for the RSW frame (i.e., $\hat{R}$, $\hat{S}$, and $\hat{W}$, respectively, denote the radial, alongtrack, and crosstrack directions). The direction of $\hat{W}$ is chosen by using the right-hand rule.

For the atmospheric drag (acceleration), we use the following form (Vallado, 2007):

$$\boldsymbol{F}_{\text{drag}} = -\frac{1}{2}\frac{C_D A}{m}\rho v_{\text{rel}}^2 \frac{\boldsymbol{v}_{\text{rel}}}{\|\boldsymbol{v}_{\text{rel}}\|} = -\frac{1}{2}\frac{C_D A}{m}\rho v_{\text{rel}}\boldsymbol{v}_{\text{rel}} \tag{6.3}$$

where C_D ($C_D \sim 2.0$ to 2.2), A, ρ, and m denote the coefficient of drag, cross-sectional area, atmospheric density, and the mass of the object, respectively. The vector $\boldsymbol{v}_{\text{rel}}$ is the velocity of the object relative to the Earth atmosphere expressed in the Earth-Centered Inertial (ECI) frame:

$$\boldsymbol{v}_{\text{rel}} = \frac{\mathrm{d}\boldsymbol{r}}{\mathrm{d}t} - \boldsymbol{\omega}_e \times \boldsymbol{r} \tag{6.4}$$

where $\boldsymbol{r}$ denotes the position of the object in the ECI frame, $\boldsymbol{\omega}_e$ the angular velocity of the rotating atmosphere with respect to the ECI frame.

Therefore, the governing equations under the J_2 perturbation and atmospheric drag can be obtained as

$$\begin{aligned}\ddot{\boldsymbol{r}} &= -\nabla U + \boldsymbol{F}_{\text{drag}} \\ &= -\frac{\mu}{r^2}\hat{R} - \frac{\mathfrak{J}_2}{r^4}\left(1 - 3s_i^2 s_\theta^2\right)\hat{R} - \frac{\mathfrak{J}_2 s_i^2 s_{2\theta}}{r^4}\hat{S} - \frac{\mathfrak{J}_2 s_{2i} s_\theta}{r^4}\hat{W} - \frac{1}{2}\frac{C_D A}{m}\rho v_{\text{rel}}\boldsymbol{R}\boldsymbol{v}_{\text{rel}}\end{aligned} \tag{6.5}$$

where $\boldsymbol{R}$ is the 3-1-3 Euler rotation matrix such that $[\mathrm{RSW}] = \boldsymbol{R}[\mathrm{ECI}]$, defined as

$$\boldsymbol{R}(\theta,\ i,\ \Omega) = \begin{bmatrix}\boldsymbol{R}_1 \\ \boldsymbol{R}_2 \\ \boldsymbol{R}_3\end{bmatrix} = \begin{bmatrix} c_\theta c_\Omega - s_\theta c_i s_\Omega & c_\theta s_\Omega + s_\theta c_i c_\Omega & s_\theta s_i \\ -s_\theta c_\Omega - c_\theta c_i s_\Omega & -s_\theta s_\Omega + c_\theta c_i c_\Omega & c_\theta s_i \\ s_i s_\Omega & -s_i c_\Omega & c_i \end{bmatrix} \tag{6.6}$$

where $\theta,\ i,\ \Omega$ are argument of latitude, inclination, right ascension of the ascending node, respectively.

From the equations, the specific disturbance forces (accelerations) expressed in the RSW frame have the following forms:

$$\begin{aligned} F_R &= -\frac{\mathfrak{J}_2}{r^4}\left(1 - 3s_i^2 s_\theta^2\right) - \frac{1}{2}\frac{C_D A}{m}\rho v_{\text{rel}}\boldsymbol{R}_1\boldsymbol{v}_{\text{rel}}, \\ F_S &= -\frac{\mathfrak{J}_2 s_i^2 s_{2\theta}}{r^4} - \frac{1}{2}\frac{C_D A}{m}\rho v_{\text{rel}}\boldsymbol{R}_2\boldsymbol{v}_{\text{rel}}, \\ F_W &= -\frac{\mathfrak{J}_2 s_{2i} s_\theta}{r^4} - \frac{1}{2}\frac{C_D A}{m}\rho v_{\text{rel}}\boldsymbol{R}_3\boldsymbol{v}_{\text{rel}}. \end{aligned} \tag{6.7}$$

The motion of the object orbiting around the Earth is governed by Gauss Variational Equation (GVE) (Vallado, 2007; Alfriend et al., 2010). In order to avoid the singularities of the orbital elements, new vari-

ables are used (Schaub and Junkins, 2003):

$$q_1 := es_\omega, \quad q_2 := ec_\omega \tag{6.8}$$

where e denotes the eccentricity and ω the argument of periapsis.

By using the new variables, the motion of the chief spacecraft can be described by using the following six equations (Chang et al., 2010a):

$$\begin{aligned}
\frac{\mathrm{d}a}{\mathrm{d}t} &= \frac{2}{n\sqrt{1-e^2}}\left(es_\nu F_R + \frac{p}{r}F_S\right) = \frac{2es_\nu}{n\sqrt{1-e^2}}F_R + \frac{2(1+ec_\nu)}{n\sqrt{1-e^2}}F_S, \\
\frac{\mathrm{d}q_1}{\mathrm{d}t} &= \dot{e}s_\omega + e\dot{\omega}c_\omega \\
&= \frac{\sqrt{1-e^2}}{na}\left[-c_\theta F_R + \left\{s_\theta\left(1+\frac{1}{1+ec_\nu}\right) + \frac{q_1}{1+ec_\nu}\right\}F_S - \frac{q_2 c_i s_\theta}{s_i(1+ec_\nu)}F_W\right], \\
\frac{\mathrm{d}q_2}{\mathrm{d}t} &= \dot{e}c_\omega - e\dot{\omega}s_\omega \\
&= \frac{\sqrt{1-e^2}}{na}\left[s_\theta F_R + \left\{c_\theta\left(1+\frac{1}{1+ec_\nu}\right) + \frac{q_2}{1+ec_\nu}\right\}F_S + \frac{q_1 c_i s_\theta}{s_i(1+ec_\nu)}F_W\right], \\
\frac{\mathrm{d}i}{\mathrm{d}t} &= \frac{\sqrt{1-e^2}}{na}\frac{c_\theta}{1+ec_\nu}F_W, \\
\frac{\mathrm{d}\Omega}{\mathrm{d}t} &= \frac{\sqrt{1-e^2}}{na}\frac{s_\theta}{s_i(1+ec_\nu)}F_W, \\
\frac{\mathrm{d}\theta}{\mathrm{d}t} &= \frac{\mathrm{d}\omega}{\mathrm{d}t} + \frac{\mathrm{d}\nu}{\mathrm{d}t} = \frac{h}{r^2} - \frac{\sqrt{1-e^2}}{na}\frac{c_i s_\theta}{s_i(1+ec_\nu)}F_W
\end{aligned} \tag{6.9}$$

where a denotes the semimajor axis and $n := \sqrt{\mu/a^3}$ is the mean motion of the chief spacecraft.

By defining $\chi := 1 + ec_\nu$ and $\kappa := \sqrt{1-e^2}$ and substituting the disturbance forces in (6.7) into (6.9), the

modified GVEs can be rewritten as follows:

$$
\begin{aligned}
\frac{\mathrm{d}a}{\mathrm{d}t} &= -\frac{2\mathfrak{J}_2\chi^4}{na^4\kappa^9}\left\{es_\nu\left(1-3s_i^2s_\theta^2\right)+\chi s_i^2 s_{2\theta}\right\} - \frac{1}{n\kappa}\frac{C_DA}{m}\rho v_{\text{rel}}\left(es_\nu\boldsymbol{R}_1+\chi\boldsymbol{R}_2\right)\boldsymbol{v}_{\text{rel}},\\
\frac{\mathrm{d}q_1}{\mathrm{d}t} &= \frac{\mathfrak{J}_2\chi^3}{na^5\kappa^7}\Big[c_\theta\left\{\chi-s_i^2s_\theta^2(5\chi+2)\right\}-q_1s_i^2s_{2\theta}+2q_2c_i^2s_\theta^2\Big]\\
&\quad+\frac{\kappa}{na\chi}\frac{C_DA}{2m}\rho v_{\text{rel}}\left[\chi\boldsymbol{R}_1-\left\{s_\theta(\chi+1)+q_1\right\}\boldsymbol{R}_2+\frac{q_2c_is_\theta}{s_i}\boldsymbol{R}_3\right]\boldsymbol{v}_{\text{rel}},\\
\frac{\mathrm{d}q_2}{\mathrm{d}t} &= -\frac{\mathfrak{J}_2\chi^3}{na^5\kappa^7}\Big[s_\theta\left\{\chi-s_i^2s_\theta^2(5\chi+2)+2s_i^2(\chi+1)\right\}+2q_1c_i^2s_\theta^2+q_2s_i^2s_{2\theta}\Big]\\
&\quad-\frac{\kappa}{na\chi}\frac{C_DA}{2m}\rho v_{\text{rel}}\left[\chi\boldsymbol{R}_1+\left\{c_\theta(\chi+1)+q_2\right\}\boldsymbol{R}_2+\frac{q_1c_is_\theta}{s_i}\boldsymbol{R}_3\right]\boldsymbol{v}_{\text{rel}},\\
\frac{\mathrm{d}i}{\mathrm{d}t} &= -\frac{\mathfrak{J}_2\chi^3}{2na^5\kappa^7}s_{2i}s_{2\theta}-\frac{\kappa c_\theta}{na\chi}\frac{C_DA}{2m}\rho v_{\text{rel}}\boldsymbol{R}_3\boldsymbol{v}_{\text{rel}},\\
\frac{\mathrm{d}\Omega}{\mathrm{d}t} &= -\frac{2\mathfrak{J}_2\chi^3}{na^5\kappa^7}c_is_\theta^2-\frac{\kappa s_\theta}{na\chi s_i}\frac{C_DA}{2m}\rho v_{\text{rel}}\boldsymbol{R}_3\boldsymbol{v}_{\text{rel}},\\
\frac{\mathrm{d}\theta}{\mathrm{d}t} &= \frac{n\chi^2}{\kappa^3}+\frac{2\mathfrak{J}_2\chi^3}{na^5\kappa^7}c_i^2s_\theta^2+\frac{\kappa c_is_\theta}{na\chi s_i}\frac{C_DA}{2m}\rho v_{\text{rel}}\boldsymbol{R}_3\boldsymbol{v}_{\text{rel}}.
\end{aligned}
\tag{6.10}
$$

6.2.2 Nonlinear Dynamic Models Relative Orbits (Deputy Spacecraft)

We derive the exact nonlinear dynamic model for the deputy spacecraft to describe their accurate motions. The relative dynamic models of the deputy spacecraft can be directly found as follows:

$$
\begin{aligned}
&(\dot{\boldsymbol{r}}_j-\dot{\boldsymbol{r}})^{\mathcal{I}} = (\dot{\boldsymbol{r}}_j-\dot{\boldsymbol{r}})^{\mathcal{R}}+\boldsymbol{\omega}\times(\dot{\boldsymbol{r}}_j-\dot{\boldsymbol{r}})^{\mathcal{R}},\\
&(\ddot{\boldsymbol{r}}_j-\ddot{\boldsymbol{r}})^{\mathcal{I}} = (\ddot{\boldsymbol{r}}_j-\ddot{\boldsymbol{r}})^{\mathcal{R}}+\dot{\boldsymbol{\omega}}\times(\dot{\boldsymbol{r}}_j-\dot{\boldsymbol{r}})^{\mathcal{R}}+2\boldsymbol{\omega}\times(\dot{\boldsymbol{r}}_j-\dot{\boldsymbol{r}})^{\mathcal{R}}+\boldsymbol{\omega}\times\left(\boldsymbol{\omega}\times(\boldsymbol{r}_j-\boldsymbol{r})^{\mathcal{R}}\right)
\end{aligned}
\tag{6.11}
$$

where the subscripts $\mathcal{I}$ and $\mathcal{R}$ denote the ECI and RSW frames, respectively. The angular velocity $\boldsymbol{\omega}$ can be found by the following equation (Kechichian, 1998; Xu and Wang, 2008):

$$
\boldsymbol{\omega} = \begin{bmatrix} \dot{i}c_\theta+\dot{\Omega}s_is_\theta \\ -\dot{i}s_\theta+\dot{\Omega}s_ic_\theta \\ \dot{\theta}+\dot{\Omega}c_i \end{bmatrix} = \begin{bmatrix} \dot{i}c_\theta+\dot{\Omega}s_is_\theta \\ 0 \\ \dot{\theta}+\dot{\Omega}c_i \end{bmatrix} =: \begin{bmatrix} \omega_x \\ 0 \\ \omega_z \end{bmatrix}. \tag{6.12}
$$

Defining $\boldsymbol{\rho}_j = \boldsymbol{r}_j - \boldsymbol{r} = [x_j \;\; y_j \;\; z_j]^\top$ and applying (6.5) to (6.11) with an assumption of a virtual chief spacecraft yields

$$\begin{aligned}\ddot{\boldsymbol{\rho}}_j^{\mathcal{I}} &= \ddot{\boldsymbol{\rho}}_j^{\mathcal{R}} + \dot{\boldsymbol{\omega}} \times \dot{\boldsymbol{\rho}}_j^{\mathcal{R}} + 2\boldsymbol{\omega} \times \dot{\boldsymbol{\rho}}_j^{\mathcal{R}} + \boldsymbol{\omega} \times \left(\boldsymbol{\omega} \times \boldsymbol{\rho}_j^{\mathcal{R}}\right) \\ &= -\nabla\left(U_j - U\right) + \boldsymbol{F}_{\text{drag},j}\end{aligned} \tag{6.13}$$

where $\dot{\boldsymbol{\omega}} \times \boldsymbol{\rho}_j^{\mathcal{R}} = \begin{bmatrix} -\dot{\omega}_z y_j \\ \dot{\omega}_z x_j - \dot{\omega}_x z_j \\ \dot{\omega}_x y_j \end{bmatrix}$, $\boldsymbol{\omega} \times \dot{\boldsymbol{\rho}}_j^{\mathcal{R}} = \begin{bmatrix} -\omega_z \dot{y}_j \\ \omega_z \dot{x}_j - \omega_x \dot{z}_j \\ \omega_x \dot{y}_j \end{bmatrix}$, $\boldsymbol{\omega} \times \left(\boldsymbol{\omega} \times \boldsymbol{\rho}_j^{\mathcal{R}}\right) = \begin{bmatrix} -\omega_z^2 x_j + \omega_x \omega_z z_j \\ -\omega_z^2 y_j - \omega_x^2 y_j \\ \omega_x \omega_z x_j - \omega_x^2 z_j \end{bmatrix}$. Hence, we need $\nabla\left(U_j - U\right)$ to obtain the dynamic model. The gravitational potential of the jth spacecraft can be expressed from (6.1) (Xu and Wang, 2008)

$$U_j = -\frac{\mu}{r_j} - \frac{\mathfrak{J}_2}{r_j^3}\left(\frac{1}{3} - s_{\phi_j}^2\right) = -\frac{\mu}{r_j} - \frac{\mathfrak{J}_2}{3r_j^2} + \frac{\mathfrak{J}_2 r_{jZ}^2}{r_j^5} \tag{6.14}$$

where $r_{jZ} := (r + x_j)s_i s_\theta + y_j s_i c_\theta + z_j c_i$ and $r_j = \sqrt{(r + x_j)^2 + y_j^2 + z_j^2}$.

Therefore, each element of ∇U_j can be derived as

$$\begin{aligned}\frac{\partial U_j}{\partial x_j} &= \frac{\mathrm{d}U_j}{\mathrm{d}r_j}\frac{\partial r_j}{\partial x_j} = \frac{\mu}{r_j^2} + \frac{r + x_j}{r_j} + \frac{\mathfrak{J}_2}{r_j^4}\frac{r + x_j}{r_j} - \frac{5\mathfrak{J}_2 r_{jZ}^2}{r_j^6}\frac{r + x_j}{r_j} + \frac{\mathfrak{J}_2}{r_j^5}2r_{jZ}s_i s_\theta \\ &= (r + x_j)\left(\frac{\mu}{r_j^3} + \frac{\mathfrak{J}_2}{r_j^5} - \frac{5\mathfrak{J}_2 r_{jZ}^2}{r_j^7}\right) + \frac{2\mathfrak{J}_2 r_{jZ}}{r_j^5}s_i s_\theta, \\ \frac{\partial U_j}{\partial y_j} &= \frac{\mathrm{d}U_j}{\mathrm{d}r_j}\frac{\partial r_j}{\partial y_j} = \frac{\mu}{r_j^2}\frac{y_j}{r_j} + \frac{\mathfrak{J}_2}{r_j^4}\frac{y_j}{r_j} - \frac{5\mathfrak{J}_2 r_{jZ}^2}{r_j^6}\frac{y_j}{r_j} + \frac{\mathfrak{J}_2}{r_j^5}2r_{jZ}s_i c_\theta \\ &= y_j\left(\frac{\mu}{r_j^3} + \frac{\mathfrak{J}_2}{r_j^5} - \frac{5\mathfrak{J}_2 r_{jZ}^2}{r_j^7}\right) + \frac{2\mathfrak{J}_2 r_{jZ}}{r_j^5}s_i c_\theta, \\ \frac{\partial U_j}{\partial z_j} &= \frac{\mathrm{d}U_j}{\mathrm{d}r_j}\frac{\partial r_j}{\partial z_j} = \frac{\mu}{r_j^2} + \frac{z_j}{r_j} + \frac{\mathfrak{J}_2}{r_j^4}\frac{z_j}{r_j} - \frac{5\mathfrak{J}_2 r_{jZ}^2}{r_j^6}\frac{z_j}{r_j} + \frac{\mathfrak{J}_2}{r_j^5}2r_{jZ}c_i \\ &= z_j\left(\frac{\mu}{r_j^3} + \frac{\mathfrak{J}_2}{r_j^5} - \frac{5\mathfrak{J}_2 r_{jZ}^2}{r_j^7}\right) + \frac{2\mathfrak{J}_2 r_{jZ}}{r_j^5}c_i.\end{aligned} \tag{6.15}$$

Hence, by defining $\xi_j := \sqrt{\frac{\mu}{r_j^3} + \frac{\mathfrak{J}_2}{r_j^5} - \frac{5\mathfrak{J}_2 r_{jZ}^2}{r_j^7}}$ (physically, it is an angular velocity) and $\alpha_j := \frac{2\mathfrak{J}_2 r_{jZ}}{r_j^5}$ (physically, it is an angular acceleration), the gradient of the gravitational potential of the jth spacecraft,

∇U_j, becomes

$$\nabla U_j = \begin{bmatrix} \frac{\partial U_j}{\partial x_j} \\ \frac{\partial U_j}{\partial y_j} \\ \frac{\partial U_j}{\partial z_j} \end{bmatrix} = \begin{bmatrix} \xi_j^2(r+x_j) + \alpha_j s_i s_\theta \\ \xi_j^2 y_j + \alpha_j s_i c_\theta \\ \xi_j^2 z_j + \alpha_j c_i \end{bmatrix}. \tag{6.16}$$

From (6.2) and (6.16), $-\nabla\left(U_j - U\right)$ can be obtained as follows:

$$-\nabla\left(U_j - U\right) = -\nabla U_j + \nabla U = \begin{bmatrix} -\xi_j^2(r+x_j) - \alpha_j s_i s_\theta + \frac{\mu}{r^2} + \frac{\mathfrak{J}_2}{r^4} - \frac{3\mathfrak{J}_2 s_i^2 s_\theta^2}{r^4} \\ -\xi_j^2 y_j - \alpha_j s_i c_\theta + \frac{\mathfrak{J}_2 s_i^2 s_{2\theta}}{r^4} \\ -\xi_j^2 z_j - \alpha_j c_i + \frac{\mathfrak{J}_2 s_{2i} s_\theta}{r^4} \end{bmatrix}. \tag{6.17}$$

Therefore, from (6.13), (6.17), and (6.3), the relative dynamic models of the jth spacecraft with respect to the formation center expressed in the RSW frame is expressed as

$$\begin{aligned}
\ddot{x}_j &= \dot{\omega}_z y_j + 2\omega_z \dot{y}_j + \omega_z^2 x_j - \omega_x \omega_z z_j - (r+x_j)\xi_j^2 - \alpha_j s_i s_\theta \\
&\quad + r\left(\frac{\mu}{r^3} + \frac{\mathfrak{J}_2}{r^5} - \frac{3\mathfrak{J}_2 s_i^2 s_\theta^2}{r^5}\right) - \frac{C_D A_j}{2m_j}\rho_j v_{j,\text{rel}} \boldsymbol{R}_1 \boldsymbol{v}_{j,\text{rel}} + F_{j,x} \\
&= 2\omega_z \dot{y}_j - \left(\xi_j^2 - \omega_z^2\right) x_j + \dot{\omega}_z y_j - \omega_x \omega_z z_j - \xi_j^2 r - \alpha_j s_i s_\theta \\
&\quad + \left(\frac{\mu}{r^3} + \frac{\mathfrak{J}_2}{r^5} - \frac{5\mathfrak{J}_2 s_i^2 s_\theta^2}{r^5}\right) r + \frac{2\mathfrak{J}_2 s_i s_\theta}{r^4} s_i s_\theta - \frac{C_D A_j}{2m_j}\rho_j v_{j,\text{rel}} \boldsymbol{R}_1 \boldsymbol{v}_{j,\text{rel}} + F_{j,x}, \\
\ddot{y}_j &= -\dot{\omega}_z x_j + \dot{\omega}_x z_j - 2\omega_z \dot{x}_j + 2\omega_x \dot{z}_j + \omega_z^2 y_j + \omega_x^2 y_j - \xi_j^2 y_j - \alpha_j s_i c_\theta \\
&\quad + \frac{2\mathfrak{J}_2 s_i s_\theta}{r^4} s_i c_\theta - \frac{C_D A_j}{2m_j}\rho_j v_{j,\text{rel}} \boldsymbol{R}_2 \boldsymbol{v}_{j,\text{rel}} + F_{j,y}, \\
\ddot{z}_j &= -\dot{\omega}_x y_j - 2\omega_x \dot{y}_j - \omega_x \omega_z x_j + \omega_x^2 z_j - \xi_j^2 z_j - \alpha_j c_i \\
&\quad + \frac{2\mathfrak{J}_2 s_i s_\theta}{r^4} c_i - \frac{C_D A_j}{2m_j}\rho_j v_{j,\text{rel}} \boldsymbol{R}_3 \boldsymbol{v}_{j,\text{rel}} + F_{j,z}.
\end{aligned} \tag{6.18}$$

By defining $\xi := \sqrt{\frac{\mu}{r^3} + \frac{\mathfrak{J}_2}{r^5} - \frac{5\mathfrak{J}_2 s_i^2 s_\theta^2}{r^5}}$ and $\alpha := \frac{2\mathfrak{J}_2 s_i s_\theta}{r^4}$, the exact nonlinear dynamic models for the deputy spacecraft is obtained as

$$\begin{aligned}
\ddot{x}_j &= 2\omega_z \dot{y}_j - \left(\xi_j^2 - \omega_z^2\right) x_j + \dot{\omega}_z y_j - \omega_x \omega_z z_j - \left(\xi_j^2 - \xi^2\right) r \\
&\quad - \left(\alpha_j - \alpha\right) s_i s_\theta - \frac{C_D A_j}{2m_j} \rho_j v_{j,\text{rel}} \boldsymbol{R}_1 \boldsymbol{v}_{j,\text{rel}} + F_{j,x}, \\
\ddot{y}_j &= -2\omega_z \dot{x}_j + 2\omega_x \dot{z}_j - \dot{\omega}_z x_j - \left(\xi_j^2 - \omega_x^2 - \omega_z^2\right) y_j + \dot{\omega}_x z_j \\
&\quad - \left(\alpha_j - \alpha\right) s_i c_\theta - \frac{C_D A_j}{2m_j} \rho_j v_{j,\text{rel}} \boldsymbol{R}_2 \boldsymbol{v}_{j,\text{rel}} + F_{j,y}, \\
\ddot{z}_j &= -2\omega_x \dot{y}_j - \omega_x \omega_z x_j - \dot{\omega}_x y_j - \left(\xi_j^2 - \omega_x^2\right) z_j \\
&\quad - \left(\alpha_j - \alpha\right) c_i - \frac{C_D A_j}{2m_j} \rho_j v_{j,\text{rel}} \boldsymbol{R}_3 \boldsymbol{v}_{j,\text{rel}} + F_{j,z}.
\end{aligned} \tag{6.19}$$

Notice that (6.19) must be discretized to be used in the CD-SDRE controller.

6.2.3 The Discretization of Dynamic Models of the Relative Motion

For the discretization of the relative dynamic models, the sampling time is set to T. Then, (6.20) and (6.21) show the discretization of the kinematics and dynamics of the relative motion:[1]

$$x_j(k+1) = x_j + T\dot{x}_j, \quad y_j(k+1) = y_j + T\dot{y}_j, \quad \text{and} \quad z_j(k+1) = z_j + T\dot{z}_j \tag{6.20}$$

and the discretization of the dynamics of the relative motion (6.19):

$$\begin{aligned}
\dot{x}_j(k+1) &= \dot{x}_j + 2T\omega_z \dot{y}_j - T\left(\xi_j^2 - \omega_z^2\right) x_j + T\dot{\omega}_z y_j - T\omega_x \omega_z z_j - T\left(\xi_j^2 - \xi^2\right) r \\
&\quad - T\left(\alpha_j - \alpha\right) s_i s_\theta - T\frac{C_D A_j}{2m_j} \rho_j v_{j,\text{rel}} \boldsymbol{R}_1 \boldsymbol{v}_{j,\text{rel}} + TF_{j,x}, \\
\dot{y}_j(k+1) &= -2T\omega_z \dot{x}_j + \dot{y}_j + 2T\omega_x \dot{z}_j - T\dot{\omega}_z x_j - T\left(\xi_j^2 - \omega_x^2 - \omega_z^2\right) y_j + T\dot{\omega}_x z_j \\
&\quad - T\left(\alpha_j - \alpha\right) s_i c_\theta - T\frac{C_D A_j}{2m_j} \rho_j v_{j,\text{rel}} \boldsymbol{R}_2 \boldsymbol{v}_{j,\text{rel}} + TF_{j,y}, \\
\dot{z}_j(k+1) &= -2T\omega_x \dot{y}_j + \dot{z}_j - T\omega_x \omega_z x_j - T\dot{\omega}_x y_j - T\left(\xi_j^2 - \omega_x^2\right) z_j \\
&\quad - T\left(\alpha_j - \alpha\right) c_i - T\frac{C_D A_j}{2m_j} \rho_j v_{j,\text{rel}} \boldsymbol{R}_3 \boldsymbol{v}_{j,\text{rel}} + TF_{j,z}.
\end{aligned} \tag{6.21}$$

[1] It should be noted that the time variable k at the right-hand side was removed for brevity.

By combining (6.20) and (6.21), the state-space equations of the relative motion are obtained:

$$\underbrace{\begin{bmatrix} x_j \\ y_j \\ z_j \\ \dot{x}_j \\ \dot{y}_j \\ \dot{z}_j \end{bmatrix}^+}_{=:\boldsymbol{x}_j^+} = \underbrace{\begin{bmatrix} 1 & 0 & 0 & T & 0 & 0 \\ 0 & 1 & 0 & 0 & T & 0 \\ 0 & 0 & 1 & 0 & 0 & T \\ -T(\xi_j^2-\omega_z^2) & T\dot{\omega}_z & -T\omega_x\omega_z & 1 & 2T\omega_z & 0 \\ -T\dot{\omega}_z & -T(\xi_j^2-\omega_x^2-\omega_z^2) & T\dot{\omega}_x & -2T\omega_z & 1 & 2T\omega_x \\ -T\omega_x\omega_z & -T\dot{\omega}_x & -T(\xi_j^2-\omega_x^2) & 0 & -2T\omega_x & 1 \end{bmatrix}}_{=:\boldsymbol{A}_j(\boldsymbol{x}_j)} \underbrace{\begin{bmatrix} x_j \\ y_j \\ z_j \\ \dot{x}_j \\ \dot{y}_j \\ \dot{z}_j \end{bmatrix}}_{=:\boldsymbol{x}_j}$$

$$+ \underbrace{\begin{bmatrix} 0 & 0 & 0 \\ 0 & 0 & 0 \\ 0 & 0 & 0 \\ T & 0 & 0 \\ 0 & T & 0 \\ 0 & 0 & T \end{bmatrix}}_{=:\boldsymbol{B}_j} \underbrace{\begin{bmatrix} F_{j,x} \\ F_{j,y} \\ F_{j,z} \end{bmatrix}}_{\boldsymbol{u}_j} + \underbrace{\begin{bmatrix} 0 \\ 0 \\ 0 \\ -T(\xi_j^2-\xi^2)r - T(\alpha_j-\alpha)s_i s_\theta - T\frac{C_D A_j}{2m_j}\rho_j v_{j,\text{rel}}\boldsymbol{R}_1\boldsymbol{v}_{j,\text{rel}} \\ -T(\alpha_j-\alpha)s_i c_\theta - T\frac{C_D A_j}{2m_j}\rho_j v_{j,\text{rel}}\boldsymbol{R}_2\boldsymbol{v}_{j,\text{rel}} \\ -T(\alpha_j-\alpha)c_i - T\frac{C_D A_j}{2m_j}\rho_j v_{j,\text{rel}}\boldsymbol{R}_3\boldsymbol{v}_{j,\text{rel}} \end{bmatrix}}_{=:\boldsymbol{\Delta}_j}$$

or in a simple form as

$$\boldsymbol{x}_j^+ = \boldsymbol{A}_j(\boldsymbol{x}_j)\boldsymbol{x}_j + \boldsymbol{B}_j\boldsymbol{u}_j + \boldsymbol{\Delta}_j. \tag{6.22}$$

6.2.4 Extension to a Multiple Spacecraft System

In this part, we design the whole system of a multiple spacecraft system through the use of (6.22). For notational simplicity, we will omit the time k in the following equations unless otherwise needed for clarification. It is supposed that jth spacecraft can communicate with other spacecraft in the formation. The controller for the jth spacecraft can be designed as follows:

$$\boldsymbol{u}_j = -\boldsymbol{K}_{\boldsymbol{x}_j}(\boldsymbol{x}_j)\boldsymbol{x}_j + \boldsymbol{K}_{\boldsymbol{\omega}_j}(\boldsymbol{x}_j)\boldsymbol{\omega}_j + \sum_{l\in\mathcal{N}_j, l\neq j}\left(\boldsymbol{K}_{\boldsymbol{x}_l}\boldsymbol{R}^{l,j}\boldsymbol{x}_l - \boldsymbol{K}_{\boldsymbol{\omega}_l}\boldsymbol{R}^{l,j}\boldsymbol{\omega}_l\right) \tag{6.23}$$

where $\mathcal{N}_j \subset \mathbb{Z}_{1:N}$ includes the indices for the spacecraft communicating with the jth spacecraft in the formation. The matrix for a phase angle shift $\boldsymbol{R}^{l,j}$ is used to rotate the coordinates by a phase angle difference

between the jth and lth spacecraft. Readers are referred to (Chang et al., 2011) for more information on the phase angle shift and coordinate transformation methods.

Substituting (6.23) into (6.22) yields

$$\begin{aligned}\boldsymbol{x}_j^+ = &\Big(\boldsymbol{A}_j(\boldsymbol{x}_j) - \boldsymbol{B}_j(\boldsymbol{x}_j)\boldsymbol{K}_{\boldsymbol{x}_j}(\boldsymbol{x}_j)\Big)\boldsymbol{x}_j + \boldsymbol{B}_j(\boldsymbol{x}_j)\boldsymbol{K}_{\boldsymbol{\omega}_j}\boldsymbol{\omega}_j \\ &+ \boldsymbol{B}_j(\boldsymbol{x}_j)\sum_{l\in\mathcal{N}_j, l\neq j}\Big(\boldsymbol{K}_{\boldsymbol{x}_l}\boldsymbol{R}^{l,j}\boldsymbol{x}_l - \boldsymbol{K}_{\boldsymbol{\omega}_l}\boldsymbol{R}^{l,j}\boldsymbol{\omega}_l\Big) + \boldsymbol{\Delta}_j. \end{aligned} \tag{6.24}$$

Therefore, from (6.24), the state-space equations for the whole system comprised of p spacecraft are obtained:

$$\begin{aligned}\begin{bmatrix}\boldsymbol{x}_1\\ \boldsymbol{x}_2\\ \vdots\\ \boldsymbol{x}_p\end{bmatrix}^+ = &\begin{bmatrix}\boldsymbol{A}_{\mathrm{cl},1}(\boldsymbol{x}_1) & \delta_{1,2}\boldsymbol{B}_1(\boldsymbol{x}_1)\boldsymbol{K}_{\boldsymbol{x}_2}\boldsymbol{R}^{2,1} & \cdots & \delta_{1,p}\boldsymbol{B}_1(\boldsymbol{x}_1\boldsymbol{K}_{\boldsymbol{x}_p}\boldsymbol{R}^{p,1}\\ \delta_{2,1}\boldsymbol{B}_2(\boldsymbol{x}_2)\boldsymbol{K}_{\boldsymbol{x}_1}\boldsymbol{R}^{1,2} & \boldsymbol{A}_{\mathrm{cl},2}(\boldsymbol{x}_2) & \cdots & \delta_{2,p}\boldsymbol{B}_2(\boldsymbol{x}_2)\boldsymbol{K}_{\boldsymbol{x}_p}\boldsymbol{R}^{p,2}\\ \vdots & \vdots & \ddots & \vdots\\ \delta_{p,1}\boldsymbol{B}_p(\boldsymbol{x}_p)\boldsymbol{K}_{\boldsymbol{x}_1}\boldsymbol{R}^{1,p} & \delta_{p,2}\boldsymbol{B}_p(\boldsymbol{x}_p)\boldsymbol{K}_{\boldsymbol{x}_2}\boldsymbol{R}^{2,p} & \cdots & \boldsymbol{A}_{\mathrm{cl},p}(\boldsymbol{x}_p)\end{bmatrix}\begin{bmatrix}\boldsymbol{x}_1\\ \boldsymbol{x}_2\\ \vdots\\ \boldsymbol{x}_p\end{bmatrix}\\ &+\begin{bmatrix}\boldsymbol{B}_1(\boldsymbol{x}_1)\boldsymbol{K}_{\boldsymbol{\omega}_1} & -\delta_{1,2}\boldsymbol{B}_1(\boldsymbol{x}_1)\boldsymbol{K}_{\boldsymbol{\omega}_2}\boldsymbol{R}^{2,1} & \cdots & -\delta_{1,p}\boldsymbol{B}_1(\boldsymbol{x}_1)\boldsymbol{K}_{\boldsymbol{\omega}_p}\boldsymbol{R}^{p,1}\\ -\delta_{2,1}\boldsymbol{B}_2(\boldsymbol{x}_2)\boldsymbol{K}_{\boldsymbol{\omega}_1}\boldsymbol{R}^{1,2} & \boldsymbol{B}_2(\boldsymbol{x}_2)\boldsymbol{K}_{\boldsymbol{\omega}_2} & \cdots & -\delta_{2,p}\boldsymbol{B}_2(\boldsymbol{x}_2)\boldsymbol{K}_{\boldsymbol{\omega}_p}\boldsymbol{R}^{p,2}\\ \vdots & \vdots & \ddots & \vdots\\ -\delta_{p,1}\boldsymbol{B}_p(\boldsymbol{x}_p)\boldsymbol{K}_{\boldsymbol{\omega}_1}\boldsymbol{R}^{1,p} & -\delta_{p,1}\boldsymbol{B}_p(\boldsymbol{x}_p)\boldsymbol{K}_{\boldsymbol{\omega}_2}\boldsymbol{R}^{2,p} & \cdots & \boldsymbol{B}_p(\boldsymbol{x}_p)\boldsymbol{K}_{\boldsymbol{\omega}_p}\end{bmatrix}\begin{bmatrix}\boldsymbol{\omega}_1\\ \boldsymbol{\omega}_2\\ \vdots\\ \boldsymbol{\omega}_p\end{bmatrix}.\end{aligned} \tag{6.25}$$

6.3 Simulation

In this section, we evaluate the proposed CD-SDRE controller by applying it to reconfiguration problem of the spacecraft. Two simulations are tested: 1) demanding initial conditions and 2) combination of guidance and control via CD-SDRE. For the simulations, the initial values of the six orbital elements of the LVLH frame are given as follows: $a = 6778.137$ km, $e = 0$, $i = 45^\circ$, $\Omega = 30^\circ$, $\omega = 0^\circ$, and $\nu = 10^\circ$. For the atmospheric drag, $m_j = 100$ kg, $C_D = 2.2$, and $A_j = 1$ m^2 are assumed.

6.3.1 Controller Test with Extreme Initial Conditions

The purpose of the test is to show the reliability of the proposed CD-SDRE even with extremely demanding initial condition. To this end, the desired trajectory of the spacecraft is generated by using the Hill-Clohessy-Whiltshire (HCW) equation (Clohessy and Wiltshire, 1960) with the periodic conditions (Chang et al., 2010a): $\dot{y}_0 = -2nx_0$ and $y_0 = 2\dot{x}_0/n$. We define such an orbit as a periodic relative orbit (PRO). The initial conditions of the desired trajectory are $x_0 = y_0 = 1\ \mathrm{km}$, $z_0 = 0.5\ \mathrm{km}$, $\dot{z}_0 = 10^{-3}\ \mathrm{km/s}$. We want to show how the spacecraft, initially at rest in the origin of the LVLH frame, follows its desired trajectory in the presence of different levels of actuator saturations. The performance of the CD-SDRE is compared with that by the linear MPC. For a consistent comparison, the same weights of the controllers are chosen: $\boldsymbol{Q}_k = \boldsymbol{Q} = \mathrm{diag}\big([10^{-5},\ 10^{-5},\ 10^{-5},\ 10^{-6},\ 10^{-6},\ 10^{-6}]\big)$ and $\boldsymbol{R}_k = \boldsymbol{R} = \mathrm{diag}\big([1,\ 1,\ 1]\big)$. For the CD-SDRE and the Linear MPC, $N = 30$ and $T = 1\ \mathrm{sec}$. Three different input constraints are considered: $0.5\ \mathrm{m/s^2}$, $0.3\ \mathrm{m/s^2}$, and $0.1\ \mathrm{m/s^2}$, i.e., $-5 \times 10^{-4} \leq F_x, F_y, F_z \leq 5 \times 10^{-4}$, $-3 \times 10^{-4} \leq F_x, F_y, F_z \leq 3 \times 10^{-4}$, and $-10^{-4} \leq F_x, F_y, F_z \leq 10^{-4}$, $j = 1, 2, 3$ for all k.

Figure 6.1 shows control profiles, state errors, and trajectories of the spacecraft with weak saturations: $-0.5\ \mathrm{m/s^2} \leq F_x,\ F_y,\ F_z \leq 0.5\ \mathrm{m/s^2}$. Although the constraints are relatively lenient, the propose CD-SDRE effectively converge to the desire trajectory with less fuel consumption than that by the linear MPC. As the constrains on the actuators become stringent (Figures 6.2 and 6.3), the spacecraft spent longer time tracking and converging to its desired trajectory. The reason of having fluctuated trajectories before converging to its desired trajectory is because of short length of the control horizon $N = 30$. In other words, the proposed CD-SDRE and the linear MPC can look ahead only 30 steps (i.e., 30 sec because the sampling time is 1 sec.). The short control horizon can increase difficulties for the controllers to generate optimal control signals. However, even with such difficulties, the proposed CD-SDRE controller makes the spacecraft converge to its desired trajectory faster (Table 6.1) with less fuel consumptions (ΔV, Table 6.2).

We have shown the reliability of the proposed CD-SDRE controller. In general, however, spacecraft does not have such fluctuated orbits while transferring its orbit although our main purpose of the test is to show the reliability of the proposed CD-SDRE. In the next section, we evaluate guidance and control of spacecraft with the proposed CD-SDRE to see the applicability of the proposed CD-SDRE in a realistic space mission.

Table 6.1: Comparison of Convergent Time [s] (Error < 0.1 m, $i = x, y, z$)

Constraints	$\lvert F_i \rvert \leq 0.5 \mathrm{m/s^2}$	$\lvert F_i \rvert \leq 0.3 \mathrm{m/s^2}$	$\lvert F_i \rvert \leq 0.1 \mathrm{m/s^2}$
LMPC	175	230	636
CD-SDRE	106	184	461

Table 6.2: Comparison of Total Fuel Consumption (ΔV [km/s])

Constraints	$\lvert F_i \rvert \leq 0.5 \mathrm{m/s^2}$	$\lvert F_i \rvert \leq 0.3 \mathrm{m/s^2}$	$\lvert F_i \rvert \leq 0.1 \mathrm{m/s^2}$
LMPC	0.09431	0.09306	0.09336
CD-SDRE	0.06755	0.06828	0.06839

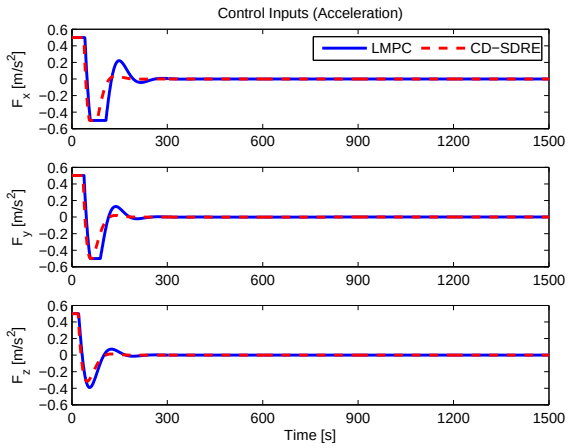

(a) Control inputs (acceleration)

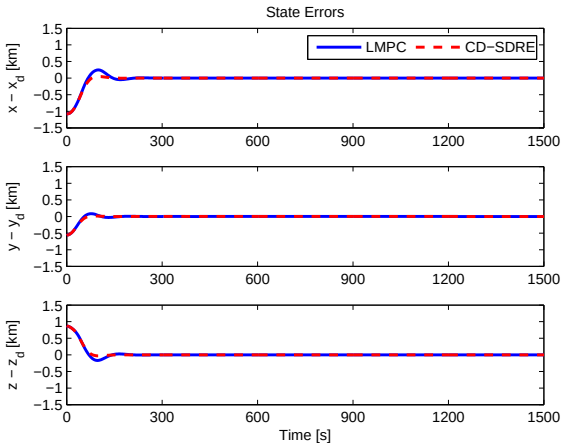

(b) State errors

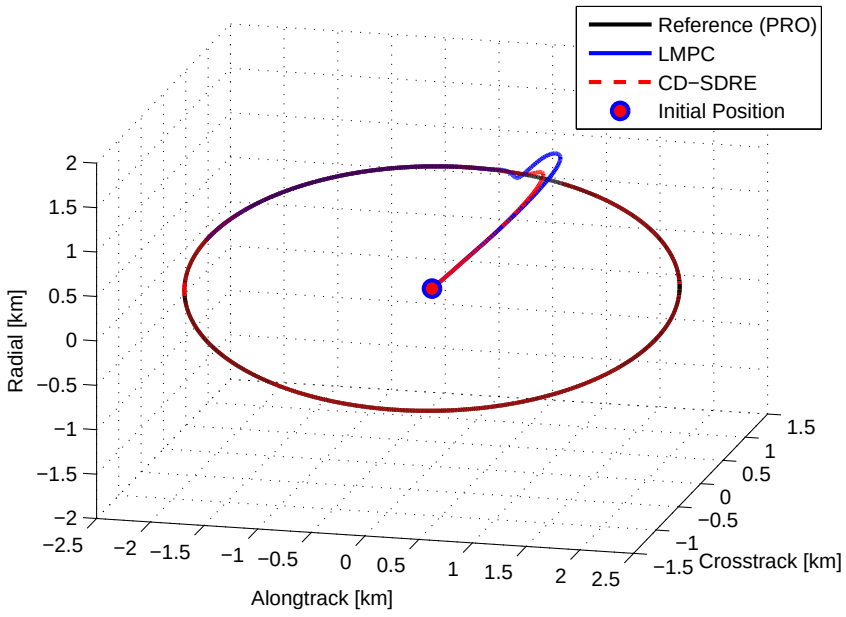

(c) Trajectories

Figure 6.1: Time histories of the control inputs, state errors, and trajectories with $|F_i| \leq 0.5\ \mathrm{m/s^2}$

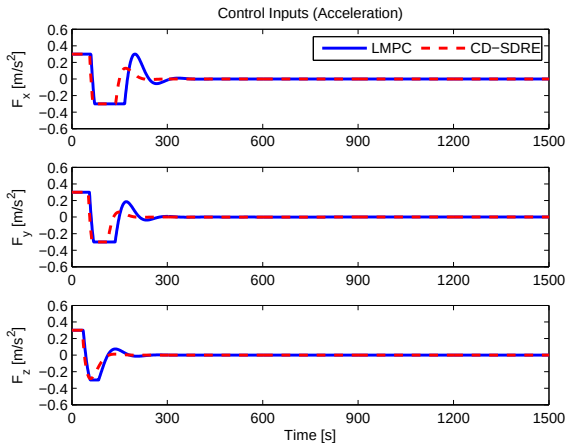

(a) Control inputs (acceleration)

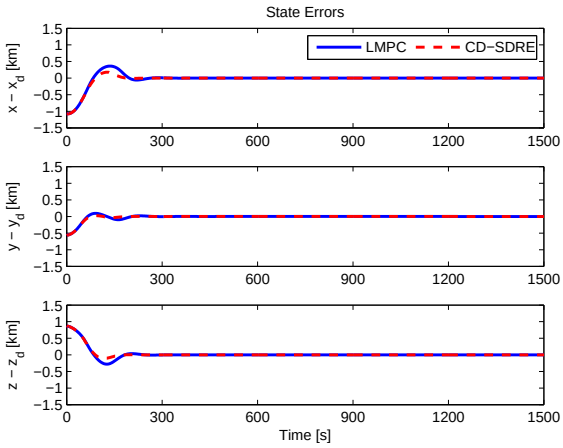

(b) State errors

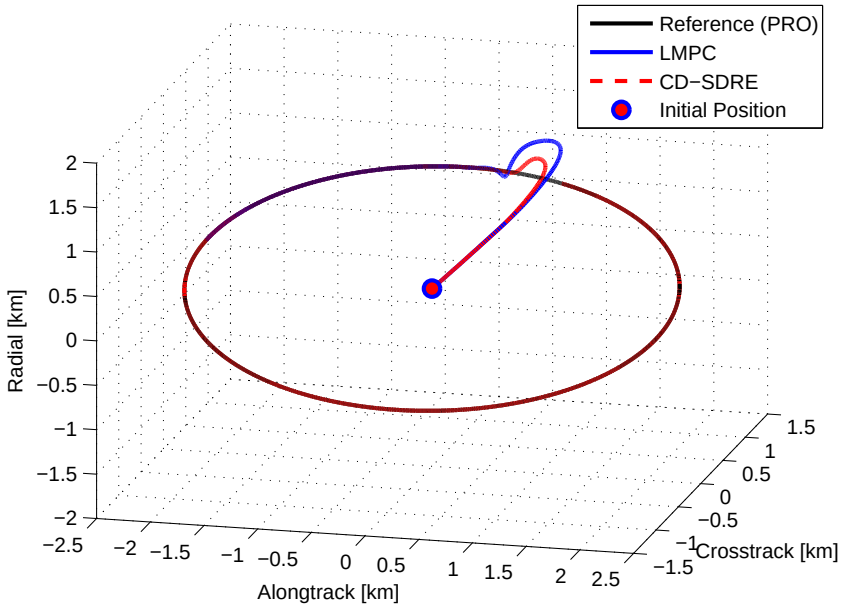

(c) Trajectories

Figure 6.2: Time histories of the control inputs, state errors, and trajectories with $|F_i| \leq 0.3\ \mathrm{m/s^2}$

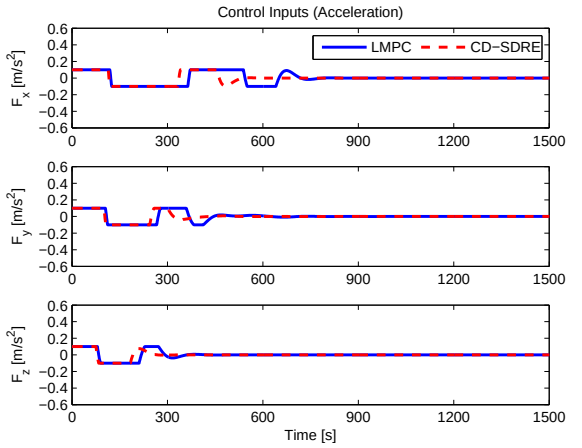

(a) Control inputs (acceleration)

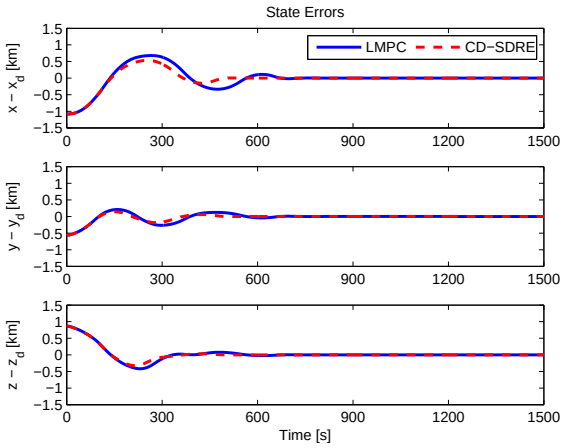

(b) State errors

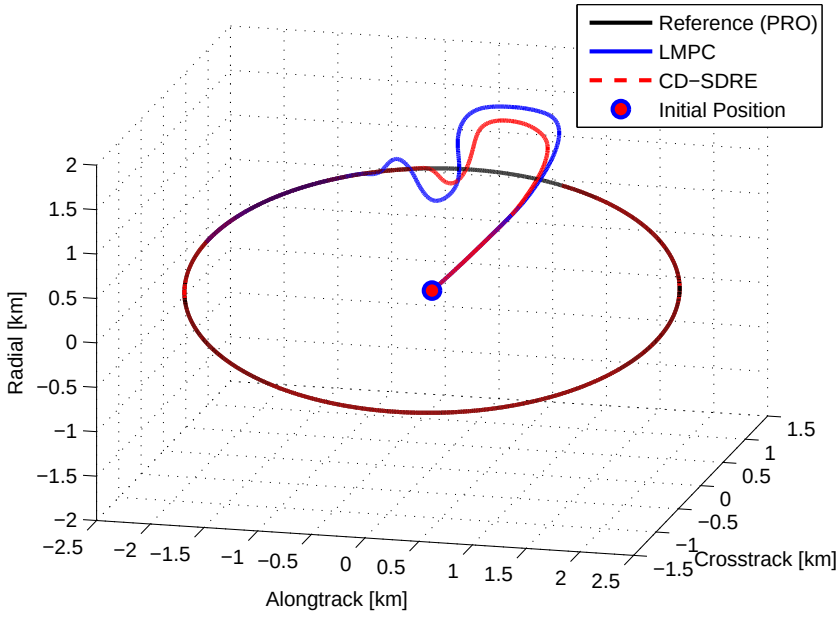

(c) Trajectories

Figure 6.3: Time histories of the control inputs, state errors, and trajectories with $|F_i| \leq 0.1 \text{ m/s}^2$

6.3.2 Extension to a Multiple Spacecraft System

In this section, we evaluate the proposed distributed CD-SDRE controller. From the formation flying system obtained in the previous section, three different controllers are applied: a distributed CD-SDRE, a linear MPC, and an infinite horizon LQR controller. For the simulation, the initial values of the six orbital elements are given as follows: $a = 6778.137$ km, $e = 0$, $i = 45°$, $\Omega = 30°$, $\omega = 0°$, and $\nu = 10°$. For the atmospheric drag, $m_j = 100$ kg, $C_D = 2.2$, and $A_j = 1$ m^2 are assumed. The desired trajectories of the spacecraft are generated by using the Hill-Clohessy-Whiltshire (HCW) equation (Clohessy and Wiltshire, 1960) with the periodic conditions (Chang et al., 2010a): $\dot{y}_0 = -2nx_0$ and $y_0 = 2\dot{x}_0/n$. We define such an orbit as a periodic relative orbit (PRO). The initial conditions of the desired trajectories are $x_0 = y_0 = 1$ km, $z_0 = 0.5$ km, $\dot{z}_0 = 10^{-3}$ km. The desired trajectories of the three spacecraft are generated by using $120°$ as the phase shift angle (Chang et al., 2011). Three spacecraft have random initial positions and zero initial velocities. We want to show how the spacecraft, initially at rest, follow their desired trajectories. For a consistent comparison, the same weights of the controllers are chosen: $\boldsymbol{Q}_k = \boldsymbol{Q} = \mathrm{diag}\big([10^{-5},\ 10^{-5},\ 10^{-5},\ 10^{-6},\ 10^{-6},\ 10^{-6}]\big)$ and $\boldsymbol{R}_k = \boldsymbol{R} = \mathrm{diag}\big([1,\ 1,\ 1]\big)$. For the distributed CD-SDRE and the Linear MPC, $N = 30$ and $T = 1$ sec. Three different input constraints are considered: 0.5 m/s^2, 0.3 m/s^2, and 0.1 m/s^2, i.e., $-5 \times 10^{-4} \leq F_{x,j}, F_{y,j}, F_{z,j} \leq 5 \times 10^{-4}$, $-3 \times 10^{-4} \leq F_{x,j}, F_{y,j}, F_{z,j} \leq 3 \times 10^{-4}$, and $-10^{-4} \leq F_{x,j}, F_{y,j}, F_{z,j} \leq 10^{-4}$, $j = 1, 2, 3$ for all k.

The trajectories, state errors, and control inputs with different constraints on the control inputs. The red circles show the initial positions of the spacecraft.

Figures 6.4 – 6.6 show simulation results of the trajectories, state errors, and control inputs of spacecraft with different constraints on the control inputs. Notice that figures in Figures 6.4 – 6.6 show the state errors and control inputs of the radial direction of the first spacecraft for clarity since the results of the other directions for three spacecraft are similar. From these results, the spacecraft with the proposed distributed CD-SDRE controller are seen to converge to their trajectories faster and with smaller control effort than those with the infinite LQR and the linear MPC. The LQR controller and the linear MPC have similar results when the constraints are 0.5 m/s^2 and 0.3 m/s^2. However, the LQR controller makes the controlled system unstable as the constraint become stringent. Moreover, we can also find the bigger wave motions in the state trajectories as the constraints tighten. In the distributed CD-SDRE case, the wave motions could be attenuated as the length of horizon increases, although also increasing the computational time. Therefore,

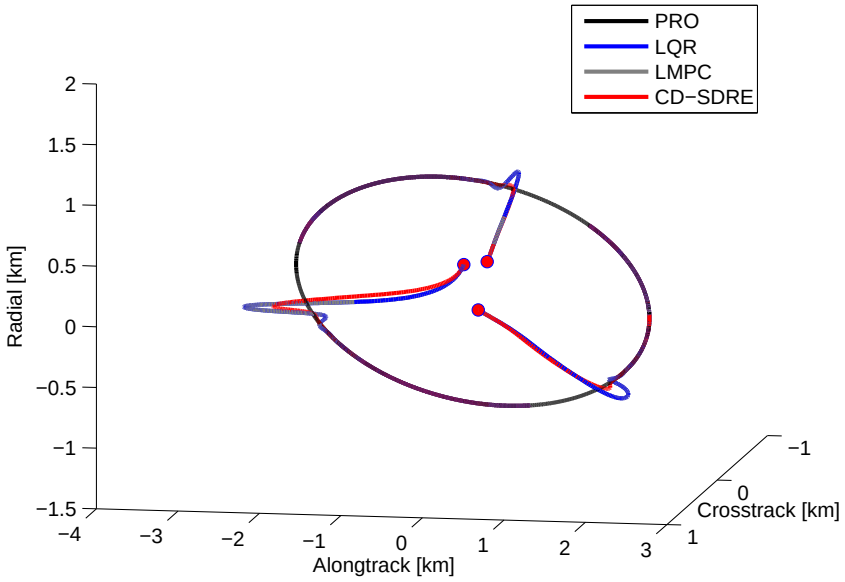

(a) Trajectories

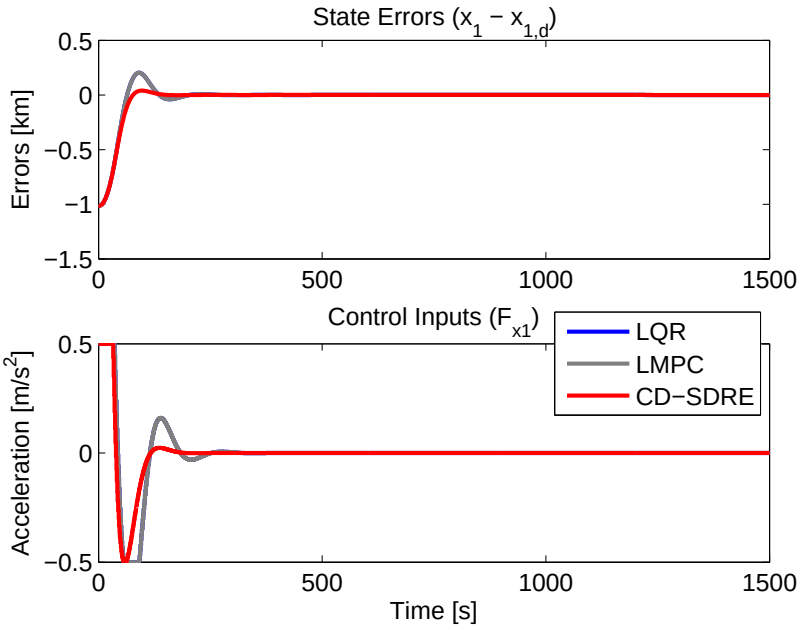

(b) State errors and control inputs

Figure 6.4: Time histories of the control inputs, state errors, and trajectories with $|F_i| \leq 0.5\ \mathrm{m/s^2}$

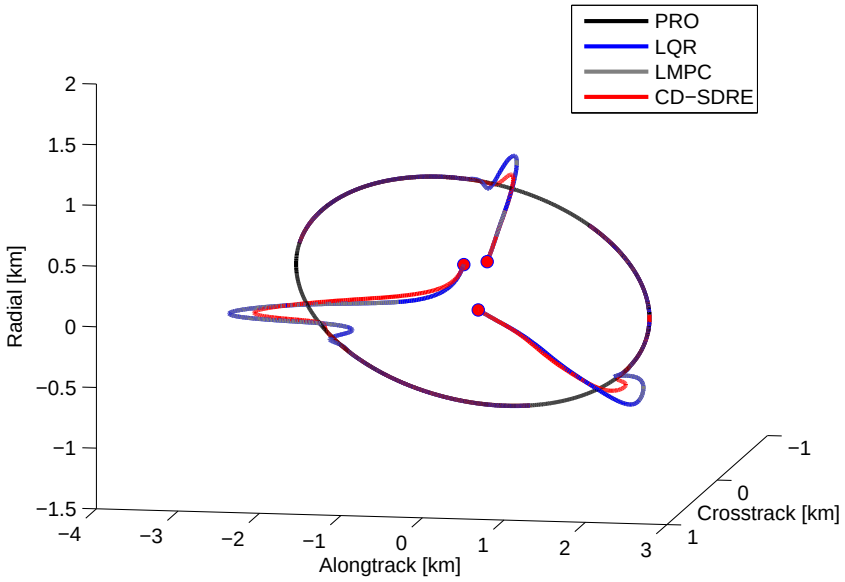

(a) Trajectories

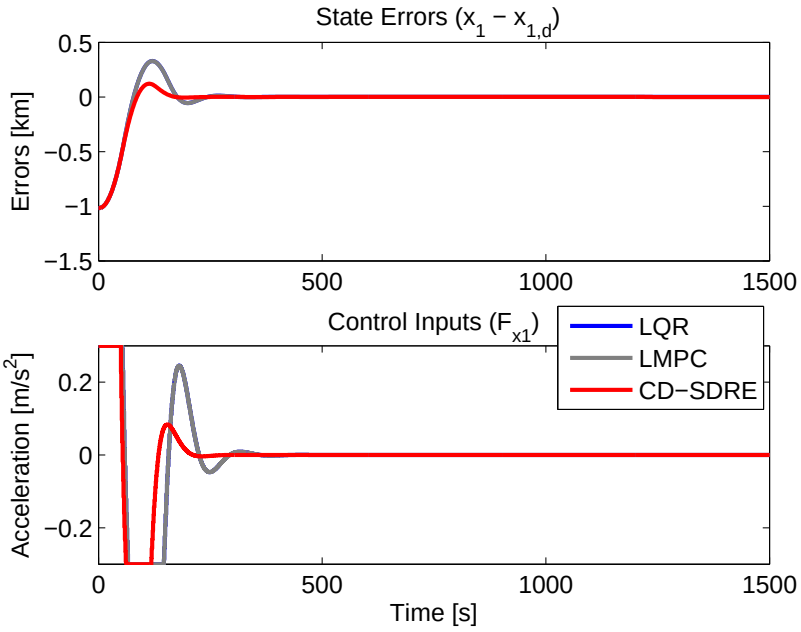

(b) State errors and control inputs

Figure 6.5: Time histories of the control inputs, state errors, and trajectories with $|F_i| \leq 0.3\ \mathrm{m/s^2}$

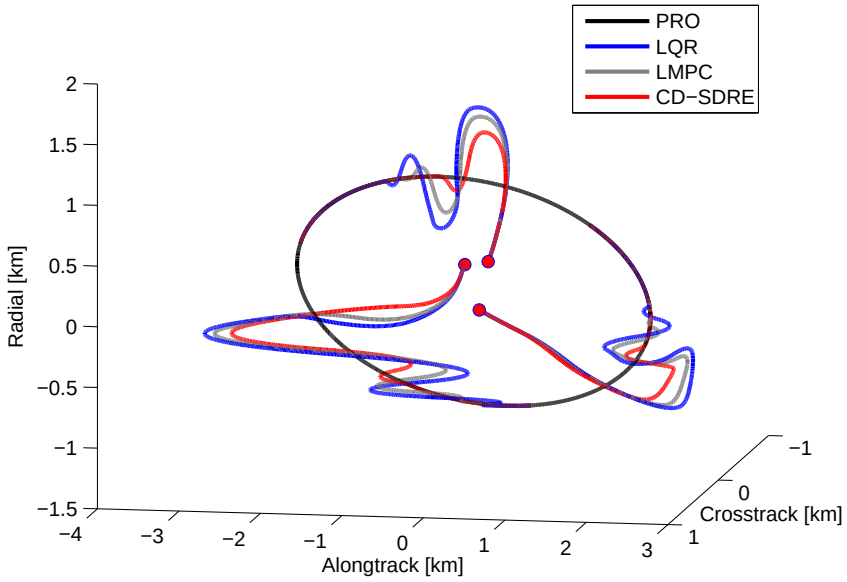

(a) Trajectories

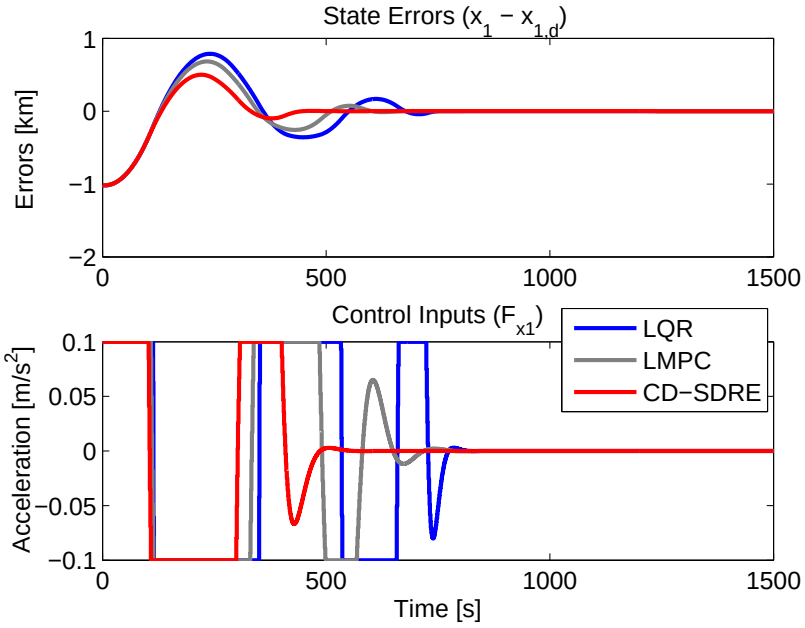

(b) State errors and control inputs

Figure 6.6: Time histories of the control inputs, state errors, and trajectories with $|F_i| \leq 0.1$ m/s^2

an appropriate horizon should be chosen depending on the application.

6.3.3 Guidance and Control via CD-SDRE

Unlike the previous simulations, a more realistic simulation is tested. A spacecraft, randomly located at rest in $|x_0|,\ |y_0|,\ |z_0| \leq 1$ km, will approach a pre-defined final position in one orbital period ($t_f = 5554$ sec). The final position is located in a PRO, which is defined in the previous section but with different initial conditions: $x_0 = y_0 = 100$ km, $z_0 = 50$ km, $\dot{z}_0 = 0.01$ km/s. The final destination is set up to $x_{T_f} = 0.35$ km, $y_{T_f} = 100$ km, $z_{T_f} = 1.3$ km. In order to generate optimal trajectory, PSO was used under the assumptions that there is no constraint on its controller performance and the orbit can be transferred with a single burn. It should be emphasized that PSO assumed that the spacecraft is located in the origin of the LVLH frame, which can give the spacecraft more challenge due to the discrepancy between the actual initial position and the optimal initial position. Therefore, the spacecraft should generate more control signals at the beginning of the orbit transfer. For the optimal trajectory and its associated optimal control profile, $N_{\text{guidance}} = 5554$ was used. Then, the spacecraft used the desired trajectory and control signals to track the spacecraft to the final position. For the spacecraft orbit control, $N = 15$ and $T = 1$ sec were used, and $-5 \times 10^{-4}\ \text{km/s}^2 \leq F_{x,j}, F_y, F_z \leq 5 \times 10^{-4}\ \text{km/s}^2$ for all $k \in \mathbb{Z}_{\geq 0}$ were applied to the actuator saturation.

Figure 6.7 shows the simulation results of the control profile, state errors, and its trajectory in the LVLH frame. As discussed earlier, the spacecraft generated more control signals at the beginning of the orbit transfer due to the different values of the actual initial location and the pre-calculated optimal initial position. However, the proposed CD-SDRE could track the desired trajectory in 500 sec.

6.4 Conclusions

Comprehensive dynamical modeling of the spacecraft orbit reconfiguration problem and its tracking controller design by using the proposed CD-SDRE showed the possibility of implementing the controller to sophisticated and real-time guidance and control problems.

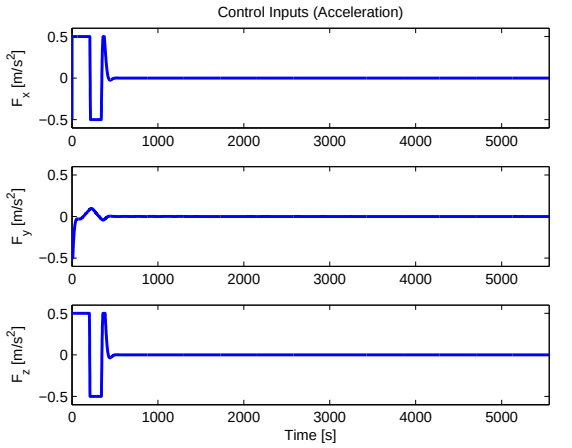

(a) Control inputs (acceleration)

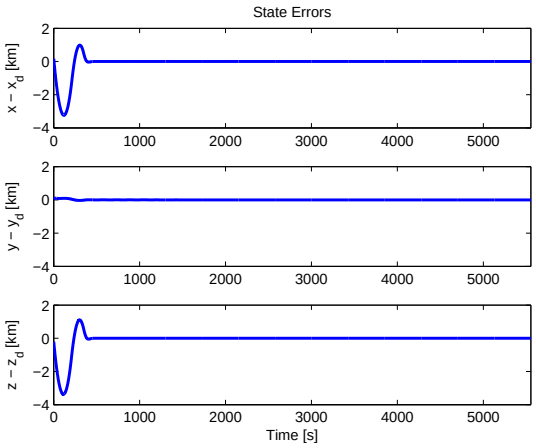

(b) State errors

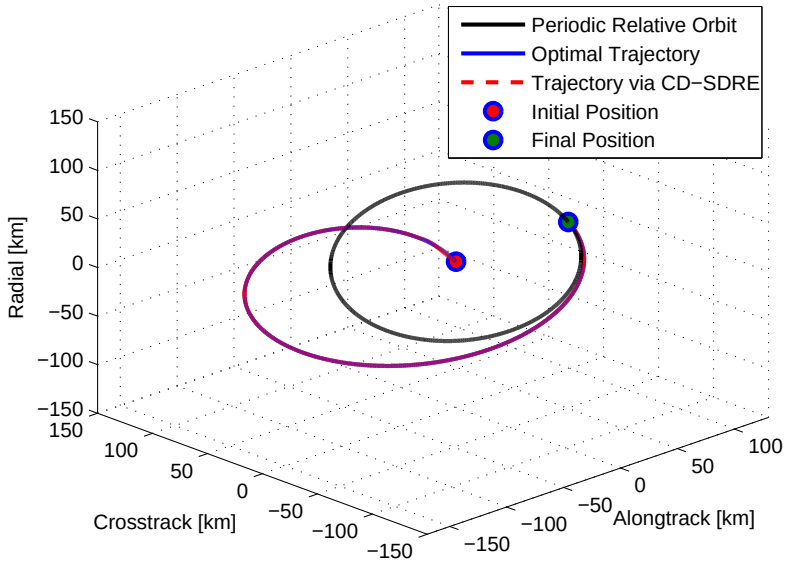

(c) Trajectories

Figure 6.7: Time histories of the control inputs, state errors, and trajectories with $|F_i| \leq 0.5\ \mathrm{m/s^2}$

Chapter 7

Robust Constrained Discrete-Time State-Dependent Riccati Equation Controller

7.1 Introduction

THE constrained discrete-time state-dependent Riccati equation (CD-SDRE) technique in the presence of uncertainties in the nonlinear system to be controlled is presented. The proposed robust CD-SDRE controller is given by a switched control law that incorporates D-SDRE and MPC-based controllers. First, the system stability under each of the latter controllers is separately established. The stability of the closed loop system under a robust CD-SDRE controller is then proven based on the stability of each control system comprising switching configuration. A high fidelity dynamical model of spacecraft attitude motion in 3-dimensional space is derived with a partially filled fuel tank, assumed to have the first fuel slosh mode. The proposed robust CD-SDRE controller is then applied to the spacecraft attitude control system to stabilize its motion in the presence of uncertainly characterized by the first fuel slosh mode. The resulting performance demonstrates the reliability of the proposed robust CD-SDRE technique.

This chapter is organized as follows. In the following section, the robust D-SDRE feedback controller in the presence of uncertainties is investigated. Stability conditions of robust MPC mode and finally the robust CD-SDRE in the presence of uncertainties are provided in Section 7.4. In Section 7.5, nonlinear dynamics of spacecraft attitude dynamics is derived and simulated with the proposed CD-SDRE controller. Finally, concluding remarks are made in Section 7.6.

7.2 Review of D-SDRE Technique

The D-SDRE technique was investigated in Chapter 5. However, we briefly review it here for notational clarification.

7.2.1 Derivation of the D-SDRE Feedback Controller

Consider the discrete-time deterministic nonlinear control-affine system described by the nonlinear difference equation:

$$\boldsymbol{z}_{k+1} = \bar{\boldsymbol{f}}(\boldsymbol{z}_k, \bar{\boldsymbol{u}}_k) = \boldsymbol{A}(\boldsymbol{z}_k)\boldsymbol{z}_k + \boldsymbol{B}(\boldsymbol{z}_k)\bar{\boldsymbol{u}}_k \tag{7.1}$$

where $\boldsymbol{z}_k \in X \subseteq \mathbb{R}^n$ and $\bar{\boldsymbol{u}}_k \in U \subseteq \mathbb{R}^m$. It is assumed that $\bar{\boldsymbol{f}}(\boldsymbol{0}) = \boldsymbol{0}$ and $\bar{\boldsymbol{f}}(\boldsymbol{z}_k)$ is continuously differentiable. We assume that $(\boldsymbol{A}(\boldsymbol{z}_k), \boldsymbol{B}(\boldsymbol{z}_k))$ is piecewise controllable for all $\boldsymbol{z}_k \in X$. For this system, the D-SDRE technique finds a control input $\bar{\boldsymbol{u}}_k \in U$ at each time that minimizes the following performance index:

$$J_0 = \frac{1}{2}\sum_{j=k}^{k+N-1}\Big(\boldsymbol{z}_j^\top \boldsymbol{Q}(\boldsymbol{z}_j)\boldsymbol{z}_j + \bar{\boldsymbol{u}}_j^\top \boldsymbol{R}(\boldsymbol{z}_j)\bar{\boldsymbol{u}}_j\Big) \tag{7.2}$$

where the weights $\boldsymbol{Q}(\boldsymbol{z}_j)$ and $\boldsymbol{R}(\boldsymbol{z}_j)$ are assumed to be symmetric positive semi-definite and symmetric positive definite, respectively.

The optimal feedback control $\bar{\boldsymbol{u}}_k$ for the deterministic system (7.1) is defined as follows:

$$\bar{\boldsymbol{u}}(\boldsymbol{z}_k) = -\Big(\boldsymbol{R}(\boldsymbol{z}_k) + \boldsymbol{B}(\boldsymbol{z}_k)^\top \boldsymbol{P}_{k+1}\boldsymbol{B}(\boldsymbol{z}_k)\Big)^{-1}\boldsymbol{B}(\boldsymbol{z}_k)^\top \boldsymbol{P}_{k+1}\boldsymbol{A}(\boldsymbol{z}_k)\boldsymbol{z}_k =: -\bar{\boldsymbol{K}}(\boldsymbol{z}_k)\boldsymbol{z}_k \tag{7.3}$$

where $\bar{\boldsymbol{K}}(\boldsymbol{z}_k) \in \mathbb{R}^{m\times n}$ is the optimal feedback control gain of the D-SDRE technique.
It should be noted that $\boldsymbol{P}_k$ and $\boldsymbol{P}_{k+1}$ are needed to obtain $\bar{\boldsymbol{K}}(\boldsymbol{z}_k)$ where $\boldsymbol{P}_k$ and $\boldsymbol{P}_{k+1}$ are the solutions of the generalized discrete-time Riccati equation (GD-RE) at times k and $k+1$, respectively:

$$\begin{aligned}\boldsymbol{P}_k = &\left(\boldsymbol{Q}(\boldsymbol{z}_k) + \frac{1}{2}\boldsymbol{z}_k^\top \frac{\partial \boldsymbol{Q}(\boldsymbol{z}_k)}{\partial \boldsymbol{z}_k} - \frac{1}{2}\bar{\boldsymbol{u}}_k^\top \frac{\partial \boldsymbol{R}(\boldsymbol{z}_k)}{\partial \boldsymbol{z}_k}\bar{\boldsymbol{K}}(\boldsymbol{z}_k)\right)\\ &+ \bar{\boldsymbol{A}}^\top \boldsymbol{P}_{k+1}\Big(\boldsymbol{I} + \boldsymbol{B}(\boldsymbol{z}_k)\boldsymbol{R}(\boldsymbol{z}_k)^{-1}\boldsymbol{B}(\boldsymbol{z}_k)^\top \boldsymbol{P}_{k+1}\Big)^{-1}\boldsymbol{A}(\boldsymbol{z}_k).\end{aligned} \tag{7.4}$$

7.3 D-SDRE for Uncertain Nonlinear Systems

Consider the discrete-time nonlinear system with uncertainties:

$$\boldsymbol{x}_{k+1} = \boldsymbol{f}(\boldsymbol{x}_k, \boldsymbol{u}_k, \boldsymbol{\Delta}_k) = (\boldsymbol{A}(\boldsymbol{x}_k) + \boldsymbol{\Delta}_{\boldsymbol{A}_k})\boldsymbol{x}_k + (\boldsymbol{B}(\boldsymbol{x}_k) + \boldsymbol{\Delta}_{\boldsymbol{B}_k})\boldsymbol{u}_k \tag{7.5}$$

where $\boldsymbol{x}_k \in X \subseteq \mathbb{R}^n$ and $\boldsymbol{u}_k \in U \subseteq \mathbb{R}^m$. The parameters $\boldsymbol{\Delta}_{\boldsymbol{A}_k}$ and $\boldsymbol{\Delta}_{\boldsymbol{B}_k}$ are, respectively, uncertainties of $\boldsymbol{A}(\boldsymbol{x}_k)$ and $\boldsymbol{B}(\boldsymbol{x}_k)$ with the following assumptions

$$\|\boldsymbol{\Delta}_{\boldsymbol{A}_k}\| \leq a \text{ and } \|\boldsymbol{\Delta}_{\boldsymbol{B}_k}\| \leq b \tag{7.6}$$

for all $\boldsymbol{x}_k \in X$.

By means of the D-SDRE controller for the deterministic nonlinear system (7.1), we want to find a control input $\boldsymbol{u}_k$ such that the uncertain nonlinear system (7.5) is stabilized. It should be noted that the deterministic nonlinear system (7.1) will be considered to be a nominal system of (7.5) throughout this chapter. The following lemma will play an important role in proving the stability of the D-SDRE feedback controller of (7.5) in the presence of uncertainties.

Lemma 18 *Consider a linear discrete-time system*

$$\boldsymbol{x}_{k+1} = \boldsymbol{A}(\alpha)\boldsymbol{x}_k + \boldsymbol{B}(\beta)\boldsymbol{u}_k \tag{7.7}$$

where $\boldsymbol{A}(\alpha) \in \mathcal{A} := \{\boldsymbol{A}(\alpha) : \boldsymbol{A}(\alpha) = \sum_{i=1}^{L_A} \alpha_i \boldsymbol{A}_i,\ \sum_{i=1}^{L_A} \alpha_i = 1, \alpha_i \geq 0\}$ *and* $\boldsymbol{B}(\beta) \in \mathcal{B} := \{\boldsymbol{B}(\beta) : \boldsymbol{B}(\beta) = \sum_{i=1}^{L_B} \beta_j \boldsymbol{B}_j,\ \sum_{j=1}^{L_B} \beta_j = 1, \beta_j \geq 0\}$. *Then (7.7) is robustly stable in* $\mathcal{A}$ *and* $\mathcal{B}$ *if there exist* $\boldsymbol{P}_{ij} = \boldsymbol{P}_{ij}^\top > \boldsymbol{0}$ *and* $\boldsymbol{G}$ *such that*

$$\begin{bmatrix} \boldsymbol{P}_{ij} & \boldsymbol{A}_i\boldsymbol{G} - \boldsymbol{B}_j\bar{\boldsymbol{K}} \\ \boldsymbol{G}^\top\boldsymbol{A}_i^\top - \bar{\boldsymbol{K}}^\top\boldsymbol{B}_j^\top & \boldsymbol{G} + \boldsymbol{G}^\top - \boldsymbol{P}_{ij} \end{bmatrix} > \boldsymbol{0} \tag{7.8}$$

for all $i \in \mathbb{Z}_{1:L_A}$ *and* $j \in \mathbb{Z}_{1:L_B}$. *Then a robust state feedback controller is obtained by*

$$\boldsymbol{u}_k = -\boldsymbol{K}\boldsymbol{x}_k = -\bar{\boldsymbol{K}}\boldsymbol{G}^{-1}\boldsymbol{x}_k. \tag{7.9}$$

Proof See de Oliveira et al. (1999). □

For the stability proof, the uncertain nonlinear system (7.5) can be rewritten in the following form:

$$\boldsymbol{x}_{k+1} = \boldsymbol{A}_{\boldsymbol{x}_k}(\alpha)\boldsymbol{x}_k + \boldsymbol{B}_{\boldsymbol{x}_k}(\beta)\boldsymbol{u}_k \tag{7.10}$$

where $\boldsymbol{A}_{\boldsymbol{x}_k}(\alpha) \in \mathcal{A}_{\boldsymbol{x}_k} := \{\boldsymbol{A}_{\boldsymbol{x}_k}(\alpha) : \boldsymbol{A}_{\boldsymbol{x}_k}(\alpha) = \sum_{i=1}^{L_A} \alpha_i \boldsymbol{A}_{\boldsymbol{x}_k,i}; \sum_{i=1}^{L_A} = 1, \alpha_i \geq 0\}$ and $\boldsymbol{B}_{\boldsymbol{x}_k}(\beta) \in \mathcal{B}_{\boldsymbol{x}_k} := \{\boldsymbol{B}_{\boldsymbol{x}_k}(\beta) : \boldsymbol{B}_{\boldsymbol{x}_k}(\beta) = \sum_{j=1}^{L_B} \beta_j \boldsymbol{B}_{\boldsymbol{x}_k,j}; \sum_{j=1}^{L_B} = 1, \beta_j \geq 0\}$ where $\boldsymbol{A}_{\boldsymbol{x}_k,i}$ and $\boldsymbol{B}_{\boldsymbol{x}_k,j}$ are the vertices of the polytopes $\mathcal{A}_{\boldsymbol{x}_k}$ and $\mathcal{B}_{\boldsymbol{x}_k}$, respectively.

With the uncertain nonlinear system, we can design a robust state feedback controller via the discrete-time state-dependent Riccati equation.

Theorem 19 *Given the nonlinear system (7.10) and the nominal state feedback control input $\bar{\boldsymbol{u}}_k = -\bar{\boldsymbol{K}}(\boldsymbol{z}_k)\boldsymbol{z}_k$, there exists a matrix $\boldsymbol{G}_k$ satisfying*

$$\begin{bmatrix} \boldsymbol{P}_{ij} & \boldsymbol{A}_{\boldsymbol{x}_k,i}\boldsymbol{G}_k - \boldsymbol{B}_{\boldsymbol{x}_k,j}\bar{\boldsymbol{K}}(\boldsymbol{z}_k) \\ \boldsymbol{G}_k^\top \boldsymbol{A}_{\boldsymbol{x}_k,i}^\top - \bar{\boldsymbol{K}}^\top(\boldsymbol{z}_k)\boldsymbol{B}_{\boldsymbol{x}_k,j}^\top & \boldsymbol{G}_k + \boldsymbol{G}_k^\top - \boldsymbol{P}_{ij} \end{bmatrix} > \boldsymbol{0} \tag{7.11}$$

for all $i \in \mathbb{Z}_{1:L_A}$, $j \in \mathbb{Z}_{1:L_B}$ $\forall \boldsymbol{x}_k \in X \in \mathbb{R}^n$ such that the state feedback controller $\boldsymbol{u}_k = -\boldsymbol{K}(\boldsymbol{x}_k)\boldsymbol{x}_k = -\bar{\boldsymbol{K}}(\boldsymbol{z}_k)\boldsymbol{G}_k^{-1}\boldsymbol{x}_k$ robustly stabilizes the uncertain nonlinear system.

Proof The proof is straightforward from Lemma 18 by using piecewise $\boldsymbol{x}_k$ for all $k \in \mathbb{Z}_{\geq 0}$. □

7.4 CD-SDRE for Uncertain Nonlinear Systems

As one of the control modes in CD-SDRE, the robust MPC is analyzed in this section. Then, we investigate the CD-SDRE technique to control uncertain nonlinear systems.

7.4.1 Robust Stability Analysis of MPC Mode

The robust MPC controller contains two controllers: a nominal MPC-based controller and a supplemental controller to handle uncertainties in the nominal systems, which is the same as the uncertain nonlinear system (Rawlings and Mayne, 2009). First, we consider the nominal controller. Given a discrete-time nonlinear control-affine system (7.1), we want to find a sequence of optimal control signals:

$$\bar{\boldsymbol{\mu}}_N(\boldsymbol{z}_k, k) := \{\bar{\mu}_k(\boldsymbol{z}_k, k), \bar{\mu}_{k+1}(\boldsymbol{z}_k, k), \cdots, \bar{\mu}_{k+N-1}(\boldsymbol{z}_k, k)\} \tag{7.12}$$

that minimizes the following performance index

$$J_N(\boldsymbol{z}_k) = \sum_{i=k}^{k+N-1} \left(\boldsymbol{z}_i^\top \boldsymbol{Q}(\boldsymbol{z}_i)\boldsymbol{z}_i + \bar{\boldsymbol{u}}_i^\top \boldsymbol{R}(\boldsymbol{z}_i)\bar{\boldsymbol{u}}_i \right) + \boldsymbol{z}_{k+N}^\top \boldsymbol{S}(\boldsymbol{z}_{k+N})\boldsymbol{z}_{k+N} \tag{7.13}$$

subject to (7.1), $\boldsymbol{z}_k \in \mathbb{X}$, and $\boldsymbol{u}_k \in \mathbb{U}$ where $\mathbb{X}$ is convex and closed in $\mathbb{R}^n$ and $\mathbb{U}$ is convex and compact in $\mathbb{R}^m$ both of which contain their origins.

By solving the constrained optimization problem, an optimal control sequence $\bar{\boldsymbol{\mu}}_N(\boldsymbol{z}_k, k)$ can be obtained. Then the the nominal MPC-based controller is designed as $\bar{\boldsymbol{u}}_k := \bar{\mu}_k(\boldsymbol{z}_k, k)$ where $\bar{\mu}_k(\boldsymbol{z}_k, k)$ is in (7.12). The following assumptions are needed to prove the stability of the nominal system controlled by MPC.

Assumption 20 *The stage cost and the terminal cost satisfy the bound conditions*

$$\begin{aligned} &\textstyle\sum_{i=k}^{k+N-1} \boldsymbol{z}_i^\top \boldsymbol{Q}(\boldsymbol{z}_i)\boldsymbol{z}_i + \bar{\boldsymbol{u}}_i^\top \boldsymbol{R}(\boldsymbol{z}_i)\bar{\boldsymbol{u}}_i \geq \alpha_1(|\boldsymbol{z}_k|) \\ &\boldsymbol{z}_{k+N}^\top \boldsymbol{S}(\boldsymbol{z}_{k+N})\boldsymbol{z}_{k+N} \leq \alpha_2(|\boldsymbol{z}_k|) \end{aligned}$$

$\forall \boldsymbol{z}_k \in \mathcal{X}_N,\ \forall \bar{\boldsymbol{u}}_k \in \mathbb{U}$ *and* $\forall \boldsymbol{z}_k \in \mathcal{X}_N$ *where* $\alpha_1(\cdot),\ \alpha_2(\cdot) \in \mathcal{K}_\infty$ *and* $\mathcal{X}_N \in \mathbb{X}$ *is the ROA of the system controlled by MPC.*

Assumption 21 *The following inequality holds for all* $k \in \mathbb{Z}_{\geq 0}$*:*

$$\min_{\bar{\boldsymbol{u}} \in \mathbb{U}} \sum_{i=k}^{k+N-1} \left(\boldsymbol{z}_i^\top \boldsymbol{Q}(\boldsymbol{z}_i)\boldsymbol{z}_i + \bar{\boldsymbol{u}}_i^\top \boldsymbol{R}(\boldsymbol{z}_i)\bar{\boldsymbol{u}}_i \right) + \boldsymbol{z}_{k+N}^\top \boldsymbol{S}(\boldsymbol{z}_{k+N})\boldsymbol{z}_{k+N} \leq \boldsymbol{z}_{k+N-1}^\top \boldsymbol{S}(\boldsymbol{z}_{k+N-1})\boldsymbol{z}_{k+N-1}. \tag{7.14}$$

The following theorem can be proven with the assumptions.

Theorem 22 *Given the discrete-time deterministic nonlinear control-affine system (7.1), the performance index in (7.13), and the optimal control sequence (7.12), there exist* $\alpha_1(\cdot),\ \alpha_2(\cdot) \in \mathcal{K}_\infty$ *such that* $J_N(\cdot)$ *satisfies the following inequalities:*

$$\begin{aligned} &J_N(\boldsymbol{z}_k) \geq \alpha_1(|\boldsymbol{z}_k|) \quad \forall \boldsymbol{z}_k \in \mathcal{X}_N \\ &J_N(\boldsymbol{z}_k) \leq \alpha_2(|\boldsymbol{z}_k|) \quad \forall \boldsymbol{z}_k \in \mathcal{X}_N \\ &J_N(\boldsymbol{z}_{k+1}) - J_N(\boldsymbol{z}_k) \leq -\alpha_1(|\boldsymbol{z}_k|) \quad \forall \boldsymbol{z}_k \in \mathcal{X}_N. \end{aligned} \tag{7.15}$$

Proof See Proposition 2.18 in Rawlings and Mayne (2009). □

Theorem 22 shows that the system controlled by MPC is exponentially stable in $\mathcal{X}_N$.

In order to design the second part of the MPC-based controller which is responsible for reducing the error between actual states $\boldsymbol{x}_k$ and the nominal states $\boldsymbol{z}_k$, we consider the following composite system:

$$\begin{aligned} \boldsymbol{x}_{k+1} &= \boldsymbol{A}(\boldsymbol{x}_k)\boldsymbol{x}_k + \boldsymbol{B}(\boldsymbol{x}_k)\boldsymbol{u}_k \\ \boldsymbol{z}_{k+1} &= \boldsymbol{A}(\boldsymbol{z}_k)\boldsymbol{z}_k + \boldsymbol{B}(\boldsymbol{z}_k)\bar{\boldsymbol{u}}_k. \end{aligned} \tag{7.16}$$

We want to design a sequence of optimal control signals:

$$\boldsymbol{\mu}_N(\boldsymbol{x}_k, \boldsymbol{z}_k, k) := \left\{\mu_k(\boldsymbol{x}_k, \boldsymbol{z}_k, k), \mu_{k+1}(\boldsymbol{x}_k, \boldsymbol{z}_k, k), \cdots, \mu_{k+N-1}(\boldsymbol{x}_k, \boldsymbol{z}_k, k)\right\} \tag{7.17}$$

that minimizes the following performance index

$$J_N(\boldsymbol{x}_k, \boldsymbol{z}_k) = \sum_{i=k}^{k+N-1} \Big((\boldsymbol{x}_i - \boldsymbol{z}_i)^\top \boldsymbol{Q}(\boldsymbol{z}_i)(\boldsymbol{x}_i - \boldsymbol{z}_i) + (\boldsymbol{u}_i - \bar{\boldsymbol{u}}_i)^\top \boldsymbol{R}(\boldsymbol{z}_i)(\boldsymbol{u}_i - \bar{\boldsymbol{u}}_i)\Big) \tag{7.18}$$

subject to (7.16), $\boldsymbol{x}_k, \boldsymbol{z}_k \in \mathbb{X}$, and $\boldsymbol{u}_k, \bar{\boldsymbol{u}}_k \in \mathbb{U}$ where $\mathbb{X}$ is convex and closed in $\mathbb{R}^n$ and $\mathbb{U}$ is convex and compact in $\mathbb{R}^m$ both of which contain their origins.

Theorem 23 *The composite system (7.16) together with $\boldsymbol{u}_k = \mu_k(\boldsymbol{x}_k, \boldsymbol{z}_k, k)$ and $\bar{\boldsymbol{u}}_k = \bar{\mu}_k(\boldsymbol{x}_k, \boldsymbol{z}_k, k)$ is exponentially stable in the ROA $\mathcal{X}_N \in \mathbb{X}$ where $\boldsymbol{x}_k, \boldsymbol{z}_k \in \mathcal{X}_N \ \forall k \in \mathbb{Z}_{\geq 0}$.*

Proof To prove the robust stability of the MPC mode, it is assumed that the control signals can be expressed as

$$\begin{aligned} \boldsymbol{u}_k &= -\boldsymbol{K}_{\mathrm{MPC}}\boldsymbol{x}_k - \boldsymbol{K}'_{\mathrm{MPC}}\boldsymbol{z}_k - \boldsymbol{K}_{\mathrm{MPC},0} \\ \bar{\boldsymbol{u}}_k &= -\boldsymbol{K}_{\mathrm{MPC}}\boldsymbol{z}_k - \boldsymbol{K}'_{\mathrm{MPC}}\boldsymbol{z}_k - \boldsymbol{K}_{\mathrm{MPC},0}. \end{aligned} \tag{7.19}$$

Substituting (7.19) into (7.16) yields

$$\breve{\boldsymbol{x}}_{k+1} = \breve{\boldsymbol{A}}_{cl}(\breve{\boldsymbol{x}}_k)\breve{\boldsymbol{x}}_k \tag{7.20}$$

where $\breve{\boldsymbol{x}}_k = \begin{bmatrix} \boldsymbol{x}_k^\top & \boldsymbol{z}_k^\top & \mathbf{1} \end{bmatrix}^\top$.

The stability is proven straightforwardly from Theorem 7 by replacing $\boldsymbol{A}(\boldsymbol{x}_k)$ by $\breve{\boldsymbol{A}}_{cl}(\breve{\boldsymbol{x}}_k)$. □

We have shown that the uncertain nonlinear discrete-time system controlled by D-SDRE and MPC is exponentially stable in its ROA. Since only one controller is activated during each sampling time, the proposed

CD-SDRE controller can be viewed as a switched system (Daafouz et al., 2002; Hovd and Olaru, 2010). In the next section, we will discuss the stability condition of such a switched system.

7.4.2 Stability Analysis of the Switched System (CD-SDRE)

As discussed in the previous sections, the proposed CD-SDRE controller contains two different controllers: D-SDRE and MPC, i.e.,

$$\boldsymbol{u}_k = \begin{cases} -\boldsymbol{K}_1(\boldsymbol{x}_k)\boldsymbol{x}_k, & \text{for robust D-SDRE} \\ -\breve{\boldsymbol{K}}_2(\breve{\boldsymbol{x}}_k)\breve{\boldsymbol{x}}_k, & \text{for robust MPC} \end{cases} \tag{7.21}$$

where $\breve{\boldsymbol{K}}_2(\breve{\boldsymbol{x}}_k) := \begin{bmatrix} \boldsymbol{K}_{\mathrm{MPC}} & \boldsymbol{K}'_{\mathrm{MPC}} & \boldsymbol{K}_{\mathrm{MPC},0} \end{bmatrix}$.

Depending on the location of the estimates of the states and the inputs, the CD-SDRE activates only one controller to generate the proper control signals. An indicator function is defined to augment the two controllers to the nonlinear discrete-time system:

$$\boldsymbol{\eta}_k := \begin{bmatrix} \eta_k^1 & \eta_k^2 \end{bmatrix}^\top \tag{7.22}$$

where

$$\eta_k^i = \begin{cases} 1, & \text{if } \boldsymbol{K}_i \text{ is activated at } k, \\ 0, & \text{otherwise}. \end{cases} \tag{7.23}$$

Substituting (7.21) and (7.22) into the nonlinear discrete-time system yields

$$\begin{aligned} \breve{\boldsymbol{x}}_{k+1} &= \left(\sum_{i=1}^{2} \eta_k^i \left(\breve{\boldsymbol{A}}_i(\breve{\boldsymbol{x}}_k) - \breve{\boldsymbol{B}}(\breve{\boldsymbol{x}}_k)\breve{\boldsymbol{K}}_i(\breve{\boldsymbol{x}}_k) \right) \right) \breve{\boldsymbol{x}}_k \\ &=: \breve{\boldsymbol{A}}_{cl}(\breve{\boldsymbol{x}}_k, \boldsymbol{\eta}_k)\breve{\boldsymbol{x}}_k = \sum_{i=1}^{2} \eta_k^i \breve{\boldsymbol{A}}_{cl}^{\,i}(\breve{\boldsymbol{x}}_k)\breve{\boldsymbol{x}}_k \end{aligned} \tag{7.24}$$

where $\breve{\boldsymbol{A}}_1(\breve{\boldsymbol{x}}_k) := \begin{bmatrix} \boldsymbol{A}(\boldsymbol{x}_k) & \boldsymbol{0} & \boldsymbol{0} \\ \boldsymbol{0} & \boldsymbol{0} & \boldsymbol{0} \\ \boldsymbol{0} & \boldsymbol{0} & \boldsymbol{0} \end{bmatrix}$, $\breve{\boldsymbol{A}}_2(\boldsymbol{x}_k) := \begin{bmatrix} \boldsymbol{A}(\boldsymbol{x}_k) & \boldsymbol{0} & \boldsymbol{0} \\ \boldsymbol{0} & \boldsymbol{A}(\boldsymbol{z}_k) & \boldsymbol{0} \\ \boldsymbol{0} & \boldsymbol{0} & \boldsymbol{0} \end{bmatrix}$, $\breve{\boldsymbol{B}}_1(\breve{\boldsymbol{x}}_k) := \begin{bmatrix} \boldsymbol{B}(\boldsymbol{x}_k) \\ \boldsymbol{0} \\ \boldsymbol{0} \end{bmatrix}$, $\breve{\boldsymbol{B}}_2(\breve{\boldsymbol{x}}_k) :=$

$$\begin{bmatrix} \boldsymbol{B}(\boldsymbol{x}_k) \\ \boldsymbol{B}(\boldsymbol{z}_k) \\ \boldsymbol{0} \end{bmatrix}, \text{ and } \breve{\boldsymbol{K}}_1(\boldsymbol{x}_k) := \begin{bmatrix} \boldsymbol{K}_1(\boldsymbol{x}_k) & \boldsymbol{0} & \boldsymbol{0} \end{bmatrix}.$$

The following theorem shows the stability condition of the switched system.

Theorem 24 *Suppose there exist symmetric positive definite matrices $\boldsymbol{M}_k^1$ (D-SDRE) and $\boldsymbol{M}_k^2$ (MPC) such that*

$$\begin{bmatrix} \boldsymbol{M}_k^i & \breve{\boldsymbol{A}}_{cl}^{i\top} \boldsymbol{M}_k^j \\ \boldsymbol{M}_k^j \breve{\boldsymbol{A}}_{cl}^{i} & \boldsymbol{M}_k^j \end{bmatrix} > \boldsymbol{0} \quad \forall i,\ j \in \mathbb{Z}_{0:1}. \tag{7.25}$$

Then, the switched system (7.24) is exponentially stable in $\mathcal{X}_N$.

Proof Since the stability condition of the nonlinear discrete-time system controlled by D-SDRE and MPC was proven, there exist $\boldsymbol{M}_k^1$ and $\boldsymbol{M}_k^2$ such that

$$\begin{bmatrix} \boldsymbol{M}_k^1 & \breve{\boldsymbol{A}}_{cl}^{1\top} \boldsymbol{M}_k^1 \\ \boldsymbol{M}_k^1 \breve{\boldsymbol{A}}_{cl}^{1} & \boldsymbol{M}_k^1 \end{bmatrix} > \boldsymbol{0}, \quad \text{and} \quad \begin{bmatrix} \boldsymbol{M}_k^2 & \breve{\boldsymbol{A}}_{cl}^{2\top} \boldsymbol{M}_k^2 \\ \boldsymbol{M}_k^2 \breve{\boldsymbol{A}}_{cl}^{2} & \boldsymbol{M}_k^2 \end{bmatrix} > \boldsymbol{0} \quad \forall k \in \mathbb{Z}_{\geq 0}. \tag{7.26}$$

Since we consider the two modes (D-SDRE and the MPC) together, we need to combine matrices in (7.26):

$$\begin{bmatrix} \boldsymbol{M}_k^i \sum_{l=1}^2 \eta_k^l & \breve{\boldsymbol{A}}_{cl}^{i\top} \boldsymbol{M}_k^j \sum_{l=1}^2 \eta_k^l \\ \boldsymbol{M}_k^j \sum_{l=1}^2 \eta_k^l \breve{\boldsymbol{A}}_{cl}^{i} & \boldsymbol{M}_k^j \sum_{l=1}^2 \eta_k^l \end{bmatrix} > \boldsymbol{0}. \tag{7.27}$$

It is sufficient to show that the inequality holds for $i \neq j$. Let $\eta_k^1 = 1$ at time k and $\eta_k^2 = 1$ at time $k+1$ since the inequalities in (7.26) hold for $\eta_k^1 = 1\ \forall k \in \mathbb{Z}_{\geq 0}$ and $\eta_k^2 = 1\ \forall k \in \mathbb{Z}_{\geq 0}$, respectively. Then

$$\begin{bmatrix} \boldsymbol{M}_k^i & \breve{\boldsymbol{A}}_{cl}^{i\top} \boldsymbol{M}_{k+1}^j \\ \boldsymbol{M}_{k+1}^j \breve{\boldsymbol{A}}_{cl}^{i} & \boldsymbol{M}_{k+1}^j \end{bmatrix} > \boldsymbol{0}. \tag{7.28}$$

By Schur complement (Boyd et al., 1994), it is equivalent to the following inequality,

$$\breve{\boldsymbol{x}}_k^\top \left(\boldsymbol{M}_k^i - \breve{\boldsymbol{A}}_{cl}^{i\top} \boldsymbol{M}_{k+1}^j \breve{\boldsymbol{A}}_{cl}^{i} \right) \breve{\boldsymbol{x}}_k > \boldsymbol{0}. \tag{7.29}$$

The Lyapunov function candidate for the switched system is defined as

$$V(\breve{\boldsymbol{x}}_k) := \breve{\boldsymbol{x}}_k^\top \boldsymbol{M}_k(\boldsymbol{\eta}_k)\breve{\boldsymbol{x}}_k = \breve{\boldsymbol{x}}_k^\top \left(\sum_{l=1}^{2} \eta_k^l \boldsymbol{M}_k^l\right) \breve{\boldsymbol{x}}_k \tag{7.30}$$

where $\boldsymbol{M}_k^i$ is symmetric positive definite, defined in (7.26).

Hence, the following inequalities hold due to the definition of the $V(\breve{\boldsymbol{x}}_k)$ and $\boldsymbol{M}_k^i$:

$$\begin{aligned} V(\breve{\boldsymbol{x}}_k) &\geq \lambda_{min}(\min\{\boldsymbol{M}_k^1,\ \boldsymbol{M}_k^2\})|\breve{\boldsymbol{x}}_k| =: \alpha_1(|\breve{\boldsymbol{x}}_k|) \\ V(\breve{\boldsymbol{x}}_k) &\leq \lambda_{max}(\max\{\boldsymbol{M}_k^1,\ \boldsymbol{M}_k^2\})|\breve{\boldsymbol{x}}_k| =: \alpha_2(|\breve{\boldsymbol{x}}_k|). \end{aligned} \tag{7.31}$$

The following inequality can be derived by the definition of the Lyapunov function

$$\begin{aligned} V(\boldsymbol{x}_{k+1}) - V(\boldsymbol{x}_k) &= \breve{\boldsymbol{x}}_{k+1}^\top \left(\sum_{l=1}^{2} \eta_{k+1}^l \boldsymbol{M}_{k+1}^l\right) \breve{\boldsymbol{x}}_{k+1} - \breve{\boldsymbol{x}}_k^\top \left(\sum_{l=1}^{2} \eta_k^l \boldsymbol{M}_k^l\right) \breve{\boldsymbol{x}}_k \\ &= -\breve{\boldsymbol{x}}_k^\top \left(\boldsymbol{M}_k^i - \breve{\boldsymbol{A}}_{cl}^{i\top} \boldsymbol{M}_{k+1}^j \breve{\boldsymbol{A}}_{cl,k}^{i}\right) \breve{\boldsymbol{x}}_k \\ &\leq -\alpha_3(|\boldsymbol{x}_k|) < 0 \end{aligned} \tag{7.32}$$

where $\alpha_3 \in \mathcal{K}_\infty$.

This proves the theorem. $\square$

We have shown the concept, the mechanism, and the stability condition of the CD-SDRE controller in the presence of uncertainties. We evaluate the proposed controller in the following section.

7.5 Numerical Evaluation

In order to evaluate the performance of the proposed CD-SDRE controller in the presence of uncertainties in the plant, a challenging problem is considered: spacecraft attitude control in the presence fuel slosh effect and limited actuator performance. To this end, we first derive the equations of motion for the spacecraft attitude.

7.5.1 Generalized Attitude Dynamics in the Presence of Fuel Slosh Effect

In this chapter, it is assumed that the fuel tank has a spherical shape. The first fuel sloshing mode in the spherical tank is considered (Bryson, Jr., 1994). Figure 7.1 shows the coordinates and variables of the spacecraft considered in this chapter. The dynamics of the rigid spacecraft with the first fuel sloshing mode is analogous to that of tether-connected spacecraft with inelastic tethers (Chang et al., 2010b).

The rotational matrix from the spacecraft body-fixed frame ($\hat{\boldsymbol{b}}_1,\ \hat{\boldsymbol{b}}_2,\ \hat{\boldsymbol{b}}_3$) to the inertial frame ($\hat{\boldsymbol{i}},\ \hat{\boldsymbol{j}},\ \hat{\boldsymbol{k}}$) is obtained by using a series of 3 rotations (Hughes, 1986):

$$\begin{aligned}\boldsymbol{C}^{bi}(\phi,\theta,\psi) &= \left(\boldsymbol{C}^{ib}\right)^{\top}(\phi,\theta,\psi) = \boldsymbol{C}_3^{\top}(\psi)\boldsymbol{C}_2^{\top}(\theta)\boldsymbol{C}_1^{\top}(\phi) \\ &= \begin{bmatrix} c\theta c\psi & s\phi s\theta c\psi - c\phi s\psi & c\phi s\theta c\psi + s\phi s\psi \\ c\theta s\psi & s\phi s\theta s\psi + c\phi c\psi & c\phi s\theta s\psi - s\phi c\psi \\ -s\theta & s\phi c\theta & c\phi c\theta \end{bmatrix}\end{aligned} \tag{7.33}$$

where $c(\cdot) := \cos(\cdot)$ and $s(\cdot) := \sin(\cdot)$.

The distance between the mass center of the spacecraft and the center of the fuel tank, expressed in the inertial frame, can be found by using (7.33):

$${}^{i}\boldsymbol{l} = \boldsymbol{C}^{bi}\,{}^{b}\boldsymbol{l} = l \begin{bmatrix} c\theta c\psi \\ c\theta s\psi \\ -s\theta \end{bmatrix}. \tag{7.34}$$

Likewise, the distance between the center of the fuel tank and the mass center of the fuel in the tank, expressed in the inertial frame, can be described as

$${}^{i}\boldsymbol{r}_{\mathrm{f}} = \boldsymbol{C}^{si}\,{}^{s}\boldsymbol{r}_{\mathrm{f}} = r_{\mathrm{f}} \begin{bmatrix} c\theta_{\mathrm{f}} c\psi_{\mathrm{f}} \\ c\theta_{\mathrm{f}} s\psi_{\mathrm{f}} \\ -s\theta_{\mathrm{f}} \end{bmatrix}. \tag{7.35}$$

Therefore, the distance between the mass center of the spacecraft and the mass center of the fuel, expressed

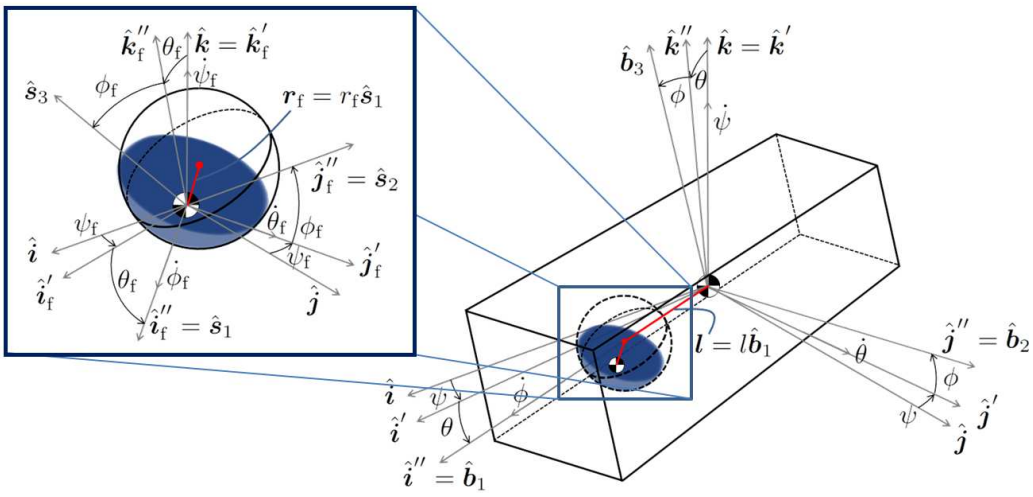

Figure 7.1: Coordinates and variables of the spacecraft and the fuel slosh dynamics

in the inertial frame, can be obtained from (7.34) and (7.35) as follows:

$$ {}^{i}\boldsymbol{d}_{\mathrm{f}} = {}^{i}\boldsymbol{l} + {}^{i}\boldsymbol{r}_{\mathrm{f}} = \begin{bmatrix} lc\theta c\psi + r_{\mathrm{f}}c\theta_{\mathrm{f}}c\psi_{\mathrm{f}} \\ lc\theta s\psi + r_{\mathrm{f}}c\theta_{\mathrm{f}}s\psi_{\mathrm{f}} \\ -ls\theta - r_{\mathrm{f}}s\theta_{\mathrm{f}} \end{bmatrix}. \tag{7.36} $$

By differentiating (7.36) with respect to time, the velocity of the mass center of the fuel is obtained:

$$ {}^{i}\dot{\boldsymbol{d}}_{\mathrm{f}} = \begin{bmatrix} -l\dot{\theta}s\theta c\psi - l\dot{\psi}c\theta s\psi - r_{\mathrm{f}}\dot{\theta}_{\mathrm{f}}s\theta_{\mathrm{f}}c\psi_{\mathrm{f}} - r_{\mathrm{f}}\dot{\psi}_{\mathrm{f}}c\theta_{\mathrm{f}}s\psi_{\mathrm{f}} \\ -l\dot{\theta}s\theta s\psi + l\dot{\psi}c\theta c\psi - r_{\mathrm{f}}\dot{\theta}_{\mathrm{f}}s\theta_{\mathrm{f}}s\psi_{\mathrm{f}} + r_{\mathrm{f}}\dot{\psi}_{\mathrm{f}}c\theta_{\mathrm{f}}c\psi_{\mathrm{f}} \\ -l\dot{\theta}c\theta - r_{\mathrm{f}}\dot{\theta}_{\mathrm{f}}c\theta_{\mathrm{f}} \end{bmatrix}. \tag{7.37} $$

Then, the translational kinetic energy of the fuel is obtained by using (7.37) as

$$ \begin{aligned} \mathcal{T}_{\text{rot,f}} &= \frac{1}{2}m_{\mathrm{f}}\|\dot{\boldsymbol{d}}_{\mathrm{f}}\|^2 \\ &= \frac{1}{2}m_{\mathrm{f}}l^2\left(\dot{\theta}^2 + \dot{\psi}^2c^2\theta\right) + \frac{1}{2}m_{\mathrm{f}}r_{\mathrm{f}}^2\left(\dot{\theta}_{\mathrm{f}}^2 + \dot{\psi}_{\mathrm{f}}^2c^2\theta_{\mathrm{f}}\right) + m_{\mathrm{f}}lr_{\mathrm{f}}\Big[\dot{\theta}\Big\{\dot{\theta}_{\mathrm{f}}\big(c\theta c\theta_{\mathrm{f}} + s\theta s\theta_{\mathrm{f}}c(\psi-\psi_{\mathrm{f}})\big) \\ &\quad - \dot{\psi}_{\mathrm{f}}s\theta c\theta_{\mathrm{f}}s(\psi-\psi_{\mathrm{f}})\Big\} + \dot{\psi}\Big\{\dot{\theta}_{\mathrm{f}}c\theta s\theta_{\mathrm{f}}s(\psi-\psi_{\mathrm{f}}) + \dot{\psi}_{\mathrm{f}}c\theta c\theta_{\mathrm{f}}c(\psi-\psi_{\mathrm{f}})\Big\}\Big]. \end{aligned} \tag{7.38} $$

Therefore, the total kinetic energy of the spacecraft with the fuel slosh effect can be expressed as follows:

$$ \begin{aligned} \mathcal{T} &= \big(\mathcal{T}_{\text{rot,b}} + \mathcal{T}_{\text{trans,b}}\big) + \big(\mathcal{T}_{\text{rot,f}} + \mathcal{T}_{\text{trans,f}}\big) \\ &= \frac{1}{2}\boldsymbol{\omega}^{\top}\boldsymbol{I}_{\mathrm{b}}\boldsymbol{\omega} + \frac{1}{2}\boldsymbol{\omega}_{\mathrm{f}}^{\top}\boldsymbol{I}_{\mathrm{f}}\boldsymbol{\omega}_{\mathrm{f}} + \frac{1}{2}m_{\mathrm{f}}l^2\Big(\dot{\theta}^2 + \dot{\psi}^2c^2\theta\Big) + \frac{1}{2}m_{\mathrm{f}}r_{\mathrm{f}}^2\Big(\dot{\theta}_{\mathrm{f}}^2 + \dot{\psi}_{\mathrm{f}}^2c^2\theta_{\mathrm{f}}\Big) \\ &\quad + m_{\mathrm{f}}lr_{\mathrm{f}}\Big[\dot{\theta}\Big\{\dot{\theta}_{\mathrm{f}}\big(c\theta c\theta_{\mathrm{f}} + s\theta s\theta_{\mathrm{f}}c(\psi-\psi_{\mathrm{f}})\big) - \dot{\psi}_{\mathrm{f}}s\theta c\theta_{\mathrm{f}}s(\psi-\psi_{\mathrm{f}})\Big\} + \dot{\psi}\Big\{\dot{\theta}_{\mathrm{f}}c\theta s\theta_{\mathrm{f}}s(\psi-\psi_{\mathrm{f}}) \\ &\quad + \dot{\psi}_{\mathrm{f}}c\theta c\theta_{\mathrm{f}}c(\psi-\psi_{\mathrm{f}})\Big\}\Big] \end{aligned} \tag{7.39} $$

where $\mathcal{T}_{\text{trans,b}} = 0$ is assumed, i.e., there is no translational motion, to confine our interest in the rotational motion of the spacecraft in the presence of the fuel slosh effect. Moreover, the angular velocities of the body

and the fuel respect to the inertial frame, respectively, can be expressed as

$$\boldsymbol{\omega} := \begin{bmatrix} \omega_1 \\ \omega_2 \\ \omega_3 \end{bmatrix} = \begin{bmatrix} \dot{\phi} - \dot{\psi} s\theta \\ \dot{\theta} c\phi + \dot{\psi} c\theta s\phi \\ -\dot{\theta} s\phi + \dot{\psi} c\theta c\phi \end{bmatrix} \quad \text{and} \quad \boldsymbol{\omega}_{\mathrm{f}} := \begin{bmatrix} \omega_{\mathrm{f},1} \\ \omega_{\mathrm{f},2} \\ \omega_{\mathrm{f},3} \end{bmatrix} = \begin{bmatrix} \dot{\phi}_{\mathrm{f}} - \dot{\psi}_{\mathrm{f}} s\theta_{\mathrm{f}} \\ \dot{\theta}_{\mathrm{f}} c\phi_{\mathrm{f}} + \dot{\psi}_{\mathrm{f}} c\theta_{\mathrm{f}} s\phi_{\mathrm{f}} \\ -\dot{\theta}_{\mathrm{f}} s\phi_{\mathrm{f}} + \dot{\psi}_{\mathrm{f}} c\theta_{\mathrm{f}} c\phi_{\mathrm{f}} \end{bmatrix}. \tag{7.40}$$

By assuming that the potential energy of the spacecraft is negligible (i.e., $\mathcal{V} \approx 0$), the Lagrangian of the system is the same as the total kinetic energy in (7.39), i.e.,

$$\mathcal{L} = \mathcal{T} - \mathcal{V} = \mathcal{T}. \tag{7.41}$$

In order to derive the equations of motion of the spacecraft in the presence of the fuel slosh effect, Lagrange's equations of motion is used (Goldstein et al., 2002):

$$\frac{d}{dt}\left(\frac{\partial \mathcal{L}}{\partial \dot{\boldsymbol{q}}}\right) - \frac{\partial \mathcal{L}}{\partial \boldsymbol{q}} + \frac{\partial \mathcal{R}}{\partial \dot{\boldsymbol{q}}} = \boldsymbol{\tau} \tag{7.42}$$

where $\boldsymbol{q} := [\phi \;\; \theta \;\; \psi \;\; \phi_{\mathrm{f}} \;\; \theta_{\mathrm{f}} \;\; \psi_{\mathrm{f}}]^{\top}$ is the generalized coordinates and $\mathcal{R} := \sum \varepsilon_i \dot{q}_i^2$ is Rayleigh's dissipation function.

By the assumption of the first fuel slosh mode, we can obtain constraints in the rotational motion of the fuel slosh:

$$\begin{aligned} \dot{\theta}_{\mathrm{f}} c\phi_{\mathrm{f}} &= -\dot{\psi}_{\mathrm{f}} c\theta_{\mathrm{f}} s\phi_{\mathrm{f}} \\ \dot{\theta}_{\mathrm{f}} s\phi_{\mathrm{f}} &= \dot{\psi}_{\mathrm{f}} c\theta_{\mathrm{f}} c\phi_{\mathrm{f}}. \end{aligned} \tag{7.43}$$

The nonlinear equations of motion of the spacecraft with the first fuel slosh mode are derived by solving (7.42) together with the constraints (7.43). The equations of motion of the spacecraft attitude in the presence

of the first fuel slosh mode are obtained by solving (7.42):

$$
\begin{aligned}
\phi \;:\;& I_{\mathrm{b},1}\Big(\ddot{\phi}-\ddot{\psi}s\theta-\dot{\psi}\dot{\theta}c\theta\Big)+I_{\mathrm{b},2}\Big(\dot{\theta}c\phi+\dot{\psi}s\phi c\theta\Big)\Big(\dot{\theta}s\phi-\dot{\psi}c\phi c\theta\Big)\\
&-I_{\mathrm{b},3}\Big(\dot{\theta}s\phi-\dot{\psi}c\phi c\theta\Big)\Big(\dot{\theta}c\phi+\dot{\psi}s\phi c\theta\Big)=\tau_1\\
\theta \;:\;& I_{\mathrm{b},2}\Big(\ddot{\theta}c^2\phi+\ddot{\psi}c\phi s\phi c\theta-2\dot{\phi}\dot{\theta}c\phi s\phi+\dot{\phi}\dot{\psi}c2\phi c\theta\Big)+I_{\mathrm{b},3}\Big(\ddot{\theta}s^2\phi-\ddot{\psi}c\phi s\phi c\theta+2\dot{\phi}\dot{\theta}c\phi s\phi\\
&-\dot{\phi}\dot{\psi}c2\phi c\theta\Big)+m_{\mathrm{f}}l^2\ddot{\theta}+m_{\mathrm{f}}lr_{\mathrm{f}}\Big\{\ddot{\theta}_{\mathrm{f}}\Big(c\theta c\theta_{\mathrm{f}}+s\theta s\theta_{\mathrm{f}}c(\psi-\psi_{\mathrm{f}})\Big)-\dot{\theta}_{\mathrm{f}}\Big(\dot{\theta}_{\mathrm{f}}c\theta s\theta_{\mathrm{f}}-\dot{\theta}_{\mathrm{f}}s\theta c\theta_{\mathrm{f}}c(\psi-\psi_{\mathrm{f}})\\
&-\dot{\psi}_{\mathrm{f}}s\theta s\theta_{\mathrm{f}}s(\psi-\psi_{\mathrm{f}})\Big)-\ddot{\psi}_{\mathrm{f}}s\theta c\theta_{\mathrm{f}}s(\psi-\psi_{\mathrm{f}})+\dot{\theta}_{\mathrm{f}}\dot{\psi}_{\mathrm{f}}s\theta s\theta_{\mathrm{f}}s(\psi-\psi_{\mathrm{f}})+\dot{\psi}_{\mathrm{f}}^2s\theta c\theta_{\mathrm{f}}c(\psi-\psi_{\mathrm{f}})\Big\}\\
&+I_{\mathrm{b},1}\Big(\dot{\phi}-\dot{\psi}s\theta\Big)\dot{\psi}c\theta+I_{\mathrm{b},2}\dot{\psi}^2s^2\phi c\theta s\theta+I_{\mathrm{b},3}\dot{\psi}^2c^2\phi c\theta s\theta+m_{\mathrm{f}}l^2\dot{\psi}^2c\theta s\theta=\tau_2 \qquad (7.44)\\
\psi \;:\;& I_{\mathrm{b},1}\Big(-\ddot{\phi}s\theta+\ddot{\psi}s^2\theta-\dot{\phi}\dot{\theta}c\theta+2\dot{\theta}\dot{\psi}c\theta s\theta\Big)+I_{\mathrm{b},2}\Big(\ddot{\theta}c\phi s\phi c\theta+\ddot{\psi}s^2\phi c^2\theta+\dot{\phi}\dot{\theta}c2\phi c\theta\\
&+2\dot{\phi}\dot{\psi}c\phi s\phi c^2\theta-\dot{\theta}^2c\phi s\phi s\theta-2\dot{\theta}\dot{\psi}s^2\phi c\theta s\theta\Big)+I_{\mathrm{b},3}\Big(-\ddot{\theta}c\phi s\phi c\theta+\ddot{\psi}c^2\phi c^2\theta-\dot{\phi}\dot{\theta}c2\phi c\theta\\
&-2\dot{\phi}\dot{\psi}c\phi s\phi c^2\theta+\dot{\theta}^2c\phi s\phi s\theta-2\dot{\theta}\dot{\psi}c^2\phi c\theta s\theta\Big)+m_{\mathrm{f}}l^2\Big(\ddot{\psi}c^2\theta-2\dot{\theta}\dot{\psi}c\theta s\theta\Big)\\
&+m_{\mathrm{f}}lr_{\mathrm{f}}\Big\{\ddot{\theta}_{\mathrm{f}}c\theta s\theta_{\mathrm{f}}s(\psi-\psi_{\mathrm{f}})+\ddot{\psi}_{\mathrm{f}}c\theta c\theta_{\mathrm{f}}c(\psi-\psi_{\mathrm{f}})+\dot{\theta}_{\mathrm{f}}^2c\theta c\theta_{\mathrm{f}}s(\psi-\psi_{\mathrm{f}})-\dot{\theta}_{\mathrm{f}}\dot{\psi}_{\mathrm{f}}c\theta s\theta_{\mathrm{f}}c(\psi-\psi_{\mathrm{f}})\\
&-\dot{\theta}_{\mathrm{f}}\dot{\psi}_{\mathrm{f}}c\theta s\theta_{\mathrm{f}}c(\psi-\psi_{\mathrm{f}})+\dot{\psi}_{\mathrm{f}}^2c\theta c\theta_{\mathrm{f}}s(\psi-\psi_{\mathrm{f}})\Big\}=\tau_3.
\end{aligned}
$$

The equations of motion of the fuel with the first fuel slosh mode can be expressed as

$$
\begin{aligned}
\phi_{\mathrm{f}} \;:\;& I_{\mathrm{f},1}\Big(\ddot{\phi}_{\mathrm{f}}-\ddot{\psi}_{\mathrm{f}}s\theta_{\mathrm{f}}-\dot{\theta}_{\mathrm{f}}\dot{\psi}_{\mathrm{f}}c\theta_{\mathrm{f}}\Big)+2\varepsilon_1\dot{\phi}_{\mathrm{f}}=0\\
\theta_{\mathrm{f}} \;:\;& m_{\mathrm{f}}lr_{\mathrm{f}}\Big\{\ddot{\theta}\Big(c\theta c\theta_{\mathrm{f}}+s\theta s\theta_{\mathrm{f}}c(\psi-\psi_{\mathrm{f}})\Big)-\dot{\theta}\Big(\dot{\theta}s\theta c\theta_{\mathrm{f}}-\dot{\theta}c\theta s\theta_{\mathrm{f}}c(\psi-\psi_{\mathrm{f}})+\dot{\psi}s\theta s\theta_{\mathrm{f}}s(\psi-\psi_{\mathrm{f}})\Big)\\
&+\ddot{\psi}c\theta s\theta_{\mathrm{f}}s(\psi-\psi_{\mathrm{f}})-\dot{\theta}\dot{\psi}s\theta s\theta_{\mathrm{f}}s(\psi-\psi_{\mathrm{f}})+\dot{\psi}^2c\theta s\theta_{\mathrm{f}}c(\psi-\psi_{\mathrm{f}})\Big\}+I_{\mathrm{f},1}\Big(\dot{\phi}_{\mathrm{f}}-\dot{\psi}_{\mathrm{f}}s\theta_{\mathrm{f}}\Big)\dot{\psi}_{\mathrm{f}}c\theta_{\mathrm{f}}\\
&+m_{\mathrm{f}}r_{\mathrm{f}}^2\dot{\psi}_{\mathrm{f}}^2c\theta_{\mathrm{f}}s\theta_{\mathrm{f}}+2\varepsilon_2\dot{\theta}_{\mathrm{f}}=0 \qquad (7.45)\\
\psi_{\mathrm{f}} \;:\;& I_{\mathrm{f},1}\Big(-\ddot{\phi}_{\mathrm{f}}s\theta_{\mathrm{f}}+\ddot{\psi}_{\mathrm{f}}s^2\theta_{\mathrm{f}}-\dot{\phi}_{\mathrm{f}}\dot{\theta}_{\mathrm{f}}c\theta_{\mathrm{f}}+2\dot{\theta}_{\mathrm{f}}\dot{\psi}_{\mathrm{f}}c\theta_{\mathrm{f}}s\theta_{\mathrm{f}}\Big)+m_{\mathrm{f}}r_{\mathrm{f}}^2\ddot{\psi}_{\mathrm{f}}c^2\theta_{\mathrm{f}}-2m_{\mathrm{f}}r_{\mathrm{f}}^2\dot{\psi}_{\mathrm{f}}\dot{\theta}_{\mathrm{f}}c\theta_{\mathrm{f}}s\theta_{\mathrm{f}}\\
&+m_{\mathrm{f}}lr_{\mathrm{f}}\Big\{-\ddot{\theta}s\theta c\theta_{\mathrm{f}}s(\psi-\psi_{\mathrm{f}})-\dot{\theta}^2c\theta c\theta_{\mathrm{f}}s(\psi-\psi_{\mathrm{f}})-\dot{\theta}\dot{\psi}s\theta c\theta_{\mathrm{f}}c(\psi-\psi_{\mathrm{f}})+\ddot{\psi}c\theta c\theta_{\mathrm{f}}c(\psi-\psi_{\mathrm{f}})\\
&-\dot{\theta}\dot{\psi}s\theta c\theta_{\mathrm{f}}c(\psi-\psi_{\mathrm{f}})-\dot{\psi}^2c\theta c\theta_{\mathrm{f}}s(\psi-\psi_{\mathrm{f}})\Big\}+2\varepsilon_3\dot{\psi}_{\mathrm{f}}=0.
\end{aligned}
$$

Combining (7.44) and (7.45) yields a matrix form as

$$
\boldsymbol{\mathcal{M}}(\boldsymbol{q})\ddot{\boldsymbol{q}}+\boldsymbol{\mathcal{C}}(\boldsymbol{q},\dot{\boldsymbol{q}})\dot{\boldsymbol{q}}=\boldsymbol{\tau} \qquad (7.46)
$$

where $\boldsymbol{q} := [\phi \;\; \theta \;\; \psi \;\; \phi_\mathrm{f} \;\; \theta_\mathrm{f} \;\; \psi_\mathrm{f}]^\top$.

It is assumed that the states of the fuel ($\phi_\mathrm{f},\ \theta_\mathrm{f},\ \psi_\mathrm{f}$) and their rates are not measurable. In order to apply the proposed CD-SDRE controller, we use the nonlinear dynamic model of the spacecraft body (7.44) and the terms with states of the fuel are considered to be uncertainties. Then the equations of motion of the spacecraft body can be expressed from (7.44) as

$$\boldsymbol{\mathcal{M}}_\mathrm{b}(\boldsymbol{q}_\mathrm{b})\ddot{\boldsymbol{q}}_\mathrm{b} + \boldsymbol{\mathcal{C}}_\mathrm{b}(\boldsymbol{q}_\mathrm{b}, \dot{\boldsymbol{q}}_\mathrm{b})\dot{\boldsymbol{q}}_\mathrm{b} = \boldsymbol{\tau}_\mathrm{b} + \boldsymbol{\Delta}(\boldsymbol{q}_\mathrm{b}, \boldsymbol{q}_\mathrm{f}, \dot{\boldsymbol{q}}_\mathrm{f}, \ddot{\boldsymbol{q}}_\mathrm{f}) \tag{7.47}$$

where $\boldsymbol{q}_\mathrm{b} := [\phi \;\; \theta \;\; \psi]^\top$ and $\boldsymbol{q}_\mathrm{f} := [\phi_\mathrm{f} \;\; \theta_\mathrm{f} \;\; \psi_\mathrm{f}]^\top$. The uncertainty $\boldsymbol{\Delta}(\boldsymbol{q}_\mathrm{b}, \boldsymbol{q}_\mathrm{f}, \dot{\boldsymbol{q}}_\mathrm{f}, \ddot{\boldsymbol{q}}_\mathrm{f})$ consists of terms in (7.44) which include at least one element of the fuel (e.g., $\boldsymbol{q}_\mathrm{f}$, $\dot{\boldsymbol{q}}_\mathrm{f}$, $\ddot{\boldsymbol{q}}_\mathrm{f}$. Therefore, it has the following form

$$\boldsymbol{\Delta} = [0 \;\; \boldsymbol{\Delta}_2 \;\; \boldsymbol{\Delta}_3]^\top \tag{7.48}$$

where

$$\begin{aligned}
\boldsymbol{\Delta}_2 = m_\mathrm{f} l r_\mathrm{f}\Big(&- \ddot{\theta}_\mathrm{f}\Big(c\theta c\theta_\mathrm{f} + s\theta s\theta_\mathrm{f} c(\psi - \psi_\mathrm{f})\Big) + \ddot{\psi}_\mathrm{f} s\theta c\theta_\mathrm{f} s(\psi - \psi_\mathrm{f}) - \dot{\theta}_\mathrm{f}^2 s\theta c\theta_\mathrm{f} c(\psi - \psi_\mathrm{f}) \\
&- 2\dot{\theta}_\mathrm{f}\dot{\psi}_\mathrm{f} s\theta s\theta_\mathrm{f} s(\psi - \psi_\mathrm{f}) - \dot{\psi}_\mathrm{f}^2 s\theta c\theta_\mathrm{f} c(\psi - \psi_\mathrm{f})\Big) \\
\boldsymbol{\Delta}_3 = m_\mathrm{f} l r_\mathrm{f}\Big(&- \ddot{\theta}_\mathrm{f} c\theta s\theta_\mathrm{f} s(\psi - \psi_\mathrm{f}) - \ddot{\psi}_\mathrm{f} c\theta c\theta_\mathrm{f} c(\psi - \psi_\mathrm{f}) - \dot{\theta}_\mathrm{f}^2 c\theta c\theta_\mathrm{f} s(\psi - \psi_\mathrm{f}) + 2\dot{\theta}_\mathrm{f}\dot{\psi}_\mathrm{f} c\theta s\theta_\mathrm{f} c(\psi - \psi_\mathrm{f}) \\
&- \dot{\psi}_\mathrm{f}^2 c\theta c\theta_\mathrm{f} s(\psi - \psi_\mathrm{f})\Big).
\end{aligned}$$

The matrices $\boldsymbol{\mathcal{M}}_\mathrm{b}(\boldsymbol{q}_\mathrm{b})$ and $\boldsymbol{\mathcal{C}}_\mathrm{b}(\boldsymbol{q}_\mathrm{b}, \dot{\boldsymbol{q}}_\mathrm{b})$ are defined as

$$\boldsymbol{\mathcal{M}}_\mathrm{b}(\boldsymbol{q}_\mathrm{b}) := \begin{bmatrix} I_{\mathrm{b},1} & 0 & -I_{\mathrm{b},1} s\theta \\ 0 & I_{\mathrm{b},2} c^2\phi + I_{\mathrm{b},3} s^2\phi & (I_{\mathrm{b},2} - I_{\mathrm{b},3}) c\phi s\phi c\theta \\ -I_{\mathrm{b},1} s\theta & (I_{\mathrm{b},2} - I_{\mathrm{b},3}) c\phi s\phi c\theta & I_{\mathrm{b},1} s^2\theta + I_{\mathrm{b},2} s^2\phi c^2\theta + I_{\mathrm{b},3} c^2\phi c^2\theta \end{bmatrix}$$

$$\boldsymbol{\mathcal{C}}_\mathrm{b}(\boldsymbol{q}_\mathrm{b}, \dot{\boldsymbol{q}}_\mathrm{b}) := \begin{bmatrix} 0 & \mathcal{C}_{1,2} & \mathcal{C}_{1,3} \\ \mathcal{C}_{2,1} & 0 & \mathcal{C}_{2,3} \\ \mathcal{C}_{3,1} & \mathcal{C}_{3,2} & 0 \end{bmatrix}$$

where

$$\mathcal{C}_{1,2} = (I_{\mathrm{b},2} - I_{\mathrm{b},3})\dot{\theta}c\phi s\phi + I_{\mathrm{b},2}\dot{\psi}c2\phi c\theta$$

$$\mathcal{C}_{1,3} = -I_{\mathrm{b},1}\dot{\theta}c\theta - (I_{\mathrm{b},2} - I_{\mathrm{b},3})\dot{\psi}c\phi s\phi c^2\theta - I_{\mathrm{b},3}\dot{\theta}c2\phi c\theta$$

$$\mathcal{C}_{2,1} = I_{\mathrm{b},1}\dot{\psi}c\theta - 2(I_{\mathrm{b},2} - I_{\mathrm{b},3})\dot{\theta}c\phi s\phi + I_{\mathrm{b},2}\dot{\psi}c2\phi c\theta$$

$$\mathcal{C}_{2,3} = -I_{\mathrm{b},1}\dot{\psi}c\theta s\theta - I_{\mathrm{b},3}\dot{\phi}c2\phi c\theta + (I_{\mathrm{b},2}s^2\phi + I_{\mathrm{b},3}c^2\phi)\dot{\psi}c\theta s\theta + m_{\mathrm{f}}l^2\dot{\psi}c\theta s\theta$$

$$\mathcal{C}_{3,1} = I_{\mathrm{b},1}\dot{\theta}c\theta + 2(I_{\mathrm{b},2} - I_{\mathrm{b},3})\dot{\psi}c\phi s\phi c^2\theta - I_{\mathrm{b},3} - \dot{\theta}c2\phi c\theta$$

$$\mathcal{C}_{3,2} = 2I_{\mathrm{b},1}\dot{\psi}c\theta s\theta + I_{\mathrm{b},2}\dot{\phi}c2\phi c\theta - (I_{\mathrm{b},2} - I_{\mathrm{b},3})\dot{\theta}c\phi s\phi s\theta - 2(I_{\mathrm{b},2}s^2\phi + I_{\mathrm{b},3}c^2\phi)\dot{\psi}c\theta s\theta - 2m_{\mathrm{f}}l^2\dot{\psi}c\theta s\theta.$$

Therefore, the state-space equation of the equations of motion of the spacecraft is written as

$$\underbrace{\begin{bmatrix}\dot{\boldsymbol{q}}_{\mathrm{b}}\\ \ddot{\boldsymbol{q}}_{\mathrm{b}}\end{bmatrix}}_{=:\dot{\boldsymbol{x}}} = \left(\underbrace{\begin{bmatrix}\boldsymbol{0}_{3\times3} & \boldsymbol{I}_{3\times3}\\ \boldsymbol{0}_{3\times3} & -\boldsymbol{\mathcal{M}}^{-1}\boldsymbol{\mathcal{C}}\end{bmatrix}}_{=:\boldsymbol{\mathcal{A}}(\boldsymbol{x})} + \underbrace{\begin{bmatrix}\boldsymbol{0}_{3\times3} & \boldsymbol{0}_{3\times3}\\ \boldsymbol{\mathcal{M}}^{-1}\begin{bmatrix}\boldsymbol{0}_{3\times1} & \boldsymbol{\Delta}\theta^{-1} & \boldsymbol{0}_{3\times1}\end{bmatrix} & \boldsymbol{0}_{3\times3}\end{bmatrix}}_{=:\boldsymbol{\Delta}_{\boldsymbol{\mathcal{A}}}}\right)\underbrace{\begin{bmatrix}\boldsymbol{q}_{\mathrm{b}}\\ \dot{\boldsymbol{q}}_{\mathrm{b}}\end{bmatrix}}_{=:\boldsymbol{x}} + \underbrace{\begin{bmatrix}\boldsymbol{0}_{3\times3}\\ \boldsymbol{\mathcal{M}}^{-1}\end{bmatrix}}_{=:\boldsymbol{\mathcal{B}}(\boldsymbol{x})}\underbrace{\boldsymbol{\tau}_{\mathrm{b}}}_{=:\boldsymbol{u}}. \tag{7.49}$$

Discretizing (7.49) with T as a sampling time yields the discrete-time state-space equation of the dynamic motion of the spacecraft attitude as follow:

$$\boldsymbol{x}_{k+1} = \Big(\underbrace{\boldsymbol{I}_{6\times6} + T\boldsymbol{\mathcal{A}}(\boldsymbol{x}_k)}_{=:\boldsymbol{A}(\boldsymbol{x}_k)} + \underbrace{T\boldsymbol{\Delta}_{\boldsymbol{\mathcal{A}}}}_{=:\boldsymbol{\Delta}_{\boldsymbol{A}}}\Big)\boldsymbol{x}_k + \underbrace{T\boldsymbol{\mathcal{B}}(\boldsymbol{x}_k)}_{=:\boldsymbol{B}(\boldsymbol{x}_k)}\boldsymbol{u}_k \tag{7.50}$$

which has the same structure of (7.5). Therefore, we can design the robust CD-SDRE controller.

For simulation, we consider a spacecraft with an assumption that the fuel tank is filled with half fuel and the fuel is rigid for a simple simulation (hemisphere). However the fuel can move freely with the viscosity of $\varepsilon_i = 0.005\ \mathrm{Ns/m^2}\ \forall i \in \mathbb{Z}_{1:3}$. The physical parameters of the spacecraft are set as $\boldsymbol{I}_{\mathrm{b}} = diag(150,\ 300,\ 250)\ \mathrm{kgm^2}$, $\boldsymbol{I}_{\mathrm{f}} = \frac{2m_{\mathrm{f}}^2}{5}diag(1,\ 1,\ 1)\ \mathrm{kgm^2}$, $m_{\mathrm{f}} = 50\ \mathrm{kg}$, $l = 1\ \mathrm{m}$, and $r_{\mathrm{f}} = 0.3\ \mathrm{m}$. For the proposed controller $\boldsymbol{Q} = diag(2,\ 2,\ 2,\ 1,\ 1,\ 1)$, $\boldsymbol{R} = \boldsymbol{I}_{3\times3}$, $N = 30$, and $T = 0.1\ \mathrm{sec}$. The initial conditions of the states are $\phi_0 = -\frac{\pi}{4}\ \mathrm{rad}$, $\theta_0 = \frac{\pi}{4}\ \mathrm{rad}$, $\psi_0 = \frac{\pi}{4}\ \mathrm{rad}$, $\dot{\phi}_0 = \dot{\theta}_0 = \dot{\psi}_0 = 0\ \mathrm{rad/s}$. The motion of the fuel cannot be measured by the spacecraft sensor thereby it causes uncertainties in the spacecraft dynamics. We want to investigate the proposed CD-SDRE controller to see if it can stabilize the attitude

motion of the spacecraft in the presence of such uncertainties under limited actuator torques.

Figures 7.2 and 7.4 show the simulation results under four different conditions of the saturation of the actuators: no saturation, $|\boldsymbol{u}_k| \leq 1.0\ \mathrm{Nm}$, $0.6\ \mathrm{Nm}$, $0.2\ \mathrm{Nm}$. Figures 7.2 and 7.3 show the state errors, i.e., the angular errors and angular rate errors, respectively. As the constrained becomes stringent, the time to converge the state errors to zeros increases. However, they finally converge to zero errors in the presence of uncertainties. It should be noted that there are relatively big changes in angular rate errors (Figure 7.3) and the applied torque (Figure 7.4) in 20–50 sec for $|\boldsymbol{u}_k| \leq 1.0,\ 0.6\ \mathrm{Nm}$ and 40–120 sec for $|\boldsymbol{u}_k| \leq 0.2\ \mathrm{Nm}$. It is mainly because of the motion of the fuel in the fuel tank. Regardless of the effect of the uncertainties caused by the fuel slosh effect and the actuator saturations, the proposed CD-SDRE controller effectively made the attitude motion of the spacecraft stable.

7.6 Conclusions

In this chapter, we investigated the robust CD-SDRE technique in the presence of uncertainties in the controlled nonlinear system. The CD-SDRE controller was considered to be a switched system containing a robust D-SDRE and MPC-based controller. Rigorous stability proofs were provided showing that the robust CD-SDRE feedback system is ISS in its ROA in the presence of uncertainties of the system. Finally, an accurate dynamical model of the spacecraft attitude motion in the presence of the first fuel slosh effect in 3-dimensional space was derived. The robust CD-SDRE controller was applied to the spacecraft to evaluate its performance in the presence of unpredictable motion of the fuel generated while spacecraft rotates its body. The results of this application showed the effectiveness and the reliability of the proposed CD-SDRE technique in controlling an uncertain system.

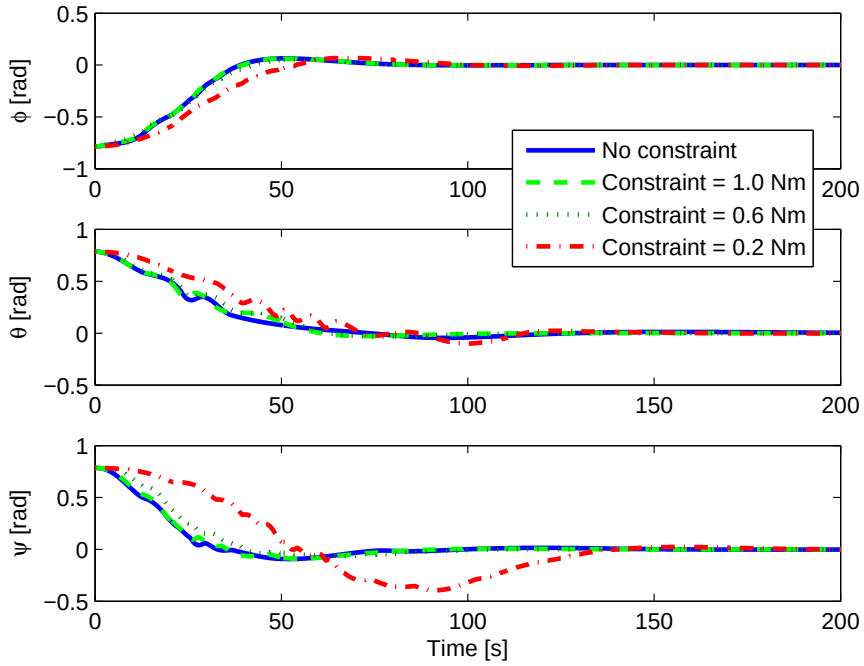

Figure 7.2: Time histories of the angular errors of the spacecraft in the presence of different actuator saturations (no constraints, ± 1.0 Nm, ± 0.6 Nm, ± 0.2 Nm).

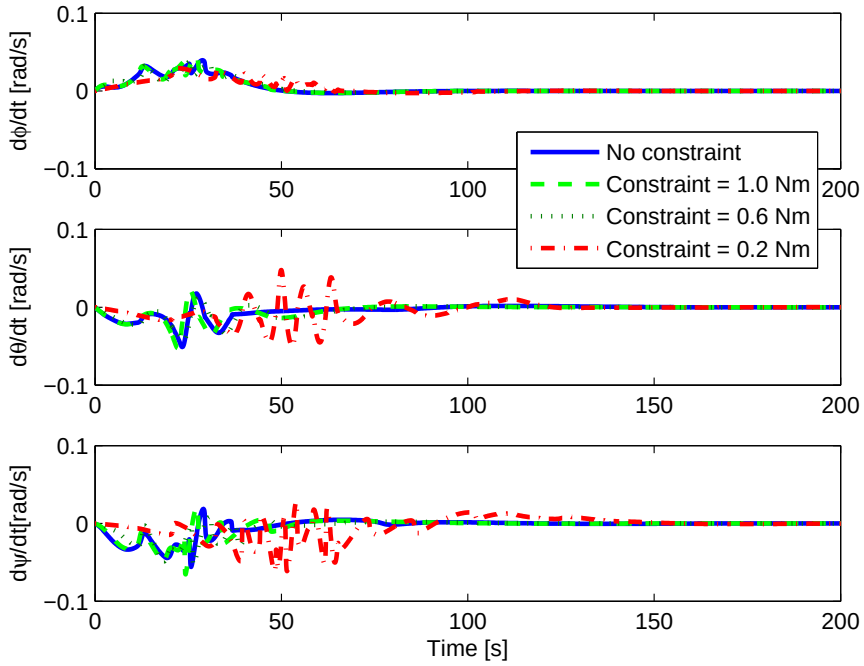

Figure 7.3: Time histories of the angular rate errors of the spacecraft in the presence of different actuator saturations (no constraints, ± 1.0 Nm, ± 0.6 Nm, ± 0.2 Nm).

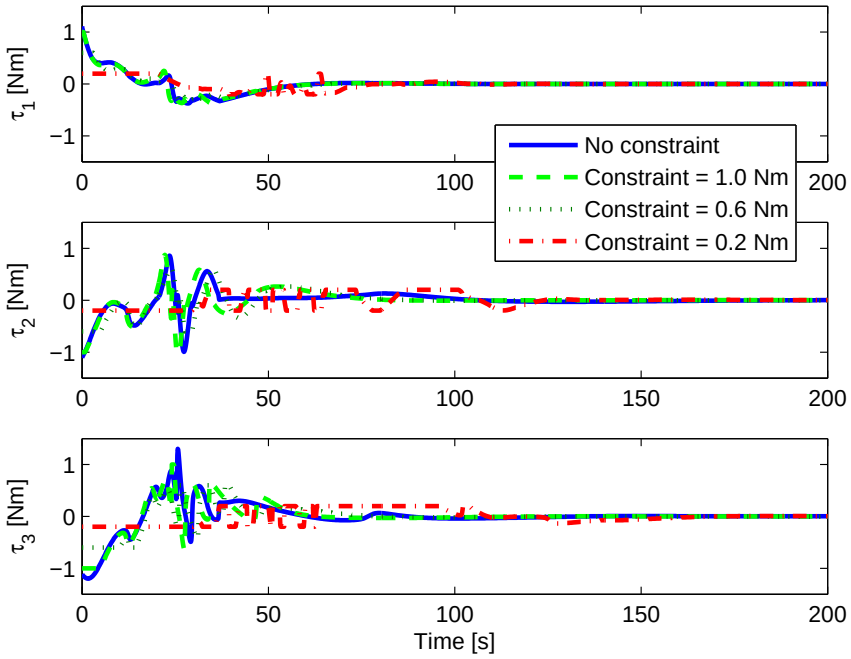

Figure 7.4: Time histories of the applied torques of the spacecraft in the presence of different actuator saturations (no constraints, ± 1.0 Nm, ± 0.6 Nm, ± 0.2 Nm).

Part III

Filtering Design via D-SDRE

Chapter 8

Observer Design via D-SDRE Technique

In the current and the following chapters, we discuss estimation techniques of the unmeasurable state parameters in a deterministic or a stochastic nonlinear system, respectively. In this chapter, the observer based on the D-SDRE technique, called D-SDRE Observer, is investigated in this chapter.

8.1 Discrete-Time State-Dependent Riccati Equation-Based Observer (D-SDRE Observer)

Suppose that there is a discrete-time deterministic nonlinear system:

$$\begin{aligned} \boldsymbol{x}_{k+1} &= \boldsymbol{f}(\boldsymbol{x}_k) \\ \boldsymbol{y}_k &= \boldsymbol{h}(\boldsymbol{x}_k) \end{aligned} \tag{8.1}$$

where $\boldsymbol{x}_k \in \mathbb{R}^n$ and $\boldsymbol{y}_k \in \mathbb{R}^p$ denote the states and the outputs of the system, respectively.
It is emphasized that the nonlinear dynamical system (8.1) can be reconstructed by using the SDC factorization:

$$\begin{aligned} \boldsymbol{x}_{k+1} &= \boldsymbol{f}(\boldsymbol{x}_k) &&= \boldsymbol{A}(\boldsymbol{x}_k)\boldsymbol{x}_k \\ \boldsymbol{y}_k &= \boldsymbol{h}(\boldsymbol{x}_k) &&= \boldsymbol{C}(\boldsymbol{x}_k)\boldsymbol{x}_k. \end{aligned} \tag{8.2}$$

A one-step procedure is considered for the design of the observer via the D-SDRE technique. Then the D-SDRE Observer for the nonlinear system can be designed as follows:

$$\begin{aligned} \hat{\boldsymbol{x}}_{k+1} &= \boldsymbol{A}(\hat{\boldsymbol{x}}_k)\hat{\boldsymbol{x}}_k + \boldsymbol{L}(\hat{\boldsymbol{x}}_k)\big(\boldsymbol{y}_k - \hat{\boldsymbol{y}}_k\big) \\ \hat{\boldsymbol{y}}_k &= \boldsymbol{C}(\hat{\boldsymbol{x}}_k)\hat{\boldsymbol{x}}_k \end{aligned} \tag{8.3}$$

where $\boldsymbol{L}(\hat{\boldsymbol{x}}_k) \in \mathbb{R}^{n\times p}$ is the observer gain, defined as (Song and Grizzle, 1992)

$$\boldsymbol{L}(\hat{\boldsymbol{x}}_k) := \boldsymbol{P}_k\boldsymbol{C}^\top(\hat{\boldsymbol{x}}_k)\Big(\boldsymbol{R}_k + \boldsymbol{C}(\hat{\boldsymbol{x}}_k)\boldsymbol{P}_k\boldsymbol{C}^\top(\hat{\boldsymbol{x}}_k)\Big)^{-1} \tag{8.4}$$

where the symmetric positive definite solution $\boldsymbol{P}_k$ of the D-SDRE can be updated by using the following equation:

$$\begin{aligned}\boldsymbol{P}_{k+1} &= \boldsymbol{Q}_k + \boldsymbol{A}(\hat{\boldsymbol{x}}_k)\Big\{\boldsymbol{P}_k - \boldsymbol{P}_k\boldsymbol{C}^\top(\hat{\boldsymbol{x}}_k)\Big(\boldsymbol{C}(\hat{\boldsymbol{x}}_k)\boldsymbol{P}_k\boldsymbol{C}^\top(\hat{\boldsymbol{x}}_k) + \boldsymbol{R}_k\Big)^{-1}\boldsymbol{C}(\hat{\boldsymbol{x}}_k)\boldsymbol{P}_k\Big\}\boldsymbol{A}^\top(\hat{\boldsymbol{x}}_k)\\ &= \boldsymbol{Q}_k + \boldsymbol{A}(\hat{\boldsymbol{x}}_k)\Big(\boldsymbol{P}_k^{-1} + \boldsymbol{C}^\top(\hat{\boldsymbol{x}}_k)\boldsymbol{R}_k^{-1}\boldsymbol{C}(\hat{\boldsymbol{x}}_k)\Big)^{-1}\boldsymbol{A}^\top(\hat{\boldsymbol{x}}_k).\end{aligned} \tag{8.5}$$

It is noted that (8.5) can be rewritten by using the observer gain in (8.4) and the matrix inversion lemma (Lewis et al., 2012):

$$\begin{aligned}\boldsymbol{P}_{k+1} &= \boldsymbol{Q}_k + \boldsymbol{A}(\hat{\boldsymbol{x}}_k)\Big\{\boldsymbol{P}_k - \boldsymbol{P}_k\boldsymbol{C}^\top(\hat{\boldsymbol{x}}_k)\Big(\boldsymbol{C}(\hat{\boldsymbol{x}}_k)\boldsymbol{P}_k\boldsymbol{C}^\top(\hat{\boldsymbol{x}}_k) + \boldsymbol{R}_k\Big)^{-1}\boldsymbol{C}(\hat{\boldsymbol{x}}_k)\boldsymbol{P}_k\Big\}\boldsymbol{A}^\top(\hat{\boldsymbol{x}}_k)\\ &= \boldsymbol{Q}_k + \boldsymbol{A}(\hat{\boldsymbol{x}}_k)\Big(\boldsymbol{P}_k - \boldsymbol{L}(\hat{\boldsymbol{x}}_k)\boldsymbol{C}(\hat{\boldsymbol{x}}_k)\boldsymbol{P}_k\Big)\boldsymbol{A}^\top(\hat{\boldsymbol{x}}_k)\\ &= \boldsymbol{Q}_k + \boldsymbol{A}(\hat{\boldsymbol{x}}_k)\Big(\boldsymbol{I} - \boldsymbol{L}(\hat{\boldsymbol{x}}_k)\boldsymbol{C}(\hat{\boldsymbol{x}}_k)\Big)\boldsymbol{P}_k\boldsymbol{A}^\top(\hat{\boldsymbol{x}}_k).\end{aligned} \tag{8.6}$$

For the stability analysis of the nonlinear system with the D-SDRE Observer, the error dynamics is analyzed. The error of the system is defined as follows:

$$\boldsymbol{e}_k := \boldsymbol{x}_k - \hat{\boldsymbol{x}}_k \tag{8.7}$$

where $\hat{\boldsymbol{x}}_k$ denotes the estimated state of the real state $\boldsymbol{x}_k$ by using the D-SDRE Observer.
There are some assumptions for the stability analysis:

Assumption 25 For $\boldsymbol{A}(\boldsymbol{x}_k)$ and $\boldsymbol{C}(\boldsymbol{x}_k)$ in (8.3), the following Lipschitz conditions hold for all $i \in \mathbb{Z}_{\leq 0}$:

$$\begin{aligned}\|\boldsymbol{A}(\boldsymbol{x}_i) - \boldsymbol{A}(\hat{\boldsymbol{x}}_i)\| &\leq \rho_A|\boldsymbol{x}_i - \hat{\boldsymbol{x}}_i|\\ \|\boldsymbol{C}(\boldsymbol{x}_i) - \boldsymbol{C}(\hat{\boldsymbol{x}}_i)\| &\leq \rho_C|\boldsymbol{x}_i - \hat{\boldsymbol{x}}_i|\end{aligned} \tag{8.8}$$

for some $\rho_A > 0$ and $\rho_C > 0$.

Assumption 26 For $\boldsymbol{A}(\boldsymbol{x}_k)$ and $\boldsymbol{C}(\boldsymbol{x}_k)$ in (8.3) and associated matrices $\boldsymbol{P}_k$ in (8.5) and $\boldsymbol{L}(\hat{\boldsymbol{x}}_k)$ in (8.4), the following inequalities hold for all $i \in \mathbb{Z}_{\leq 0}$:

$$\begin{aligned} a_{\min} &\leq \|\boldsymbol{A}(\boldsymbol{x}_i)\| \leq a_{\max} \\ c_{\min} &\leq \|\boldsymbol{C}(\boldsymbol{x}_i)\| \leq a_{\max} \\ p_{\min} &\leq \|\boldsymbol{P}_i\| \leq p_{\max} \\ l_{\min} &\leq \|\boldsymbol{L}(\hat{\boldsymbol{x}}_i)\| \leq l_{\max} \\ |\boldsymbol{x}_i| &\leq \chi. \end{aligned} \tag{8.9}$$

Prior to the stability analysis of the system with the D-SDRE Observer, we prove two lemmas first.

Lemma 27 *[Similar to Theorem 2.4 in (Song and Grizzle, 1992)] For invertible $\boldsymbol{P}k$, $\boldsymbol{Q}_k$, and $\boldsymbol{R}_k$, the following equality holds for all $k \in \mathbb{Z}_{\geq 0}$:*

$$\begin{aligned} \boldsymbol{A}^\top(\hat{\boldsymbol{x}}_k)\boldsymbol{P}_{k+1}^{-1}\boldsymbol{A}(\hat{\boldsymbol{x}}_k) = \Big\{\boldsymbol{P}_k^{-1} - \boldsymbol{P}_k^{-1}\Big(\boldsymbol{I} - \boldsymbol{L}(\hat{\boldsymbol{x}}_k)\boldsymbol{C}(\hat{\boldsymbol{x}}_k)\Big)^{-1}\Big(\boldsymbol{P}_k^{-1} + \boldsymbol{C}^\top(\hat{\boldsymbol{x}}_k)\boldsymbol{R}_k^{-1}\boldsymbol{C}(\hat{\boldsymbol{x}}_k) \\ + \boldsymbol{A}^\top(\hat{\boldsymbol{x}}_k)\boldsymbol{Q}_k^{-1}\boldsymbol{A}(\hat{\boldsymbol{x}}_k)\Big)^{-1}\boldsymbol{P}_k^{-1}\Big\}\Big(\boldsymbol{I} - \boldsymbol{L}(\hat{\boldsymbol{x}}_k)\boldsymbol{C}(\hat{\boldsymbol{x}}_k)\Big)^{-1}. \end{aligned} \tag{8.10}$$

Proof Taking the inverse of (8.6), left-multiplying it by $\boldsymbol{A}^\top(\hat{\boldsymbol{x}}_k)$, and right-multiplying it by $\boldsymbol{A}(\hat{\boldsymbol{x}}_k)$ yields

$$\boldsymbol{A}^\top(\hat{\boldsymbol{x}}_k)\boldsymbol{P}_{k+1}^{-1}\boldsymbol{A}(\hat{\boldsymbol{x}}_k) = \Big\{\boldsymbol{A}^{-1}(\hat{\boldsymbol{x}}_k)\boldsymbol{Q}_k\boldsymbol{A}^{-\top}(\hat{\boldsymbol{x}}_k) + \Big(\boldsymbol{I} - \boldsymbol{L}(\hat{\boldsymbol{x}}_k)\boldsymbol{C}(\hat{\boldsymbol{x}}_k)\Big)\boldsymbol{P}_k\Big\}^{-1}. \tag{8.11}$$

We can derive the following equations by applying the matrix inversion lemma (Lewis et al., 2012) to (8.11),

$$\begin{aligned} \boldsymbol{A}^\top(\hat{\boldsymbol{x}}_k)\boldsymbol{P}_{k+1}^{-1}\boldsymbol{A}(\hat{\boldsymbol{x}}_k) &= \Big\{\Big(\boldsymbol{I} - \boldsymbol{L}(\hat{\boldsymbol{x}}_k)\boldsymbol{C}(\hat{\boldsymbol{x}}_k)\Big)\boldsymbol{P}_k\Big\}^{-1} - \Big\{\Big(\boldsymbol{I} - \boldsymbol{L}(\hat{\boldsymbol{x}}_k)\boldsymbol{C}(\hat{\boldsymbol{x}}_k)\Big)\boldsymbol{P}_k\Big\}^{-1} \\ &\quad \times \Big[\Big\{\Big(\boldsymbol{I} - \boldsymbol{L}(\hat{\boldsymbol{x}}_k)\boldsymbol{C}(\hat{\boldsymbol{x}}_k)\Big)\boldsymbol{P}_k\Big\}^{-1} + \boldsymbol{A}^\top(\hat{\boldsymbol{x}}_k)\boldsymbol{Q}_k^{-1}\boldsymbol{A}(\hat{\boldsymbol{x}}_k)\Big]^{-1} \\ &\quad \times \Big\{\Big(\boldsymbol{I} - \boldsymbol{L}(\hat{\boldsymbol{x}}_k)\boldsymbol{C}(\hat{\boldsymbol{x}}_k)\Big)\boldsymbol{P}_k\Big\}^{-1} \\ &= \Big[\boldsymbol{P}_k^{-1} - \boldsymbol{P}_k^{-1}\Big(\boldsymbol{I} - \boldsymbol{L}(\hat{\boldsymbol{x}}_k)\boldsymbol{C}(\hat{\boldsymbol{x}}_k)\Big)^{-1}\Big[\Big\{\Big(\boldsymbol{I} - \boldsymbol{L}(\hat{\boldsymbol{x}}_k)\boldsymbol{C}(\hat{\boldsymbol{x}}_k)\Big)\boldsymbol{P}_k\Big\}^{-1} \\ &\quad + \boldsymbol{A}^\top(\hat{\boldsymbol{x}}_k)\boldsymbol{Q}_k^{-1}\boldsymbol{A}(\hat{\boldsymbol{x}}_k)\Big]^{-1}\boldsymbol{P}_k^{-1}\Big]\Big(\boldsymbol{I} - \boldsymbol{L}(\hat{\boldsymbol{x}}_k)\boldsymbol{C}(\hat{\boldsymbol{x}}_k)\Big)^{-1} \\ &= \Big\{\boldsymbol{P}_k^{-1} - \boldsymbol{P}_k^{-1}\Big(\boldsymbol{I} - \boldsymbol{L}(\hat{\boldsymbol{x}}_k)\boldsymbol{C}(\hat{\boldsymbol{x}}_k)\Big)^{-1}\Big(\boldsymbol{P}_k^{-1} + \boldsymbol{C}^\top(\hat{\boldsymbol{x}}_k)\boldsymbol{R}_k^{-1}\boldsymbol{C}(\hat{\boldsymbol{x}}_k) \\ &\quad + \boldsymbol{A}^\top(\hat{\boldsymbol{x}}_k)\boldsymbol{Q}_k^{-1}\boldsymbol{A}(\hat{\boldsymbol{x}}_k)\Big)^{-1}\boldsymbol{P}_k^{-1}\Big\}\Big(\boldsymbol{I} - \boldsymbol{L}(\hat{\boldsymbol{x}}_k)\boldsymbol{C}(\hat{\boldsymbol{x}}_k)\Big)^{-1}. \end{aligned} \tag{8.12}$$

This proves the lemma. □

Lemma 28 *For invertible $\boldsymbol{P}k$, $\boldsymbol{Q}_k$, and $\boldsymbol{R}_k$, the following equality holds for all $k \in \mathbb{Z}_{\geq 0}$:*

$$\begin{aligned}
&\boldsymbol{e}_k^\top \Big(\boldsymbol{I} - \boldsymbol{L}(\hat{\boldsymbol{x}}_k)\boldsymbol{C}(\hat{\boldsymbol{x}}_k)\Big)^\top \boldsymbol{A}^\top(\hat{\boldsymbol{x}}_k)\boldsymbol{P}_{k+1}^{-1}\boldsymbol{A}(\hat{\boldsymbol{x}}_k)\Big(\boldsymbol{I} - \boldsymbol{L}(\hat{\boldsymbol{x}}_k)\boldsymbol{C}(\hat{\boldsymbol{x}}_k)\Big)\boldsymbol{e}_k \\
&\quad = \boldsymbol{e}_k^\top \boldsymbol{P}_k^{-1}\boldsymbol{e}_k - \boldsymbol{e}_k^\top \boldsymbol{C}^\top(\hat{\boldsymbol{x}}_k)\Big(\boldsymbol{R}_k + \boldsymbol{C}(\hat{\boldsymbol{x}}_k)\boldsymbol{P}_k\boldsymbol{C}^\top(\hat{\boldsymbol{x}}_k)\Big)^{-1}\boldsymbol{C}(\hat{\boldsymbol{x}}_k)\boldsymbol{e}_k \\
&\qquad - \boldsymbol{e}_k^\top \boldsymbol{P}_k^{-1}\Big(\boldsymbol{P}_k^{-1} + \boldsymbol{C}^\top(\hat{\boldsymbol{x}}_k)\boldsymbol{R}_k^{-1}\boldsymbol{C}(\hat{\boldsymbol{x}}_k) + \boldsymbol{A}^\top(\hat{\boldsymbol{x}}_k)\boldsymbol{Q}_k^{-1}\boldsymbol{A}(\hat{\boldsymbol{x}}_k)\Big)^{-1}\boldsymbol{P}_k^{-1}\boldsymbol{e}_k. \qquad (8.13)
\end{aligned}$$

Proof This lemma can be proven through the use of Lemma 27. That is, by substituting (8.11) into the left-hand side of (8.13) yields,

$$\begin{aligned}
&\boldsymbol{e}_k^\top \Big(\boldsymbol{I} - \boldsymbol{L}(\hat{\boldsymbol{x}}_k)\boldsymbol{C}(\hat{\boldsymbol{x}}_k)\Big)^\top \boldsymbol{A}^\top(\hat{\boldsymbol{x}}_k)\boldsymbol{P}_{k+1}^{-1}\boldsymbol{A}(\hat{\boldsymbol{x}}_k)\Big(\boldsymbol{I} - \boldsymbol{L}(\hat{\boldsymbol{x}}_k)\boldsymbol{C}(\hat{\boldsymbol{x}}_k)\Big)\boldsymbol{e}_k \\
&\quad = \boldsymbol{e}_k^\top \Big(\boldsymbol{I} - \boldsymbol{L}(\hat{\boldsymbol{x}}_k)\boldsymbol{C}(\hat{\boldsymbol{x}}_k)\Big)^\top \Big\{\boldsymbol{P}_k^{-1} - \boldsymbol{P}_k^{-1}\Big(\boldsymbol{I} - \boldsymbol{L}(\hat{\boldsymbol{x}}_k)\boldsymbol{C}(\hat{\boldsymbol{x}}_k)\Big)^{-1} \\
&\qquad \times \Big(\boldsymbol{P}_k^{-1} + \boldsymbol{C}^\top(\hat{\boldsymbol{x}}_k)\boldsymbol{R}_k^{-1}\boldsymbol{C}(\hat{\boldsymbol{x}}_k) + \boldsymbol{A}^\top(\hat{\boldsymbol{x}}_k)\boldsymbol{Q}_k^{-1}\boldsymbol{A}(\hat{\boldsymbol{x}}_k)\Big)^{-1}\boldsymbol{P}_k^{-1}\Big\}\boldsymbol{e}_k \\
&\quad = \boldsymbol{e}_k^\top \Big(\boldsymbol{I} - \boldsymbol{L}(\hat{\boldsymbol{x}}_k)\boldsymbol{C}(\hat{\boldsymbol{x}}_k)\Big)^\top \boldsymbol{P}_k^{-1}\boldsymbol{e}_k - \boldsymbol{e}_k^\top \Big(\boldsymbol{I} - \boldsymbol{L}(\hat{\boldsymbol{x}}_k)\boldsymbol{C}(\hat{\boldsymbol{x}}_k)\Big)^\top \Big\{\boldsymbol{P}_k^{-1}\Big(\boldsymbol{I} - \boldsymbol{L}(\hat{\boldsymbol{x}}_k)\boldsymbol{C}(\hat{\boldsymbol{x}}_k)\Big)^{-1} \\
&\qquad \times \Big(\boldsymbol{P}_k^{-1} + \boldsymbol{C}^\top(\hat{\boldsymbol{x}}_k)\boldsymbol{R}_k^{-1}\boldsymbol{C}(\hat{\boldsymbol{x}}_k) + \boldsymbol{A}^\top(\hat{\boldsymbol{x}}_k)\boldsymbol{Q}_k^{-1}\boldsymbol{A}(\hat{\boldsymbol{x}}_k)\Big)^{-1}\boldsymbol{P}_k^{-1}\Big\}\boldsymbol{e}_k. \qquad (8.14)
\end{aligned}$$

Since $\left(\boldsymbol{I} - \boldsymbol{L}(\hat{\boldsymbol{x}}_k)\boldsymbol{C}(\hat{\boldsymbol{x}}_k)\right)\boldsymbol{P}_k$ is symmetric,

$$\Big(\boldsymbol{I} - \boldsymbol{L}(\hat{\boldsymbol{x}}_k)\boldsymbol{C}(\hat{\boldsymbol{x}}_k)\Big)^\top = \boldsymbol{P}_k^{-1}\Big(\boldsymbol{I} - \boldsymbol{L}(\hat{\boldsymbol{x}}_k)\boldsymbol{C}(\hat{\boldsymbol{x}}_k)\Big)\boldsymbol{P}_k. \qquad (8.15)$$

Therefore, substituting (8.15) and $\boldsymbol{L}(\hat{\boldsymbol{x}}_k) = \boldsymbol{P}_k\boldsymbol{C}^\top(\hat{\boldsymbol{x}}_k)\left(\boldsymbol{R}_k + \boldsymbol{C}(\hat{\boldsymbol{x}}_k)\boldsymbol{P}_k\boldsymbol{C}^\top(\hat{\boldsymbol{x}}_k)\right)^{-1}$ into (8.14) yields

$$\begin{aligned}
&\boldsymbol{e}_k^\top \Big(\boldsymbol{I} - \boldsymbol{L}(\hat{\boldsymbol{x}}_k)\boldsymbol{C}(\hat{\boldsymbol{x}}_k)\Big)^\top \boldsymbol{A}^\top(\hat{\boldsymbol{x}}_k)\boldsymbol{P}_{k+1}^{-1}\boldsymbol{A}(\hat{\boldsymbol{x}}_k)\Big(\boldsymbol{I} - \boldsymbol{L}(\hat{\boldsymbol{x}}_k)\boldsymbol{C}(\hat{\boldsymbol{x}}_k)\Big)\boldsymbol{e}_k \\
&\quad = \boldsymbol{e}_k^\top \boldsymbol{P}_k^{-1}\boldsymbol{e}_k - \boldsymbol{e}_k^\top \boldsymbol{P}_k^{-1}\boldsymbol{L}(\hat{\boldsymbol{x}}_k)\boldsymbol{C}(\hat{\boldsymbol{x}}_k)\boldsymbol{e}_k - \boldsymbol{e}_k^\top \boldsymbol{P}_k^{-1}\Big(\boldsymbol{P}_k^{-1} + \boldsymbol{C}^\top(\hat{\boldsymbol{x}}_k)\boldsymbol{R}_k^{-1}\boldsymbol{C}(\hat{\boldsymbol{x}}_k) \\
&\qquad + \boldsymbol{A}^\top(\hat{\boldsymbol{x}}_k)\boldsymbol{Q}_k^{-1}\boldsymbol{A}(\hat{\boldsymbol{x}}_k)\Big)^{-1}\boldsymbol{P}_k^{-1}\boldsymbol{e}_k \\
&\quad = \boldsymbol{e}_k^\top \boldsymbol{P}_k^{-1}\boldsymbol{e}_k - \boldsymbol{e}_k^\top \boldsymbol{C}^\top(\hat{\boldsymbol{x}}_k)\Big(\boldsymbol{R}_k + \boldsymbol{C}(\hat{\boldsymbol{x}}_k)\boldsymbol{P}_k\boldsymbol{C}^\top(\hat{\boldsymbol{x}}_k)\Big)^{-1}\boldsymbol{C}(\hat{\boldsymbol{x}}_k)\boldsymbol{e}_k \\
&\qquad - \boldsymbol{e}_k^\top \boldsymbol{P}_k^{-1}\Big(\boldsymbol{P}_k^{-1} + \boldsymbol{C}^\top(\hat{\boldsymbol{x}}_k)\boldsymbol{R}_k^{-1}\boldsymbol{C}(\hat{\boldsymbol{x}}_k) + \boldsymbol{A}^\top(\hat{\boldsymbol{x}}_k)\boldsymbol{Q}_k^{-1}\boldsymbol{A}(\hat{\boldsymbol{x}}_k)\Big)^{-1}\boldsymbol{P}_k^{-1}\boldsymbol{e}_k. \qquad (8.16)
\end{aligned}$$

Therefore, the equality in (8.13) holds for all $k \in \mathbb{Z}_{\geq 0}$. $\square$

Theorem 29 The error dynamics between the actual states of the discrete-time deterministic nonlinear system in (8.1) and the estimated states of the D-SDRE Observer in (8.3) is ISS.

Proof In order to prove the theorem, we use the definition of the error of the system at time k in (8.17). The objective of the stability is to make the error $\boldsymbol{e}_k$ bounded for all k. The error at time $k+1$, i.e., $\boldsymbol{e}_{k+1}$ can be obtained by substituting (8.1) and (8.3) into (8.17):

$$\begin{aligned}
\boldsymbol{e}_{k+1} &= \boldsymbol{x}_{k+1} - \hat{\boldsymbol{x}}_{k+1} \\
&= \boldsymbol{A}(\boldsymbol{x}_k)\boldsymbol{x}_k - \boldsymbol{A}(\hat{\boldsymbol{x}}_k)\hat{\boldsymbol{x}}_k - \boldsymbol{L}(\hat{\boldsymbol{x}}_k)\Big(\boldsymbol{C}(\boldsymbol{x}_k)\boldsymbol{x}_k - \boldsymbol{C}(\hat{\boldsymbol{x}}_k)\hat{\boldsymbol{x}}_k\Big) \\
&\quad - \boldsymbol{A}(\hat{\boldsymbol{x}}_k)\boldsymbol{x}_k + \boldsymbol{A}(\hat{\boldsymbol{x}}_k)\boldsymbol{x}_k - \boldsymbol{L}(\hat{\boldsymbol{x}}_k)\Big(\boldsymbol{C}(\hat{\boldsymbol{x}}_k)\boldsymbol{x}_k - \boldsymbol{C}(\hat{\boldsymbol{x}}_k)\boldsymbol{x}_k\Big) \\
&= \boldsymbol{A}(\hat{\boldsymbol{x}}_k)\left(\boldsymbol{x}_k - \hat{\boldsymbol{x}}_k\right) - \boldsymbol{L}(\hat{\boldsymbol{x}}_k)\boldsymbol{C}(\hat{\boldsymbol{x}}_k)\left(\boldsymbol{x}_k - \hat{\boldsymbol{x}}_k\right) \\
&\quad + \Big(\boldsymbol{A}(\boldsymbol{x}_k) - \boldsymbol{A}(\hat{\boldsymbol{x}}_k)\Big)\boldsymbol{x}_k - \boldsymbol{L}(\hat{\boldsymbol{x}}_k)\Big(\boldsymbol{C}(\boldsymbol{x}_k) - \boldsymbol{C}(\hat{\boldsymbol{x}}_k)\Big)\boldsymbol{x}_k.
\end{aligned} \tag{8.17}$$

In order to prove theorem, an ISS-Lyapunov function candidate $V(\boldsymbol{e}_k)$ in Definition 2 for the systems (8.1) and (8.3) can be defined as:

$$V(\boldsymbol{e}_k) := \boldsymbol{e}_k^\top \boldsymbol{P}_k^{-1} \boldsymbol{e}_k \tag{8.18}$$

where $\boldsymbol{P}_k^{-1}$ is the inverse of the symmetric positive solution of the D-SDRE at time k in (8.5).
Then, from the definition of the ISS-Lyapunov function (8.18), we can see that the following inequalities hold for all $k \in \mathbb{Z}_{\geq 0}$ by Assumption 25,

$$\alpha_1(|\boldsymbol{e}_k|) := \frac{1}{p_{\max}}|\boldsymbol{e}_k|^2 \leq V(\boldsymbol{e}_k) \leq \frac{1}{p_{\min}}|\boldsymbol{e}_k|^2 =: \alpha_2(|\boldsymbol{e}_k|) \tag{8.19}$$

where $\alpha_1(\cdot) \in \mathcal{K}_\infty$ and $\alpha_2(\cdot) \in \mathcal{K}_\infty$.
It is sufficient to show that there exist $\alpha_3(\cdot) \in \mathcal{K}_\infty$ and $\sigma(\cdot) \in \mathcal{K}$ such that $\Delta V(\boldsymbol{e}) := V(\boldsymbol{e}_{k+1}) - V(\boldsymbol{e}_k)$ is bounded. To this end, (8.18) is used directly. By substituting (8.17) into (8.18), the following equation can be obtained:

$$
\begin{aligned}
\Delta V(\boldsymbol{e}) &:= V(\boldsymbol{e}_{k+1}) - V(\boldsymbol{e}_k) = \boldsymbol{e}_{k+1}^\top \boldsymbol{P}_{k+1}^{-1}\boldsymbol{e}_{k+1} - \boldsymbol{e}_k^\top \boldsymbol{P}_k^{-1}\boldsymbol{e}_k \\
&= \boldsymbol{e}_k^\top \Big(\boldsymbol{I} - \boldsymbol{L}(\hat{\boldsymbol{x}}_k)\boldsymbol{C}(\hat{\boldsymbol{x}}_k)\Big)^\top \boldsymbol{A}^\top(\hat{\boldsymbol{x}}_k)\boldsymbol{P}_{k+1}^{-1}\boldsymbol{A}(\hat{\boldsymbol{x}}_k)\Big(\boldsymbol{I} - \boldsymbol{L}(\hat{\boldsymbol{x}}_k)\boldsymbol{C}(\hat{\boldsymbol{x}}_k)\Big)\boldsymbol{e}_k \\
&\quad + \boldsymbol{e}_k^\top \Big(\boldsymbol{I} - \boldsymbol{L}(\hat{\boldsymbol{x}}_k)\boldsymbol{C}(\hat{\boldsymbol{x}}_k)\Big)^\top \boldsymbol{A}^\top(\hat{\boldsymbol{x}}_k)\boldsymbol{P}_{k+1}^{-1}\tilde{\boldsymbol{A}}_k\boldsymbol{x}_k \\
&\quad - \boldsymbol{e}_k^\top \Big(\boldsymbol{I} - \boldsymbol{L}(\hat{\boldsymbol{x}}_k)\boldsymbol{C}(\hat{\boldsymbol{x}}_k)\Big)^\top \boldsymbol{A}^\top(\hat{\boldsymbol{x}}_k)\boldsymbol{P}_{k+1}^{-1}\boldsymbol{A}(\hat{\boldsymbol{x}}_k)\boldsymbol{L}(\hat{\boldsymbol{x}}_k)\tilde{\boldsymbol{C}}_k\boldsymbol{x}_k \\
&\quad + \boldsymbol{x}_k^\top \tilde{\boldsymbol{A}}_k^\top \boldsymbol{P}_{k+1}^{-1}\boldsymbol{A}(\hat{\boldsymbol{x}}_k)\Big(\boldsymbol{I} - \boldsymbol{L}(\hat{\boldsymbol{x}}_k)\boldsymbol{C}(\hat{\boldsymbol{x}}_k)\Big)\boldsymbol{e}_k \\
&\quad + \boldsymbol{x}_k^\top \tilde{\boldsymbol{A}}_k^\top \boldsymbol{P}_{k+1}^{-1}\tilde{\boldsymbol{A}}_k\boldsymbol{x}_k - \boldsymbol{x}_k^\top \tilde{\boldsymbol{A}}_k^\top \boldsymbol{P}_{k+1}^{-1}\boldsymbol{A}(\hat{\boldsymbol{x}}_k)\boldsymbol{L}(\hat{\boldsymbol{x}}_k)\tilde{\boldsymbol{C}}_k\boldsymbol{x}_k \\
&\quad - \boldsymbol{x}_k^\top \tilde{\boldsymbol{C}}_k^\top \boldsymbol{L}^\top(\hat{\boldsymbol{x}}_k)\boldsymbol{A}^\top(\hat{\boldsymbol{x}}_k)\boldsymbol{P}_{k+1}^{-1}\boldsymbol{A}(\hat{\boldsymbol{x}}_k)\Big(\boldsymbol{I} - \boldsymbol{L}(\hat{\boldsymbol{x}}_k)\boldsymbol{C}(\hat{\boldsymbol{x}}_k)\Big)\boldsymbol{e}_k \\
&\quad - \boldsymbol{x}_k^\top \tilde{\boldsymbol{C}}_k^\top \boldsymbol{L}^\top(\hat{\boldsymbol{x}}_k)\boldsymbol{A}^\top(\hat{\boldsymbol{x}}_k)\boldsymbol{P}_{k+1}^{-1}\tilde{\boldsymbol{A}}_k\boldsymbol{x}_k \\
&\quad + \boldsymbol{x}_k^\top \tilde{\boldsymbol{C}}_k^\top \boldsymbol{L}^\top(\hat{\boldsymbol{x}}_k)\boldsymbol{A}^\top(\hat{\boldsymbol{x}}_k)\boldsymbol{P}_{k+1}^{-1}\boldsymbol{A}(\hat{\boldsymbol{x}}_k)\boldsymbol{L}(\hat{\boldsymbol{x}}_k)\tilde{\boldsymbol{C}}_k\boldsymbol{x}_k - \boldsymbol{e}_k^\top \boldsymbol{P}_k^{-1}\boldsymbol{e}_k. \qquad (8.20)
\end{aligned}
$$

By applying Lemmas 27 and 28, and Assumptions 25 and 26, the following inequality can be derived,

$$
\begin{aligned}
\Delta V(\boldsymbol{e}) &\le -\boldsymbol{e}_k^\top \boldsymbol{C}^\top(\hat{\boldsymbol{x}}_k)\Big(\boldsymbol{R}_k + \boldsymbol{C}(\hat{\boldsymbol{x}}_k)\boldsymbol{P}_k\boldsymbol{C}^\top(\hat{\boldsymbol{x}}_k)\Big)^{-1}\boldsymbol{C}(\hat{\boldsymbol{x}}_k)\boldsymbol{e}_k \\
&\quad - \boldsymbol{e}_k^\top \boldsymbol{P}_k^{-1}\Big(\boldsymbol{P}_k^{-1} + \boldsymbol{C}^\top(\hat{\boldsymbol{x}}_k)\boldsymbol{R}_k^{-1}\boldsymbol{C}(\hat{\boldsymbol{x}}_k) + \boldsymbol{A}^\top(\hat{\boldsymbol{x}}_k)\boldsymbol{Q}_k^{-1}\boldsymbol{A}(\hat{\boldsymbol{x}}_k)\Big)^{-1}\boldsymbol{P}_k^{-1}\boldsymbol{e}_k \\
&\quad + 2\left(1 + l_{\max}c_{\max}\right)\frac{a_{\max}\chi}{p_{\min}}\|\tilde{\boldsymbol{A}}_k\||\boldsymbol{e}_k| + 2\left(1 + l_{\max}c_{\max}\right)\frac{a_{\max}^2 l_{\max}\chi}{p_{\min}}\|\tilde{\boldsymbol{C}}_k\||\boldsymbol{e}_k| \\
&\quad + \frac{\chi^2}{p_{\min}}\|\tilde{\boldsymbol{A}}_k\|^2 + 2\frac{a_{\max}l_{\max}\chi^2}{p_{\min}}\|\tilde{\boldsymbol{A}}_k\|\|\tilde{\boldsymbol{C}}_k\| + \frac{a_{\max}^2 l_{\max}^2\chi^2}{p_{\min}}\|\tilde{\boldsymbol{C}}_k\|^2 \\
&\le -\left(\frac{c_{\min}^2}{r_{\max} + c_{\max}^2 p_{\max}} + \frac{1}{p_{\max}^2}\frac{p_{\min}q_{\min}r_{\min}}{q_{\min}r_{\min} + c_{\max}^2 p_{\min}q_{\min} + a_{\max}^2 p_{\min}q_{\min}}\right)|\boldsymbol{e}_k|^2 \\
&\quad + \frac{\chi\left(1 + a_{\max}l_{\max}\right)}{p_{\min}}\Big\{2a_{\max} + \chi + a_{\max}l_{\max}\left(2c_{\max} + \chi\right)\Big\}|\boldsymbol{\xi}_k|^2 \\
&=: -\alpha_3(|\boldsymbol{e}_k|) + \sigma(|\boldsymbol{\xi}|) \qquad (8.21)
\end{aligned}
$$

where $|\boldsymbol{\xi}| = \max\big\{\|\tilde{\boldsymbol{A}}_k\|,\ \|\tilde{\boldsymbol{C}}_k\|,\ |\boldsymbol{e}_k|\big\}$, $\alpha_3(\cdot) \in \mathcal{K}_\infty$, and $\sigma(\cdot) \in \mathcal{K}$.

Therefore, the error dynamics between the actual states of the discrete-time deterministic nonlinear system and the estimated states of the D-SDRE Observer is ISS. □

We derived the D-SDRE Observer and showed that the D-SDRE Observer can estimate the actual state $\boldsymbol{x}_k$ accurately with founded error as proven in Theorem 29. Table 8.1 summarizes the algorithm of the

Table 8.1: Algorithm of the D-SDRE Observer ($\hat{\boldsymbol{x}}_k \rightarrow \hat{\boldsymbol{x}}_{k+1}$)

Initialization

Define $\boldsymbol{P}_0$, $\boldsymbol{Q}_0$, and $\boldsymbol{R}_0$.

For $k = 0,\ 1,\ 2, \cdots$

$\hat{\boldsymbol{x}}_k,\ k \quad \rightarrow \quad \boldsymbol{A}(\hat{\boldsymbol{x}}_k),\ \boldsymbol{B}(\hat{\boldsymbol{x}}_k),\ \boldsymbol{Q}_k,\ \boldsymbol{R}_k$

Update

Observer Gain

$$\boldsymbol{L}(\hat{\boldsymbol{x}}_k) \quad = \quad \boldsymbol{P}_k \boldsymbol{C}^\top(\hat{\boldsymbol{x}}_k)\Big(\boldsymbol{R}_k + \boldsymbol{C}(\hat{\boldsymbol{x}}_k)\boldsymbol{P}_k\boldsymbol{C}^\top(\hat{\boldsymbol{x}}_k)\Big)^{-1}$$

Riccati Solution

$$\boldsymbol{P}_{k+1} \quad = \quad \boldsymbol{Q}_k + \boldsymbol{A}(\hat{\boldsymbol{x}}_k)\Big(\boldsymbol{P}_k^{-1} + \boldsymbol{C}^\top(\hat{\boldsymbol{x}}_k)\boldsymbol{R}_k^{-1}\boldsymbol{C}(\hat{\boldsymbol{x}}_k)\Big)^{-1}\boldsymbol{A}^\top(\hat{\boldsymbol{x}}_k)$$

Predicted Measurement

$$\hat{\boldsymbol{y}}_k \quad = \quad \boldsymbol{C}(\hat{\boldsymbol{x}}_k)\hat{\boldsymbol{x}}_k$$

State Estimate

$$\hat{\boldsymbol{x}}_{k+1} \quad = \quad \boldsymbol{A}(\hat{\boldsymbol{x}}_k)\hat{\boldsymbol{x}}_k + \boldsymbol{L}(\hat{\boldsymbol{x}}_k)\big(\boldsymbol{y}_k - \hat{\boldsymbol{y}}_k\big)$$

End

D-SDRE Observer.

In the next section, we evaluate the performance of the D-SDRE Observer by using a chaotic dynamical system.

8.2 Numerical Validation

Based on the algorithm of the D-SDRE Observer in Table 8.1, we evaluate its performance by using the Lorenz attractor (Lorenz, 1963). The Lorenz attractor, a nonlinear deterministic 3-dimensional system, is a simplified mathematical model for atmospheric convection, which has chaotic solutions for certain initial conditions and parameters in the equation. It has the following form:

$$\begin{aligned} \dot{x} &= \sigma(y - x) \\ \dot{y} &= x(\rho - z) - y \\ \dot{z} &= xy - \beta z \end{aligned} \tag{8.22}$$

where x, y, and z denote the states of the system and σ, ρ, and β design parameters.

In order to apply the D-SDRE Observer, (8.22) needs to be discretized. Defining T as a sampling time of the system yields the discretization of the states: $\dot{x} = \frac{x_{k+1} - x_k}{T}$, $\dot{y} = \frac{y_{k+1} - y_k}{T}$, and $\dot{z} = \frac{z_{k+1} - z_k}{T}$. Substituting theses equations into (8.22) yields the discrete-time Lorenz attractor as

$$\begin{aligned} x_{k+1} &= x_k + T\sigma(y_k - x_k) \\ y_{k+1} &= y_k + Tx_k(\rho - z_k) - Ty_k \\ z_{k+1} &= z_k + Tx_k y_k - T\beta z_k. \end{aligned} \tag{8.23}$$

These equations can be expressed in a compact form by using a matrix structure as follows:

$$\underbrace{\begin{bmatrix} x_{k+1} \\ y_{k+1} \\ z_{k+1} \end{bmatrix}}_{=:\boldsymbol{x}_{k+1}} = \underbrace{\begin{bmatrix} 1 - T\sigma & T\sigma & 0 \\ T\rho & 1 - T & -Tx_k \\ 0 & Tx_k & 1 - T\beta \end{bmatrix}}_{=:\boldsymbol{A}(\boldsymbol{x}_k)} \underbrace{\begin{bmatrix} x_k \\ y_k \\ z_k \end{bmatrix}}_{=:\boldsymbol{x}_k}. \tag{8.24}$$

It is assumed that only x can be measured. Then, the equation of the output is expressed as

$$\boldsymbol{y}_k = \begin{bmatrix} 1 & 0 & 0 \end{bmatrix} \boldsymbol{x}_k := \boldsymbol{C}\boldsymbol{x}_k. \tag{8.25}$$

The system of (8.24) and (8.25) shows the form in (8.2). Therefore, we can design the D-SDRE Observer by using (8.24) and (8.25) as:

$$\begin{aligned} \hat{\boldsymbol{x}}_{k+1} &= \boldsymbol{A}(\hat{\boldsymbol{x}}_k)\hat{\boldsymbol{x}}_k + \boldsymbol{L}(\hat{\boldsymbol{x}}_k)\big(\boldsymbol{y}_k - \hat{\boldsymbol{y}}_k\big) \\ \hat{\boldsymbol{y}}_k &= \boldsymbol{C}(\hat{\boldsymbol{x}}_k)\hat{\boldsymbol{x}}_k \end{aligned} \tag{8.26}$$

where $\boldsymbol{L}(\hat{\boldsymbol{x}}_k)$ is the observer gain of the D-SDRE Observer which can be calculated by using (8.4) and (8.5) at each sampling time.

For simulations, the parameters σ, ρ, and β in (8.23) need to be defined: We set up the values of the parameters as $\sigma = 10$, $\rho = 28$, and $\beta = 8/3$. The sampling time of the system is defined as $T = 0.01$ sec. The initial conditions of the state are set up as $[x_0,\ y_0,\ z_0] = [0 \ \ 1 \ \ 1]$. Figure 8.1 shows the simulation result of the Lorenz attractor (8.23).

For the investigation of the D-SDRE Observer, it is assumed that the initial conditions of the state estimates are $[\hat{x}_0,\ \hat{y}_0,\ \hat{z}_0] = [-5 \ \ 5 \ \ 0]$. By changing the values of $\boldsymbol{Q}_k = \boldsymbol{Q}_k^\top \in \mathbb{R}^{3\times 3}$ and $\boldsymbol{R}_k \in \mathbb{R}$, the performance of the D-SDRE Observer is evaluated. Three cases are tested with different $\boldsymbol{Q}_k$ and $\boldsymbol{R}_k$ as:

$$\begin{cases} \text{Case I} & : \ \boldsymbol{Q}_k = diag(0.001,\ 0.001,\ 0.001),\ \boldsymbol{R}_k = 0.01 \\ \text{Case II} & : \ \boldsymbol{Q}_k = diag(0.01,\ 0.01,\ 0.01),\ \boldsymbol{R}_k = 0.001 \\ \text{Case III} & : \ \boldsymbol{Q}_k = diag(0.01,\ 0.01,\ 0.01),\ \boldsymbol{R}_k = 0.01. \end{cases} \tag{8.27}$$

Figure 8.2 shows a simulation result of trajectory of the Lorenz attractor (black) and the estimated trajectory (red) by the D-SDRE Observer with $\boldsymbol{Q}_k = diag(0.01,\ 0.01,\ 0.01)$ and $\boldsymbol{R}_k = 0.01$ and $[\hat{x}_0,\ \hat{y}_0,\ \hat{z}_0] = [-5 \ \ 5 \ \ 0]$. Figures 8.3 – 8.5 show the trajectory of the each state of the Lorenz attractor and a corresponding signal by the D-SDRE Observer, and the root mean square (RMS) error of the estimated states by the D-SDRE Observer with $\boldsymbol{Q}_k = diag(0.001,\ 0.001,\ 0.001),\ \boldsymbol{R}_k = 0.01$, $\boldsymbol{Q}_k = diag(0.01,\ 0.01,\ 0.01),\ \boldsymbol{R}_k = 0.001$, and $\boldsymbol{Q}_k = diag(0.01,\ 0.01,\ 0.01),\ \boldsymbol{R}_k = 0.01$, respectively. Based on the first figures in Figures 8.3 – 8.5, the estimated states are very closed the actual states of the Lorenz attractor. This can be proven

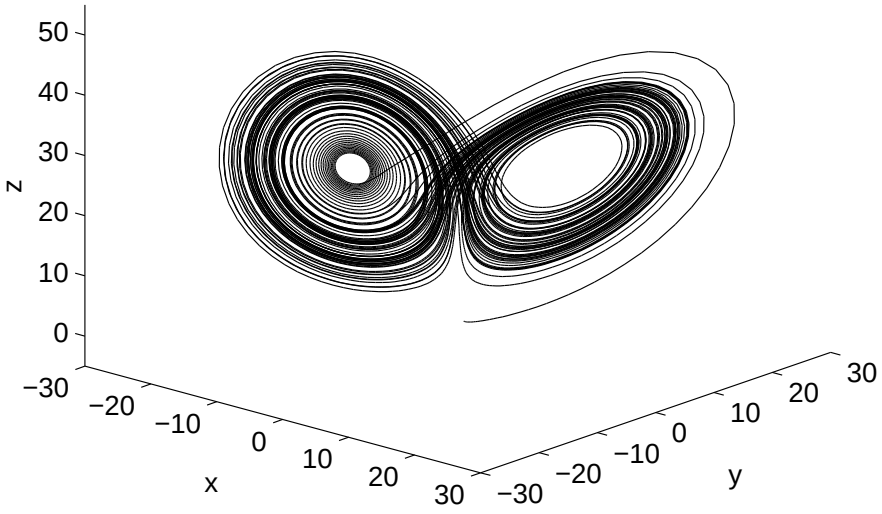

Figure 8.1: Trajectory of the Lorenz attractor with $\sigma = 10$, $\rho = 28$, $\beta = 8/3$, and $[x_0,\ y_0,\ z_0] = [0\ \ 1\ \ 1]$

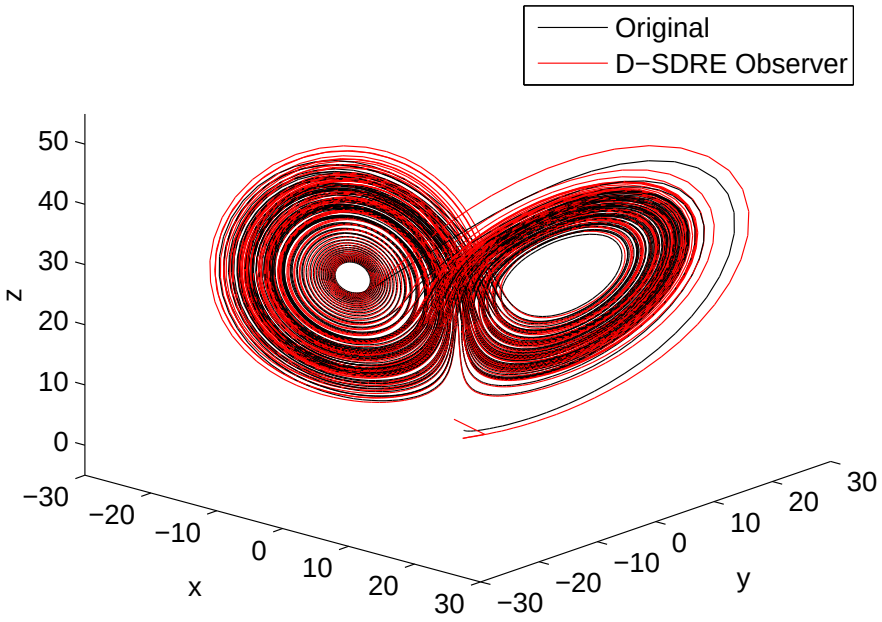

Figure 8.2: Comparison of the trajectories: the original system and D-SDRE Observer with $\sigma = 10$, $\rho = 28$, $\beta = 8/3$, $[x_0,\ y_0,\ z_0] = [0\ \ 1\ \ 1]$, and $[\hat{x}_0,\ \hat{y}_0,\ \hat{z}_0] = [-5\ \ 5\ \ 0]$

more clearly by using the second figures in Figures 8.3 – 8.5. Due to the mismatches of the initial conditions between the actual state values and the the D-SDRE Observer, the RMS errors have large values at the beginning of the simulations (0–1 sec). However, after the effect of the initial mismatches, the average values of the RMS errors converge to certain values. The results show that the estimation of the states by using the D-SDRE Observer is reliable regardless of the values of $\boldsymbol{Q}_k$ and $\boldsymbol{R}_k$.

8.3 Conclusion

In this chapter, we introduced the D-SDRE Observer, based on the D-SDRE technique introduced in the Chapter 5. We have investigated condition of the error between the actual state of the nonlinear deterministic system and the estimated one by using the D-SDRE Observer and have proven that the error dynamics is ISS. We applied the D-SDRE Observer to the Lorenz attractor to estimate the states and the results showed that the Observer is reliable regardless of the values of the $\boldsymbol{Q}_k$ and $\boldsymbol{R}_k$.

However, it should be noted that the D-SDRE Observer was designed for the *deterministic* system. Therefore, we should investigate the case where there are stochastic terms in the dynamical systems, which is the topic for the next chapter.

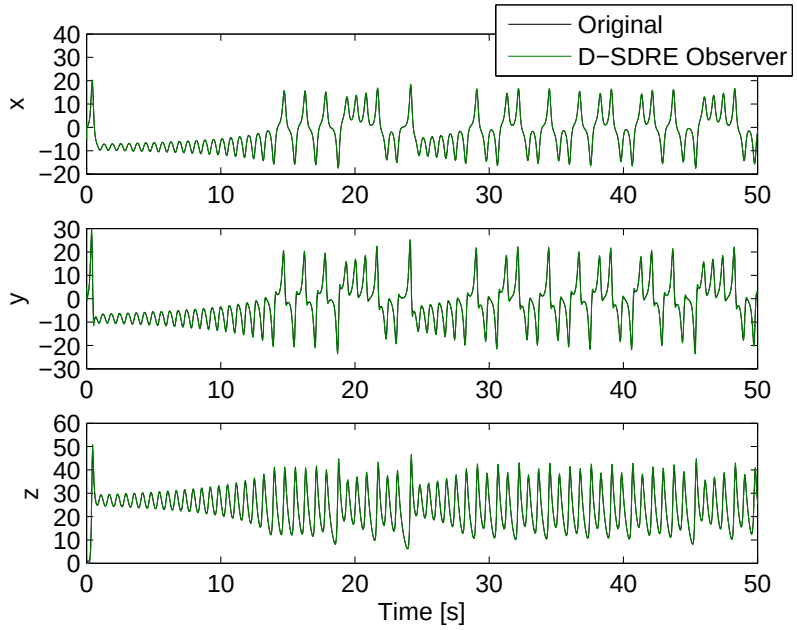

(a) Trajectories of the Lorenz attractor and corresponding signals by the D-SDRE Observer

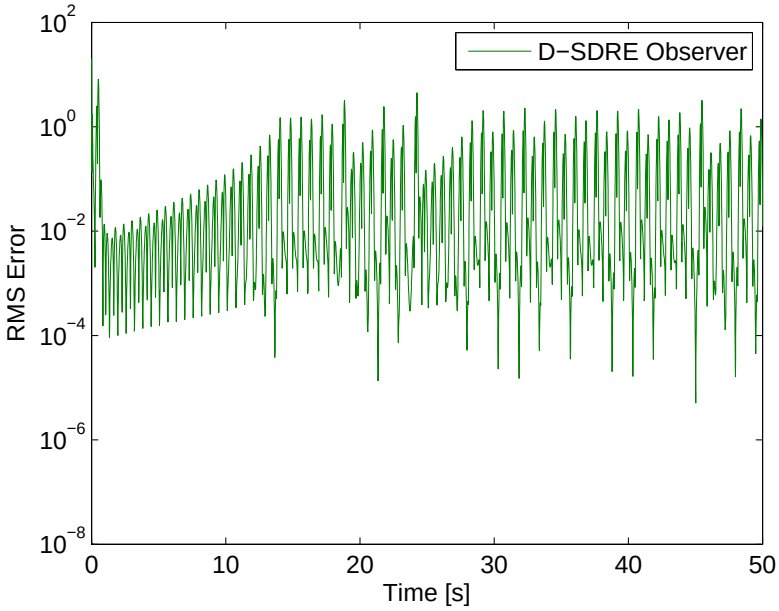

(b) RMS error of the D-SDRE Observer signal

Figure 8.3: Trajectory of the Lorenz attractor and the time histories of RMS errors with $\boldsymbol{Q}_k = diag(0.001,\ 0.001,\ 0.001),\ \boldsymbol{R}_k = 0.01$

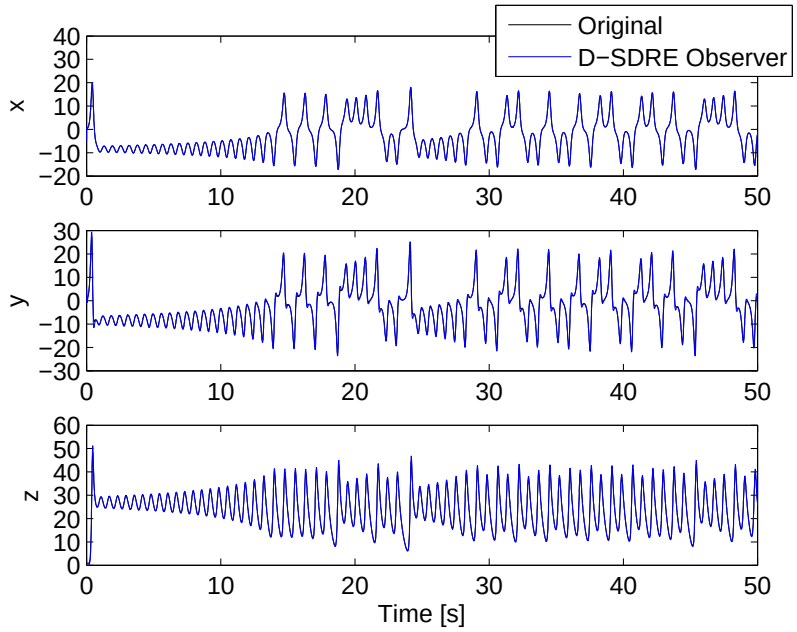

(a) Trajectories of the Lorenz attractor and corresponding signals by the D-SDRE Observer

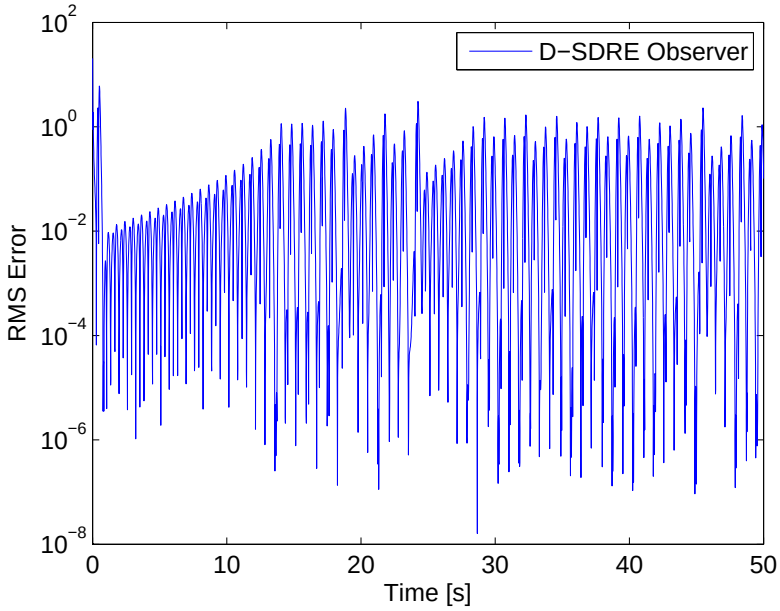

(b) RMS error of the D-SDRE Observer signal

Figure 8.4: Trajectory of the Lorenz attractor and the time histories of RMS errors with $\boldsymbol{Q}_k = diag(0.01,\ 0.01,\ 0.01),\ \boldsymbol{R}_k = 0.001$

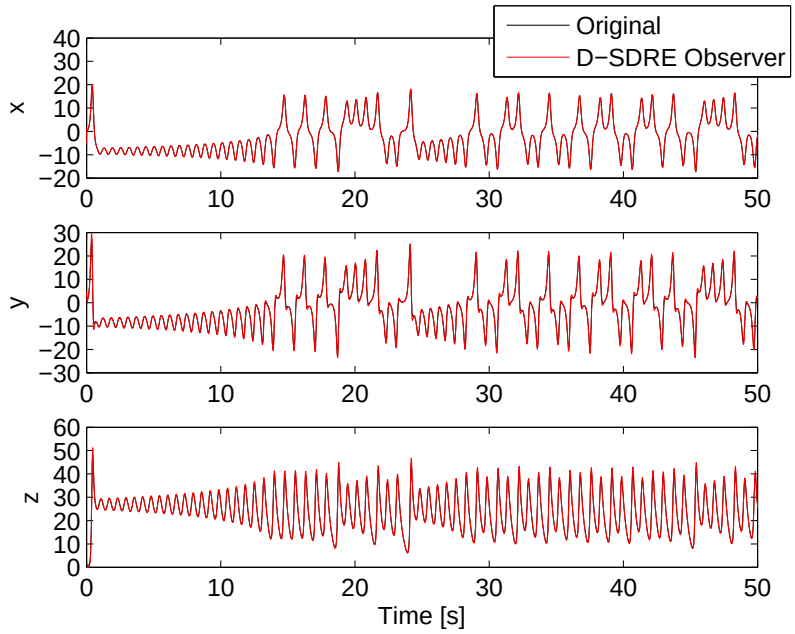

(a) Trajectories of the Lorenz attractor and corresponding signals by the D-SDRE Observer

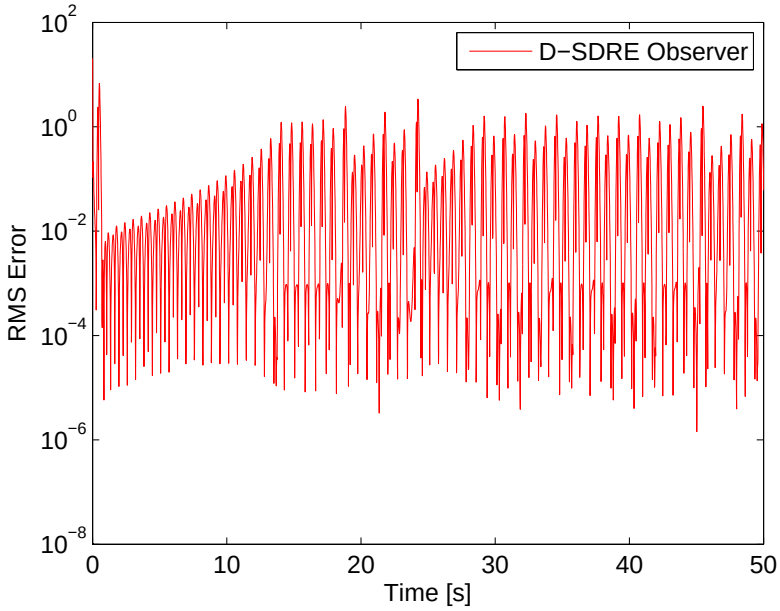

(b) RMS error of the D-SDRE Observer signal

Figure 8.5: Trajectory of the Lorenz attractor and the time histories of RMS errors with $\boldsymbol{Q}_k = diag(0.01,\ 0.01,\ 0.01),\ \boldsymbol{R}_k = 0.01$

Chapter 9

The D-SDRE-Based Filter Design

9.1 Introduction

TWO filtering techniques are investigated by using the discrete-time state-dependent Riccati equation (D-SDRE) technique. Detailed derivation of the D-SDRE-based filter (D-SDREF) is provided under the assumption of Gaussian noises and the stability condition of the error signal between the measured signal and the estimated signals is proven to be input-to-state stable. For the non-Gaussian distributed noises, we propose a filter by combining the D-SDREF and the particle filter (PF), named the combined D-SDRE/PF. Two algorithms for the filtering techniques are provided. Several filtering techniques are compared with challenging numerical examples to show the reliability and efficacy of the proposed D-SDREF and the combined D-SDRE/particle filter.

The rest of the chapter is organized as follows: The D-SDREF is derived in Section 9.2. Its stability condition is rigorously investigated in Section 9.3. The combined D-SDRE/PF is introduced in Section 9.4. In Section 9.5, the proposed D-SDREF and the combined D-SDRE/PF are evaluated by using two challenging examples. Finally, concluding remarks are made in Section 9.6.

9.2 Discrete-Time State-Dependent Riccati Equation-Based Filter (D-SDREF)

In this section, we derive the D-SDREF technique. Consider a discrete-time nonlinear stochastic system:

$$\begin{aligned} \boldsymbol{x}_k &= \boldsymbol{f}(\boldsymbol{x}_{k-1}, \boldsymbol{w}_{k-1}) &&= \boldsymbol{A}(\boldsymbol{x}_{k-1})\boldsymbol{x}_{k-1} + \boldsymbol{G}_{k-1}\boldsymbol{\omega}_{k-1} \\ \boldsymbol{y}_k &= \boldsymbol{h}(\boldsymbol{x}_k, \boldsymbol{\nu}_k) &&= \boldsymbol{C}(\boldsymbol{x}_k)\boldsymbol{x}_k + \boldsymbol{\Gamma}_k\boldsymbol{\nu}_k \end{aligned} \tag{9.1}$$

where $\boldsymbol{x}_k \in \mathbb{R}^n$ denotes the state and $\boldsymbol{y}_k \in \mathbb{R}^p$ the output of the system. The variables $\boldsymbol{\omega}_k \in \mathbb{R}^p$ and $\boldsymbol{\nu}_q \in \mathbb{R}^p$, respectively, represent a process noise and a measurement noise with $\boldsymbol{\omega}_k \sim \mathcal{N}(\mathbf{0}, \boldsymbol{I}_p)$ and $\boldsymbol{\nu}_k \sim \mathcal{N}(\mathbf{0}, \boldsymbol{I}_q)$. The time-varying matrices $\boldsymbol{G}_k \in \mathbb{R}^{n\times p}$ and $\boldsymbol{\Gamma}_k \in \mathbb{R}^{n\times q}$ are assumed to be known.

A two-step procedure is used to design the D-SDREF: state prediction ($\bar{(\cdot)}$) and state update ($\hat{(\cdot)}$). A procedure in this section can also be found in Gelb (1974); Anderson and Moore (1979), which describe EKF. We start with the updated state ($\hat{\boldsymbol{x}}_k$) to derive equations of the D-SDREF. It is assumed that the updated state $\hat{\boldsymbol{x}}_k$ can be expressed as

$$\hat{\boldsymbol{x}}_k := \boldsymbol{\vartheta}_k + \boldsymbol{L}_k \boldsymbol{y}_k \tag{9.2}$$

where $\boldsymbol{\vartheta}_k$ and $\boldsymbol{L}_k$ are variables to be determined later, and $\boldsymbol{y}_k$ is the output of the system, defined in (9.1). From the two-step procedure, two types of errors can be considered for the analysis of the D-SDREF:

$$\begin{aligned} \bar{\boldsymbol{e}}_k &:= \boldsymbol{x}_k - \bar{\boldsymbol{x}}_k \quad \text{: error of the predicted state} \\ \hat{\boldsymbol{e}}_k &:= \boldsymbol{x}_k - \hat{\boldsymbol{x}}_k \quad \text{: error of the updated state.} \end{aligned} \tag{9.3}$$

Substituting (9.3) into (9.2) yields

$$\boldsymbol{x}_k - \hat{\boldsymbol{e}}_k = \bar{\boldsymbol{e}}_k + \bar{\boldsymbol{x}}_k - \hat{\boldsymbol{e}}_k = \boldsymbol{\vartheta}_k + \boldsymbol{L}_k \boldsymbol{y}_k. \tag{9.4}$$

Since the expectations of $\bar{\boldsymbol{e}}_k$ and $\hat{\boldsymbol{e}}_k$ are zeros (i.e., $\mathbb{E}\big[\bar{\boldsymbol{e}}_k\big] = \mathbf{0},\ \mathbb{E}\big[\hat{\boldsymbol{e}}_k\big] = \mathbf{0}$), we can obtain the following equation by applying the expectation in both side of (9.4),

$$\boldsymbol{\vartheta}_k = \bar{\boldsymbol{x}}_k - \boldsymbol{L}_k \bar{\boldsymbol{y}}_k. \tag{9.5}$$

Therefore, by substituting (9.5) into (9.2), we can find the state-update process as follows:

$$\hat{\boldsymbol{x}}_k = \bar{\boldsymbol{x}}_k + \boldsymbol{L}_k\big(\boldsymbol{y}_k - \bar{\boldsymbol{y}}_k\big). \tag{9.6}$$

Then, the following estimated error can be found by substituting (9.1) and (9.3) into (9.6):

$$-\hat{\boldsymbol{e}}_k = -\bar{\boldsymbol{e}}_k + \boldsymbol{L}_k\big(\boldsymbol{h}(\boldsymbol{x}_k) - \boldsymbol{h}(\bar{\boldsymbol{x}}_k)\big) + \boldsymbol{L}_k \boldsymbol{\Gamma}_k \boldsymbol{\nu}_k. \tag{9.7}$$

An analytical form of the estimated error covariance can be derived by multiplying (9.7) and its transpose,

$$\begin{aligned}\hat{\boldsymbol{e}}_k\hat{\boldsymbol{e}}_k^\top &= \bar{\boldsymbol{e}}_k\bar{\boldsymbol{e}}_k^\top - \boldsymbol{L}_k\big(\boldsymbol{h}(\boldsymbol{x}_k)-\boldsymbol{h}(\bar{\boldsymbol{x}}_k)\big)\bar{\boldsymbol{e}}_k^\top - \boldsymbol{L}_k\boldsymbol{\Gamma}_k\boldsymbol{\nu}_k\bar{\boldsymbol{e}}_k^\top - \bar{\boldsymbol{e}}_k\big(\boldsymbol{h}(\boldsymbol{x}_k)-\boldsymbol{h}(\bar{\boldsymbol{x}}_k)\big)^\top\boldsymbol{L}_k^\top \\ &\quad + \boldsymbol{L}_k\big(\boldsymbol{h}(\boldsymbol{x}_k)-\boldsymbol{h}(\bar{\boldsymbol{x}}_k)\big)\big(\boldsymbol{h}(\boldsymbol{x}_k)-\boldsymbol{h}(\bar{\boldsymbol{x}}_k)\big)^\top\boldsymbol{L}_k^\top + \boldsymbol{L}_k\boldsymbol{\Gamma}_k\boldsymbol{\nu}_k\big(\boldsymbol{h}(\boldsymbol{x}_k)-\boldsymbol{h}(\bar{\boldsymbol{x}}_k)\big)^\top\boldsymbol{L}_k^\top \\ &\quad - \bar{\boldsymbol{e}}_k\boldsymbol{\nu}_k^\top\boldsymbol{\Gamma}_k^\top\boldsymbol{L}_k^\top + \boldsymbol{L}_k\big(\boldsymbol{h}(\boldsymbol{x}_k)-\boldsymbol{h}(\bar{\boldsymbol{x}}_k)\big)\boldsymbol{\nu}_k^\top\boldsymbol{\Gamma}_k^\top\boldsymbol{L}_k^\top + \boldsymbol{L}_k\boldsymbol{\Gamma}_k\boldsymbol{\nu}_k\boldsymbol{\nu}_k^\top\boldsymbol{\Gamma}_k^\top\boldsymbol{L}_k^\top. \end{aligned} \tag{9.8}$$

Taking the expectation of (9.8) yields the following result:

$$\begin{aligned}\mathbb{E}\big[\hat{\boldsymbol{e}}_k\hat{\boldsymbol{e}}_k^\top\big] &= \mathbb{E}\big[\bar{\boldsymbol{e}}_k\bar{\boldsymbol{e}}_k^\top\big] - \boldsymbol{L}_k\bar{\boldsymbol{C}}_k\mathbb{E}\big[\bar{\boldsymbol{e}}_k\bar{\boldsymbol{e}}_k^\top\big] - \boldsymbol{L}_k\boldsymbol{\Gamma}_k\mathbb{E}\big[\boldsymbol{\nu}_k\bar{\boldsymbol{e}}_k^\top\big] - \mathbb{E}\big[\bar{\boldsymbol{e}}_k\bar{\boldsymbol{e}}_k^\top\big]\bar{\boldsymbol{C}}_k^\top\boldsymbol{L}_k^\top \\ &\quad + \boldsymbol{L}_k\bar{\boldsymbol{C}}_k\mathbb{E}\big[\bar{\boldsymbol{e}}_k\bar{\boldsymbol{e}}_k^\top\big]\bar{\boldsymbol{C}}_k^\top\boldsymbol{L}_k^\top + \boldsymbol{L}_k\boldsymbol{\Gamma}_k\mathbb{E}\big[\boldsymbol{\nu}_k\bar{\boldsymbol{e}}_k^\top\big]\bar{\boldsymbol{C}}_k^\top\boldsymbol{L}_k^\top - \mathbb{E}\big[\bar{\boldsymbol{e}}_k\boldsymbol{\nu}_k^\top\big]\boldsymbol{\Gamma}_k^\top\boldsymbol{L}_k^\top \\ &\quad + \boldsymbol{L}_k\bar{\boldsymbol{C}}_k\mathbb{E}\big[\hat{\boldsymbol{e}}_k\boldsymbol{\nu}_k^\top\big]\boldsymbol{\Gamma}_k^\top\boldsymbol{\mathfrak{L}}_k^\top + \boldsymbol{\mathfrak{L}}_k\boldsymbol{\Gamma}_k\mathbb{E}\big[\boldsymbol{\nu}_k\boldsymbol{\nu}_k^\top\big]\boldsymbol{\Gamma}_k^\top\boldsymbol{\mathfrak{L}}_k^\top \end{aligned} \tag{9.9}$$

where $\bar{\boldsymbol{C}}_k = \boldsymbol{C}(\bar{\boldsymbol{x}}_k)$ and it is frozen at time k.

Then, the estimate of the error covariance ($\hat{\boldsymbol{P}}_k$) at time k is obtained from (9.9):

$$\hat{\boldsymbol{P}}_k = \bar{\boldsymbol{P}}_k - \boldsymbol{L}_k\bar{\boldsymbol{C}}_k\bar{\boldsymbol{P}}_k - \bar{\boldsymbol{P}}_k\bar{\boldsymbol{C}}_k^\top\boldsymbol{L}_k^\top + \boldsymbol{L}_k\bar{\boldsymbol{C}}_k\bar{\boldsymbol{P}}_k\bar{\boldsymbol{C}}_k^\top\boldsymbol{L}_k^\top + \boldsymbol{L}_k\boldsymbol{R}_k\boldsymbol{L}_k^\top \tag{9.10}$$

where $\bar{\boldsymbol{P}}_k$ represents the predicted error covariance.

The purpose of the D-SDREF is to minimize the mean error of the states, i.e., $\min_{\boldsymbol{L}_k}\mathbb{E}\big[\hat{\boldsymbol{e}}_k\hat{\boldsymbol{e}}_k^\top\big] = \min_{\boldsymbol{L}_k}\mathrm{tr}(\hat{\boldsymbol{P}}_k)$.

Thus,

$$\frac{\partial\mathrm{tr}\big(\hat{\boldsymbol{P}}_k\big)}{\partial\boldsymbol{L}_k} = \boldsymbol{0}. \tag{9.11}$$

The filter gain $\boldsymbol{\mathfrak{L}}_k$ is obtained by solving (9.11) for $\boldsymbol{L}_k$:

$$\boldsymbol{L}_k = \bar{\boldsymbol{P}}_k\bar{\boldsymbol{C}}_k^\top\big(\bar{\boldsymbol{C}}_k\bar{\boldsymbol{P}}_k\bar{\boldsymbol{C}}_k^\top + \boldsymbol{R}_k\big)^{-1}. \tag{9.12}$$

Substituting (9.12) into (9.10) simplifies the updated covariance matrix $\hat{\boldsymbol{P}}_k$,

$$\begin{aligned}\hat{\boldsymbol{P}}_k &= \big(\boldsymbol{I} - \boldsymbol{L}_k\bar{\boldsymbol{C}}_k\big)\bar{\boldsymbol{P}}_k - \bar{\boldsymbol{P}}_k\bar{\boldsymbol{C}}_k^\top\boldsymbol{L}_k^\top + \boldsymbol{L}_k\big(\bar{\boldsymbol{C}}_k\bar{\boldsymbol{P}}_k\bar{\boldsymbol{C}}_k^\top + \boldsymbol{R}_k\big)\boldsymbol{L}_k^\top \\ &= \big(\boldsymbol{I} - \boldsymbol{L}_k\bar{\boldsymbol{C}}_k\big)\bar{\boldsymbol{P}}_k \end{aligned} \tag{9.13}$$

which is known as the Joseph algorithm (Gelb, 1974; Stengel, 1994) for a linearized system.

The predicted error covariance matrix $\bar{\boldsymbol{P}}_k$ can be obtained directly from its definition:

$$\bar{\boldsymbol{P}}_k = \mathrm{cov}\left[\bar{\boldsymbol{e}}_k\right] = \hat{\boldsymbol{A}}_{k-1}\hat{\boldsymbol{P}}_{k-1}\hat{\boldsymbol{A}}_{k-1}^{\top} + \boldsymbol{Q}_{k-1} \tag{9.14}$$

where $\hat{\boldsymbol{A}}_{k-1} := \boldsymbol{A}(\hat{\boldsymbol{x}}_{k-1})$.

Table 9.1 summarizes the algorithm of the D-SDREF discussed so far.

Based on the derivation of the D-SDREF, its error bounds are investigated in the following section.

9.3 Error Bounds for the D-SDREF

In this section, we want to show that the errors between the actual states and the estimated ones by using the D-SDREF are bounded in the presence of disturbances sources such as process noise, measurement noise, model uncertainties, etc. Prior to that, we consider the following assumptions of the states and the values of the matrices in the dynamical model (9.1) and the filtering model in Table 30.

Assumption 30 *Given the nonlinear stochastic system (9.1), the following assumptions hold for all* $k \in \mathbb{Z}_{\geq 0}$*:*

$$\begin{aligned}
&\|\boldsymbol{A}(\boldsymbol{x}_k) - \boldsymbol{A}(\hat{\boldsymbol{x}}_k)\| \leq \rho_A |\boldsymbol{x}_k - \hat{\boldsymbol{x}}_k| \\
&\|\boldsymbol{C}(\boldsymbol{x}_k) - \boldsymbol{C}(\bar{\boldsymbol{x}}_k)\| \leq \rho_C |\boldsymbol{x}_k - \bar{\boldsymbol{x}}_k| \\
&a_{\min} \leq \|\boldsymbol{A}(\boldsymbol{x}_k)\| \leq a_{\max} \\
&c_{\min} \leq \|\boldsymbol{C}(\boldsymbol{x}_k)\| \leq c_{\max} \\
&p_{\min} \leq \|\boldsymbol{P}_k\| \leq p_{\max} \\
&l_{\min} \leq \|\boldsymbol{L}(\hat{\boldsymbol{x}}_k)\| \leq l_{\max} \\
&|\boldsymbol{x}_k| \leq \chi
\end{aligned} \tag{9.15}$$

for some $\rho_A > 0$ *and* $\rho_C > 0$*.*

The first two in Assumption 30 show the Lipschitz condition and the last one shows that the states of the system are bounded.

Prior to the stability analysis of the system with the D-SDREF, we discuss two useful lemmas first that will be used to prove the stability of the error bounds.

Table 9.1: Algorithm of the D-SDREF

Initialization ($k = 0$)

Define $\boldsymbol{P}_0$, $\boldsymbol{Q}_0$, and $\boldsymbol{R}_0$.

For $k = 1,\ 2,\ 3, \cdots$

Prediction ($\hat{\boldsymbol{x}}_{k-1},\ \hat{\boldsymbol{P}}_{k-1}, \rightarrow \bar{\boldsymbol{x}}_k,\ \bar{\boldsymbol{P}}_k$)

Predicted State

$$\bar{\boldsymbol{x}}_k \quad = \quad \boldsymbol{f}(\hat{\boldsymbol{x}}_{k-1}) = \boldsymbol{A}(\hat{\boldsymbol{x}}_{k-1})\hat{\boldsymbol{x}}_{k-1} = \hat{\boldsymbol{A}}_{k-1}\hat{\boldsymbol{x}}_{k-1}$$

Predicted Measurement

$$\bar{\boldsymbol{y}}_k \quad = \quad \boldsymbol{h}(\bar{\boldsymbol{x}}_k) = \boldsymbol{C}(\bar{\boldsymbol{x}}_k)\bar{\boldsymbol{x}}_k = \bar{\boldsymbol{C}}_k\bar{\boldsymbol{x}}_k$$

Predicted Error Covariance

$$\bar{\boldsymbol{P}}_k \quad = \quad \hat{\boldsymbol{A}}_{k-1}\hat{\boldsymbol{P}}_{k-1}\hat{\boldsymbol{A}}_{k-1}^{\top} + \boldsymbol{Q}_{k-1}$$

Update ($\bar{\boldsymbol{x}}_k,\ \bar{\boldsymbol{P}}_k \rightarrow \hat{\boldsymbol{x}}_k,\ \hat{\boldsymbol{P}}_k$)

Filter Gain

$$\boldsymbol{L}_k \quad = \quad \bar{\boldsymbol{P}}_k\bar{\boldsymbol{C}}_k^{\top}\left(\bar{\boldsymbol{C}}_k\bar{\boldsymbol{P}}_k\bar{\boldsymbol{C}}_k^{\top} + \boldsymbol{R}_k\right)^{-1}$$

State Estimate

$$\hat{\boldsymbol{x}}_k \quad = \quad \bar{\boldsymbol{x}}_k + \boldsymbol{L}_k\left(\boldsymbol{y}_k - \bar{\boldsymbol{y}}_k\right)$$

Error Covariance Estimate

$$\hat{\boldsymbol{P}}_k \quad = \quad \left(\boldsymbol{I} - \boldsymbol{L}_k\bar{\boldsymbol{C}}_k\right)\bar{\boldsymbol{P}}_k$$

End

Lemma 31 *For invertible $\hat{\boldsymbol{A}}_k$, $\hat{\boldsymbol{P}}_k$ and $\boldsymbol{Q}_k$, the following inequality holds for all $k \in \mathbb{Z}_{\geq 0}$:*

$$\left(\hat{\boldsymbol{A}}_k \hat{\boldsymbol{P}}_k \hat{\boldsymbol{A}}_k^\top + \boldsymbol{Q}_k\right)^{-1} = \hat{\boldsymbol{A}}_k^{-\top}\left[\hat{\boldsymbol{P}}_k^{-1} - \hat{\boldsymbol{P}}_k^{-1}\left(\hat{\boldsymbol{P}}_k^{-1} + \hat{\boldsymbol{A}}_k^\top \boldsymbol{Q}_k^{-1}\hat{\boldsymbol{A}}_k\right)^{-1}\hat{\boldsymbol{P}}_k^{-1}\right]\hat{\boldsymbol{A}}_k^{-1}. \tag{9.16}$$

Proof The left-hand side of (9.16) can be rearranged as follows:

$$\begin{aligned}\left(\hat{\boldsymbol{A}}_k \hat{\boldsymbol{P}}_k \hat{\boldsymbol{A}}_k^\top + \boldsymbol{Q}_k\right)^{-1} &= \left(\hat{\boldsymbol{A}}_k(\hat{\boldsymbol{P}}_k + \hat{\boldsymbol{A}}_k^{-1}\boldsymbol{Q}_k\hat{\boldsymbol{A}}_k^{-\top})\hat{\boldsymbol{A}}_k^\top\right)^{-1} \\ &= \hat{\boldsymbol{A}}_k^{-\top}(\hat{\boldsymbol{P}}_k + \hat{\boldsymbol{A}}_k^{-1}\boldsymbol{Q}_k\hat{\boldsymbol{A}}_k^{-\top})^{-1}\hat{\boldsymbol{A}}_k^{-1}.\end{aligned} \tag{9.17}$$

Finally, applying the matrix inversion lemma (Lewis et al., 2012) yields

$$\begin{aligned}\left(\hat{\boldsymbol{A}}_k \hat{\boldsymbol{P}}_k \hat{\boldsymbol{A}}_k^\top + \boldsymbol{Q}_k\right)^{-1} &= \hat{\boldsymbol{A}}_k^{-\top}\left(\hat{\boldsymbol{P}}_k^{-1} - \hat{\boldsymbol{P}}_k^{-1}\hat{\boldsymbol{A}}_k^{-1}(\hat{\boldsymbol{A}}_k^{-\top}\hat{\boldsymbol{P}}_k^{-1}\hat{\boldsymbol{A}}_k^{-1} + \boldsymbol{Q}_k^{-1})^{-1}\hat{\boldsymbol{A}}_k^{-\top}\hat{\boldsymbol{P}}_k^{-1}\right)\hat{\boldsymbol{A}}_k^{-1} \\ &= \hat{\boldsymbol{A}}_k^{-\top}\left(\hat{\boldsymbol{P}}_k^{-1} - \hat{\boldsymbol{P}}_k^{-1}(\hat{\boldsymbol{P}}_k^{-1} + \hat{\boldsymbol{A}}_k^\top\boldsymbol{Q}_k^{-1}\hat{\boldsymbol{A}}_k)^{-1}\hat{\boldsymbol{P}}_k^{-1}\right)\hat{\boldsymbol{A}}_k^{-1}.\end{aligned} \tag{9.18}$$

This proves the lemma. □

Lemma 32 *For invertible $\hat{\boldsymbol{A}}_k$, $\hat{\boldsymbol{P}}_k$ and $\boldsymbol{Q}_k$, the following inequality holds for all $k \in \mathbb{Z}_{\geq 0}$:*

$$\hat{\boldsymbol{P}}_k^{-1} \leq (\boldsymbol{I} - \boldsymbol{L}_k\bar{\boldsymbol{C}}_k)^{-\top}\hat{\boldsymbol{A}}_{k-1}^{-\top}(\hat{\boldsymbol{P}}_{k-1}^{-1} - \hat{\boldsymbol{P}}_{k-1}^{-1}(\hat{\boldsymbol{P}}_{k-1}^{-1} + \hat{\boldsymbol{A}}_{k-1}^\top\boldsymbol{Q}_{k-1}^{-1}\hat{\boldsymbol{A}}_{k-1})^{-1}\hat{\boldsymbol{P}}_{k-1}^{-1})\hat{\boldsymbol{A}}_{k-1}^{-1}(\boldsymbol{I} - \boldsymbol{L}_k\hat{\boldsymbol{C}}_k)^{-1}.$$

Proof Since $\boldsymbol{L}_k\boldsymbol{R}_k\boldsymbol{L}_k^\top \geq \boldsymbol{0}$, the inequality holds from (9.10):

$$\hat{\boldsymbol{P}}_k \geq (\boldsymbol{I} - \boldsymbol{L}_k\bar{\boldsymbol{C}}_k)\bar{\boldsymbol{P}}_k(\boldsymbol{I} - \boldsymbol{L}_k\bar{\boldsymbol{C}}_k)^\top. \tag{9.19}$$

By taking the inverse in both sides of (9.19), it follows that

$$\hat{\boldsymbol{P}}_k^{-1} \leq (\boldsymbol{I} - \boldsymbol{L}_k\bar{\boldsymbol{C}}_k)^{-\top}\bar{\boldsymbol{P}}_k^{-1}(\boldsymbol{I} - \boldsymbol{L}_k\bar{\boldsymbol{C}}_k)^{-1}. \tag{9.20}$$

The lemma can be proven by the definition of $\bar{\boldsymbol{P}}_k$ and Lemma 31:

$$\begin{aligned}\hat{\boldsymbol{P}}_k^{-1} &\leq \big(\boldsymbol{I} - \boldsymbol{L}_k\bar{\boldsymbol{C}}_k\big)^{-\top}\Big(\hat{\boldsymbol{A}}_{k-1}\hat{\boldsymbol{P}}_{k-1}\hat{\boldsymbol{A}}_{k-1} + \boldsymbol{Q}_{k-1}\Big)^{-1}\big(\boldsymbol{I} - \boldsymbol{L}_k\bar{\boldsymbol{C}}_k\big)^{-1} \\ &= \big(\boldsymbol{I} - \boldsymbol{L}_k\bar{\boldsymbol{C}}_k\big)^{-\top}\hat{\boldsymbol{A}}_{k-1}^{-\top}\Big(\hat{\boldsymbol{P}}_{k-1}^{-1} - \hat{\boldsymbol{P}}_{k-1}^{-1}\big(\hat{\boldsymbol{P}}_{k-1}^{-1} + \hat{\boldsymbol{A}}_{k-1}^{\top}\boldsymbol{Q}_{k-1}^{-1}\hat{\boldsymbol{A}}_{k-1}\big)^{-1}\hat{\boldsymbol{P}}_{k-1}^{-1}\Big) \\ &\quad \times \hat{\boldsymbol{A}}_{k-1}^{-1}\big(\boldsymbol{I} - \boldsymbol{L}_k\bar{\boldsymbol{C}}_k\big)^{-1}. \end{aligned} \tag{9.21}$$

Therefore, the inequality holds for all $k \in \mathbb{Z}_{\geq 0}$. □

Theorem 33 *The error dynamics between the actual states of the discrete-time stochastic nonlinear system (9.1) and the estimated states of the D-SDREF in Table 9.1 is ISS.*

Proof In order to prove the stable error bound on states, we recall the definition of the state error in (9.3). Then, substituting (9.1) and (9.6) into (9.3) yields

$$\begin{aligned}\hat{\boldsymbol{e}}_k &= \boldsymbol{x}_k - \hat{\boldsymbol{x}}_k \\ &= \boldsymbol{A}_{k-1}\boldsymbol{x}_{k-1} + \boldsymbol{G}_{k-1}\boldsymbol{\omega}_{k-1} - \bar{\boldsymbol{x}}_k - \boldsymbol{L}_k\big(\boldsymbol{y}_k - \bar{\boldsymbol{y}}_k\big) \\ &= \hat{\boldsymbol{A}}_{k-1}\big(\boldsymbol{x}_{k-1} - \hat{\boldsymbol{x}}_{k-1}\big) - \boldsymbol{L}_k\bar{\boldsymbol{C}}_k\bar{\boldsymbol{e}}_k + \big(\boldsymbol{A}_{k-1} - \hat{\boldsymbol{A}}_{k-1}\big)\boldsymbol{x}_{k-1} + \boldsymbol{G}_{k-1}\boldsymbol{\omega}_{k-1} - \boldsymbol{L}_k\boldsymbol{\Gamma}_k\boldsymbol{\nu}_k \\ &= \hat{\boldsymbol{A}}_{k-1}\hat{\boldsymbol{e}}_{k-1} - \boldsymbol{L}_k\bar{\boldsymbol{C}}_k\hat{\boldsymbol{A}}_{k-1}\hat{\boldsymbol{e}}_{k-1} - \boldsymbol{L}_k\bar{\boldsymbol{C}}_k\boldsymbol{G}_{k-1}\boldsymbol{\omega}_{k-1} + \tilde{\boldsymbol{A}}_{k-1}\boldsymbol{x}_{k-1} \\ &\quad + \boldsymbol{G}_{k-1}\boldsymbol{\omega}_{k-1} - \boldsymbol{L}_k\boldsymbol{\Gamma}_k\boldsymbol{\nu}_k \end{aligned} \tag{9.22}$$

where $\tilde{\boldsymbol{A}}_{k-1} := \boldsymbol{A}_{k-1} - \hat{\boldsymbol{A}}_{k-1}$.

For the proof, we define an ISS-Lyapunov function candidate as follows:

$$V(\hat{\boldsymbol{e}}_k) := \hat{\boldsymbol{e}}_k^{\top}\hat{\boldsymbol{P}}_k^{-1}\hat{\boldsymbol{e}}_k \tag{9.23}$$

where $\hat{\boldsymbol{P}}_k^{-1}$ is the inverse of the updated error covariance of the system.

By substituting (9.22) into (9.23), the following derivation can be obtained:

$$
\begin{aligned}
V(\hat{\boldsymbol{e}}_k) = & \Big(\big(\boldsymbol{I} - \boldsymbol{L}_k \bar{\boldsymbol{C}}_k\big) \hat{\boldsymbol{A}}_{k-1} \hat{\boldsymbol{e}}_{k-1} + \tilde{\boldsymbol{A}}_{k-1} \boldsymbol{x}_{k-1} + \big(\boldsymbol{I} - \boldsymbol{L}_k \bar{\boldsymbol{C}}_k\big) \boldsymbol{G}_{k-1} \boldsymbol{\omega}_{k-1} - \boldsymbol{L}_k \boldsymbol{\Gamma}_k \boldsymbol{\nu}_k \Big)^\top \hat{\boldsymbol{P}}_k^{-1} \\
& \times \Big(\big(\boldsymbol{I} - \boldsymbol{L}_k \bar{\boldsymbol{C}}_k\big) \hat{\boldsymbol{A}}_{k-1} \hat{\boldsymbol{e}}_{k-1} + \tilde{\boldsymbol{A}}_{k-1} \boldsymbol{x}_{k-1} + \big(\boldsymbol{I} - \boldsymbol{L}_k \bar{\boldsymbol{C}}_k\big) \boldsymbol{G}_{k-1} \boldsymbol{\omega}_{k-1} - \boldsymbol{L}_k \boldsymbol{\Gamma}_k \boldsymbol{\nu}_k \Big) \\
= & \hat{\boldsymbol{e}}_{k-1}^\top \Big(\big(\boldsymbol{I} - \boldsymbol{L}_k \bar{\boldsymbol{C}}_k\big) \hat{\boldsymbol{A}}_{k-1} \Big)^\top \hat{\boldsymbol{P}}_k^{-1} \Big(\big(\boldsymbol{I} - \boldsymbol{L}_k \bar{\boldsymbol{C}}_k\big) \hat{\boldsymbol{A}}_{k-1} \Big) \hat{\boldsymbol{e}}_{k-1} \\
& + \hat{\boldsymbol{e}}_{k-1}^\top \Big(\big(\boldsymbol{I} - \boldsymbol{L}_k \bar{\boldsymbol{C}}_k\big) \hat{\boldsymbol{A}}_{k-1} \Big)^\top \hat{\boldsymbol{P}}_k^{-1} \tilde{\boldsymbol{A}}_{k-1} \boldsymbol{x}_{k-1} \\
& + \hat{\boldsymbol{e}}_{k-1}^\top \Big(\big(\boldsymbol{I} - \boldsymbol{L}_k \bar{\boldsymbol{C}}_k\big) \hat{\boldsymbol{A}}_{k-1} \Big)^\top \hat{\boldsymbol{P}}_k^{-1} \big(\boldsymbol{I} - \boldsymbol{L}_k \bar{\boldsymbol{C}}_k\big) \boldsymbol{G}_{k-1} \boldsymbol{\omega}_{k-1} \\
& - \hat{\boldsymbol{e}}_{k-1}^\top \Big(\big(\boldsymbol{I} - \boldsymbol{L}_k \bar{\boldsymbol{C}}_k\big) \hat{\boldsymbol{A}}_{k-1} \Big)^\top \hat{\boldsymbol{P}}_k^{-1} \boldsymbol{L}_k \boldsymbol{\Gamma}_k \boldsymbol{\nu}_k \\
& + \boldsymbol{x}_{k-1}^\top \tilde{\boldsymbol{A}}_{k-1}^\top \hat{\boldsymbol{P}}_k^{-1} \Big(\big(\boldsymbol{I} - \boldsymbol{L}_k \bar{\boldsymbol{C}}_k\big) \hat{\boldsymbol{A}}_{k-1} \Big) \hat{\boldsymbol{e}}_{k-1} + \boldsymbol{x}_{k-1}^\top \tilde{\boldsymbol{A}}_{k-1}^\top \hat{\boldsymbol{P}}_k^{-1} \tilde{\boldsymbol{A}}_{k-1} \boldsymbol{x}_{k-1} \\
& + \boldsymbol{x}_{k-1}^\top \tilde{\boldsymbol{A}}_{k-1}^\top \hat{\boldsymbol{P}}_k^{-1} \big(\boldsymbol{I} - \boldsymbol{L}_k \bar{\boldsymbol{C}}_k\big) \boldsymbol{G}_{k-1} \boldsymbol{\omega}_{k-1} - \boldsymbol{x}_{k-1}^\top \tilde{\boldsymbol{A}}_{k-1}^\top \hat{\boldsymbol{P}}_k^{-1} \boldsymbol{L}_k \boldsymbol{\Gamma}_k \boldsymbol{\nu}_k \\
& + \boldsymbol{\omega}_{k-1}^\top \boldsymbol{G}_{k-1}^\top \big(\boldsymbol{I} - \boldsymbol{L}_k \bar{\boldsymbol{C}}_k\big)^\top \hat{\boldsymbol{P}}_k^{-1} \Big(\big(\boldsymbol{I} - \boldsymbol{L}_k \bar{\boldsymbol{C}}_k\big) \hat{\boldsymbol{A}}_{k-1} \Big) \hat{\boldsymbol{e}}_{k-1} \\
& + \boldsymbol{\omega}_{k-1}^\top \boldsymbol{G}_{k-1}^\top \big(\boldsymbol{I} - \boldsymbol{L}_k \bar{\boldsymbol{C}}_k\big)^\top \hat{\boldsymbol{P}}_k^{-1} \tilde{\boldsymbol{A}}_{k-1} \boldsymbol{x}_{k-1} \\
& + \boldsymbol{\omega}_{k-1}^\top \boldsymbol{G}_{k-1}^\top \big(\boldsymbol{I} - \boldsymbol{L}_k \bar{\boldsymbol{C}}_k\big)^\top \hat{\boldsymbol{P}}_k^{-1} \big(\boldsymbol{I} - \boldsymbol{L}_k \bar{\boldsymbol{C}}_k\big) \boldsymbol{G}_{k-1} \boldsymbol{\omega}_{k-1} \\
& - \boldsymbol{\omega}_{k-1}^\top \boldsymbol{G}_{k-1}^\top \big(\boldsymbol{I} - \boldsymbol{L}_k \bar{\boldsymbol{C}}_k\big)^\top \hat{\boldsymbol{P}}_k^{-1} \boldsymbol{L}_k \boldsymbol{\Gamma}_k \boldsymbol{\nu}_k \\
& - \boldsymbol{\nu}_k \boldsymbol{\Gamma}_k^\top \boldsymbol{L}_k^\top \hat{\boldsymbol{P}}_k^{-1} \Big(\big(\boldsymbol{I} - \boldsymbol{L}_k \bar{\boldsymbol{C}}_k\big) \hat{\boldsymbol{A}}_{k-1} \Big) \hat{\boldsymbol{e}}_{k-1} - \boldsymbol{\nu}_k \boldsymbol{\Gamma}_k^\top \boldsymbol{L}_k^\top \hat{\boldsymbol{P}}_k^{-1} \tilde{\boldsymbol{A}}_{k-1} \boldsymbol{x}_{k-1} \\
& - \boldsymbol{\nu}_k \boldsymbol{\Gamma}_k^\top \boldsymbol{L}_k^\top \hat{\boldsymbol{P}}_k^{-1} \big(\boldsymbol{I} - \boldsymbol{L}_k \bar{\boldsymbol{C}}_k\big) \boldsymbol{G}_{k-1} \boldsymbol{\omega}_{k-1} + \boldsymbol{\nu}_k \boldsymbol{\Gamma}_k^\top \boldsymbol{L}_k^\top \hat{\boldsymbol{P}}_k^{-1} \boldsymbol{L}_k \boldsymbol{\Gamma}_k \boldsymbol{\nu}_k . \qquad (9.24)
\end{aligned}
$$

Applying Lemma 32 into (9.24) yields the following inequality:

$$
\begin{aligned}
V(\hat{\boldsymbol{e}}) &:= V(\hat{\boldsymbol{e}}_k) - V(\hat{\boldsymbol{e}}_{k-1}) \\
&\leq -\hat{\boldsymbol{e}}_{k-1}^{\top}\hat{\boldsymbol{P}}_{k-1}^{-1}\left(\hat{\boldsymbol{P}}_{k-1}^{-1} + \hat{\boldsymbol{A}}_{k-1}^{\top}\boldsymbol{Q}_{k-1}^{-1}\bar{\boldsymbol{A}}_{k-1}\right)^{-1}\hat{\boldsymbol{P}}_{k-1}^{-1}\hat{\boldsymbol{e}}_{k-1} \\
&\quad + \frac{2(1+l_{\max}c_{\max})a_{\max}\chi}{p_{\min}}\|\tilde{\boldsymbol{A}}_{k-1}\||\hat{\boldsymbol{e}}_{k-1}| + \frac{2(1+l_{\max}c_{\max})^2 a_{\max}}{p_{\min}}\|\boldsymbol{G}_{k-1}\||\hat{\boldsymbol{e}}_{k-1}| \\
&\quad + \frac{2(1+l_{\max}c_{\max})a_{\max}l_{\max}}{p_{\min}}\|\boldsymbol{\Gamma}_k\||\hat{\boldsymbol{e}}_{k-1}| + \frac{\chi^2}{p_{\min}}\|\tilde{\boldsymbol{A}}_{k-1}\|^2 \\
&\quad + \frac{2(1+l_{\max}c_{\max})\chi}{p_{\min}}\|\tilde{\boldsymbol{A}}_{k-1}\|\|\boldsymbol{G}_{k-1}\| + \frac{2l_{\max}\chi}{p_{\min}}\|\tilde{\boldsymbol{A}}_{k-1}\|\|\boldsymbol{\Gamma}_k\| \\
&\quad + \frac{(1+l_{\max}c_{\max})^2}{p_{\min}}\|\boldsymbol{G}_{k-1}\|^2 + \frac{2(1+l_{\max}c_{\max})l_{\max}}{p_{\min}}\|\boldsymbol{G}_{k-1}\|\|\boldsymbol{\Gamma}_k\| + \frac{l_{\max}^2}{p_{\min}}\|\boldsymbol{\Gamma}_k\|^2 \\
&\leq -\frac{p_{\min}q_{\min}}{p_{\max}^2\left(q_{\min}+p_{\min}a_{\max}^2\right)}|\hat{\boldsymbol{e}}_k|^2 + \frac{1}{p_{\min}}\Big((\chi+l_{\max})^2 + 2(1+l_{\max}c_{\max})(a_{\max}+1)(\chi+l_{\max}) \\
&\quad + (1+l_{\max}c_{\max})^2(2a_{\max}+1)\Big)|\boldsymbol{\xi}_k|^2 \\
&=: -\alpha_3(|\hat{\boldsymbol{e}}_k|) + \sigma(|\boldsymbol{\xi}_k|) \qquad (9.25)
\end{aligned}
$$

where $|\boldsymbol{\xi}_k| := \max\{\|\tilde{\boldsymbol{A}}_k\|,\ \|\boldsymbol{G}_k\|,\ \|\boldsymbol{\Gamma}_k\|,\ |\hat{\boldsymbol{e}}_k|\}$.

Therefore, the system is ISS by Definitions 1 and 2. □

In this section, we derived analytical forms of the D-SDREF and showed the stability condition between the measured signal and the estimated one under the assumption of Gaussian noises. In the next section, we investigate a new filter to improve the performance of the filter in the presence of non-Gaussian noises.

9.4 Combined D-SDRE/Particle Filter

In this section, we want to extend the D-SDREF to the case where the noises in a system follow non-Gaussian distribution. It should be noted that the D-SDREF was developed based on the assumption of Gaussian distribution. We propose a new filtering technique by combining the D-SDREF with particle filters (PF), named the combined D-SDRE/PF. Prior to discussing the benefits of D-SDRE/PF, we summarize the advantages of the proposed D-SDREF compared to other filtering techniques discussed:

1. D-SDREF propagates the states by using the full nonlinear model (more accurate propagation).

2. The full nonlinear model is factorized by using the SDC factorization without explicit calculation of

Jacobians or Hessians.

3. The computational burden is less than EKF (no linearization), UKF (no sigma points), MHE (no horizon of measurements), or PF (no samples).

However, it should be noted that the D-SDREF was designed under the assumption of the Gaussian noises. Therefore, the D-SDREF is not suitable for a system with non-Gaussian noises. Among filtering techniques that can handle non-Gaussian noises, PF shows its reliability as well as simplicity to be implemented in a system. It is interesting to note that PF is one of the filtering techniques that can handle Gaussian/non-Gaussian noises. The advantages of the PF are as follows (Rawlings and Mayne, 2009):

1. PF uses the full nonlinear model to propagate the samples.

2. The PF sampled density can represent a general conditional density.

3. PF is simple to program and executes quickly for small sample sizes.

However, PF has weaknesses to be operated alone in a system. For examples, the performance of PF becomes worse as the state dimensions increases. It is also sensitive to unmodeled disturbances (Rawlings and Mayne, 2009). There have been studies to investigate the benefits of filtering techniques by combining them with PF not only to overcome their weaknesses but also to take advantage of PF. Notable outcomes are extended Kalman particle filter (de Freitas et al., 2000), unscented particle filter (van der Merwe et al., 2000), and the combined MHE/particle filter (Rawlings and Mayne, 2009). These combined filters use their original filters to locate/relocate the samples of the PF. Then PF is used to obtain fast recursive estimation. However, extended Kalman particle filter has a linearization problem. The unscented particle filter and the combined MHE/PF show outstanding performance. However, the computational load cannot be underestimated due to the characteristics of UKF and MHE.

We propose the combined D-SDRE/PF by combining D-SDRE and PF. The two filters have different roles in the combined filter: the D-SDREF locates the samples while the PF is responsible for obtaining fast recursive estimation. By doing so, the combined D-SDRE/PF can overcome the drawbacks of each filtering techniques: simpler calculation and increased robustness to unmodeled disturbances, etc. The proposed D-SDRE/PF has benefits compared to the combined filters listed above:

1. D-SDRE/PF uses the full nonlinear model to propagate the samples.

2. D-SDRE/PF does not use many particles that can increase computational burden. It is computationally less expensive than unscented particle filter or combined MHE/PF.

The proposed D-SDRE/PF is summarized in Table 9.2.

9.5 Numerical Evaluation

9.5.1 Motion Estimates of Pendubot with Gaussian Noises

In this part, the D-SDREF is evaluated. To this end, the pendubot (Spong and Block, 1995; Fantoni et al., 2000) is to used to estimate the angles and the rates of angles of the rods in the presence of Gaussian noises. Figure 9.1 describe motion of the pendubot. There are two rods each of which has m_i, I_i, and L_i ($i = 1, 2$) as its mass, moment of inertia, and total length, respectively. The rod 1 is pivoted at the center of the inertial frame (x-y) and the rod 2 is connected to the other edge of the rod 1. The gravitation is applied to $-y$ direction (g in Figure 9.1 denotes the gravitational acceleration ($\approx 9.81\ \mathrm{m/s^2}$)). The length l_1 denotes the distance of the center of mass of the rod 1 from the origin and l_2 the distance of the center of mass of the rod 2 from the hinge with the rod 1. There are two angles in the system: $\theta_1(\mathrm{rad})$ denotes the angle measured from the x axis to the rod 1 and $\theta_2(\mathrm{rad})$ the angle measured from the rod 1 to the rod 2. There is an actuator that generates the torque τ_1 for the rod 1 at the origin. It is assumed that there is no friction in the system. Then, the equations of motion of the pendubot are described as follows (Fantoni et al., 2000):

$$\boldsymbol{M}(\boldsymbol{q})\ddot{\boldsymbol{q}} + \boldsymbol{V}(\boldsymbol{q}, \dot{\boldsymbol{q}})\dot{\boldsymbol{q}} + \boldsymbol{g}(\boldsymbol{q}) = \boldsymbol{\tau} \tag{9.26}$$

where $\boldsymbol{q} := [\theta_1 \quad \theta_2]^\top$ and $\boldsymbol{\tau} := [\tau_1 \quad 0]^\top$. The matrices $\boldsymbol{M}(\boldsymbol{q})$ and $\boldsymbol{V}(\boldsymbol{q}, \dot{\boldsymbol{q}})$ and the vector $\boldsymbol{g}(\boldsymbol{q})$ are defined as

$$\boldsymbol{M}(\boldsymbol{q}) := \begin{bmatrix} \ell_1 + \ell_2 + 2\ell_3 \cos\theta_2 & \ell_2 + \ell_3 cos\theta_2 \\ \ell_2 + \ell_3 \cos\theta_2 & \ell_2 \end{bmatrix}, \quad \boldsymbol{V}(\boldsymbol{q}, \dot{\boldsymbol{q}}) := \ell_3 \sin\theta_2 \begin{bmatrix} -\dot{\theta}_2 & -\dot{\theta}_1 - \dot{\theta}_2 \\ \dot{\theta}_1 & 0 \end{bmatrix},$$

$$\boldsymbol{g}(\boldsymbol{q}) := \begin{bmatrix} \ell_4 g \cos\theta_1 + \ell_5 g \cos(\theta_1 + \theta_2) \\ \ell_5 g \cos(\theta_1 + \theta_2) \end{bmatrix}$$

Table 9.2: Combined D-SDRE/Particle Filter

I. Initialization $(k = 0)$

$$\boldsymbol{x}_0^{(i)} \sim \Pr(\boldsymbol{x}_0)$$
$$w_0^{(i)} = \tfrac{1}{N_p} \qquad i = 1, 2, \cdots, N_p$$

II. For $k = 1,\ 2,\ 3,\ \cdots$

1. Importance Sampling

(1) SDC Factorization

- Calculate $\boldsymbol{A}^{(i)}(\hat{\boldsymbol{x}}_{k-1}^{(i)})$ by using SDC factorization for $i = 1, 2, 3, \cdots, N_p$.

(2) Particle Updates via D-SDREF

$$\bar{\boldsymbol{x}}_k^{(i)} = \boldsymbol{f}^{(i)}(\hat{\boldsymbol{x}}_{k-1}^{(i)}) = \boldsymbol{A}^{(i)}(\hat{\boldsymbol{x}}_{k-1}^{(i)})\hat{\boldsymbol{x}}_{k-1}^{(i)}$$
$$\bar{\boldsymbol{P}}_k^{(i)} = \boldsymbol{A}^{(i)}(\hat{\boldsymbol{x}}_{k-1}^{(i)})\hat{\boldsymbol{P}}_{k-1}^{(i)}\boldsymbol{A}^{\top(i)}(\hat{\boldsymbol{x}}_{k-1}^{(i)}) + \boldsymbol{Q}_{k-1}^{(i)}$$
$$\boldsymbol{L}_k^{(i)} = \bar{\boldsymbol{P}}_k^{(i)}\boldsymbol{C}^{\top(i)}(\bar{\boldsymbol{x}}_k^{(i)})\big(\boldsymbol{C}^{(i)}(\bar{\boldsymbol{x}}_k^{(i)})\bar{\boldsymbol{P}}_k^{(i)}\boldsymbol{C}^{\top(i)}(\bar{\boldsymbol{x}}_k^{(i)}) + \boldsymbol{R}_k^{(i)}\big)^{-1}$$
$$\hat{\boldsymbol{x}}_k^{(i)} = \bar{\boldsymbol{x}}_k^{(i)} + \boldsymbol{L}_k^{(i)}\big(\boldsymbol{y}_k - \bar{\boldsymbol{y}}_k^{(i)}\big)$$
$$\hat{\boldsymbol{P}}_k^{(i)} = \big(\boldsymbol{I} - \boldsymbol{L}_k^{(i)}\boldsymbol{C}^{(i)}(\bar{\boldsymbol{x}}_k^{(i)})\big)\bar{\boldsymbol{P}}_k^{(i)}$$

(3) Measurement Likelyhood

$$\boldsymbol{y}_k \sim \Pr(\boldsymbol{y}_k|\boldsymbol{x}_k^{(i)})$$

(4) Weight Update

$$w_k^{(i)} = w_{k-1}^{(i)}\frac{\Pr(\boldsymbol{y}_k|\boldsymbol{x}_k^{(i)})\Pr(\boldsymbol{x}_k|\boldsymbol{x}_{k-1}^{(i)})}{q(\boldsymbol{x}_k|\boldsymbol{x}_{k-1}^{(i)},\boldsymbol{y}_k)}$$

(5) Weight Normalization

$$\tilde{w}_k^{(i)} = w_k^{(i)}\left(\sum_{j=1}^{N_p} w_k^{(i)}\right)^{-1}$$

2. Resampling Decision

$$N_{\text{eff}} = \frac{1}{\sum_{i=1}^{N_p}\left(w_k^{(i)}\right)^2}$$

if $N_{\text{eff}} < N_{\text{tres}}$ (Resampling)

- Generate (resample) a set of "new" particles $\hat{\boldsymbol{x}}_k^{(i)}$: $\Pr(\hat{\boldsymbol{x}}_k = \boldsymbol{x}_k^{(i)}) = \tilde{w}_k^{(i)}$ for $i = 1, 2, 3, \cdot, N_p$.
- Set $\tilde{w}_k^{(i)} = \frac{1}{N_p}$ for $i = 1, 2, 3, \cdots, N_p$.

3. Posterior Distribution

$$\Pr(\boldsymbol{x}_k|\boldsymbol{Y}_k) \simeq \hat{\Pr}(\boldsymbol{x}_k|\boldsymbol{Y}_k) \simeq \sum_{i=1}^{N_p}\tilde{w}_k^{(i)}\delta(\boldsymbol{x}_k - \boldsymbol{x}_k^{(i)})$$

4. State Estimation

(1) Conditional Mean

$$\hat{\boldsymbol{x}}_k = \mathbb{E}\big[\boldsymbol{x}_k|\boldsymbol{Y}_k\big] \simeq \sum_{i=1}^{N_p}\tilde{w}_k^{(i)}\boldsymbol{x}_k^{(i)}$$

(2) Conditional Covariance

$$\hat{\boldsymbol{P}}_k = \hat{\boldsymbol{x}}_k\hat{\boldsymbol{x}}_k^{\top} - \mathbb{E}\big[\boldsymbol{x}_k|\boldsymbol{Y}_k\big]\mathbb{E}^{\top}\big[\boldsymbol{x}_k|\boldsymbol{Y}_k\big]$$

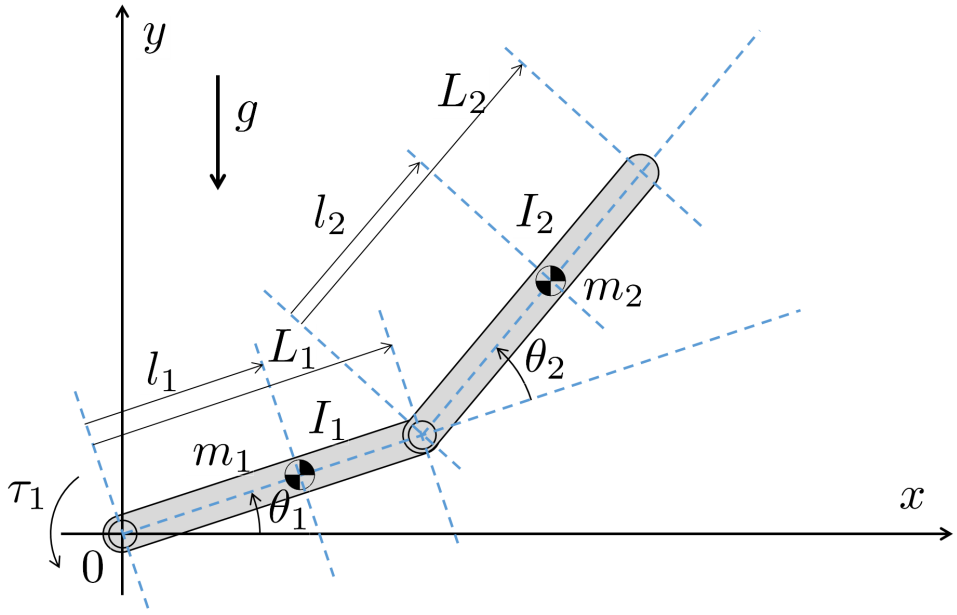

Figure 9.1: Description of the pendubot in the inertial frame (x-y)

where ℓ_i $(i = 1, 2, \cdots, 5)$ are parameters defined as

$$\begin{aligned}
\ell_1 &= m_1 l_1^2 + m_2 L_1^2 + I_1 \\
\ell_2 &= m_2 l_2^2 + I_2 \\
\ell_3 &= m_2 L_1 l_2 \\
\ell_4 &= m_1 l_1 + m_2 L_1 \\
\ell_5 &= m_2 l_2.
\end{aligned}$$

Assuming that there is no actuator in the system, i.e., $\tau_1 = 0$, the state-space equation of the pendubot system can be derived from (9.26):

$$\underbrace{\begin{bmatrix} \dot{\boldsymbol{q}} \\ \ddot{\boldsymbol{q}} \end{bmatrix}}_{=:\dot{\boldsymbol{x}}} = \underbrace{\begin{bmatrix} \boldsymbol{0} & \boldsymbol{I}_{2\times 2} \\ -\boldsymbol{M}^{-1}\boldsymbol{g}\begin{bmatrix} q_1^{-1}\eta_{q_1} & q_2^{-1}\eta_{q_2} \end{bmatrix} & -\boldsymbol{M}^{-1}\left(\boldsymbol{V} + \boldsymbol{g}\begin{bmatrix} \dot{q}_1^{-1}\eta_{\dot{q}_1} & \dot{q}_2^{-1}\eta_{\dot{q}_2} \end{bmatrix}\right) \end{bmatrix}}_{=:\boldsymbol{A}(\boldsymbol{x})} \underbrace{\begin{bmatrix} \boldsymbol{q} \\ \dot{\boldsymbol{q}} \end{bmatrix}}_{=:\boldsymbol{x}} \tag{9.27}$$

where $\boldsymbol{I}_{2\times 2} \in \mathbb{R}^{2\times 2}$ is the identity matrix and η_i $(i = q_1, q_2, \dot{q}_1, \dot{q}_2)$ is an indicator function such that

$$\begin{cases} \eta_i = 1 & \text{if } |i| = \max\{|q_1|, |q_2|, |\dot{q}_1|, |\dot{q}_2|\} \\ \eta_i = 0 & \text{otherwise.} \end{cases} \tag{9.28}$$

It is assumed that only $\boldsymbol{q} = [\theta_1 \quad \theta_2]^\top$ is measurable. Defining $\dot{\boldsymbol{x}} = \frac{\boldsymbol{x}_{k+1} - \boldsymbol{x}_k}{T}$ where T is the sampling time and adding $\boldsymbol{G}_k\boldsymbol{\omega}_k$ ($\boldsymbol{G}_k := T\boldsymbol{Q}_k^{\frac{1}{2}}$, $\boldsymbol{\omega}_k \sim \mathcal{N}(\boldsymbol{0}_4, \boldsymbol{I}_4)$) as a process noise and $\boldsymbol{\Gamma}\boldsymbol{\nu}_k$ ($\boldsymbol{\Gamma}_k := T\boldsymbol{R}_k^{\frac{1}{2}}$, $\boldsymbol{\nu}_k \sim \mathcal{N}(\boldsymbol{0}_2, \boldsymbol{I}_2)$) as a measurement noise yield the discrete-time state-space equation of (9.27):

$$\begin{aligned}
\boldsymbol{x}_{k+1} &= \Big(\boldsymbol{I}_{4\times 4} + T\boldsymbol{A}(\boldsymbol{x}_k)\Big)\boldsymbol{x}_k + \boldsymbol{G}_k\boldsymbol{\omega}_k \\
\boldsymbol{y}_k &= \underbrace{\begin{bmatrix} \boldsymbol{I}_{2\times 2} & \boldsymbol{0}_{2\times 2} \end{bmatrix}}_{\boldsymbol{C}_k} \boldsymbol{x}_k + \boldsymbol{\Gamma}_k\boldsymbol{\nu}_k.
\end{aligned} \tag{9.29}$$

The physical parameters of the pendubot for simulation are as follows: $m_1 = m_2 = 1$ kg, $I_1 = 1$ kgm^2, $I_2 = 0.6$ kgm^2, $L_1 = 1$ m, $L_2 = 1.3$ m, $l_1 = 0.5$ m, and $l_2 = 0.6$ m. The sampling time is $T = 0.01$ sec. The initial conditions of the states are $[\theta_{1,0} \quad \theta_{2,0} \quad \dot{\theta}_{1,0} \quad \dot{\theta}_{2,0}]^\top = [\frac{\pi}{2} \quad \frac{\pi}{12} \quad 0 \quad 0]^\top$. Three different filters are performed to evaluate the performance of the D-SDREF: EKF, UKF, and the D-SDREF. The initial

estimates of the states for the filters are set to $[\hat{\theta}_{1,0} \quad \hat{\theta}_{2,0} \quad \hat{\dot{\theta}}_{1,0} \quad \hat{\dot{\theta}}_{2,0}]^\top = [\frac{\pi}{3} \quad -\frac{\pi}{6} \quad 0 \quad 0]^\top$.

Two cases are simulated with different $\boldsymbol{Q}_k$ and $\boldsymbol{R}_k$. For the first simulation, we set up $\boldsymbol{Q}_k$ and $\boldsymbol{R}_k$ as $\boldsymbol{Q}_k = diag([0.001,\ 0.001,\ 0.001,\ 0.001])$ and $\boldsymbol{R}_k = diag([0.1,\ 0.1])$, which defines smaller Gaussian noises in the pendubot system. Figure 9.2 shows the simulation results of the state trajectories and root-mean square (RMS) errors by the EKF, UKF, and D-SDREF. When such small noises were applied, the performance of the D-SDREF is similar to that by the UKF while the EKF failed, especially to estimate accurate rates of angles ($\hat{\dot{\theta}}_1$ and $\hat{\dot{\theta}}_2$ in Figure 9.2(a)). It shows that the linearization of the dynamical system can affect the performance of the filters, which is one of the main drawbacks of using EKF in a highly nonlinear system.

Increasing the values of $\boldsymbol{Q}_k$ and $\boldsymbol{R}_k$, the reliability of the proposed D-SDREF can be evaluated. Figure 9.3 shows the simulation results of the filters with $\boldsymbol{Q}_k = diag([0.1,\ 0.1,\ 0.1,\ 0.1])$ and $\boldsymbol{R}_k = diag([1.0,\ 1.0])$ which show relatively larger Gaussian noises in the pendubot system. It is interesting to note that EKF and UKF failed to obtain accurate state estimates while the proposed D-SDREF shows the estimated the angles and the rates of angles with smaller errors regardless of $\boldsymbol{Q}_k$ and $\boldsymbol{R}_k$.

In the next part, we evaluate the combined D-SDRE/PF for a nonlinear system in the presence non-Gaussian noises.

9.5.2 Motion Estimates of the Rössler Attractor with Non-Gaussian Noises

In this section, the proposed D-SDREF and the combined D-SDRE/PF are evaluated. To this end, we use Rössler attractor (Rössler, 1976; Pikovsky et al., 1996), which shows chaotic behaviors with different fractal properties of the attractor. The equations of the Rössler attractor have the following set of ordinary differential equations:

$$\begin{aligned} \dot{x} &= -y - z \\ \dot{y} &= x + ay \\ \dot{z} &= b + z(x - c) \end{aligned} \tag{9.30}$$

where a, b, and c are design parameters. Figure 9.4 shows the trajectories of x, y, and z of the Rössler attractor in the 3-dimensional space with $a = 0.2$, $b = 0.2$, and $c = 5.7$.

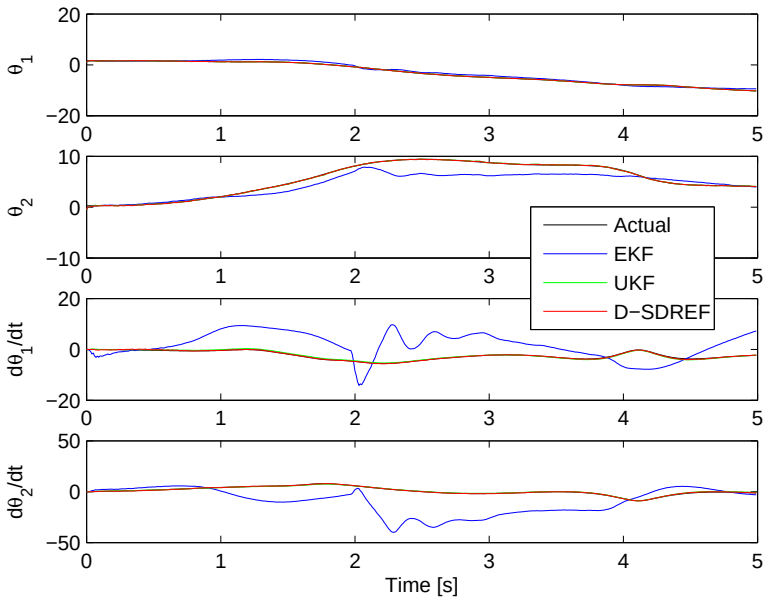

(a) State trajectories and corresponding estimates by EKF, UKF, and D-SDREF

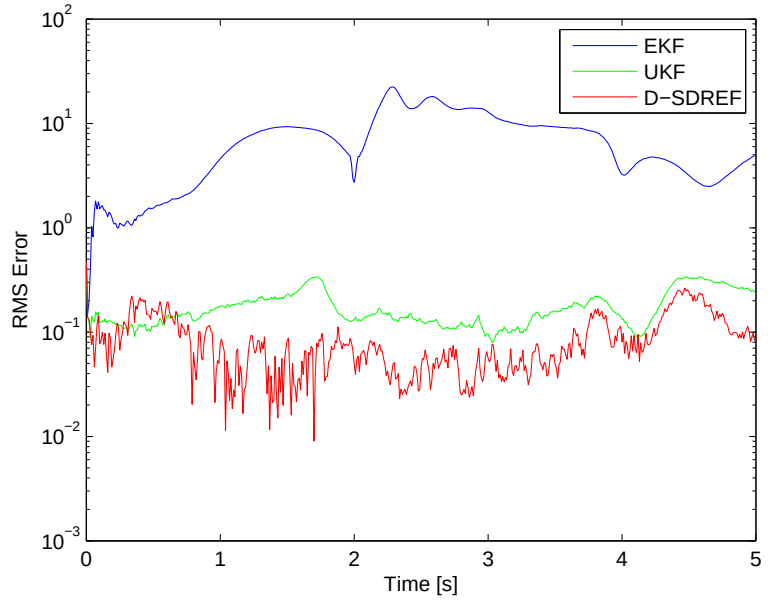

(b) RMS errors of EKF, UKF, and D-SDREF

Figure 9.2: State trajectories of the pendubot and RMS errors by EKF, UKF, and D-SDREF with $\boldsymbol{Q}_k = diag([0.001,\ 0.001,\ 0.001,\ 0.001])$ and $\boldsymbol{R}_k = diag([0.1,\ 0.1])$

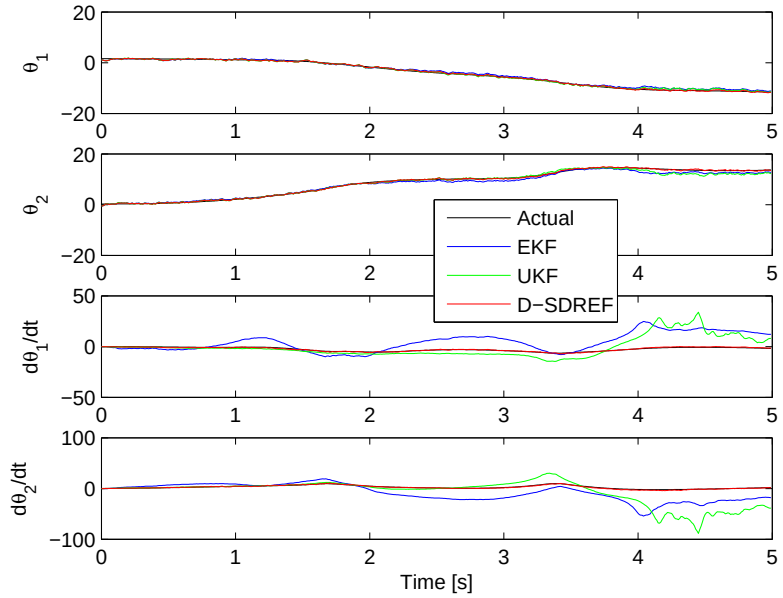

(a) State trajectories and corresponding estimates by EKF, UKF, and D-SDREF

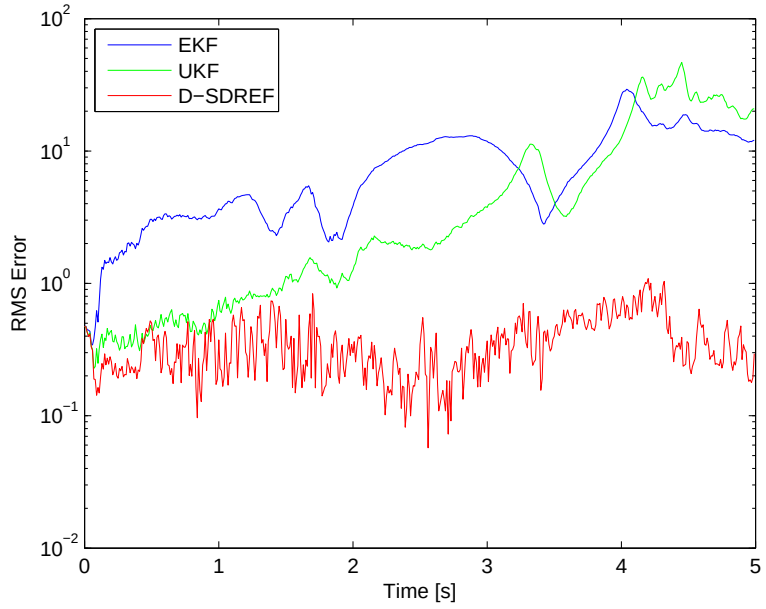

(b) RMS errors of EKF, UKF, and D-SDREF

Figure 9.3: State trajectories of the pendubot and RMS errors by EKF, UKF, and D-SDREF with $\boldsymbol{Q}_k = diag([0.1,\ 0.1,\ 0.1,\ 0.1])$ and $\boldsymbol{R}_k = diag([1.0,\ 1.0])$

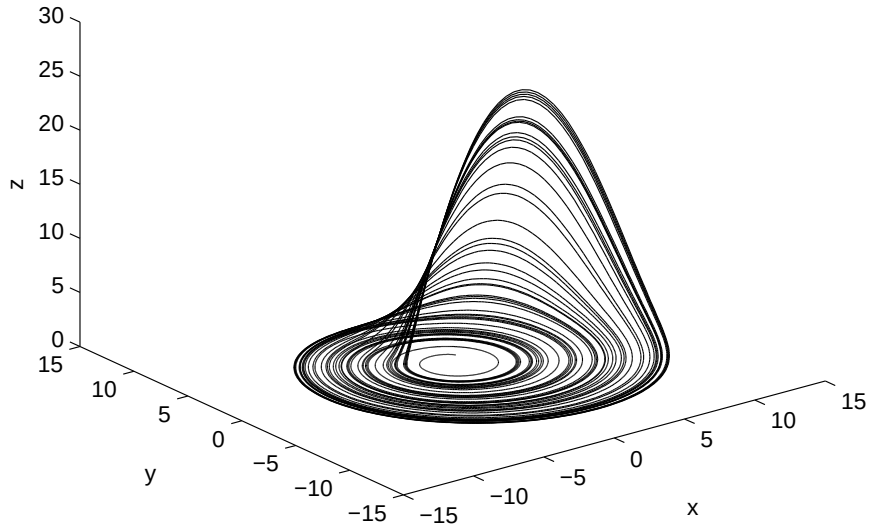

Figure 9.4: Trajectory of the Rössler attractor with $a = 0.2$, $b = 0.2$,$c = 5.7$, and $[x_0,\ y_0,\ z_0] = [1,\ 1,\ 0]$

Thus, the state-space equation of the Rössler attractor can be derived from (9.30):

$$\underbrace{\begin{bmatrix} \dot{x} \\ \dot{y} \\ \dot{z} \end{bmatrix}}_{=:\dot{\boldsymbol{x}}} = \underbrace{\begin{bmatrix} 0 & -1 & -1 \\ 1 & a & 0 \\ z + \frac{b}{x}\eta_x & \frac{b}{y}\eta_y & -c + \frac{b}{z}\eta_z \end{bmatrix}}_{=:\boldsymbol{A}(\boldsymbol{x})} \underbrace{\begin{bmatrix} x \\ y \\ z \end{bmatrix}}_{\boldsymbol{x}} \tag{9.31}$$

where η_i ($i = x,\ y,\ z$) is an indicator function defined as follows:

$$\begin{cases} \eta_i = 1 & \text{if } |i| = \max\{|x|, |y|, |z|\} \\ \eta_i = 0 & \text{otherwise.} \end{cases} \tag{9.32}$$

As done in the previous example, (9.31) can be discretized by defining $\dot{\boldsymbol{x}} := \frac{\boldsymbol{x}_{k+1} - \boldsymbol{x}_k}{T}$ and applying it to (9.31). Assuming that only x is measurable and adding $\boldsymbol{G}_k\boldsymbol{\omega}_k$ ($\boldsymbol{G}_k := T\boldsymbol{Q}_k^{\frac{1}{2}}$) as a process noise and $\boldsymbol{\Gamma}\boldsymbol{\nu}_k$ ($\boldsymbol{\Gamma}_k := T\boldsymbol{R}_k^{\frac{1}{2}}$) as a measurement noise to the system yield the discrete-time state-space equation of (9.31):

$$\begin{aligned} \boldsymbol{x}_{k+1} &= \Big(\boldsymbol{I}_{3\times 3} - T\boldsymbol{A}(\boldsymbol{x}_k)\Big)\boldsymbol{x}_k + \boldsymbol{G}_k\boldsymbol{\omega}_k \\ \boldsymbol{y}_k &= \underbrace{\begin{bmatrix} 1 & 0 & 0 \end{bmatrix}}_{=:\boldsymbol{C}_k} \boldsymbol{x}_k + \boldsymbol{\Gamma}_k\boldsymbol{\nu}_k. \end{aligned} \tag{9.33}$$

It should be noted that unlike in the previous example, $\boldsymbol{\omega}_k$ or $\boldsymbol{\nu}_k$ do not have to be Gaussian noises. In this simulation, elements of $\boldsymbol{\omega}_k$ and $\boldsymbol{\nu}_k$ are uniformly distributed between -1 and $+1$.

For the simulation, $T = 0.02$ sec, $a = 0.2$, $b = 0.2$, and $c = 5.7$ are used. The initial conditions of the states of the attractor are set to $[x_0,\ y_0,\ z_0] = [1,\ 1,\ 0]$ while filters to be compared in this simulation have $[\hat{x}_0,\ \hat{y}_0,\ \hat{z}_0] = [-1,\ 0,\ 0]$. The weighting matrix $\boldsymbol{Q}_k$ is defined as $\boldsymbol{Q}_k = diag([0.01,\ 0.01,\ 0.01])$ while $\boldsymbol{R}_k = 0.05$ and $\boldsymbol{R}_k = 0.1$ are considered.

We tested the estimates of the state by using different filtering techniques: EKF, UKF, PF, D-SDREF, and the combined D-SDRE/PF. Figure 9.4 shows the trajectories of x, y, and z in the 3-dimensional space. Figures 9.5 and 9.6 show the histories of the x, y, and z and the root-mean square (RMS) errors over first 40 sec with $\boldsymbol{R}_k = 0.01$ and $\boldsymbol{R}_k = 0.1$, respectively. The proposed combined D-SDRE/PF shows better performance in the sense that the RMS converged to a smaller value with a faster speed than those by

other filters and remained the small value while UKF and PF were more sensitive to $\boldsymbol{R}_k$ than other filters. Although UKF showed relatively similar performance to D-SDREF and the combined D-SDRE/PF, the time to converge to small RMS is longer than the D-SDREF and the combined D-SDRE/PF.

9.6 Concluding Remarks

In this chapter, we introduced D-SDREF and derived its analytical form with two-step procedure. The error bounds by the D-SDREF were investigated and the difference between the measured signal and the estimated signals was proven to be ISS. We further extended the D-SDREF to deal with non-Gaussian distributed noises. We suggested algorithms of the D-SDREF and the combined D-SDRE/PF. Finally, the proposed filtering techniques were evaluated by using two challenging dynamical examples and the results showed how the proposed filtering techniques could estimate the actual values of the states of the dynamical systems more accurately.

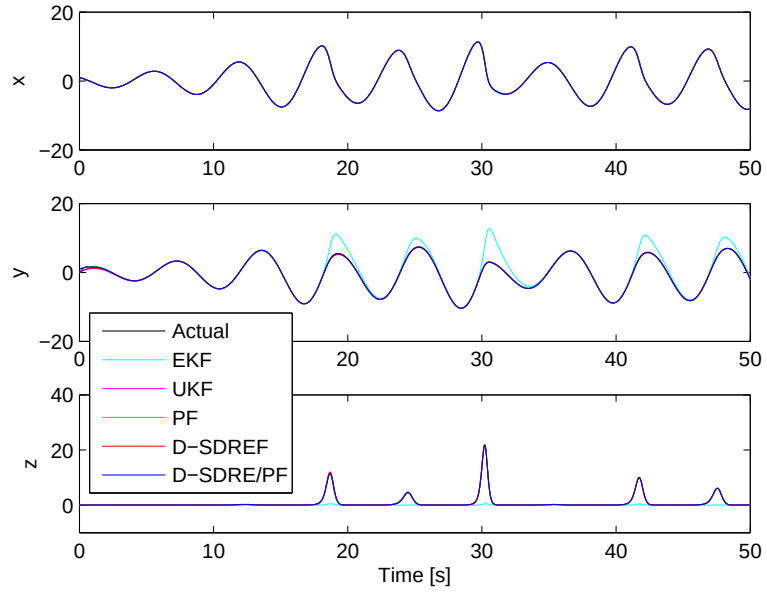

(a) State trajectory of the Rössler attractor and its corresponding estimates by filters

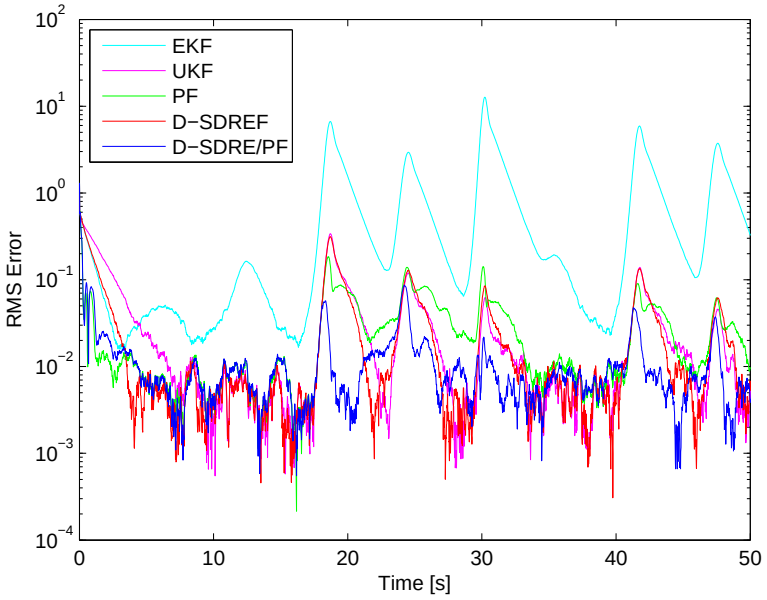

(b) RMS errors of the estimates

Figure 9.5: State trajectory/estimates of the Rössler attractor and RMS errors by EKF, UKF, particle filter, D-SDREF, and combined D-SDRE/PF under uniform noises with $\boldsymbol{Q}_k = diag([0.01,\ 0.01,\ 0.01]),\ \boldsymbol{R}_k = 0.01$

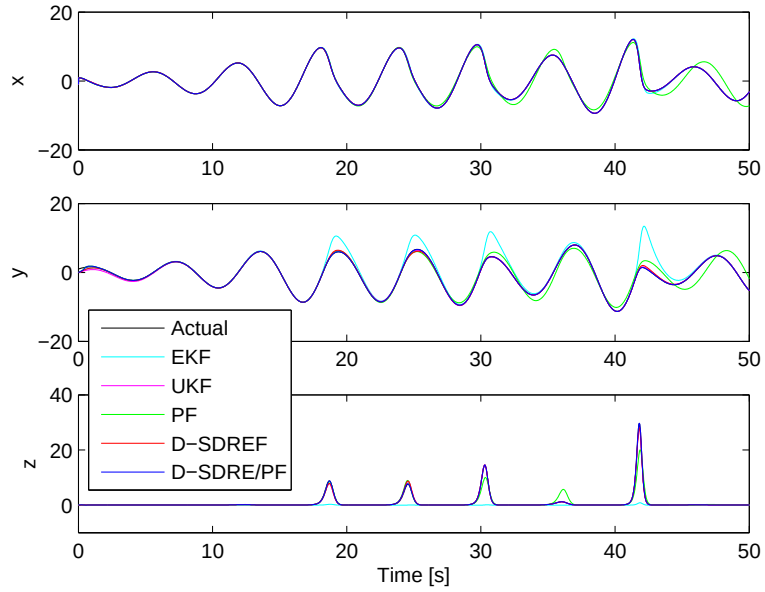

(a) State trajectory of the Rössler attractor and its corresponding estimates by filters

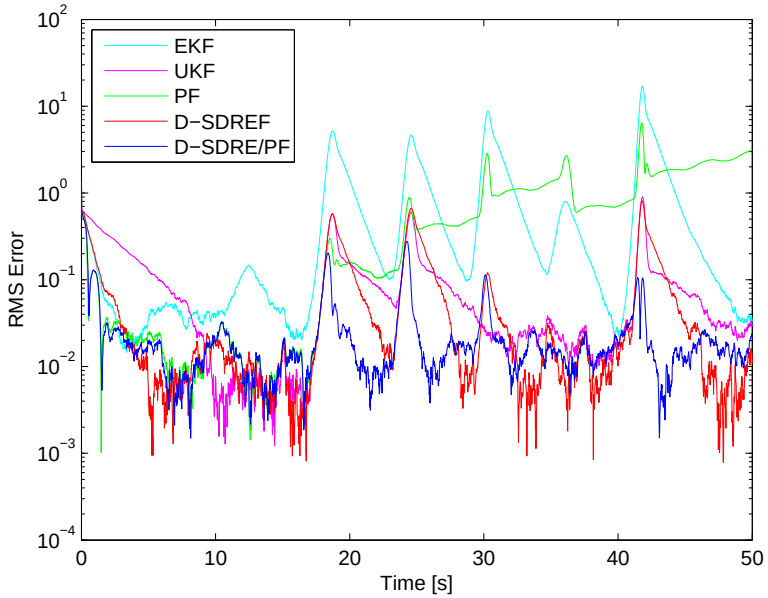

(b) RMS errors of the estimates

Figure 9.6: State trajectory/estimates of the Rössler attractor and RMS errors by EKF, UKF, particle filter, D-SDREF, and combined D-SDRE/PF under uniform noises with $\boldsymbol{Q}_k = diag([0.01,\ 0.01,\ 0.01]),\ \boldsymbol{R}_k = 0.1$

Part IV

Conclusions and Future Work

Chapter 10

Conclusions and Future Research

To conclude, the main contributions of the thesis are summarized and some directions of future research are presented next.

10.1 Summary

In this thesis, we have discussed control and estimation methodologies by using the D-SDRE and CD-SDRE technique, specifically in the presence of constraints on the inputs or states.

In Part II, we investigated the design of the D-SDRE and CD-SDRE controllers. In Chapter 5, Detailed procedures of deriving the D-SDRE and CD-SDRE were provided for the deterministic nonlinear systems. A concept of model predictive control was used not only to provide estimated values of the parameters in the D-SDRE technique, but also to handle constraints on the states/inputs. The proofs of the stability condition for the D-SDRE and the CD-SDRE feedback systems were analyzed to show the exponential stability in their ROAs. In the subsequent chapter, the proposed CD-SDRE controller was evaluated by using challenging problems in spacecraft orbit reconfiguration. We also derived high-fidelity models of the reference and the relative orbit in the presence of the oblateness of the Earth (J_2 perturbation). The proposed CD-SDRE controller successfully generated control signals to transfer the orbit even with demanding initial conditions and the stringent input saturations.

In Chapter 7, the robust CD-SDRE controller was studied for a class of uncertain nonlinear systems. Two controllers were used as in the CD-SDRE discussed in the previous chapter: the robust D-SDRE controller and the robust MPC. The proposed robust CD-SDRE controller comprises the two controllers and they are activated exclusively, which can be viewed as a switched system. We derived 3-dimensional equations of motion of the spacecraft attitude in the presence of fuel slosh effect. Applications of the robust CD-SDRE controller to stabilizing the attitude motion showed its reliability in the presence of uncertainties due to the

motion of the fuel while moving the spacecraft attitude and the saturations on its applied torques.

In Part III, we discussed the filtering design based on the D-SDRE technique. In Chapter 8, the D-SDRE Observer was derived and the stability analysis of the error between the actual states and their associated signals estimated by the D-SDRE Observer was provided to be input-to-state stable.

In Chapter 9, two filters were proposed: the D-SDRE-based filter and the combined D-SDRE/particle filter. The D-SDREF can be used for the nonlinear system with Gaussian noises while the combined D-SDRE/PF for the system with non-Gaussian noises as well as Gaussian noises. The error bounds for the D-SDREF were analyzed. Algorithms of the D-SDREF and the combined D-SDRE/PF were provided.

We also provided related studies to the CD-SDRE technique. In Chapter 3, exponential stability of the continuous-time SDRE feedback system was investigated through the use of contraction analysis and the incremental stability analysis. A way to estimate the ROA was provided which is guaranteed to be invariant. In Chapter 4, a gain-tuning algorithm was discussed, called the AGT-PSO. It provides systematic way to find optimal values of the tuning parameters such as controller gains, system parameters, etc. Due to the model independence of the AGT-PSO and the characteristics of the non-gradient-based method, it is easily applicable to various practical problems. We applied the AGT-PSO to industry applications and showed its effectiveness.

10.2 Future Research

10.2.1 Output-Feedback Control via the CD-SDRE Technique

In this thesis, we discussed the CD-SDRE controller for the full-state feedback system. Moreover, we designed an observer and the filters via the D-SDRE technique. Therefore, output-feedback control of the CD-SDRE controller can be investigated by combining the two systems. In this case, the stability of the combined system will be a main issue.

10.2.2 Adaptive D-SDRE/CD-SDRE Controller

In Chapter 7, we discussed uncertainties in a nonlinear model to be controlled by the CD-SDRE technique. The model uncertainties can be estimated or the effect of the model mismatches can be compensated by using a concept of adaptive control (Narendra and Annaswamy, 1989; Krstić et al., 1995; Ioannou and Sun,

1995). Therefore, it is worthwhile to investigate the adaptive version of the D-SDRE/CD-SDRE technique.

10.2.3 SDRE-Based $\mathcal{H}_\infty$ Control

The SDRE (or D-SDRE) can be applied to design a robust controller via $\mathcal{H}_\infty$ control (Doyle et al., 1991; Zhou et al., 1996). As discussed briefly in (Cloutier, 1997), the SDRE technique can be extended to non-linear $\mathcal{H}_\infty$ control due to its analogy to linear quadratic regulation or linear quadratic Gaussian controllers. However, more rigorous analysis of the stability condition should be investigated in case of a finite horizon problem. Unlike the infinite horizon problem, which makes the control problem similar to LQR and LQG controllers, the generalized continuous-time (or discrete-time) Riccati equation as discussed in Chapter 5 should be used if a finite horizon is considered.

References

Agrawal, B. N., July–August 1993. Dynamic Characteristics of Liquid Motion in Partially Filled Tanks of a Spinning Spacecraft. AIAA Journal of Guidance, Control, and Dynamics 16 (4), 636–640.

Alfriend, K. T., Vadali, S. R., Gurfil, P., How, J. P., Breger, L. S., 2010. Spacecraft Formation Flying: Dynamics, Control and Navigation. Elsevier, Oxford, England.

Anderson, B. D. O., Moore, J. B., 1979. Optimal Filtering. Prentice-Hall, Inc., Englewood Cliffs, NJ, reprinted by Dover, Mineola, NY, 2005.

Anderson, R. T., May 2010. Results and Control Law Derivations for Hystat Pressure Control (HPC), Hystat Torque Control (HTC), and Variable ePOR Features. Tech. Rep. 23-03233, Caterpillar Inc., Mossville, IL.

Angeli, D., March 2002. A Lyapunov Approach to Incremental Stability Properties. IEEE Transactions on Automatic Control 47 (3), 410–421.

Åström, K. J., Hägglund, T., Hang, C. C., Ho, W. K., August 1993. Automatic Tuning and Adaptation for PID Controllers — A Survey. Control Engineering Practice 1 (4), 699–714.

Banks, H. T., Kwon, H.-D., Toivanen, J. A., Tran, H. T., March–April 2006. A State-Dependent Riccati Equation-Based Estimator Approach for HIV Feedback Control. Optimal Control Applications and Methods 27 (2), 93–121.

Batmani, Y., Khaloozadeh, H., September/October 2012. Optimal Chemotheraph in Cancer Treatment: State Dependent Riccati Equation Control and Extended Kalman Filter. Optimal Control Applications and Methods 34 (5), 562–577.

Beikzadeh, H., Taghirad, H. D., August 2012a. Exponential Nonlinear Observer Based on the Differential State-Dependent Riccati Equation. International Journal of Automation and Computing 9 (4), 358–368.

Beikzadeh, H., Taghirad, H. D., January 2012b. Robust SDRE Filter Design for Nonlinear Uncertain Systems with an H_∞ Performance Criterion. ISA Transactions 51 (1), 146–152.

Bemporad, A., Morari, M., Dua, V., Pistikopoulos, E. N., January 2002. The Explicit Linear Quadratic Regulator for Constrained Systems. Automatica 38 (1), 3–20.

Bentsman, J., Chang, I., Li, W., August 2012. Demonstration of Automatic Gain-Tuners via Iterative Feedback Tuning and Particle Swarm Optimization: Feasibility Study. Tech. rep., Caterpillar Inc., Mossville, IL, CAT-1065512.

Bogdanov, A., Wan, E., January–February 2007. State-Dependent Riccati Equation Control for Small Autonomous Helicopters. AIAA Journal of Guidance, Control, and Dynamics 30 (1), 47–60.

Boyd, S., Ghaoui, L. E., Feron, E., Balakrishnan, V., 1994. Linear Matrix Inequalities in System and Control Theory. SIAM, Philadelphia, PA.

Bracci, A., Innocenti, M., Pollini, L., November–December 2006. Estimation of the Region of Attraction for State-Dependent Riccati Equation Controllers. AIAA Journal of Guidance, Control, and Dynamics 29 (6), 1427–1430.

Brown, R. G., Hwang, P. Y. C., 1997. Introduction to Random Signals and Applied Kalman Filtering, 3rd Edition. John Wiley & Sons, New York, NY.

Bryson, Jr., A. E., 1994. Control of Spacecraft and Aircraft. Princeton University Press, Princeton, NJ.

Bryson, Jr., A. E., Ho, Y.-C., 1975. Applied Optimal Control: Optimization, Estimation, and Control. Taylor & Francis, New York, NY.

Campi, M. C., Lecchini, A., Savaresi, S. M., August 2002. Virtual Reference Feedback Tuning: A direct Method for the Design of Feedback Controllers. Automatica 38 (8), 1337–1346.

Campi, M. C., Savaresi, S. M., January 2006. Direct Nonlinear Control Design: The Virtual Reference Feedback Tuning (VRFT) Approach. IEEE Transactions on Automatic Control 51 (1), 14–27.

Chang, I., Chung, S.-J., Blackmore, L., December 2010a. Cooperative Control with Adaptive Graph Laplacians for Spacecraft Formation Flying. In: 49th IEEE Conference on Decision and Control. Atlanta, GA, pp. 4926–4933.

Chang, I., Chung, S.-J., Hadaegh, F. Y., May 2011. Novel Coordinate Transformation and Robust Cooperative Formation Control for Swarms of Spacecraft. In: 4th International Conference on Spacecraft Formation Flying Missions & Technologies. St. Hubert, Québec, Canada.

Chang, I., Li, W., Bentsman, J., February 2013. Development and Performance Evaluation of Automatic Gain-Tuner. Tech. rep., Caterpillar Inc., Mossville, IL, CAT-1067515.

Chang, I., Park, S.-Y., Choi, K.-H., October 2009. Decentralized Coordinated Attitude Control for Satellite Formation Flying via the State-Dependent Riccati Equation Technique. International Journal of Non-Linear Mechanics 44 (8), 891–904.

Chang, I., Park, S.-Y., Choi, K.-H., October 2010b. Nonlinear Attitude Control of a Tether-Connected Multi-Satellite in Three-Dimensional Space. IEEE Transactions on Aerospace and Electronic Systems 46 (4), 1950–1968.

Chen, C.-C., Liang, Y.-W., Jhu, W.-M., October 2015. Global Stability of a System with State-Dependent Riccati Equation Controller. AIAA Journal of Guidance, Control, and Dynamics 38 (10), 2050–2054.

Çimen, T., June 2008. State-Dependent Riccati Equation (SDRE) Control: A Survey. In: 17th IFAC World Congress. Seoul, Korea, pp. 3761–3775.

Çimen, T., April 2010. Systematic and Effective Design of Nonlinear Feedback Controllers via the State-Dependent Riccati Equation (SDRE) Method. Annual Reviews in Control 34 (1), 32–51.

Çimen, T., July–August 2012. Survey of State-Dependent Riccati Equation in Nonlinear Optimal Feedback Control Synthesis. AIAA Journal of Guidance, Control, and Dynamics 35 (4), 1025–1047.

Çimen, T., Merttopçuoğlu, A. O., June 2008. Asymptotically Optimal Nonlinear Filtering: Theory and Examples with Application to Target State Estimation. In: 17th IFAC World Congress. Seoul, Korea, pp. 8611–8617.

Clarke, D. W., Mohtadi, C., Tuffs, P. S., March 1987a. Generalized Predictive Control – Part I. The Basic Algorithm. Automatica 23 (2), 137–148.

Clarke, D. W., Mohtadi, C., Tuffs, P. S., March 1987b. Generalized Predictive Control – Part II. Extensions and Interpretations. Automatica 23 (2), 149–160.

Clerc, M., 2006. Particle Swarm Optimization. ISTE, London, UK.

Clerc, M., Kennedy, J., February 2002. The Particle Swarm - Explosion, Stability, and Convergence in a Multidimensional Complex Space. IEEE Transactions on Evolutionary Computation 6 (1), 58–73.

Clohessy, W. H., Wiltshire, R. S., 1960. Terminal Guidance System for Satellite Rendezvous. Journal of the Aerospace Science 27 (9), 653–658.

Cloutier, J. R., June 1997. State-Dependent Riccati Equation Techniques: An Overview. In: American Control Conference. Albuquerque, NM, pp. 932–936.

Cloutier, J. R., Stansbery, D. T., August 2001. Nonlinear, Hybrid Bank-to-Turn/Skid-to-Turn Missile Autopilot Design. In: AIAA Guidance, Navigation, and Control Conference. Montreal, Canada, AIAA 2001-4158.

Crowe, J., Johnson, M. A., Grimble, M. J., August 2003. PID Parameter Cycling to Tune Industrial Controllers: a New Model-Free Approach. In: 13th IFAC Symposium on System Identification. Rotterdam, The Netherlands.

Daafouz, J., Riedinger, P., Iung, C., November 2002. Stability Analysis and Control Synthesis for Switched Systems: A Switched Lyapunov Function Approach. IEEE Transactions on Automatic Control 47 (11), 1883–1887.

de Freitas, J. F. G., Niranjan, M., Gee, A. H., Doucet, A., 2000. Sequential Monte Carlo Methods to Train Neural Network Models. Neural Computation 12 (4), 955–993.

de Oliveira, M. C., Bernussou, J., Geromel, J. C., July 1999. A New Discrete-Time Robust Stability Condition. Systems and Control Letters 37 (4), 261–265.

Ding, B., Sun, H., Yang, P., Tang, H., Wang, B., December 2004. A Design Approach of Constrained Linear Time-Varying Quadratic Regulation. In: 43rd IEEE Conference on Decision and Control. Atlantis, Paradise Island, Bahamas, pp. 2954–2959.

Doucet, A., Godsill, S., Andrieu, C., July 2000. On Sequential Monte Carlo Sampling Methods for Bayesian Filtering. Staticstics and Computing 10 (3), 197–208.

Doyle, J. C., Francis, B., Tannenbaum, A., 1991. Feedback Control Theory. Macmillan Publishing Co., New York, NY.

Dutka, A. S., Ordys, A. W., Grimble, M. J., June 2005. Optimized Discrete-Time State Dependent Riccati Equation Regulator. In: American Control Conference. Portland, OR, pp. 2293–2298.

Eberhart, R. C., Shi, Y., March 1998. Comparison between Genetic Algorithms and Particle Swarm Optimization. In: 7th International Conference on Evolutionary Programming VII. San Diego, CA, pp. 611–616.

Erdem, E. B., 2001. Analysis and Real-Time Implementation of State-Dependent Riccati Equation Controlled Systems. Ph.D. thesis, University of Illinois at Urbana-Champaign, Urbana, IL, USA.

Erdem, E. B., Alleyne, A. G., June 2002. Estimation of Stability Regions of SDRE Controlled Systems Using Vector Norms. In: American Control Conference. Anchorage, AK, pp. 80–85.

Erdem, E. B., Alleyne, A. G., January 2004. Design of a Class of Nonlinear Controllers via State Dependent Riccati Equations. IEEE Transactions on Control Systems Technology 12 (1), 133–137.

Etkin, B., 1972. Dynamics of Atmospheric Flight. John Wiley & Son, New York, NY.

Fantoni, I., Lozano, R., Spong, M. W., April 2000. Energy Based Control of the Pendubot. IEEE Transactions on Automatic Control 45 (4), 725–729.

Ferrante, A., Ntogramatzidis, L., February 2013. The Generalised Discrete Algebraic Riccati Equation in Linear-Quadratic Optimal Control. Automatica 49 (2), 471–478.

Gaing, Z.-L., June 2004. A Particle Swarm Optimization Approach for Optimum Design of PID Controller in AVR System. IEEE Transactions on Energy Conversion 19 (2), 384–391.

Gao, Z., June 2003. Scaling and Bandwidth-Parameterization Based Controller Tuning. In: American Control Conference. Denver, CO, pp. 4989–4996.

Gelb, A., 1974. Applied Optimal Estimation. The MIT press, Cambridge, MA.

Geranmehr, B., Nekoo, S. R., March 2015. Nonlinear Suboptimal Control of Fully Coupled Non-Affine Six-DOF Autonomous Underwater Vehicle Using the State-Dependent Riccati Equation. Ocean Engineering 96 (1), 248–257.

Goldstein, H., Poole, C., Safko, J., 2002. Classical Mechanics, 3rd Edition. Addision-Wesley, San Francisco, CA.

Goodwin, G. C., Sin, K. S., 1984. Adaptive Filtering Prediction and Control. Prentice-Hall, Englewood Cliffs, NJ, reprinted by Dover, Mineola, NY, 2009.

Gordon, N. J., Salmond, D. J., Smith, A. F. M., April 1993. Novel Approach to Nonlinear/Non-Gaussian Bayesian State Estimation. IEE Proceedings F (Radar and Signal Processing) 140 (2), 107–113.

Grieder, P., Borrelli, F., Torrisi, F., Morari, M., April 2004. Computation of the Constrained Infinite Time Linear Quadratic Regulator. Automatica 40 (4), 701–708.

Grüne, L., Pannek, J., 2011. Nonlinear Model Predictive Control: Theory and Algorithms. Springer, London, United Kingdom.

Hassan, M. F., October 2012. Observer-Based Controller for Discrete-Time Systems: a State Dependent Riccati Equation Approach. Nonlinear Dynamics 70 (1), 693–707.

Hassan, R., Cohanim, B., de Weck, O., Venter, G., April 2005. A Comparison of Particle Swarm Optimization and the Genetic Algorithm. In: 46th AIAA/ASME/ASCE/AHS/ASC Structures, Structural Dynamics and Materials Conference. Austin, TX, AIAA 2005-1897.

Hervas, J. R., Reyhanoglu, M., Tang, H., October 2013. Thrust-Vector Control of a Three-Axis Stabilized Spacecraft with Fuel Slosh Dynamics. In: 13th International Conference on Control, Automation and Systems. Gwangju, Korea, pp. 761–766.

Hjalmarsson, H., June 2002. Iterative Feedback Tuning–An Overview. International Journal of Adaptive Control and Signal Processing 16 (5), 373–395.

Hjalmarsson, H., Gevers, M., Gunnarsson, S., Lequin, O., August 1998. Iterative Feedback Tuning: Theory and Applications. IEEE Control Systems 18 (4), 26–41.

Hovd, M., Olaru, S., 2010. Piecewise Quadratic Lyapunov Functions for Stability Verification of Approximate Explicit MPC. Journal of Modeling, Identification and Control 31 (2), 45–53.

Hughes, P. C., 1986. Spacecraft Attitude Dynamics. John Wiley & Sons, New York, NY.

Ioannou, P. A., Sun, J., 1995. Robust Adaptive Control. Prentice Hall, Upper Saddle River, NJ.

Jaganath, C., Ridley, A., Bernstein, D. S., June 2005. A SDRE-Based Asymptotic Observer for Nonlinear Discrete-Time Systems. In: American Control Conference. Portland, OR, pp. 3630–3635.

Jiang, Z.-P., Wang, Y., June 2001. Input-to-State Stability for Discrete-Time Nonlinear Systems. Automatica 37 (6), 857–869.

Jiménez-Lizárraga, M., Basin, M., Rodríguez, V., Rodríguez, P., March 2015. Open-Loop Nash Equilibrium in Polynomial Differential Games via State-Dependent Riccati Equation. Automatica 53, 155–163.

Johansen, T. A., May 2003. Reduced explicit constrained linear quadratic regulators. IEEE Transactions on Automatic Control 48 (5), 823–828.

Johansen, T. A., Petersen, I., Slupphaug, O., July 2002. Explicit Sub-Optimal Linear Quadratic Regulation with State and Input Constraints. Automatica 38 (7), 1099–1111.

Johnson, M. A., Moradi, M. H. (Eds.), 2005. PID Control — New Identification and Design Methods. Springer, London, UK.

Julier, S. J., Uhlmann, J. K., April 1997. A New Extension of the Kalman Filter to Nonlinear Systems. In: 11th International Symposium on Aerospace/Defense Sensing, Simulation, and Controls. Orlando, FL.

Julier, S. J., Uhlmann, J. K., March 2004. Unscented Filtering and Nonlinear Estimation. Proceedings of the IEEE 92 (2), 401–422.

Kalman, R. E., March 1960. A New Approach to Linear Filtering and Prediction Problems. Journal of Basic Engineering 82 (1), 35–45.

Kalman, R. E., Bucy, R. S., March 1961. New Results in Linear Filtering and Prediction Theory. Journal of Basic Engineering 83 (1), 95–108.

Karimi, A., Mišković, L., Bonvin, D., October 2004. Iterative Correlation-Based Controller Tuning. International Journal of Adaptive Control and Signal Processing 18 (8), 645–664.

Karimi, A., Van Heusden, K., Bonvin, D., July 2007. Noniterative Data-driven Controller Tuning Using the Correlation Approach. In: European Control Conference. Kos, Greece, pp. 5189–5195.

Kechichian, J. A., January–March 1998. Motion in General Elliptic Orbit with Respect to a Dragging and Precessing Coordinate Frame. Journal of the Astronautical Sciences 46 (1), 25–45.

Kennedy, J., Eberhart, R., November 1995. Particle Swarm Optimization. In: IEEE International Conference on Neural Networks. Washington, DC, pp. 1942–1948.

Khalil, H. K., 2002. Nonlinear Systems, 3rd Edition. Prentice Hall, Upper Saddle River, NJ.

Kim, K., Rao, P., Burnworth, J. A., July-August 2010. Self-Tuning of the PID Controller for a Digital Excitation Control System. IEEE Transactions on Industrial Applications 46 (4), 1518–1524.

Kim, T.-H., Maruta, I., Sugie, T., April 2008. Robust PID Controller Tuning Based on the Constrained Particle Swarm Optimization. Automatica 44 (4), 1104–1110.

Kirk, D. E., 1970. Optimal Control Theory: An Introduction. Prentice Hall, Englewood Cliffs, NJ, reprinted by Dover, Mineola, NY, 2004.

Kothare, M. V., Campo, P. J., Morari, M., Nett, C. N., December 1994. Unified Framework for the Study of Anti-windup Designs. Automatica 30 (12), 1869–1883.

Kothare, M. V., Morari, M., May 1999. Multiplier Theory for Stability Analysis of Anti-Windup Control Systems. Automatica 35 (5), 917–928.

Krstić, M., Kanellakopoulos, I., Kokotović, P., 1995. Nonlinear and Adaptive Control Design. John Wiley & Sons, New York, NY.

Langson, W., Alleyne, A. G., September 2002. A Stability Result with Application to Nonlinear Regulation. Journal of Dynamic Systems, Measurement, and Control 124 (3), 452–456.

Lee, J.-W., Khargonekar, P. P., October 2007. Constrained Infinite-Horizon Linear Quadratic Regulation of Discrete-Time Systems. IEEE Transactions on Automatic Control 52 (10), 1951–1958.

Lequin, O., Gevers, M., Mossberg, M., Bosmans, E., Triest, L., September 2003. Iterative Feedback Tuning of PID Parameters: Comparison with Classical Tuning Rules. Control Engineering Practice 11 (9), 1023–1033.

Lewis, F. R., Vrabie, D. L., Syrmos, V. L., 2012. Optimal Control, 3rd Edition. John Wiley & Sons, Inc., Hoboken, NJ.

Lohmiller, W., Slotine, J.-J. E., June 1998. On Contraction Analysis for Non-Linear Systems. Automatica 34 (6), 683–696.

Lorenz, E. N., March 1963. Deterministic Nonperiodic Flow. Journal of the Atmospheric Sciences 20 (2), 130–141.

Luenberger, D. G., April 1966. Observers for Multivariable Systems. IEEE Transactions on Automatic Control 11 (2), 190–197.

Magni, L., Raimondo, D. M., Allgöwer, F., 2009. Nonlinear Model Predictive Control: Towards New Challenging Applications. Springer, Berlin Heidelberg.

Mayne, D. Q., Rawlings, J. B., Rao, C. V., Scokaert, P. O. M., June 2000. Constrained Model Predictive Control: Stability and Optimality. Automatica 36 (6), 789–814.

McCaffrey, D., Banks, S. P., July 2001. Lagrangian Manifolds and Asymptotically Optimal Stabilizing Feedback Control. Systems and Control Letters 43 (3), 219–224.

Mracek, C. P., Cloutier, J. R., April 1998. Control Designs for the Nonlinear Benchmark Problem via the State-Dependent Riccati Equation Method. International Journal of Robust and Nonlinear Control 8 (4–5), 401–433.

Naik, M. S., Singh, S. N., August 2007. State-Dependent Riccati Equation-Based Robust Dive Plane Control of AUV with Control Constraints. Ocean Engineering 34 (11–12), 1711–1723.

Narendra, K. S., Annaswamy, A. M., 1989. Stable Adaptive Systems. Prentice Hall, Englewood Cliffs, NJ, reprinted by Dover, Mineola, NY, 2005.

Nazari, M., Ghaffari, A., Arab, F., 2015. Finite Duration Treatment of Cancer by Using Vaccine Therapy and Optimal Chemotherapy: State-Dependent Riccati Equation Control and Extended Kalman Filter. Journal of Biological Systems 23 (1), 1–29.

Nemra, A., Aouf, N., April 2010. Robust INS/GPS Sensor Fusion for UAV Localization Using SDRE Nonlinear Filtering. IEEE Sensors Journal 10 (4), 789–798.

Niknam, T., January 2010. A New Fuzzy Adaptive Hybrid Particle Swarm Optimization Algorithm for Non-Linear, Non-Smooth and Non-Convex Economic Dispatch Problem. Applied Energy 87 (1), 327–339.

Park, J.-B., Lee, K.-S., Shin, J.-R., Lee, K. Y., February 2005. A Particle Swarm Optimization for Economic Dispatch With Nonsmooth Cost Functions. IEEE Transactions on Power Systems 20 (1), 34–42.

Parrilo, P. A., May 2000. Structured Semi Definite Programs and Semi Algebraic Geometry Methods in Robustness and Optimization. Ph.D. thesis, California Institutte of Technology, Pasadena, CA, USA.

Parsopoulos, K. E., Vrahatis, M. N., 2002. Intelligent Technologies–Theory and Application: New Trends in Intelligent Technologies. Vol. 76. IOS Press, Amsterdam, The Netherlands, Ch. Particle swarm optimization method for constrained optimization problems, pp. 214–220.

Parsopoulos, K. E., Vrahatis, M. N., 2010. Particle Swarm Optimization and Intelligence: Advances and Applications. IGI Global, Hershey, PA.

Pearson, J. D., 1962. Approximation Methods in Optimal Control I. Suboptimal Control. Journal of Electronics and Control 13 (5), 453–469.

Peterson, L. D., Crawley, E. F., Hansman, R. J., September 1989. Nonlinear Fluid Slosh Coupled to the Dynamics of Spacecraft. AIAA Journal 27 (9), 1230–1240.

Pham, Q. C., Tabareau, N., Slotine, J.-J. E., April 2009. A Contraction Theory Approach to Stochastic Incremental Stability. IEEE Transactions on Automatic Control 54 (4), 816–820.

Pikovsky, A. S., Rosenblum, M. G., Kurths, J., 1996. Synchronization in a Population of Globally Coupled Chaotic Oscillators. Europhysics Letters 34 (3), 165–170.

Poli, R., Kennedy, J., Blackwell, T., June 2007. Particle Swarm Optimization: An Overview. Swarm Intelligence 1 (1), 33–57.

Ramos, D. C. W., Peres, P. L. D., August 2001. A Less Conservative LMI Condition for the Robust Stability of Discrete-Time Uncertain Systems. Systems and Control Letters 43 (5), 371–378.

Rao, C. V., Rawlings, J. B., Mayne, D. Q., February 2003. Constrained State Estimation for Nonlinear Discrete-Time Systems: Stability and Moving Horizon Approximations. IEEE Transactions on Automatic Control 48 (2), 246–258.

Rawlings, J. B., Mayne, D. Q., 2009. Model Predictive Control: Theory and Design. Nob Hill Publishing, Madison, WI.

Reyhanoglu, M., Hervas, J. R., December 2011. Nonlinear Control of a Spacecraft with Multiple Fuel Slosh Modes. In: 50th IEEE Conference on Decision and Control. Orlando, FL, pp. 6192–6197.

Rössler, O. E., July 1976. An Equation for Continuous Chaos. Physics Letters A 57 (5), 397–398.

Rădac, M.-B., Precup, R.-E., Petriu, E. M., Preitl, S., December 2011. Application of IFT and SPSA to Servo System Control. IEEE Transactions on Neural Networks 22 (12), 2363–2375.

Sánchez, A., Katebi, M. R., Johnson, M. A., September 2004. A Tuning Algorithm for Multivariable Restricted Structure Control Systems Using Subspace Identification. International Journal of Adaptive Control and Signal Processing 18 (9–10), 745–770.

Scharf, D. P., Hadaegh, F. Y., Ploen, S. R., June 2003. A Survey of Spacecraft Formation Flying Guidance and Control (Part I): Guidance. In: American Control Conference. Denver, CO, pp. 1733–1739.

Scharf, D. P., Hadaegh, F. Y., Ploen, S. R., June 2004. A Survey of Spacecraft Formation Flying Guidance and Control (Part II): Control. In: American Control Conference. Boston, MA, pp. 2976–2984.

Schaub, H., Junkins, J. L., 2003. Analytical Mechanics of Space Systems. AIAA, Reston, VA.

Scokaert, P. O. M., Rawlings, J. B., August 1998. Constrained Linear Quadratic Regulation. IEEE Transactions on Automatic Control 43 (8), 1163–1169.

Seiler, P., June 2003. Stability Region Estimates for SDRE Controlled Systems Using Sum of Squares Optimization. In: American Control Conference. Denver, CO, pp. 1867–1872.

Selvakumar, A. I., Thanushkodi, K., February 2007. A New Particle Swarm Optimization Solution to Nonconvex Economic Dispatch Problems. IEEE Transactions on Power Systems 22 (1), 42–51.

Shamma, J. S., Cloutier, J. R., March 2003. Existence of SDRE Stabilizing Feedback. IEEE Transactions on Automatic Control 48 (3), 513–517.

Shi, Y., Eberhart, R., May 1998. A Modified Particle Swarm Optimizer. In: IEEE International Conference on Evolutionary Computation. Anchorage, AK, pp. 69–73.

Song, Y., Grizzle, J. W., June 1992. The Extended Kalman Filter as a Local Asymptotic Observer for Nonlinear Discrete-Time Systems. In: American Control Conference. Chicago, IL, pp. 3365–3369.

Sontag, E. D., April 1989. Smooth Stabilization Implies Coprime Factorization. IEEE Transactions on Automatic Control 34 (4), 435–443.

Spall, J. C., March 1992. Multivariate Stochastic Approximation Using a Simultaneous Perturbation Gradient Approximation. IEEE Transactions on Automatic Control 37 (3), 332–341.

Spall, J. C., July 1998. Implementation of the Simultaneous Perturbation Algorithm for Stochastic Optimization. IEEE Transactions on Aerospace and Electronic Systems 34 (3), 817–823.

Spong, M. W., Block, D. J., December 1995. The Pendubot: A Mechatronic System for Control Research and Education. In: 34th IEEE Conference on Decision and Control. New Orleans, LA, pp. 555–556.

Stefanutti, W., Mattavelli, P., Saggini, S., Ghioni, M., January 2007. Autotuning of Digitally Controlled DC–DC Converters Based on Relay Feedback. IEEE Transactions on Power Electronics 22 (1), 199–207.

Stengel, R. F., 1994. Optimal Control and Estimation. Dover Publications, New York, NY.

Suzuki, S., Furuta, K., Sugiki, A., Hatakeyama, S., September 2004. Nonlinear Optimal Internal Forces Control and Application to Swing-up and Stabilization of Pendulum. Journal of Dynamic Systems, Measurement, and Control 126 (3), 568–573.

Tan, K. K., Ferdous, R., Huang, S., August 2002. Closed-Loop Automatic Tuning of PID Controller for Nonlinear Systems. Chemical Engineering Science 57 (15), 3005–3011.

Trelea, I. C., March 2003. The Particle Swarm Optimization Algorithm: Convergence Analysis and Parameter Selection. Information Processing Letters 85 (6), 317–325.

Vaddi, S. S., Menon, P. K., Ohlmeyer, E. J., March–April 2009. Numerical State-Dependent Riccati Equation Approach for Missile Integrated Guidance Control. AIAA Journal of Guidance, Control, and Dynamics 32 (2), 699–703.

Vallado, D. A., 2007. Fundamentals of Astrodynamics and Applications, 3rd Edition. Microcosm Press, Hawthorne, CA.

van der Merwe, R., Doucet, A., de Freitas, N., Wan, E., August 2000. The Unscented Particle Filter. Tech. Rep. CUED/F-INFENG/TR-380, Cambridge University Engineering Department.

Vreeburg, J. P. B., June 2005. Spacecraft Maneuvers and Slosh Control. IEEE Control Systems Magazine 25 (3), 12–16.

Widrow, B., Stearns, P. N., 1985. Adaptive Signal Processing. Prentice Hall, Englewood Cliffs, NJ.

Xin, M., Balakrishnan, S. N., December 2002. A New Filtering Technique for a Class of Nonlinear Systems. In: 41st IEEE Conference on Decision and Control. Las Vegas, NV, pp. 1034–1039.

Xu, G., Wang, D., September–October 2008. Nonlinear Dynamic Equations of Satellite Relative Motion Around an Oblate Earth. AIAA Journal of Guidance, Control, and Dynamics 31 (5), 1521–1524.

Zhang, S., Taft, C. W., Bentsman, J., Hussey, A., Petrus, B., September 2012. Simultaneous Gains Tuning in Boiler/Turbine PID-Based Controller Clusters Using Iterative Feedback Tuning Methodology. ISA Transactions 51 (5), 609–621.

Zhang, S., Ye, D., Bentsman, J., Taft, C., Hussey, A., June 2010. Assessment of Global Optimizers: Particle Swarm Optimization, Simulated Annealing, and Genetic Algorithms in Local Simultaneous Multi-Loop Tuning of PID Gains. In: 53rd ISA Power Industry Division Symposium. Vol. 483. Summerlin, NV, pp. 246–281.

Zhao, X., Lin, Z., December 2008. On the Horizons in Constrained Linear Quadratic Regulation. Automatica 44 (12), 3107–3112.

Zhou, K., Doyle, J. C., Glover, K., 1996. Robust and Optimal Control. Prentice Hall, Upper Saddle River, NJ.